THE UNIVERSITY *of* EDINBURGH

Cardiac Extracellular Matrix Metabolism: The Roles of Age and Sex in Collagen Dynamics

Kalyani Pandya MScR BSc (Hons)

Doctor of Philosophy in Cardiovascular Biology

2024

Contents

Declaration

I declare that this thesis has been composed solely by myself and has not been submitted for any previous degree or qualification. The work described within this thesis comprises my own original work except where otherwise stated in the text. All external sources of data and information have been specifically referenced.

Kalyani Pandya

4th November 2024

Acknowledgements

I would first like to acknowledge the British Heart Foundation (BHF) for providing both the opportunity and funding that enabled me to complete my Master's and doctoral studies.

For her continual support and guidance during my PhD, I would like to thank my supervisor, Professor Adriana A. S. Tavares. Adriana has always been enthusiastic about introducing new scientists to the field of PET, and her willingness to teach both the fundamentals of imaging and the joy of working in an interdisciplinary field is something I am truly grateful for. Her dedication to science is unmatched, and her perseverance is something I greatly admire. Adriana's famous Portuguese sayings, like "Do not leave for tomorrow what you can do today" and "God gives nuts to those who don't have teeth," have been a source of encouragement, motivation, and occasional amusement – but always a joy.

I would also like to thank my secondary supervisor, Professor Gillian Gray, for her support and honest guidance, which has helped shape me into someone who can view my work critically and continuously strive for improvement, while also appreciating each success. I am also grateful to Gillian for reminding me of what is important in both science and life, as she has truly highlighted the value of embracing intimidating opportunities and maintaining a healthy balance between work and life.

Thank you to my supervisor, Dr. Mark G. MacAskill, for guiding me through the inner workings of research and encouraging me to participate in various aspects of academia – I'm glad we got to be good CVS citizens together! I would also like to thank my thesis committee members, Dr. Laura Denby and Professor Matthew Bailey, for their ongoing support.

To the PiW team: thank you for all your help and support over the past four years. It has been truly great to experience the dedication of our group in the face of time pressures and technical challenges. In particular, I would like to thank Carlos J. Alcaide-Corral and Islay Cranston for your incredible work and support on the tough days. I always left the PET lab with a smile, and I am grateful for your enthusiasm in giving my old boys and girls a great time! I also want to thank the facilities and administrative staff at CVS and BVS, especially Ami Onishi, Will Mungall, and Polly Elliot-Pyle, for their assistance over the years.

I would also like to acknowledge the wonderful friends I have made at CVS, including Shaden Melhem, Bronwyn Berkeley, Hongling Liu, and David Craig. I am so grateful to have met such lovely people, who I'm sure will be friends for life, and that we were able to support each other through this journey. Special thanks go to Lynne Ramage, who has been exceptionally kind, taking time out of her busy day to teach me so much in the lab, lift my spirits on difficult days, and always share a laugh. Similarly, I would like to thank Adrian Thomson for his kindness, his willingness to take stressed PhD students under his wing, and, of course, the ultrasound scans!

To the most important people in my life: my family, Jake, and Maggie. Thank you for your support – words cannot express how much I appreciate everything you have done for me. I hope to make you all proud and support you the way you have supported me. In particular,

to my partner Jake – I know I make fun of your civil servant lifestyle (only because I wish for it sometimes too!), and I know, especially over the past year, that you have shouldered the stresses of us both. I am endlessly grateful for your patience, love, and cooking. I am so lucky to have you by my side. My siblings Divya, Suraj and Anjali you're the best and thank you for tolerating me. Mum and Dad, I appreciate everything you've done for us.

Finally, I dedicate this thesis to my grandfather, Ramniklal B.S. Pandya, who we lost this year. If he were here, I would thank him for being a parent to me in every sense and would want him to know that without him, I'm not sure where I would be today. My grandfather instilled in me a deep appreciation for learning and a love for education, something that motivated me throughout my studies. I have been incredibly fortunate to have his time, guidance, and support, and truly, anything I have achieved is because of him. There are no words to describe how special he was to me and my siblings.

Abstract

Aging is a major risk factor for cardiovascular disease, making it crucial to understand physiological aging in the context of cardiovascular health. In the absence of pathology, aging leads to a reduction in cardiac output and increased heart rate variability, vascular stiffening, and cardiac fibrosis. This age-related cardiac fibrosis is characterized by increased myocardial stiffness due to excessive extracellular matrix (ECM) components like fibrillin and collagen. The mechanisms of cardiovascular aging are poorly understood, though inflammation, senescence, and oxidative stress are implicated. These factors result in adverse remodelling, collagen accumulation, cardiac stiffening, and reduced cardiac function. It remains unclear whether collagen accumulation stems from increased synthesis or reduced clearance. The overarching hypothesis of this project is that aging disrupts cardiac collagen metabolism, causing a decrease in collagen synthesis despite significant collagen accumulation, with higher rates of collagen synthesis and accumulation in males compared to females. Therefore, this thesis focuses on the effect of aging on cardiac collagen metabolism, particularly on collagen synthesis both *in vivo* and *in vitro*. It also examines the influence of sex on age-related collagen metabolism, as females are thought to be relatively protected from adverse collagen accumulation.

This thesis employs a comprehensive approach to investigate the impact of aging and sex on collagen synthesis and metabolism across the heart through *in vivo, in vitro*, and *ex vivo* methods. A longitudinal Positron Emission Tomography (PET)/Computer Tomography (CT) imaging study in male (n=7-14) and female (n=7-14) Sprague-Dawley rats across five timepoints (1, 3, 6, 12, and 18 months) was carried out. Longitudinal characterization included survival analysis, body weight, and frailty measurements to assess age-related physiological changes. Cardiovascular health was evaluated using CT-derived cardiac volume measurements, tail-cuff plethysmography for blood pressure, and echocardiography at the final experimental timepoint. PET/CT imaging utilized *cis*-4-^{18}F-fluoro-*L*-proline and *trans*-4-^{18}F-fluoro-*L*-proline proline to measure unhydroxylated and hydroxylated collagen synthesis, respectively. Images were analysed using a cardiac template defining the four heart chambers. Additional groups were used for *ex vivo* tissue analysis included hydroxyproline, soluble, and insoluble assays for collagen content, advanced glycation end-product (AGEs) ELISA for crosslinking, and picrosirius red staining (PSR) staining for total collagen. *In vitro* studies examined age, sex, and drug effects of AGEs inhibitor ALT711/Algaebrium on cardiac fibroblast collagen synthesis and utilized radiotracer assays to assess collagen synthesis types.

Characterisation of the preclinical model of aging in Sprague Dawley rats identified that survival between males and females showed no difference but that mortality increased in both sexes following

a year. Similarly, all animals showed significantly increased frailty at 18 months, suggesting that our cohort had advancing biological age. Rats had healthy cardiovascular systems, with cardiac dimensions, blood pressure, and ejection fraction all within normal ranges, indicating no obvious cardiac dysfunction and suggesting we were measuring physiological cardiovascular aging. However, 18-month-old males showed significantly lower cardiac ejection fraction and end-diastolic volume compared to their female counterparts. This suggests that aging causes a reduction in cardiac function in males compared to females, although males remain physiologically healthy.

Age and sex effects on cardiac collagen synthesis were studied in the left ventricle (LV) and right ventricle (RV). No sex differences were found in collagen synthesis types, and aging effects were assessed by collating male and female data. Hydroxylated collagen synthesis significantly declined in the LV at 12 months, as did unhydroxylated collagen synthesis. Histological analysis using PSR revealed peak total collagen in males at 12 months and in females at 6 months, with subsequent declines. Males showed increased soluble and insoluble collagen at 18 months compared to females. An AGEs crosslinking ELISA identified that males had a significant increase in crosslinking at 12 months which was not observed in female counterparts. In the RV, both hydroxylated and unhydroxylated collagen synthesis decreased with age, despite significant increases in total collagen at 6 and 12 months, followed by a decline at 18 months. These findings suggest that while collagen synthesis declines with age in both ventricles, males experience greater age-related collagen accumulation, contributing to increased cardiac stiffness and functional impairment compared to females.

Similarly, the effect of age and sex was assessed on atrial cardiac collagen synthesis and deposition. Hydroxylated and unhydroxylated collagen synthesis were measured in the left atria (LA) and right atria (RA) with no significant sex difference observed in either chamber. In the LA, hydroxylated collagen synthesis was increased at 3 months and at 18 months. Interestingly, unhydroxylated collagen synthesis showed an increase at 3 months but no other significant changes with age in LA, suggesting that collagen synthesis in the LA remains stable with age. Within the RA we observed that hydroxylated collagen synthesis increased with aging and this was also observed with unhydroxylated collagen synthesis. Interestingly, no increased deposition of collagen was identified in histological analysis.

In vitro, sex and age at the time of cell explantation appeared to have much clearer effects on collagen synthesis with male fibroblasts producing significantly more unhydroxylated collagen synthesis than female cardiac fibroblasts. We observed similar trends with hydroxylated collagen synthesis however this was not statistically significant. Aging was a key driver of both hydroxylated and unhydroxylated collagen synthesis with aged male cells having significantly higher uptake of both tracers. Interestingly,

collagen deposition analysis suggested a disruption in collagen metabolism with aged cells producing significantly lower amounts of insoluble collagen compared to younger counterparts. Drug treatment with ALT711/Algaebrium showed no effect on collagen synthesis or deposition, potentially due to suboptimal dosage or that the drug only impacted directly the established crosslinking and no other part of the collagen cascade.

In summary, this study found that aging significantly impacts cardiac collagen metabolism. For the first time collagen synthesis has been longitudinally assessed and evaluated in each cardiac chamber, revealing region specific dynamic changes. Males showed more pronounced age-related collagen accumulation and potential cardiac stiffness compared to females. In both the left and right ventricles, collagen synthesis had overall significant declines with aging. Contrastingly, in the atria, hydroxylated collagen synthesis increased significantly with age, but without corresponding increases in collagen deposition. All these findings point to a disruption in the homeostatic control of collagen turnover and suggest that synthesis is not directly responsible for collagen accumulation in aging, proving our hypothesis.

Lay summary

Aging significantly increases the risk of developing various heart diseases, including atherosclerosis, heart attacks, and heart failure. As we age, our heart muscle tends to function less efficiently, mainly because it becomes stiffer. This stiffness is likely caused by the accumulation of molecules such as collagen, which build up over time and make the heart less flexible. Furthermore, it appears that men get much more accumulation of collagen compared to women which can cause more heart problems with age. Previous studies have looked at the amount of collagen present in the tissue and the clearance of collagen in aging. However, studying collagen production in the heart has been challenging due to the lack of tools available to measure this process directly in living organisms. Some studies have tried to estimate collagen production by looking at collagen gene expression, which is the first step in the process of making proteins like collagen. These studies suggest that collagen production might decrease with age. But these results are estimations of collagen production as collagen gene expression don't always directly reflect how much collagen protein is actually being made. Therefore, this study explored the effect of aging on collagen production using an imaging method which measures collagen in the body in real time. We followed a cohort of healthy animals over 18 months (until around 50-60 in human years) to assess how the collagen production and collagen found in the tissue change with age and with sex. To understand how aging affects the body, we looked at survival rates, body weight, and signs of frailty over time. We checked heart health using various techniques: 3D x-ray scans for heart size, blood pressure measurements, and echocardiograms at the end of the study. We used a highly sensitive imaging technique called Positron Emission Tomography (PET), which relies on the injection of molecules capable of measuring collagen production in living organisms to look at the heart's collagen production over 18 months. After the study, we analysed heart tissues for different types of collagen and other changes. We also studied how aging and sex, affect collagen production in heart cells in a lab setting. In this research we identified that aged male hearts were less functional than females but that this is likely to be due to increase collagen in the tissue. Our study identified that males and females had no difference in collagen production over 18 months. We identified that the type of chambers in the heart- ventricles and atria – are affected by aging in opposite ways; The heart ventricles showed declining collagen production whereas the heart atria showed increased collagen production. Interestingly, we saw that males had much more collagen build up in the tissue compare to the females suggesting that sex influences collagen abundance in the tissue. However, when comparing collagen production to its accumulation in tissue, they don't seem to be related. This suggests that factors like collagen breakdown might contribute to the build-up over time, rather than an increase in collagen production. In cells, we saw distinct differences between males and females with males producing much more

collagen than females, and aged cells producing even more collagen. Our study confirmed findings from previous studies by aging animals over 18 months. However, for the first time this study identified distinct differences between chambers of the heart and their collagen production profiles with age it. The study highlighted the influence of both sex and age on collagen turnover and how both need to be considered further when trying to understand heart diseases.

List of Figures

List of Tables

List of Abbreviations

AFib – Atrial Fibrillation

AGEs – Advanced Glycation Endproducts

ANOVA – Analysis of Variance

BNP - brain natriuretic peptide

BP – Blood Pressure

BPM – Beats Per Minute

CBP – Collagen Binding Protein

CF – Cardiac Fibrosis

cFbs – Cardiac Fibroblasts

CRL – Charles River Line

CT – Computer Tomography

CVDs – cardiovascular diseases

DI – Deionised Water

ECG – Electrocardiogram

ECM – Extracellular Matrix

EDV – End-Diastolic Volume

EF – Ejection Fraction

EGF- epidermal growth factor

EKV - Electrocardiogram-gated Kilohertz Visualisation

ER – Oestrogen Receptor

ESV – End-Systolic Volume

EtOH – ethanol

E2 – 17β-Estradiol

FAP – Fibroblast activation protein

FAPI – Fibroblast activation protein inhibitor

FI – Frailty Index

GM-CSF - granulocyte-macrophage colony-stimulating factor

HB-EGF - heparin-binding EGF-like growth factor

HCl – Hydrochloric Acid

HF – Heart Failure

HFpEF – Heart failure preserved ejection fraction

HPLC – High Performance Liquid Chromatography

HR – Heart Rate

HSD – Harlan Sprague Dawley

IGF-1 - Insulin-like Growth Factor 1

LA – Left Atria

LC-MS – Liquid Chromatography and Mass Spectrometry

LOX – Lysyl Oxidase

LV – Left ventricle

LV-BP – left ventricle – blood pool

MA – Middle Aged

MAP – Mean Arterial Pressure

MI – Myocardial Infarction

MMP - Matrix metalloproteinase

MRI - Magnetic Resonance Imaging

NaOH – Sodium Hydroxide

OCT – optimal cutting medium

PDGF - Platelet-derived growth factor

PET – Positron Emission Tomography

PIP - Procollagen type I C-peptide

PSLAX – Parasternal Long Axis

PSR – picrosirius red

RA – Right Atria

ROI – Region of Interest

RT – Room Temperature

RV – Right Ventricle

SASP - Senescence-associated secretory phenotype

SEM – Standard Error of Mean

SD – Standard Deviation

SHR – Spotaneously Hypertensive rats

SPARC – Secreted Protein Acidic And Cysteine Rich

SPECT – Single-photon emission computed tomography

SUVr – Standard uptake value ratio

TGFβ - Transforming growth factor β

TIMP - Tissue inhibitors of metalloproteinases

VOI – Voxel of Interest

VPR – Volume Pressure Recording

WKY – Wistar-Kyoto Rats

+PSR – Positive picrosirius red stain

Chapter 1 – *Literature Review*

1.1 Aging population, incidence and causes of heart failure

Cardiovascular diseases (CVDs), including heart failure (HF), are most prevalent in aging populations and the most prominent cause of mortality globally affecting around 640 million people a year (1-3). Studies have highlighted the strong correlation between aging and CVDs, with the incidence of CVDs around 40% in the 40-59 year old population but dramatically increasing in the 60-79 year old population, rising to 75% (4). With the incidence of CVD predicted to increase by 228% in the ≥85-year population by 2050. Therefore, aging clearly presents a significant global health concern both in a social and economic capacity, and specifically in the case of CVDs (4).

Cardiac fibrosis (CF) is a major common denominator in cardiac pathophysiology occurring in many CVDs (including HF) and has been associated with increased hospitalisations and occurrence of life-threatening cardiac events (5, 6). CF is largely associated with aging and found in aging populations due to altered cardiovascular function and structure with age (7, 8). It is thought that these age-related changes impair cardiac function post-injury or dysfunction through increased tissue disruption and impaired repaired mechanisms following injury (9). Sexual dimorphism is present in human cardiac aging outcomes with human females below 74 years showing lower risk of HF compared to males (2, 8, 10). However, studies have identified that females face a higher risk of HF related hospitalisation, though some suggest this is simply due to the increased life expectancy in females (10). Regardless, CVD are the leading cause of death in both sexes worldwide, with females facing specific temporal risk factors such as the beginning and end of their reproductive lives which has been found to contribute to increased risk of onset (11).

1.2 Ageing in the myocardium and cardiac fibrosis

Aging is described as a continual decline in physiological function resulting in irreversible damage on a cellular and whole organ scale, some of these age-related cardiac changes are described in Figure 1.1. These physiological changes increase the risk of developing CVDs and lead to poorer outcomes after their onset. Aging studies in humans and rodents identified a reduction in sympathetic signalling, increased afterload and left ventricle (LV) mass, culminating in a decline in cardiac efficiency and performance (12-14). The causes of this phenomenon are unknown, nevertheless, multiple factors have been hypothesised to contribute to cardiac aging and CF. The 'Seven Pillars of Aging' have been established to encompass these factors and include: inflammation, epigenetics, macromolecular damage, proteostasis, metabolism, reaction to stress and stem cell regeneration (15). Furthermore, CF is also thought to be induced by gradual loss of cardiomyocytes over time, cardiac hypertrophy, and long-term mechanical stress. Yet, many of these hypotheses are unexplored; little is truly understood about intrinsic aging mechanisms in the heart.

Age-related CF development contributes to the development of both atrial and ventricular dysfunction, this dysfunction contributes to worse prognosis follow cardiac injury or stress and often contributes to HF development (16, 17). CF development is mediated largely by fibroblasts and other cell types present in the myocardium, cardiac fibroblasts (cFbs) make up a large proportion of cells in the heart and are predominantly (but not exclusively) involved in extracellular matrix (ECM) turnover of proteins such as collagen and fibrillin (18, 19). CF is conventionally associated with cardiac injury and stress such as myocardial infarction (MI) or pressure overload. Following dysfunction, cFbs undergo a phenotypic switch into myofibroblasts with ECM deposition increased to maintain the integrity of the myocardium leading to fibrotic tissue establishment (20, 21). However, CF is also a component of aging in the myocardium in absence of overt dysfunction. This pathological cardiac fibrosis has been observed in the context of aging in animal models such as mice (13), rats (22), pigs (23), sheep (24) and humans (25) suggesting that aging mechanisms are conserved across species (26). In aging, some resident fibroblasts have been identified to become activated into myofibroblasts. Nevertheless, research suggests that overall phenotypic switch is blunted in aging with reduced transforming growth factor beta (TGFβ) and SMAD3 expression in both cFbs and mesenchymal stem cells which also form myofibroblasts (27, 28). Previous research hypothesises that the fibrotic mechanisms in aging-related cardiac fibrosis appear to differ to the fibrotic mechanisms in injury and remain largely unexplored(29).

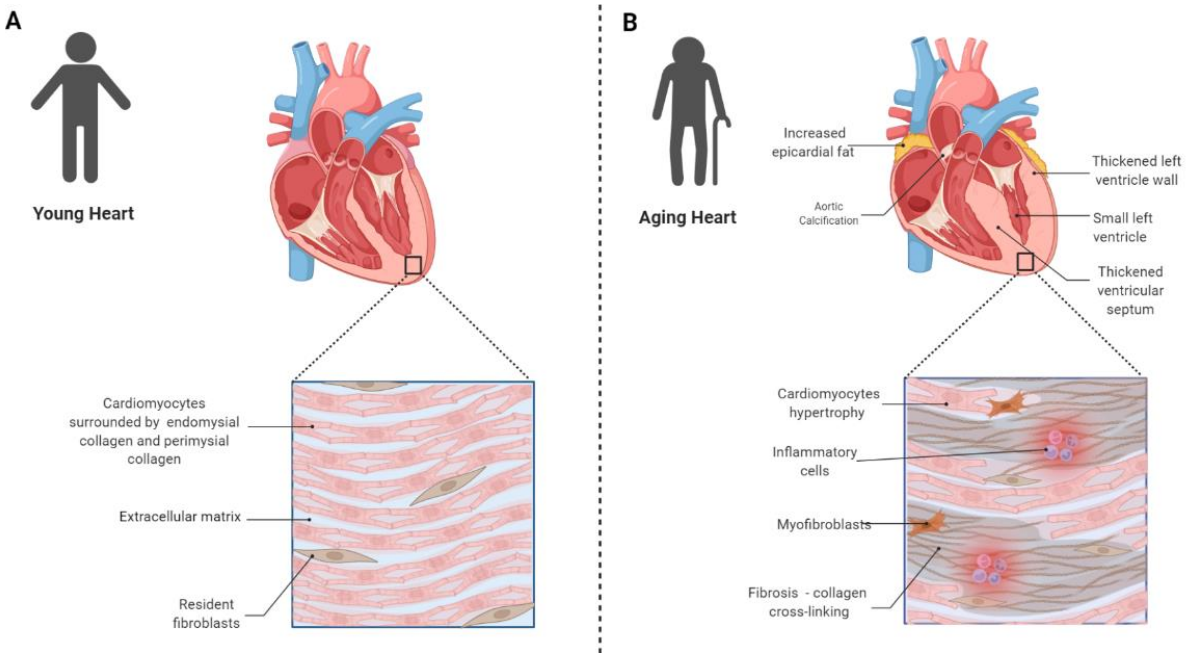

Figure 1. 1 Macro- and micro- effects of aging on cardiac structure and function. Compared to the young adult heart (A) the aged heart (B) undergoes progressive molecular and structural changes over time. In the young adult heart, tightly packed cardiomyocytes are surrounded by endomysial and perimysial collagen, along with other ECM components, maintained by resident cardiac fibroblasts. With aging, there is an increase in epicardial adipose tissue deposition (30). Over time, the progressive loss of cardiomyocytes activates apoptotic and necrotic pathways, triggering the recruitment of inflammatory cells (31, 32). This loss strains the myocardium, leading to the activation and proliferation of resident fibroblasts into myofibroblasts, which deposit ECM components. Collagen accumulation follows, resulting in interstitial fibrosis within the atria and ventricles (33, 34). On an organ-wide level, these changes cause thickening of the LV wall and a reduction in ventricular volume, thereby altering the heart's functional capacity (35, 36). Figure created using Biorender.

1.3 Collagen metabolism and important mediators of ECM in cardiac tissue

Although various ECM proteins (such as glycosaminoglycans, glycoproteins, fibronectin, and integrins) undergo age-related changes, collagen has been identified as one of the primary contributors to age-related CF (14). Comprehending the role of collagen in the healthy myocardium, along with its turnover and key regulators, is essential for unravelling how these mechanisms evolve with age. This understanding is critical for grasping the broader effects of aging on heart structure and function(29).

1.3.1 ECM Collagen

The ECM is formed through a complex network of three molecule types: non-fibrous proteins, fibrous proteins and complex networks of macromolecules (37). These molecules provide the structural scaffolding to support cellular and physiological function (37). These proteins are maintained under close homeostatic control and respond to adverse stimuli such as injury to ensure the integrity of the tissue (9).

Collagen is the predominant protein in the cardiac ECM, accounting for approximately 30% of the total ECM (38). Its primary role in the tissue is to provide structural support and flexibility to the myocardium and the majority of organs (38). In the myocardium around 28 collagen subtypes have been classified, however, in the heart the most predominant subtypes are collagen type I and III (approximately 90%) and have been identified to play a significant role in cardiac tissue function and wound healing mechanisms (37). The ECM is an important component of physiological processes in the body, with specific collagen subtypes being implicated in CVD, highlighting collagen/ECM as a target of interest in understanding pathophysiology of certain diseases such as HF with aging heart. Note other subtypes play essential roles in connective tissues, epithelial tissues and the basement membrane – however they will not be the focus of this thesis (39).

1.3.2 Cardiac fibroblasts

The development of CF plays a crucial role in ventricular dysfunction, which can lead to HF (16). cFbs, which constitute over 50% of the cells in the heart, are central to the regulation of myocardial ECM production (18, 19). Under normal physiological conditions, cFbs are typically quiescent, maintaining normal ECM turnover rates (40). However, in response to pathophysiological stimuli such as growth factors, hypoxia, and tissue injury, cFbs undergo a rapid phenotypic transition into myofibroblasts (41). Myofibroblasts actively synthesise ECM components, including collagen, contributing to fibrotic tissue formation (40). As a result, cFbs are key players in the initiation of CF (41).

Fibroblasts follow three primary phases during wound healing in the heart: inflammation, proliferation, and remodelling. The loss of cardiomyocytes due to aging, injury, or damage activates the innate immune system, which releases inflammatory mediators to the site of cell death. These mediators also stimulate fibroblast proliferation, initiating ECM synthesis. During the final remodelling phase, fibroblasts sustain ECM protein production, rebuilding collagen fibres and leading to scar tissue formation (40). Dysfunctional or excessive remodelling can result in disease phenotypes, impairing heart function by reducing contractility and causing subsequent cardiac dysfunction. Additionally, research suggests that other cell types, including endothelial cells, vascular smooth muscle cells, and

pericytes, may also contribute to the myofibroblast population (42, 43). For example, in zebrafish models, endocardial fibroblasts contribute to collagen synthesis after injury, with studies showing that inhibiting TGF-β signalling in zebrafish reduces fibroblast numbers and collagen deposition (29).

Interestingly, cFbs express both oestrogen receptor (ER) α and ERβ on their surface, and increased receptor expression of 17β-Estradiol (E2) has been shown to inhibit cFb growth *in vivo*, highlighting E2's cardioprotective effect against fibrosis (44). This effect is also observed *in vitro*, where male and female cFbs exhibit phenotypic differences under healthy and diseased conditions, despite no structural differences (44). Thus, E2 is a significant regulator of cFb proliferation in both healthy and hypertrophic cardiac tissue, and its mechanisms should be explored further for potential therapeutic applications.

1.3.3 Collagen metabolism

Collagen metabolism is defined into 3 clear stages: synthesis, deposition/accumulation and degradation, these stages are depicted in Figure 1.2. In healthy individuals, collagen homeostasis is tightly regulated to maintain tissue integrity. The synthesis of collagen predominantly occurs in cFbs, where post-translational modifications lead to the hydroxylation of the amino acid proline (incorporated almost exclusively in collagen) to form procollagen. These triple-helical procollagens consist of homo- or heterodimeric α chains, each with a repeating Gly-X-Y amino acid motif, where X and Y are typically proline and 4-hydroxyproline, respectively. This repetitive motif explains the right-handed triple-helical structure seen in collagen fibres, with glycyl residues at the centre and the X/Y residues exposed on the surface (39).

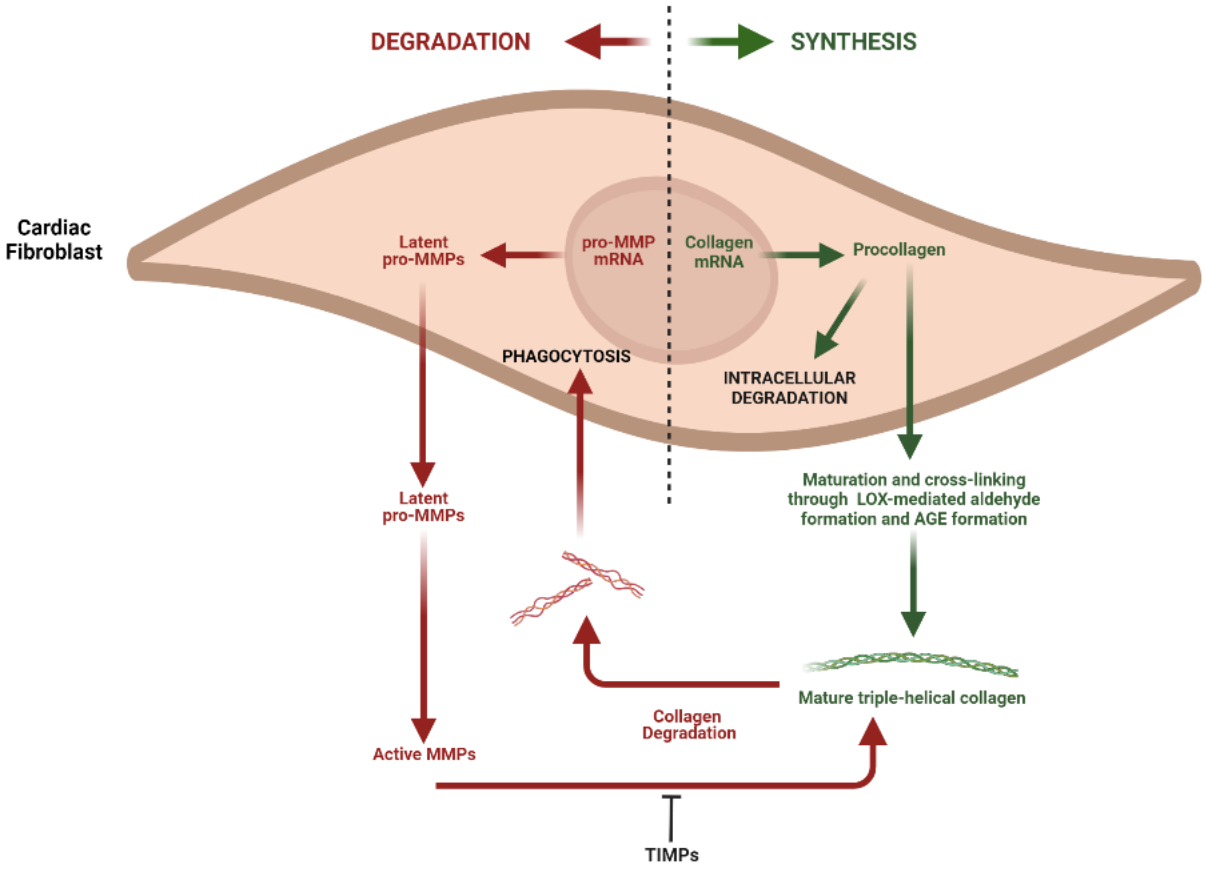

Figure 1. 2 Collagen biosynthesis and degradation pathways in the cardiac fibroblast. Collagen homeostasis is tightly regulated by the turnover pathways illustrated in the schematic. Collagen synthesis mainly takes place in cardiac fibroblasts, beginning with the expression of collagen mRNA in the nucleus, followed by the formation of procollagen in the cytosol. Procollagen contains C-terminal and N-terminal propeptide regions(45). It then follows two pathways: intracellular degradation or maturation, which leads to its exocytosis and conversion into mature triple-helical collagen through several post-synthetic steps. These maturation steps involve fibre stabilization via two processes: LOX-mediated aldehyde formation among hydroxylysine/lysine residues and the reduction of sugars, forming advanced glycation end products (AGEs) (46-49). Simultaneously, collagen degradation begins within the cardiac fibroblast through the expression of pro-MMP mRNA, followed by multiple conversion steps that produce active MMPs. Of the 25 MMPs, a subset is found in the heart, and these enzymes are responsible for degrading mature triple-helical collagen, which is then phagocytosed(50). TIMPs naturally inhibit MMPs, preventing collagen degradation. Figure created using Biorender.

Procollagen serves as the precursor to collagen, and the cross-linking of triple-helical procollagen fibrils into sheets or bundles (known as tropocollagen) leads to the formation of mature collagen fibres. These fibres play a key role in the mechanical properties of the ECM (51). Collagen cross-linking is facilitated by lysyl oxidase (LOX), which increases fibril thickness and stiffness. However, the frequency of cross-linking rises in aging, with an accumulation of AGEs found in advanced aging, contributing to hypertrophy, hypertension, and ventricular stiffness (52). Collagen type I, the predominant form in many tissues, typically features a heterotrimeric structure composed of two α chains, α1 and α2, with the former capable of forming homotrimers as well (39). With age, particularly in non-cardiovascular disease patients, collagen I content can increase by up to 200%, altering the ratio of type I to type III collagen. This imbalance affects cardiac biomechanics and conduction, contributing to age-related cardiac dysfunction (52).

As described previously, in healthy individual's collagen metabolism is closely regulated with collagen turnover/replacement occurring at a constant rate to ensure the structural integrity of the myocardium (12, 13). Collagen degradation plays a key role in this process using matrix metalloproteinases (MMPs) and these in turn are managed by tissue inhibitor matrix metalloproteinases (TIMPs)(51). These MMPs play a key role in initiating collagen degradation following an initial injury or chronic exposure to free radicals. For instance, patients with HF with preserved ejection fraction (HFpEF) exhibit increased levels of endocardial TGF-β1, which is linked to decreased MMP-1 and increased TIMP-1 levels (53). This indicates that reduced ECM degradation, coupled with increased collagen synthesis, contributes to the development of cardiac fibrosis.

Collagen turnover mechanisms shift with aging and injury, leading to changes in both collagen synthesis and maintenance, influenced by pro-fibrotic MMPs (54, 55). As individuals age, ECM turnover can become imbalanced, resulting in increased CF due to reduced levels of MMPs (such as MMP-1, MMP-2, MMP-4, and MMP-14) and elevated levels of pro-fibrotic inhibitors like TIMP-1 and TIMP-4 (13, 56).This underscores the idea that the reduced degradation of collagen, driven by lower MMP levels, is the primary cause of collagen accumulation with aging, rather than an increase in new collagen synthesis as is often assumed (9, 29). Additionally, MMPs and TIMPs are regulated by various factors, including platelet-derived growth factor (PDGF), insulin-like growth factor 1 (IGF-1), epidermal growth factor (EGF), TGF-β, heparin-binding EGF-like growth factor (HB-EGF), and granulocyte-macrophage colony-stimulating factor (GM-CSF) (53). These factors also stimulate cFbs proliferation and remodelling, contributing to the formation of fibrotic tissue (53).

Dysfunction in collagen metabolism leads to increased interstitial and perivascular collagen deposition in the aging heart, driven by altered levels of MMPs and TIMPs. This imbalance results in myocardial stiffness and cardiac dysfunction, a pattern commonly observed in elderly patients with HFpEF (9, 41).

1.4 Cardiac aging and collagen metabolism

Age-associated ECM modifications in the expression and deposition of collagen, procollagen, glycosaminoglycans, glycoproteins such as fibronectin, integrins and matricellular proteins have been observed (14). Age-related alterations in collagen metabolism are thought to contribute to CF development. Yet, much remains unknown due to the majority of cardiovascular research conducted on pathology and few aging studies. Therefore, research needs to be focused on age-related changes in the myocardium in the absence of dysfunction (57). Collagen accumulation in the aging heart has been well-defined with total collagen protein found to increase 6.5% in the LV and 12.5% in the right ventricle (RV) between 1 and 26 months in rodents (26, 36, 45). This age-related increase in total collagen protein is conserved across species(29). The current consensus is that aging impacts each component of collagen metabolism, with alterations in collagens synthesis, accumulation and degradation mechanisms observed as summarised in Table 1.1.

Table 1. 1 Summary of studies evaluating the impact of aging on cardiac collagen

Ref	Species	Groups	Effect on cardiac collagen in aging
(24)	Sheep	Young: 18 months Aged: >8 years	↑ Myocardial collagen content ↑ MMP2 activity ↓ TIMP expression failing hearts
(13)	Mice	Young: 3 months Middle-Aged (MA): 15 months Aged: 23 months	↑ Soluble collagen protein ↑ ECM degradation ↑ MMP3, MMP-9 and MMP-14 ↓ Insoluble collagen protein ↓ TIMP-4
(58)	Rat	1-5 days 10-20 days 2 months 8 months 18-26 months	↑ Myocardial collagen content ↑ Increased myocardial stiffness
(59)	Canine	Young: 1-2 years MA: 2.1-5 years Aged: 5.1- 10 years	↑ Collagen volume fraction
(36)	Human	Young: 20-25 years Aged: 67-87 years	↑ collagen type I fibres abundance and thickness ↑ Abundance of large diameter collagen fibres.

Table 1. 1 *(continued)* Summary of studies evaluating the impact of aging on cardiac collagen

(60)	Rat	7 months 12 months 18 months 23 months	↑ LV weight and end-diastolic volume index and percentage fibrosis
(61)	Rat	1 month 2 months 6 months 15 months 24 months	− Collagen fractional synthesis rates to 20%/day in hearts of rats aged 1 month − At 15 months the collagen synthesis rates in the heart were maintained. ↓ synthesis rated at 24 months around 10-fold ↑ Collagen degradation between 15- 24 months
(23)	Pig	1.5 months 6 months 6 years	↑ Collagen associated markers (Collagen III and LOX) in the aortic valve than mitral valve
(26)	Rat	1 months 3 months 6 months 12 months 22 months 24 months 26 months	↑ Collagen deposits accumulate in the LV relative to ventricular protein after 3 months and increases with aging. ↑ LV collagen from 5.5% at a 1 month old to 12% between 24-26 months old. ↑ RV in collagen content from 7% at 1 months to 19.5% in aged animals ↑ established collagen fibres increase thickened and had larger networks ↑ Fibrotic zones as animals aged
(62)	Rat	2 months 6 months 12 months 19 months	↓ Procollagen type I mRNA levels in the LV ↓ Procollagen type 3 mRNA levels rapidly decreased in LV and RV ↑ Interstitial collagen deposition during young adulthood (2-12 months old) this was further increased in the aged cohort −TGF$\beta_{1/3}$ showed no changes with age, so appears to not influence collagen pathways in ageing
(63)	Rat	5 months 15 months 26 months	↑ Myocardial collagen content − Exercise showed no significant impact on collagen accumulation over time ↓ Procollagen type I/III was observed in aging ↑ proline and hydroxyproline pools ↑ crosslinking/Hydroxylysylpyridinoline with aged ↓ collagen content/crosslinking in aged exercised animals
(57)	Mice	3 months 6 months 12 months 18 months	↑ Interstitial cardiac fibrosis compared to younger counterparts with an increase in collagen type I and III ↓ Collagen degradation progressively during aging ↑ LOX Age-dependent. ↓ Collagen triple helix repeat-containing protein 1 at 12 months and 18 months ↓ Fibrillary collagen cell surface tyrosine kinase receptor Ddt1 - Age-dependent collagen metabolism alteration causes myocardial fibrosis

Table 1. 1 *(continued)* Summary of studies evaluating the impact of aging on cardiac collagen

(64)	Mice (WT/MMP-9 KO)	Young: 6-9 months MA: 12-15 months Aged:18-24 months	↑ MMP-9 in the MA and aged group. − Aged MMP-9 KO mice did not appear to have heart failure. ↓ Collagen accumulation in the LV of aged MMP-9 KO mice than aged WT. −Collagen mRNA expression was identified in aged or MMP-9 null mice ↑ MMP-8 in MMP-9 KO mice
(65)	Rats	Between 1 day and 2 years	↑ Cardiac collagen accumulation ↑ Collagen type III proportions abundance
(66)	Rats	3 months old 16 months old 24-month-old	↑ Accumulation of collagen ↑ Hydroxyproline content ↓ Procollagen type I mRNA ↓ Procollagen type III mRNA
(67)	Mice	Young: 3 months Aged: 18 months	↑ SPARC →a key role in post-synthetic changes in collagen processing. ↑ Cardiac stiffness and fibrillary collagen content. ↑ Myocardial stiffness and collagen content in SPARC-KO mice with age, however, it was significantly ↓ than WT counterparts. ↓ Age-related collagen accumulation in the absence of SPARC
(68)	Rats	Between 13 – 30 months	↑ CD45+ fibroblasts ↑ Collagen expression. ↑ Myocardial fibrosis in aged heart due to the inflammatory system
(69)	Mice	2.5 months 12 months	↓ Fibrillary collagen in Col1a1 null mice ↓ Pro1(I) collagen mRNA at 2.5 months old and at 12 months this was reduced further to 42%. ↓ Hydroxyproline levels in the null mice.
(70)	Mice (Relaxin deficient)	8-10 months 12 months 24 months	Relaxin inhibits collagen synthesis and activating MMPs to degrade collagen ↑ Collagen content and mRNA expression in Male relaxin deficient mice as animals aged. −Females did not show any difference.
(22)	Rat	Primary cardiac fibroblast cells 4 day old 8-12 week old	↓ Collagen production in adult cFbs in 3D culture not monolayer. ↓β1 intergrin and α-SMA in adult fibroblasts −Concluded that cardiac fibroblast interactions with ECM change due to age.
(71)	Syrian Hamsters	Young (prehypertrophic): 2 months MA: 5-6 months Aged: 10-11 months	↑ Collagen III mRNA increase four-fold with age ↑ MMP-1 activity with aging ↑ MMP-2/9 activity with aging in cardio myopathy ↑ fibrillar collagen content in aged myopathic hamsters
(72)	Balb-c Mice	Young: 2 months MA: 12 Months Aged: 20 months	↑ LV collagen, fibronectin ↑ cardiac hypertrophy ↑ LV hydroxyproline

Table 1. 1 *(continued)* Summary of studies evaluating the impact of aging on cardiac collagen

(73)	Mice	Cardiac Endothelial Cells Young: 2.5 months Aged: 18 months	↑ collagen increases in whole heart
(74)	Mice	Adult: 2 months Aged: 19 months	↑ Collagen overall in aged - No difference in collagen crosslinking under polarised light
(75)	Canine	Young: 4 years Aged: 9 years	↑ collagen deposition in left atria (26% increase) ↑ cardiac fibrosis in atrial fibrillation (AF) ↑ Col1a1, Col3a1 in aged dogs in left atria ↑ MMP2/9 in aged left atria
(76)	Mice	Young: 4-5 months MA: 11-12 months Aged: 18-29 months	↑ fibrillar collagen α1 (I) and α2 (I) with age ↑ total collagen, insoluble collagen and collagen fibril diameter ↑ collagen crosslinking ↓ fibrillar collagen α1 (I) and α2 (I) following SPARC deletion - Highest collagen III & IV content at MA ↑ Collagen VI with aged
(17)	Mice	Young: 5 months Aged: 23 months	↑ interstitial fibrosis and total collagen content in LA and RA
(77)	Human	Young: 1 year Adult: 28 years Aged: 80 years	↑ Collagen Type I in LV ↓Collagen Type III in LV ↑ collagen fibril diameters in LV
(78)	Mice	Young: 7.5 months Aged: 30 months	↑ MMP-9 levels in the LV and blood plasma

1.4.1 The effect of aging on collagen synthesis

Studies examining collagen synthesis in both rodents and humans have demonstrated a reduction in mRNA expression of collagen types I and III, as well as procollagen type I, within the aging LV. Similarly, a decrease in collagen type III mRNA expression has been observed in the RV (62). Direct assessments of collagen synthesis, using flooding doses of unlabelled proline alongside [^{14}C]proline, revealed a tenfold reduction in collagen synthesis at 24 months of age (61). Interestingly, these findings contrast with the observed age-related increase in collagen protein abundance, suggesting that post-translational or post-synthetic mechanisms may drive collagen accumulation *in vivo* (79). Notably, levels of TGFβ1/3, typically associated with fibrosis, remain unchanged with aging, indicating that increased myocardial tissue stiffness may not result solely from enhanced collagen synthesis (62). However, the methods used to quantify *in vivo* collagen synthesis, which often rely on mRNA expression and *ex vivo* radioactive labelling, may lack the sensitivity needed to fully capture the complexities of collagen dynamics.

1.4.2 The effect of aging on collagen deposition

Age-related stiffening of cardiac tissue *in vivo* is largely attributed to increased interstitial fibrosis and collagen deposition, particularly of collagen types I and III (24, 58, 59, 80). With age, collagen content doubles in the absence of dysfunction from around 3.9% to 5.9% altering LV function and contribute to age-related diastolic dysfunction (81). Within the LV, collagen thickness and diameter increases in both aged humans and rodents, leading to the thickening and stiffening of the myocardium (26, 36, 45). Research in mice has highlighted specific age-related shifts in soluble and insoluble collagen proteins, suggesting that the proportions of collagen types may play a role in tissue stiffening (45, 62). Increases in the collagen I:III ratio have also been documented as part of the changes in ECM composition (36). Techniques such as hydroxyproline analysis and picrosirius red (PSR) staining have shown elevated myocardial collagen content in rodent hearts *ex vivo*, with corresponding changes in the abundance and ratio of collagen types I and III (58, 82). These alterations likely contribute to left ventricular stiffness and negatively affect heart function with age(83).

Furthermore, ECM crosslinking is crucial for maintaining ECM and myocardial integrity by binding ECM molecules into a fibrous network. During aging, crosslinking increases, largely due to the accumulation of AGEs, heightened enzymatic activity of LOX, and increased SPARC expression (84). AGEs, formed through the Maillard reaction between glucose and collagenous proteins are linked to tissue stiffness and myocardial stiffness, even without increased collagen content and have been found to accumulate specifically during the aging process (48, 63, 80, 85). AGEs contribute to CF and HF through crosslinking ECM proteins (collagen, elastin, laminin) and interacting with AGE receptors, leading to fibrosis, altered calcium metabolism, vasoconstriction, and eventual cardiac dysfunction (48, 86, 87). LOX also promotes collagen and elastin crosslinking, strengthening fibres and protecting them from protease degradation (29). Aging studies in rodents show increased LOX activity correlating with higher collagen content (80, 88). Additionally, SPARC plays a role in crosslinked collagen fibril formation, with higher expression in aged rodents linked to cardiac stiffening, a process diminished in SPARC-null mice (67). Overall, aging enhances ECM crosslinking, leading to myocardial stiffening, likely reducing normal collagen turnover and contributing to age-related fibrosis. Additionally, increased collagen cross-linking, as evidenced by higher hydroxylysylpyridinoline concentrations in myocardial tissue of older rodents, further emphasizes these age-related changes (80).

Many studies have primarily focused on the LV as it is the most frequently affected chamber in conditions like MI. As a result, there is limited understanding of collagen accumulation in other cardiac chambers. A small number of studies have begun to investigate changes in other chambers, with RV collagen deposition observed to increase in 19 month rats, however these studies are rare (62). The

atria have even less data available, with limited research showing a 26% increase in collagen deposition in canine atrial tissue (75). These gaps in research highlight the need for further investigation into collagen dynamics across all cardiac chambers to better understand the full scope of cardiac remodelling and its implications.

1.4.3 The effect of aging on collagen degradation

Degradation pathways represent the final stage of collagen metabolism and are known to be altered with aging. It is widely accepted that collagen degradation mechanisms in the heart become dysregulated as part of the aging process (57). As previously mentioned, MMPs play a key role in regulating collagen turnover, and their activity has been shown to change with age. For instance, age-related increases in MMP9 have been strongly associated with LV stiffening (88-90). A study utilising MMP9 knockout mice demonstrated reduced collagen accumulation compared to wild-type controls; however, the study also revealed that removal of one MMP can trigger compensatory mechanisms (64). In addition to MMP9, increases in MMP2 and MMP7 have been observed in aging human hearts (24). Interestingly, other MMPs, such as MMP3, MMP12, and MMP13, were found to decrease in the LV at 23 months, indicating that aging induces a spectrum of changes in MMP expression. Furthermore, alterations in TIMPs, particularly decreased TIMP4 expression, have also been observed in aged animals (38). Despite advances in understanding the impact of disrupted collagen degradation during aging, the underlying causes of these alterations remain poorly characterized, and therapeutic strategies targeting these mechanisms have seen limited success.

1.5 Age-related sexual dimorphism in collagen metabolism

Sex-differences in cardiac structure and function have long been established with changes occurring across the lifespan of humans in the case of health and dysfunction(88). This dimorphism has been attributed to hormonal, environmental and genetic factors. Studies exploring aging have assessed the impact of sex differences in age-dependent CF, with studies showing reduced collagen accumulation with age in females until the end of their reproductive life (57). With females over 50 years of age found to have rapid reduction of LV diastolic and systolic compliance, particularly following menopause (81). Research has largely attributed this protective capacity in the female myocardium to oestrogen, particularly E2 and its metabolites which are thought to dampen collagen synthesis, increase MMP production and prevent myofibroblast formation (9, 91-93). Yet, there is no consensus

currently on the effect of sex during aging on each component of collagen metabolism. The effect of sex in aging is believed to alter collagens synthesis, accumulation and degradation mechanisms, however, limited research has been conducted in 'healthy' aging male and female animals' models (88). Studies exploring the effect of sex in aging on collagen metabolism are as summarised in Table 1.2.

Table 1. 2 Summary of studies evaluating the impact of sex on cardiac collagen

Ref	Species	Groups	Findings
(57)	Mice	3 months 6 months 12 months 18 months	↑ Concentric remodelling in males compared to females suggesting that the remodelling rate is slower in females. −Collagen type I showed no sex difference with age ↑ TGFβ1 and TGFβ receptor expression in females ↑ LOX in aging females ↑ Periostin in aging males
(9)	Human	Young males: 17-40 years Young females:17-40 years Aged males: 50-68 years Aged females: 50-68 years	Younger females ↓ collagen types I,III and VI compared to male counterparts Older females (50-68 years) ↑ collagen type I, III and VI than men ↑ MMP9 in aged males compared to young counterparts ↑TIMP3 in males and older females had more TIMP2/3 compared to older males and young females ↓ SMAD2 in Young females than males ↑ SMAD 2 in older females than older males.
(94)	Mice	Aged males and female (20/21 months) C57BL/6J	↑ vitronectin, collagen type XII and Prelp (proline/arginine-rich end leucine-rich repeat protein) in aged male cardiac ECM ↑ collagen type VI in the aged female heart was found. ↑ hydroxyproline in the aged female heart compared with the old male mouse heart
(95)	Rats	Young: 3 months WT Aged: 11-12 months old WT Aged: 11-12 months old Ovarectomized plus placebo Aged: 11-12 months old Ovarectomized plus oestrogen-replaced	↑ increased LV weight on ovariectomized aged rats Collagen type I:III protein ratio ↑ 2-fold in ovarectomized rats compared to controls Collagen I was further increased whereas collagen type III was reduced ↓ MMP-2 activity in the OVX group compared to controls E2 replacement ↑ MMP-2 activity in the left ventricle Ovarian hormones removal ↑ heart remodelling. ↑ concentration of collagen type I:III prevented by oestrogen replacement. ↓ MMP2 with age especially in aged ovariectomized animal

Table 1. 2 *(continued)* Summary of studies evaluating the impact of sex on cardiac collagen

(96)	Humans	Patients with systolic HF Patients with diastolic HF Controls with CVD risk factors Controls healthy	In HF, women had significantly ↑ plasma levels of the propeptide for type I collagen (PIP) vs men,
(97)	Mice	ERβ$^{-/-}$ Males ERβ$^{-/-}$ Females WT Males WT Females	Gene expression analysis identified that male hearts had a ↑ induction of ECM-related genes e.g., procollagen type I ↑ repression of mitochondrial genes vs female hearts
(98)	Rats	Female Young: 3 months Female Aged:18 -21 months Female Aged/Ovariectomy: 18 – 21 months Female Aged/ Ovariectomy and 10% Fructose:18 - 21 months	Aging ovariectomised animals showed no further increases in collagen area fraction. ↑ myocardial fibrosis within the endocardium aged ovariectomised animals. ↑ papillary fibrosis with ovariectomy compared to age-matched controls
(99)	Rat & Human	Male cFbs Female cFbs	E2 ↓ MMP-2 E2 induces ER gene expression in rat cardiac fibroblasts in both sexes E2 ↓ collagen I and III in female cFbs E2 ↑ collagen I and III mRNA in male cells
(100)	Rat	cFbs	Treatment with 17β-estradiol ↓ collagen synthesis 17β-estradiol could exert a cardiac protective effect by reducing excessive extracellular matrix accumulation and cardiac stiffness
(101)	Mice	WT Oestrogen Receptor beta KO I infused with angiotensin II for 21 days	E2 inhibited fibrosis by around 80% in WT mice E2 acts on ERβ to prevent myofibroblast development and collagen production and Vimentin E2 administration in ovariectomised WT animals ↓ collagen deposition

Table 1. 2 *(continued)* Summary of studies evaluating the impact of sex on cardiac collagen

(102)	Rat	Intact sham-operated (SHAM) Intact with volume overload (VO) Ovariectomised sham-operated (SHOX) Ovariectomised with volume overload (VOX) Ovariectomised with volume overload with 17β-estradiol (VOX +EST)	E2 treatment improved TIMP-2/MMP-2 and TIMP-1/MMP-9 protein balance, restored ERα expression, and prevented MMP-9 activation, perivascular collagen accumulation and development of heart failure. -E2 did not prevent the increase of MMP-9 expression or loss of interstitial collagen E2 ↓ ECM remodelling and LV dilation, through modulation of ECM protein expression in ovariectomized rats.
(25)	Rat & Human	Male cFbs Female cFbs	E2 was found to protect female CFs from shifting to a myofibroblast phenotype, E2 ↓ collagens and matrix metalloproteases (MMPs) expression Collagen I and III mRNA and protein levels was regulated in a sex-specific manner by E2 in human CFs Sexually-dimorphic ER activation and collagen I and III binding in both females and male fibroblasts ↓ expression of type I and III collagens by E2 treatment in females, but ↑ male cFbs. E2 treatment inhibited expression of collagens I and III in cardiac fibroblasts from female rats, but enhanced their expression in male cells ERs bound to the promoters of collagens I and III in female CFs, while in male cells, only ERβ was bound to both promoters

1.5.1 Sexual dimorphism in collagen synthesis

Collagen synthesis, as previously discussed, is a key component of collagen metabolism that has proven difficult to measure, particularly *in vivo*. Assessments of collagen synthesis are generally conducted through mRNA analysis or via indirect markers, such as Procollagen type I C-peptide (PIP) (103). Consequently, there is a scarcity of longitudinal data that comprehensively examines the effects of sex and aging on collagen synthesis. Current evidence suggests that females exhibit lower rates of collagen synthesis compared to their male counterparts. However, few studies have explored the interaction between aging and collagen synthesis, despite the well-established connection between sex steroids and CF development (104). Notably, research into the role of E2 and its derivatives indicates that E2 suppresses collagen synthesis, inhibits MMP production, and reduces fibroblast activation (9, 91-93). Both animal and human studies have demonstrated sexually dimorphic effects of E2 on cFbs, with E2 downregulating collagen types I and III synthesis in females, while males show the opposite response (9). At the cellular level, this effect has been confirmed *in vitro*, where E2-treated rodent and human cFbs from females exhibited reduced collagen I and III mRNA expression, whereas male cFbs demonstrated increased collagen synthesis under the same conditions (25). Interestingly, although age-related CF develops in both sexes during 'healthy' aging, older females exhibit higher expression levels of collagen synthesis regulators, including TGFβ receptor 1 and SMAD2/3, when compared to age-matched males (105).These findings highlight the need for further research into sex-specific mechanisms of collagen metabolism, particularly in the context of aging and its role in cardiac remodelling.

1.5.2 Sexual dimorphism in collagen deposition

In age-related collagen accumulation sexual dimorphism has been found, with males and females showing inverse patterns in both collagen type and deposition in aging (9). Young adult hearts show lower collagen I and III deposition in females compared to male counterparts, in aged hearts the inverse occurs with higher collagen type I, III and IV in females compared to males (9, 91). Moreover, female specific regulation of collagen metabolism was identified with collagen type IV degradation biomarkers and turnover rate appeared to be significantly increased in females compared to male counterparts (106). A longitudinal study conducted by Grilo et al. revealed sex-specific regulation of cardiac ECM metabolism in mice, identifying differential patterns of collagen turnover and fibrosis between males and females (88). These alterations in ECM organization, particularly in female rodents, appear to be age-dependent and modulated by sex hormones. Additionally, aging females exhibited

increased activity of LOX, an enzyme involved in collagen crosslinking, which has been implicated in promoting cardiomyocyte senescence and myocardial stiffness (88). Yet, despite this sexual dimorphism in collagen deposition of type I and III, studies have not identified clear sex-specific differences in collagen metabolism as a whole and suggest that age has a greater influence on ECM deposition.

1.5.3 Sexual dimorphism in collagen degradation

Collagen degradation and the regulation of MMPs and TIMPs play a critical role in maintaining the ECM, with notable sex-specific differences emerging, particularly with age. Studies indicate that collagen type IV degradation biomarkers and turnover rates increase significantly in menopausal women compared to age-matched males, pointing to a distinct change in ECM turnover during menopause (106). While collagen types I and III are commonly associated with sex-specific differences in overall quantity, their turnover rates appear to be age-dependent rather than sex-dependent, suggesting that degradation is primarily influenced by aging rather than sex (106). TIMPs, especially TIMP2 and TIMP3, demonstrate sex-specific modulation with age. Older women, particularly post-menopausal, exhibit significantly higher levels of TIMP2 and TIMP3 compared to younger women and age-matched males (9, 88). This increase in TIMP levels correlates with greater collagen content in the left ventricle, which may contribute to the higher prevalence of diastolic dysfunction in women over the age of 50 (9). These findings highlight the sex-specific regulation of collagen turnover, as TIMPs, by inhibiting MMPs, play a crucial role in modulating ECM remodelling and fibrosis development. Furthermore, an age-related increase in collagen crosslinking enzymes such as LOX in females suggests a shift in ECM organization, contributing to cardiomyocyte senescence and fibrosis (88). MMP activity is also modulated by sex hormones, particularly E2, which suppresses MMP production and downregulates collagen synthesis in females. E2 has been shown to inhibit MMP2 gene expression in females, offering a protective mechanism against excessive ECM degradation and fibrosis (9, 92). Pre-menopausal levels of E2 appear to provide protection against adverse ECM remodelling and cardiac dysfunction, with E2 receptors playing a key role in the repression of ECM components (70). These findings emphasize the complex interaction between MMPs, TIMPs, and sex hormones in collagen metabolism, shedding light on the sex-specific mechanisms that govern cardiac fibrosis and ECM remodelling with age.

1.6 Current clinical methods for assessing cardiac structure and function *in vivo*

Currently, clinical assessment of CF and HF remains challenging. At present, diagnosing the extent of CF and subsequent HF is often carried out through the use of physiological tests of markers of cardiac dysfunction such as blood troponin, brain natriuretic peptide (BNP), and PIP levels (107-110). Moreover, techniques such as endomyocardial biopsy have been utilized to assess disease progression through an invasive biopsy of the myocardium and further histological and biochemical analyses (111). Additionally, electrocardiography (ECG) has been established to observe alterations in the heart's electro-mechanical coupling and is a key diagnostic tool of cardiac arrhythmias (112). However, these measurements can often vary depending on the time or region analysed, and therefore do not provide enough whole-organ context to clearly define disease progression and clinical outcomes.

1.6.1 Imaging based cardiac diagnostic tools

Imaging techniques are frequently used alongside the aforementioned tests to offer non-invasive, real-time *in vivo* analysis of cardiac structure and function. Echocardiography is commonly employed as a first-line tool for assessing HF, allowing for the measurement of the LV ejection fraction (EF), a crucial indicator of cardiac dysfunction (113, 114). It is often used together with an exercise stress test, where clinicians can compare diastolic function at rest and after exercise, indirectly identifying diastolic dysfunction by measuring pulmonary pressure (115, 116). Additionally, echocardiography can be used to perform global longitudinal strain analysis, which may detect early dysfunction in the heart or specific cardiomyopathies (117, 118). However, compared to newer and more advanced imaging techniques, echocardiography provides less detailed information and can be subjective depending on the clinician's interpretation (119).

CT imaging is another method for analysing cardiac function and offers higher spatial resolution than echocardiography (119). It is primarily used in cases of congenital cardiac dysfunction or for characterizing the heart (120). CT scans create 3D images of the thoracic region using X-rays, providing crucial structural information such as heart size and the identification of cardiac hypertrophy in heart failure patients (118). CT can also identify coronary artery obstructions using contrast agents, though it is typically employed only in low-risk cases (120). However, CT image quality can be reduced by artifacts from patient movement or inhalation, making it of limited use for heart failure assessment (118).

Currently, magnetic resonance imaging (MRI) is the gold standard imaging technique for HF detection due to its ability to determine the underlying cause, assist in diagnosis, and guide clinical decisions (121, 122). MRI provides greater accuracy, reproducibility, and higher temporal and spatial resolution than the previously mentioned techniques (123, 124). It allows for a detailed analysis of ventricle size and function, which aids in diagnosing HF and evaluating myocardial perfusion and viability (121). MRI also enables various imaging types, such as contrast-enhanced T1 and cine images, to identify infarcted tissue and assess heart function (125). Additionally, MRI with late gadolinium enhancement can detect ischemic tissue and quantify extracellular volume, enabling the identification of fibrotic tissue (123, 126). Despite its strengths, the clinical use of MRI is limited by its high setup and operating costs and, consequently, its limited availability (119).

Positron emission tomography (PET) and single-photon emission computed tomography (SPECT) are molecular imaging techniques that evaluate metabolic, cellular, and tissue processes (118, 119). Clinically, their use in cardiac fibrosis and heart failure is mainly restricted to assessing myocardial perfusion, identifying ischemic myocardial tissue, and determining myocardial viability (127). SPECT has been used for many years for diagnostic and prognostic purposes, utilizing tracers such as thallium-201 (^{201}Tl) and technetium-derived tracers (e.g., ^{99m}Tc-sestamibi and ^{99m}Tc-tetrofosmin) (128, 129). These tracers are injected intravenously and, following cardiac stress, are used to detect ischemia through reduced uptake, which can be compared with rest images (118). For example, ^{201}Tl SPECT can identify LV dysfunction by detecting increased pulmonary tracer uptake and calculating the pulmonary/cardiac uptake ratio (130). Both SPECT and PET involve exposure to ionizing radiation, though SPECT tracers may result in higher radiation doses than PET tracers (119). PET has become a key tool for assessing cardiac viability and myocardial perfusion, using tracers such as rubidium-82 (^{82}Rb) and nitrogen-13 ammonia (^{13}N-NH3) alongside ^{18}F-fluorodeoxyglucose (^{18}F-FDG) (131). These tools help diagnose MI by identifying viable cardiomyocytes, as necrotic cells do not uptake ^{18}F-FDG due to the absence of metabolic activity (132). PET offers the ability to assess specific processes such as collagen synthesis, fibroblast activation and ECM crosslinking in the myocardium, contributing to the understanding of fibrotic responses and HF development post-injury, with both clinical and preclinical applications (133-136). However, clinical use is limited due to the high cost of running PET and the limited availability of radiotracers. Finally, many limitations of these imaging modalities have been addressed with hybrid systems like PET/CT and PET/MRI. For instance, the PET/CT system combines the anatomical detail from CT imaging with the functional specificity of PET, which enhances the accuracy of diagnosis and improves clinical decision-making.

Currently medical imaging has played a vital role in assessing the effect of aging on structural, functional and molecular changes *in vivo*, providing both preclinical and clinical opportunities to assess

long-term changes. Utilisation of imaging is essential to characterise age-related changes to understand 'natural' age-related deterioration in physiological function and define clear aging hallmarks that may predispose individuals to dysfunction (137, 138).

1.7 PET radiotracers for imaging collagen biosynthesis and cardiac fibrosis

Preclinical research has highlighted the importance of developing novel imaging techniques to better understand fibrotic mechanisms. Among these, PET imaging offers a powerful tool to analyse specific biological processes with high specificity and sensitivity, crucial for characterizing CF progression and HF (139). Clinically, various PET tracers have been employed to observe myocardial perfusion, cardiac metabolism, necrosis, and autonomic innervation (140-142). However, there is a notable absence of radiotracers specifically targeting the ECM to assess cardiac fibrosis mechanisms, such as collagen biosynthesis (140-142). This gap represents a key target for the development of new radiotracers and preclinical research. Currently, there are several radiotracers targeting ECM processes in development, these are ^{68}Ga-FAPI-04, ^{18}F-FXIII, ^{64}Cu-RYM2, ^{64}Cu-CBP7/^{68}Ga-CBP8 and *trans/cis*-4-[^{18}F]-Fluoro-*L*-proline which target fibroblast activation, ECM crosslinking, collagen degradation, collagen deposition and collagen biosynthesis, respectively (142-144). These emerging radiotracers targeting ECM-specific fibrotic processes hold great promise for both preclinical and clinical use, offering the potential for early detection and detailed profiling of metabolic changes. Furthermore, it is important to note that very little longitudinal analysis of PET radiotracer uptake is conducted in healthy aging subjects and therefore little data is available on the impact of aging on radiotracer dynamics.

1.7.1 ^{68}Ga-FAPI-04 and ^{18}F-FXIII Imaging

In recent years, ^{68}Ga-FAPI-04 has been developed to track fibroblast activation in cancer research, where it is used to assess tissue remodelling (143). This radiotracer targets fibroblast activation protein (FAP) using FAP inhibitors (FAPI), as FAP is expressed by activated fibroblasts during tissue remodelling and wound healing (145). In the context of the heart, cFbs are activated in rodent models and humans following MI (146). Studies have shown that ^{68}Ga-FAPI-04 accumulates in the infarcted region of the rodent heart, primarily in the border zone, indicating its potential for imaging active fibrosis both preclinically and clinically (143). FAPI imaging has shown promising potential, especially in its prognostic capacity. Clinical studies in MI patients have demonstrated a significant association between increased ^{68}Ga-FAPI uptake and long-term reductions in LV ejection fraction (147). Additionally, studies using ^{68}Ga-DOTA-FAPI-04 indicate that FAPI imaging post-MI can predict LV remodelling 12 months after injury (148). However, the specificity of FAPI in cardiac imaging remains

poorly understood, and its role requires further investigation (147). Moreover, fibroblast activation varies among patients due to factors such as infarct size, genetic differences, or pre-existing fibroblast activation, meaning FAPI imaging may not fully capture disease burden if not performed at the optimal timepoint (147). This underscores a critical assumption: that fibroblast activation alone is sufficient to understand the remodelling process, despite evidence suggesting that different fibroblast subtypes significantly influence disease progression. Further research is needed to refine this understanding. In age-dependent CF, the absence of overt cFb activation presents a challenge for cardiac FAPI imaging, as fibrosis progresses more subtly compared to injury-induced cases. This suggests that traditional biomarkers or imaging targeting activated cFbs may be less effective in detecting subtle age-related fibrosis, requiring a deeper understanding of alternative mechanisms.

^{18}F-FXIII has been developed to assess LV remodelling by measuring ECM crosslinking, a key aspect of fibrotic mechanisms (149). In studies involving apoE-/- mice post-MI, this radiotracer effectively identified adverse LV remodelling associated with changes in ECM crosslinking (149). Whilst less research has been conducted on this radiotracer, in terms of age-related fibrosis ^{18}F-FXIII may provide key information regarding this process given that ECM crosslinking is known to dramatically increase with age and contribute to myocardial stiffening (80).

1.7.2 *trans*-4-[^{18}F]-Fluoro-*L*-proline and *cis*-4-[^{18}F]-Fluoro-*L*-proline

Collagen metabolism has emerged as a critical target for radiotracer development due to its central role in CF and HF. Given the lack of imaging tools to observe scar tissue formation, the development of ^{18}F-fluoroproline tracers has enabled *in vivo* assessment of collagen biosynthesis (136, 150). These tracers estimate the incorporation of proline, a key component of collagen, which contains approximately 23% proline and hydroxyproline in its structure (134). Proline is known to play a crucial role in wound healing through collagen synthesis with a 50% increase in plasma proline levels observed in MI patients (134). The ^{18}F-fluoroprolines focus on the *cis/trans* proline isomerization step of collagen synthesis, a rate-limiting step in collagen folding and transport to the extracellular space (151, 152). Gottlieb *et al.* first demonstrated the use of *trans*-4-[^{18}F]-Fluoro-*L*-proline and *cis*-4-[^{18}F]-Fluoro-*L*-proline in collagen synthesis (153). This research highlighted the potential of ^{18}F-fluoroprolines, as these tracers provide the opportunity to assess collagen synthesis *in vivo* which has always remained challenging, providing unique insights into collagen metabolism (154). The incorporation of *cis*-4-Fluoro-*L*-proline was believed to disrupt proper collagen folding, as newly synthesised procollagen pro-alpha chains containing *cis*-4-Fluoro-*L*-proline were unable to form the triple helical structure, resulting in irregular fibrillary collagen production (154). Whereas *trans*-4-

Fluoro-*L*-proline was thought to measure triple-helical collagen synthesis—a key feature of replacement fibrosis (155). It is important to note that in physiological conditions both *cis*-proline and *trans*-proline are present with both isomers incorporated into collagen peptides *in vivo,* however the *cis*-proline isomer is less naturally abundant (156, 157). In physiological conditions *cis*-proline incorporation leads to unfolded collagen (158). This is thought to be due to the peptide bond preferentially adopting a downward puckering with studies suggesting that around 81% of *cis*-proline bonds have this downward orientation leading a reduction in collagen stability and lack of appropriate folding (156, 158). Whereas the *trans*-proline isomer does not produce the same downward bond and is able to form stable peptide bonds and produced a triple helix structure, therefore the isomer is favoured in collagen synthesis (157). Rodent studies have shown that *cis*-4-[^{18}F]-Fluoro-*L*-proline may serve as a marker for fibrillary collagen synthesis, which is central to reactive fibrosis (155). Although ^{18}F-fluoroproline radiotracers have primarily been used in cancer imaging, their potential applications in preclinical research on cardiac, hepatic and pulmonary fibrosis are expanding (142, 144, 159, 160).

In recent times, greater focus has been placed on improving the radiosynthesis of both fluoroproline radiotracers to reduce impurities formed during radiosynthesis, to better understand the mechanisms of incorporation into collagen and to assess its role in CF post-injury (161, 162). [^{18}F]fluoroproline radiotracers demonstrate significant potential by overcoming many common issues with other radiotracers. Their high parent-free fraction (the portion of a biological sample in which the original **radiotracer** is no longer present) in plasma helps them effectively reach target tissues, while the absence of radiometabolites and favourable uptake kinetics allow for easier and more accurate quantification of PET data (162). Given that collagen synthesis rate is slow, these previous studies detected low intra-group variability suggesting that the [^{18}F]fluoroproline can sensitively assess subtle changes in the collagen synthesis rate (162, 163).

Recent studies completed by Balogh *et al.*, and Reid *et al.*, have assessed the mechanisms behind *trans*-4-[^{18}F]-Fluoro-L-proline and *cis*-4-[^{18}F]-Fluoro-*L*-proline in models of cardiac dysfunction such as angiotensin II mediated pressure overload and MI (162, 164, 165). These studies confirmed the role of *cis*-4-[^{18}F]fluoro-*L*-proline and *trans*-4-[^{18}F]fluoro-*L*-proline PET in measuring both fibrillary collagen and triple-helical collagen synthesis *in vivo,* see Figure 1.3 for full description of proposed mechanisms of action. Furthermore, Reid *et al.*, identified through a multipronged validation of *cis*-4-[^{18}F]-Fluoro-*L*-proline uptake using proteomics, hydroxyproline analysis and dansylation assays that *cis*-4-[^{18}F]-Fluoro-*L*-proline is a marker specifically of unhydroxylated collagen synthesis which is often cleared following synthesis (165-167). Conversely, *trans*-4-[^{18}F]-Fluoro-L-proline was identified to measure specifically hydroxylated collagen synthesis, with findings echoing the outcomes of the hydroxyproline assay, highlighting that *trans*-4-[^{18}F]-Fluoro-L-proline when incorporated into the collagen protein

leads to hydroxylated peptides, which are more likely to form triple helical collagen peptides (153, 165). In acute MI, the study identified that both tracers had similar patterns of uptake whilst angiotensin II treated Sprague Dawley rodents showed significant increases in hydroxylated cardiac collagen synthesis (*trans*-4-[^{18}F]-Fluoro-*L*-proline uptake) whilst unhydroxylated collagen synthesis (*cis*-4-[^{18}F]-Fluoro-*L*-proline uptake) remained unchanged following pressure overload (162, 165). This highlights the need for both tracers as together they provide an in depth understanding of the impact of a particular model of cardiac injury on collagen remodelling. These findings are consistent with current understanding of cardiac remodelling in MI which has both interstitial fibrosis and reparative fibrosis present whereas pressure overload is characterised by largely the development of interstitial fibrosis and less replacement fibrosis in the absence of ischaemic injury (168).

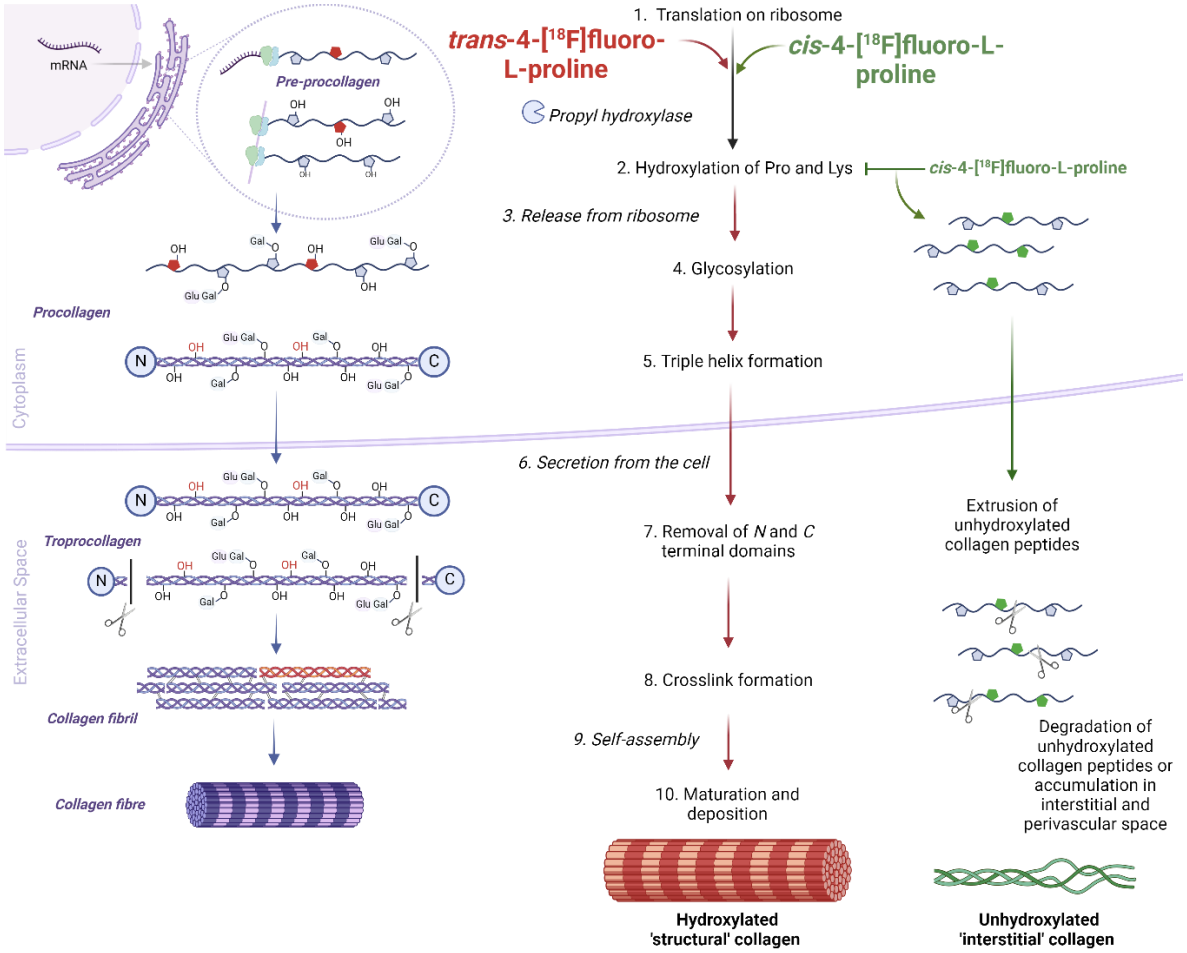

Figure 1. 3 Schematic of the mechanism of incorporation of *trans*-4-[^{18}F]-Fluoro-*L*-proline and *cis*-4-[^{18}F]-Fluoro-*L*-proline into collagen. Figure created using Biorender.

In the context of aging, collagen synthesis has remained unexplored *in vivo,* with [^{18}F]fluoroproline PET providing a key opportunity to assess the impact of aging and sex on collagen synthesis. Current understanding relies upon indirect measurements of collagen synthesis such as gene expression analysis which indicates a decline or no change (61, 70). However, these methods do not capture the specific mechanisms of collagen synthesis and turnover.

1.7.3 ^{64}Cu-CBP7, ^{68}Ga-CBP8 and ^{64}Cu-RYM2

Another critical aspect of collagen metabolism and a promising targets for imaging are collagen deposition and degradation. Both processes are essential for maintaining tissue integrity and facilitating wound healing after injury, as outlined in sections 1.4.2 and 1.4.3 (38). Addressing the current lack of accurate, quantitative assessment tools for fibrosis *in vivo*, a collagen-specific tracer, ^{64}Cu-Collagen Binding Probe (CBP) 7*,* was developed and evaluated in a preclinical model of bleomycin-induced lung fibrosis (169). ^{64}Cu-CBP7, measures deposited collagen, and studies have shown a 2- to 8-fold increase in uptake in bleomycin-treated mice compared to sham counterparts (169). This tracer demonstrated high metabolic stability, minimal retention in off-target organs, and high target-to-background ratios, highlighting its strong translational potential in fibrosis imaging (169). However, it has not yet been applied to cardiac or aging-related studies, and the longer half-life of ^{64}Cu compared to isotopes like ^{18}F or ^{68}Ga presents challenges for human translation (169).

To address these challenges, ^{68}Ga-CBP8, which specifically measures collagen type I, was developed and has been successfully used both in preclinical models (such as bleomycin-induced lung fibrosis in mice) and in clinical studies on biodistribution, dosimetry, and pharmacokinetics in humans (170, 171). Preclinically, ^{68}Ga-CBP8 uptake correlated linearly with lung collagen content in mice with lung fibrosis and those with vascular leak-related pulmonary fibrosis, suggesting that this tracer could reliably track fibrosis progression *in vivo* (170). In healthy human studies, ^{68}Ga-CBP8 has shown promising characteristics, including an absence of adverse effects, strong metabolic stability, and rapid renal clearance, suggesting its potential utility for imaging deposited collagen and fibrosis. Although these tracers have been primarily assessed in lung fibrosis models, recent research shows that ^{68}Ga-CBP8 is also effective in evaluating cardiopulmonary fibrosis in transverse aortic constriction (TAC) mice, where increased uptake in the myocardium and lungs corresponded with LV remodelling and altered cardiac function (172). The advancement of tracers such as ^{64}Cu-CBP7 and ^{68}Ga-CBP8 represents a significant step forward in fibrosis imaging, with the potential to provide valuable insights into fibrotic disease progression and to aid in the development of targeted therapies across multiple organ systems.

Collagen degradation has also emerged as a valuable target for fibrosis imaging and has been investigated preclinically in studies on abdominal aortic aneurysm and vascular health. The tracer ^{64}Cu-RYM2 was developed to assess MMP activation in aortic aneurysm, given the well-established association between MMP activity, inflammation, and the subsequent risk of aneurysm expansion and rupture (173). ^{64}Cu-RYM2 functions as a broad-spectrum MMP inhibitor, enabling the *in vivo* measurement of collagen degradation by targeting MMP activity *(173)*. Studies have demonstrated that ^{64}Cu-RYM2 uptake correlates with *ex vivo* MMP activity and CD68 expression, indicating that it provides an accurate assessment of MMP activity and collagen degradation *in vivo* (173).

The development of ^{64}Cu-RYM2 highlights the potential for targeted imaging of collagen degradation in the myocardium, especially following injury, as well as in assessing age-related cardiac fibrosis. Such applications could significantly enhance our understanding of cardiac remodelling processes, offering insights that may inform therapeutic strategies for both acute and chronic cardiac conditions.

1.8 PhD project rationale, hypothesis and aims

Aging populations face a significant health burden, particularly from conditions such as CF, HF, and other CVDs. Age is a major risk factor for cardiac dysfunction, but there is still limited understanding of how 'healthy' aging influences collagen metabolism—a key process underlying age-related CF. This knowledge gap is particularly evident in understanding how both sex and aging contribute to differences in collagen synthesis and deposition, processes that have historically been challenging to measure *in vivo*.

This project aims to address this by investigating how both sex and aging influence cardiac collagen metabolism and the development of age-related CF. While extensive research has focused on pathological cardiac conditions, studies on the natural, healthy aging process have been limited, especially in the context of sex-based differences. Additionally, much of the previous research has predominantly included male subjects, leading to an underrepresentation of females and potentially overlooking important sex-related differences in cardiac collagen metabolism. Given the established disparities in disease progression and incidence between sexes, this study will explore the intersection of sex and age in cardiac collagen metabolism to provide a more comprehensive understanding of age-related CF.

Physiological changes that accompany aging are often subtle and challenging to quantify, necessitating advanced methodologies to capture these processes accurately. To meet this challenge,

we propose the use of PET/CT imaging with *cis*-4-[^{18}F]-Fluoro-*L*-proline and *trans*-4-[^{18}F]-Fluoro-*L*-proline to sensitively and longitudinally measure both unhydroxylated and hydroxylated collagen synthesis over an 18-month period. By measuring both hydroxylated (*trans*-4-[^{18}F]-Fluoro-*L*-proline) and unhydroxylated (*cis*-4-[^{18}F]-Fluoro-L-proline) proline incorporation, we can gain a deeper understanding of the types of collagens being synthesized during aging. Hydroxylated proline is incorporated into mature, stable collagen fibres, while unhydroxylated proline reflects newly synthesized or immature collagen. Tracking both forms can reveal shifts in collagen remodelling processes, such as an increase in immature collagen during early stages of fibrosis or altered hydroxylation during chronic fibrosis. This dual measurement approach offers insights into how aging affects collagen synthesis pathways, providing a more detailed understanding of how age-related fibrosis develops at the molecular level. This comprehensive, long-term characterization has never been conducted before, offering an unprecedented view into collagen dynamics during aging. This research provides critical insights into the mechanisms of aging-related cardiac fibrosis and collagen metabolism, contributing to the broader understanding of how aging affects tissue structure and function. Clinically, the ability to characterize collagen synthesis more precisely opens new avenues for early detection and intervention in age-related cardiac conditions, which could ultimately improve patient outcomes. Additionally, by assessing the role of sex in collagen synthesis and fibrosis development, this study may lead to more personalized treatment strategies.

Given the key role cFbs play in collagen metabolism, this PhD project will also investigate the cellular-level effects of aging and sex, and explore the potential therapeutic benefits of inhibiting collagen crosslinking. By adopting a multi-pronged approach, including advanced imaging techniques and molecular analysis, this study will provide a comprehensive understanding of the collagen deposition cascade. Figure 1.4 illustrates the techniques employed throughout this investigation.

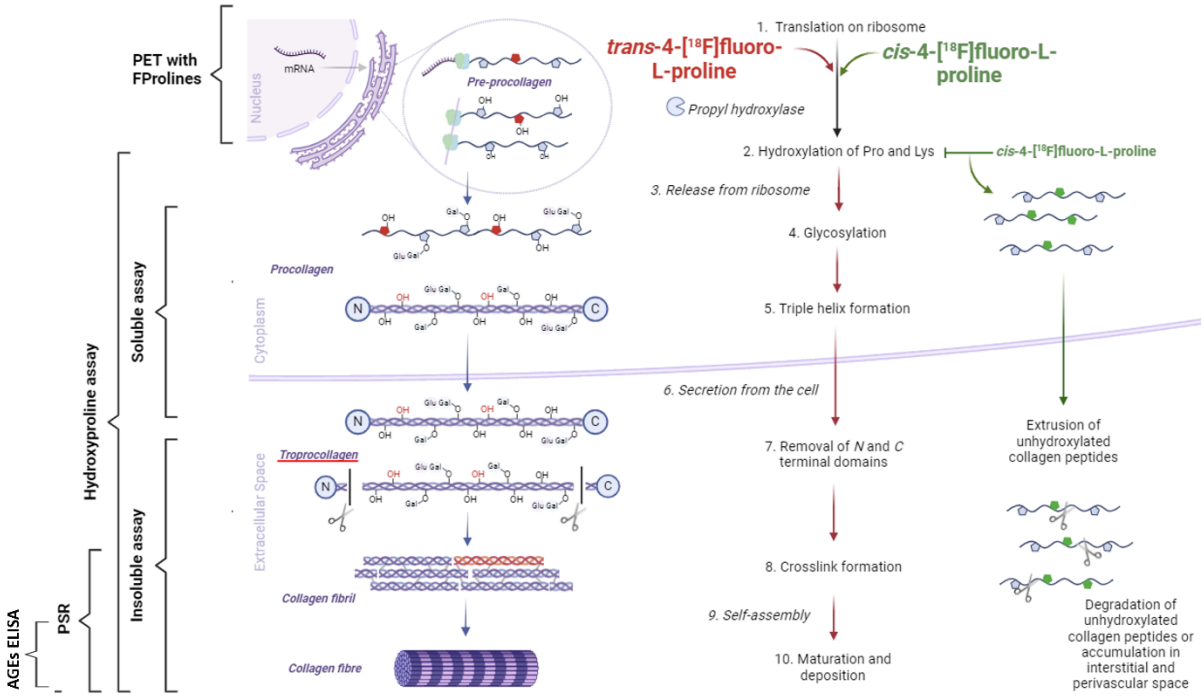

Figure 1. 4 Schematic of the scientific approach to addressing our assessing collagen metabolism in aging. Figure created using Biorender. *In vivo* and *ex vivo* analytical techniques used are described in vertical text on the left.

1.8.1 Hypothesis

Aging disrupts cardiac collagen metabolism, causing a decrease in collagen synthesis despite significant collagen accumulation, with higher rates of collagen synthesis and accumulation in males compared to females.

1.8.2 Aims

1. Characterize the effects of aging on frailty and cardiac health in Sprague Dawley rats, and investigate the relationship between frailty and cardiac health.
2. Investigate the effect of aging on cardiac collagen synthesis and accumulation.
3. Examine sex differences in cardiac collagen synthesis and accumulation during aging.
4. Identify the effect of aging and sex on cardiac collagen synthesis and accumulation on cardiac fibroblasts *in vitro.*

Chapter 2 - *Characterisation of the Effect of Aging on Survival, Frailty and Cardiac Health*

2.1 Introduction

Aging is a significant risk factor in the development of many diseases due to the gradual deterioration of physiological functions and repair mechanisms. As described in the previous chapter, aging is a major risk factor for CVD development, greatly contributing to pathological conditions such as MI, hypertension and atrial fibrillation (159, 174). Therefore, it is essential to understand what physiological changes occur with natural aging and whether sex is a key determinant of age-related dysfunction.

This thesis chapter focuses on the characterisation of natural aging in both male and female Sprague-Dawley rats to understand the effect of aging in the absence of underlying dysfunction. Preclinical aging research has always been challenging for a numerous of reasons, but primarily due to the difficultly of relating rodent age to relevant human aging timepoints and variation in the presentation of aging in different rodent species or strains (175). Therefore, this chapter is essential in providing a wider physiological context to the findings of the following thesis chapters which look to understand the effect of aging and sex on collagen synthesis and accumulation *in vivo* and *ex vivo*.

The classification of aging in preclinical research can be measured through a range of different metrics, at its crudest the chronological passing of time or lifespan studies which often do not reflect biological age (176). These assessments have been further refined through development of frailty index (FI) scorings for mice and rats which can provide a greater understanding of biological aging and comparison for human clinical frailty measurements, which will be utilised in this chapter (177-179). Conversely, cardiovascular aging assessment has been well established through evaluation of a range of parameters such as EF and cardiac dimensions derived from echocardiography analysis, which have been used to calculate cardiac aging indexes (180, 181).

Hypotheses:

- Rat survival declines with age, with a greater decrease in survival in males
- Male rats will show a greater decline in health compared to females during aging
- Rats show a decline in cardiovascular health with age, with a greater decline in males

This second thesis chapter aims to characterise and establish the effect of aging on the whole-body condition, frailty and cardiovascular physiology, using the previously mentioned metrics. Therefore, this chapter aims are threefold: (1) to investigate the impact of aging on the survival rates of rodents in experimental settings and determine if these effects differ between males and females; (2) to assess the influence of aging and sex on frailty in rodents; and (3) to characterize the effects of natural aging and sex on cardiac structure and function in rodents.

2.2 Materials & Methods

To address my hypothesis and aims, characterisation of the manifestation of aging in our male and female Sprague-Dawley rats was carried out. I conducted a longitudinal assessment of the study cohort using physiological observations, behavioural evaluation and *in vivo* imaging as shown in Figure 2.1. Rats were assessed for changes in body weight, blood pressure and cardiac volume measured by CT scanning at 1 month and then throughout to establish baseline physiological and cardiac outcomes. From 3 months onwards frailty assessments were conducted to identify whether the overall body condition and the behaviour of each animal in the study deteriorated over the course of the study leading to increased frailty. At the terminal aging timepoint ultrasound imaging was conducted to assess cardiac function and determine whether the aged animals showed any dysfunction.

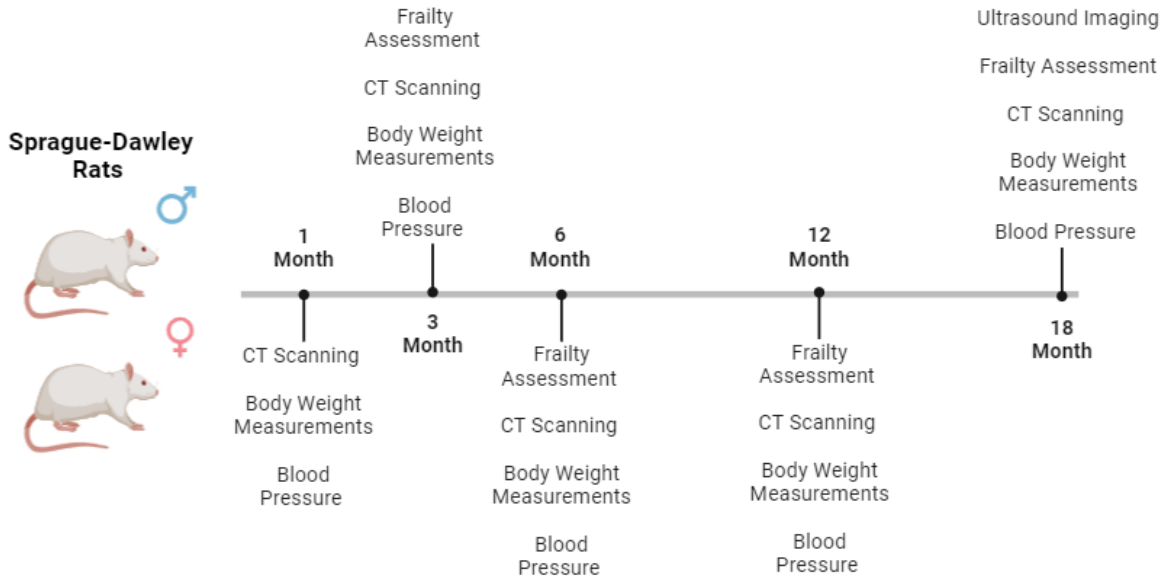

Figure 2. 1 Schematic of study design to assess the aging cohort.

2.2.1 Animal care and experimental handling

All *in vivo* experiments were carried out in accordance with the Home Office Animals (Scientific Procedures) Act 1986 and experimental plans were approved by the University of Edinburgh animal welfare and ethical review board. All *in vivo* data is reporter according to the ARRIVE recommended criteria (182). Animals used for the *in vivo* study were 3 weeks old Sprague-Dawley rats (Charles River, Tranent) and were given 1 week to acclimatise. Animals were housed initially housed on cages of 2-3

however at later stages (12-18 months) due to loss of animals some animals were single housed. Animals were housed under standard conditions with a 12 h light: 12h dark cycle (7am – 7pm lights) at 22±2◦C and 55% humidity. Animals were provided weekly with enrichment such as wooden balls, tunnels and sizzle nest. Sample sizes were calculated based on power calculations, completed prior to commencement of study. Rats were fed a standard chow diet and water available ad libitum. Both males (n=14) and female (n=14) (Table 2.1), were longitudinally assessed from 4 weeks onwards (average ages shown in Table 2.2). At each timepoint bodyweights were collected. It should be noted due to the increased prevalence of pressure sores on paws as a result of sedentary behaviour, from 12 months animals were exercised via an animal play pen filled with enrichment for 15 mins, twice a week for the remainder of the study. The number of animals on study declined over the course of the study due to the development of health issues (see section 2.3.1 for causes of death) which caused welfare concerns and were therefore culled using an overdose of anaesthetic on the advice of the named veterinary surgeon.

Table 2. 1 Longitudinal aging study animal numbers

Animal Numbers					
SEX	**1 Month**	**3 Month**	**6 Month**	**12 Month**	**18 Month**
Males	14	11	11	11	7
Females	14	12	12	9	7

Table 2. 2 Average age of animals at each time point

Average age (weeks ± SD)					
SEX	**1 Month**	**3 Month**	**6 Month**	**12 Month**	**18 Months**
Males	5.2 ± 0.6	10.0 ± 0.5	25.4 ± 2.6	47.0± 2.4	66.7 ± 6.3
Females	5.1 ± 0.6	11.2 ± 0.7	27.4 ± 2.5	52.2 ± 0.3	75.7 ± 4.6

2.2.2 Frailty assessment

Frailty measurements were carried at 3 months, 6 months, 12 months and 18 months, prior to each imaging timepoint. Criteria for frailty measurement guidelines were adapted from those set out in Yorke et al., 2017 (178). The index comprised of 9 factors: Integument, physical/musculoskeletal,

auditory, ocular/nasal, chromodacryorrhea/porphyrin, neurological, digestive/urogenital, respiratory and pain/discomfort. The criteria are described in Table 2.3, animals were placed in the playpen for observation and allowed to acclimatise prior to assessment. Animals were scored based on scoring guidelines detailed in the York et al. paper as follow 0: Absent, 0.5: mild and 1: severe. To ensure that measurements are consistent all assessment were completed by the same evaluator(178). A frailty index (FI) score was calculated based on the combined score divide by the total number of criteria.

Table 2. 3 Frailty Measurement Criteria

Classification	Category
Integument (Outer body condition)	Alopecia
	Dermatitis
	Coat condition
Physical/Musculoskeletal	Tumours
	Distended abdomen
	Hunched Posture
	Body Condition Score
	Gait Disorder
	Tremor
Vestibulocochlear (Auditory)	Hearing Loss
Ocular/Nasal	Cataracts
	Porphyrin
	Bulging Eyes
	Small Eyes
	Corneal opacity
Neurological	Malocclusion
Digestive/Urogenital	Diarrhoea
	Jaundice
	Penile/Vaginal Prolapse
	Rectal Prolapse
Respiratory	Breathing rate/depth
Pain / Discomfort	Piloerection
	Unusual Sounds

2.2.3 CT cardiac volume

Anaesthesia was induced and maintained using 1.5–2.5% isoflurane (Zoetis Ltd., London UK) with oxygen/air (50/50, 1 L/min). Body temperature was maintained at 37°C and monitored by rectal thermometer. CT (Mediso, Hungary) acquisition took place post-PET imaging, image acquisition occurred with a semi-circular full trajectory, maximum field of view, 480 projections, 50kVp, 300ms and 1:4 binning. Reconstruction was filtered back projection with a voxel size of 250x250x250 µm, 40x40x40 mm volume size, and 100% cut-off filtering. Following reconstruction, CT analysis was

carried out using PMOD version 3.7 (PMOD Technologies, Switzerland), CT images were cropped and volumes of interest (VOIs) were manually drawn by annotating every fourth slice from the slice prior to visualisation of the apex of the liver to the top of the heart. Once every fourth slice was annotated, they were combined to form a 3-dimensional VOI of the heart by interpolating the drawn slices to model the whole heart and then volume was extracted and plotted. Cardiac volume is standardly normalised to body weight and presented as ml/kg, this is often carried out to allow for comparison between subjects of different size and therefore was employed in this study(183).

2.2.4 Cardiac ultrasound

The Sprague-Dawley aging cohort of rats n=13 (males: 7; females:6 – one imaging animal was not US scanned due to technical challenges on the day) underwent high resolution cardiac ultrasound (echocardiography) at the terminal aging timepoint prior to PET/CT imaging. Rodents were anaesthetised via inhalation of 4% isoflurane (Zoetis Ltd., London UK) with 50/50 oxygen/nitrous oxide, 1 l/min and heart rate and respiration were monitored to ensure animal was stable with onset of anaesthesia defined by the loss of pedal withdrawal reflex. Rats were placed on to a heat plate for scanning, an infrared lamp was used to maintain the animals body temperature at 37◦C and body temperature was monitored using a rectal temperature probe. Fur was removed from the thoracic region using a commercially available electric shaver and the remaining fur was removed using hair removal cream (Nair, Church & Dwight, US) to optimise image quality. Anaesthesia was maintained continually, by 1-2% isoflurane administration via inhalation. Prior to the commencement of scanning, aqueous ultrasound solution (Aquasonic 100, Parker Laboratories INC) was applied to the thorax. The ultrasound probe was orientated to view the parasternal long axis (PSLAX). During ultrasound imaging two scans were acquired: Electrocardiogram-gated Kilohertz Visualisation (EKV) (all measurements bar ejection fraction (EF) and fractional shortening were acquired from this scan) B-Mode cine loops (Ejection fraction), M-Mode (Fractional Shortening) were acquired over several cardiac cycles using a Vevo 3100 micro-ultrasound imaging system (FUJIFILM VisualSonics, Canada). Due to the large body weight of the animals disrupting the imaging, Doppler scans were not acquired. Image reconstruction was performed and ultrasound image analysis was conducted using Visualsonics Vevo 770 V3.0.0 and VevoLab software (FUJIFILM, VisualSonics.Inc, Netherlands). EKV and M-Mode analysis was performed through automated identification of left ventricular end-diastole and end-systole, which were then manually checked. The endocardial and epicardial were also defined and from these values a range of cardiac structural and functional parameters were measured and calculations used to calculate parameters as described in Table 2.4 and Table 2.5 respectively.

Table 2. 4 Echocardiography measurements acquired

Measurements	Unit	Scan Type
Heart Rate	Beats per minute (BPM)	EKV
Area	mm^2	EKV
Area; Systolic	mm^2	EKV
Area; Diastolic	mm^2	EKV
Volume;s	µL	EKV
Volume;d	µL	EKV
LV Endocardial Trace	N/A	M-Mode

Table 2. 5 Structural and functional outcome measure and corresponding formulas

Outcome Measure	Unit	Formula
LV Mass	mg	$\mathbf{1.05\ x\ (\frac{5}{6}\ x\ LVAEPI\ x}$ ($\boldsymbol{LVL}$i diastolic + T)) -($\frac{5}{6}\ \boldsymbol{x\ LVAEND\ x\ LVL}$i diastolic)
Stroke Volume (SV)	µl	$\boldsymbol{LV\ end\ diastolic\ volume - LV\ end\ systolic\ volume}$
Cardiac output (CO)	µl/min	$\boldsymbol{stroke\ volume\ x\ heart\ rate}$
Ejection Fraction (EF)	%	$\left[\frac{\boldsymbol{LV\ end\ diastolic\ area - LV\ end\ systolic\ area}}{\boldsymbol{LV\ end\ diastolic\ area}}\right] \boldsymbol{x100}$
Fractional Shortening	%	$\frac{LV\ diastolic\ internal\ diameter - LV\ systolic\ internal\ diameter}{LV\ Diastolic\ Internal\ Diameter}\ x\ 100$

LVAEPI: Left Ventricular Area at the Epicardium; ***LVLi:*** Left Ventricular Longitudinal Length; ***T:*** Thickness; ***LVAEND:*** Left Ventricular Area at Endocardium

2.2.5 Tail-cuff plethysmography

Prior to the acquisition of blood pressure (BP) readings, rats were acclimatised for at least a week at each timepoint to familiarise them with the staff carrying out the experiments and the equipment used for taking blood pressure measurements. Once rats were familiar with the restraint, they underwent three consecutive acclimatisation sessions to reduce the stress response to the restraint method and reduce the likelihood of increase blood pressure due to increased stressed. Animals were placed on a heated platform and tails were placed on a heat mat to induce vasodilation which was ascertained by making sure the skin was pink in the ears and tail. Animals were placed into the clear restraining tubes and allowed to acclimatise to reduce stress levels prior to the measurements. Rats

were placed in the pre-warmed platform of the tail-cuff machine (CODA Non-invasive High Throughput Blood Pressure System, Kent Scientific Corp., USA). Then the occluding cuff and volume pressure recording (VPR) cuff were placed on the tail, and the tail temperature was measured with an infrared thermometer making sure that it was between 32-35°C for optimal readings. Animals were separated by sex and divided into groups of 2, 3 or 4. Animals' blood pressure was measured at 1.5 month, 3 months, 6 months, 12 months and 18 months of age. The blood pressure measurement included 20 cycles (1 cycle resulted in 1 blood pressure reading) which was then used for analysis. Each reading included systolic and diastolic blood pressure measurements. The initial timepoint was at 1.5 months to ensure that animals were given time to recover from first PET scans and were large enough to not move in the restraint.

2.2.6 Data Analysis

Animals were culled either due to health and welfare issues or at the terminal imaging timepoint. Survival data was collected, including the time-to-event data (in days) and the event status for each subject with event status coded as '1' for the occurrence of the event (i.e. death). Kaplan-Meier survival curves were generated using the imported data, with Prism automatically calculating the survival probabilities at different time points and plotting these probabilities against time. To compare survival curves between different groups, the log-rank (Mantel-Cox) test was employed, evaluating the null hypothesis that there is no difference in survival between the groups. The survival curves and the results of the log-rank test were examined to interpret the differences in survival between groups.

Data acquisition and analysis was not completed in a blinded manner. Data fitting, statistical analysis and production of graphs were completed using GraphPad Prism version 9 (GraphPad Software Inc., USA). Normality of the data was assessed for each group and paired or unpaired student tests were used to statistically compare two groups. If data was not normally distributed than non-parametric tests were used. Comparison of multiple groups was completed using analysis of variance (ANOVA) or mixed effect models plus post-hoc tests as indicated within the relevant figure legends. To assess survival rates and generate survival curves, survival analysis was performed using Prism version 9 (GraphPad Software Inc., USA). Data are expressed as mean± standard of the mean (SEM) in the graphical data and the threshold for statistical significance is $p<0.05$. All averages and standard deviations (SD) presented in the text were calculated using the descriptive statistics function on GraphPad Prism. All data is available upon request.

2.3 Results

This study looked to characterise and understand the effect of aging on Sprague-Dawley rats up to 18 months of age. Aging in different rodent strains has shown varying physiological outcomes and therefore it was necessary to characterise the effect of aging in this study cohort. These findings will provide physiological context to the *in vivo* and *ex vivo* findings later on this thesis.

2.3.1 Survival declines after one year of age regardless of sex

Survival was calculated based on the number of days from birth to the pre-determined end of experiment, as shown in Figure 2.2. No statistically significant difference was observed in the survival of male and female rats. Males did have a higher mean survival (514 ± 63 days) compared to females mean survival (496 ± 63 days) (p=0.90) however, this is likely due to females exhibiting a higher number of tumours (predominantly mammary tumours), as described in Table 2.6, rather than general physiological deterioration of health. Aging was shown to have an impact on survival with the earliest deaths in males around 376 days and females around 324. Of the original 11 males and 12 females, 7 males and 7 females survived to the end of the study some must have been culled. Main causes of death outside of terminal imaging timepoints in both males and females were tumours/unknown masses, however in males there were also incidences of abscesses and strokes.

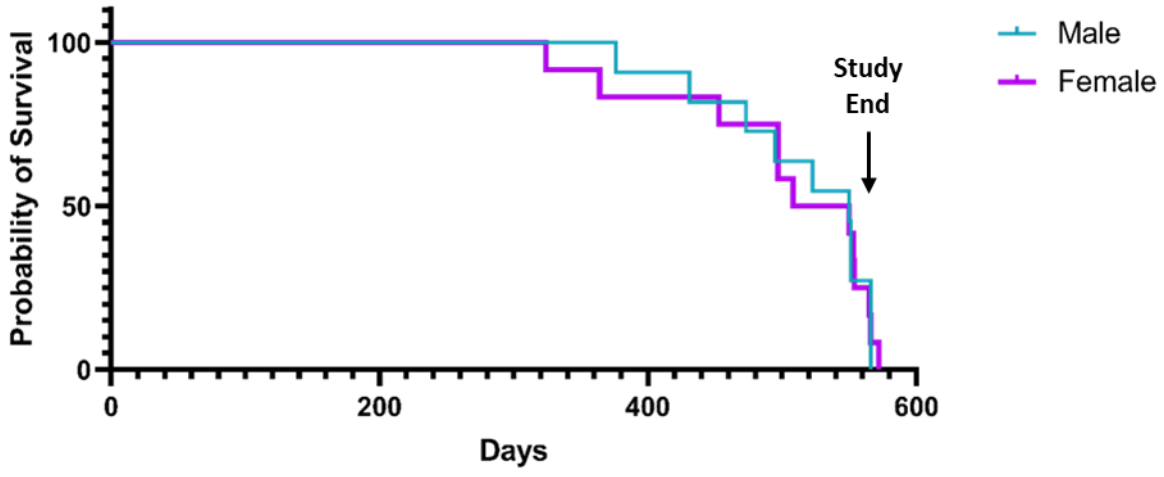

Figure 2. 2 Survival analysis of aging study cohort. Kaplan-Meier survival curves were calculated based on total days survived from the beginning of the study to intended endpoints.

Table 2. 6 Causes of death across longitudinal aging study cohort.

Cause of death	Number of deaths	
	Male	Female
Abscess	1	0
Tumour/Unknown Mass	2	5
Stroke	1	0
End of Experiment	7	7

2.3.2 Significant sex differences in body weight emerge with aging

Body weight was measured at each timepoint to assess the changes in body weightof the cohorts. At 1 month of age males and females showed no significant change in body weight with males having an average body weight of 122 ± 26 g (p=0.41), which was similar to the female's average body weight of 114 ± 26 g, see Figure 2.3 A. Following three months of age males and females showed significantly different body weight (p= <0.0001), Figure 2.3 B-E. At three months males had an average body weight of 420.2 ± 32.2g whilst female had an average body weight of 262 ± 21 g. At six months males had an average body weight of 693 ± 79 g whilst female had an average body weight of 346 ± 48 g (p=<0.0001). At 12 months males had an average body weight of 812 ± 97g whilst female had an average body weight of 395 ± 67 g (p=<0.0001). At 18 months males had an average body weight of 861 ± 121 g whilst female had an average body weight of 461 ± 60 g (p= <0.0001). Both males and females showed a significant body weight increase, which was greatest between 1-3 months which de-accelerated over time as shown in Figure 2.4.

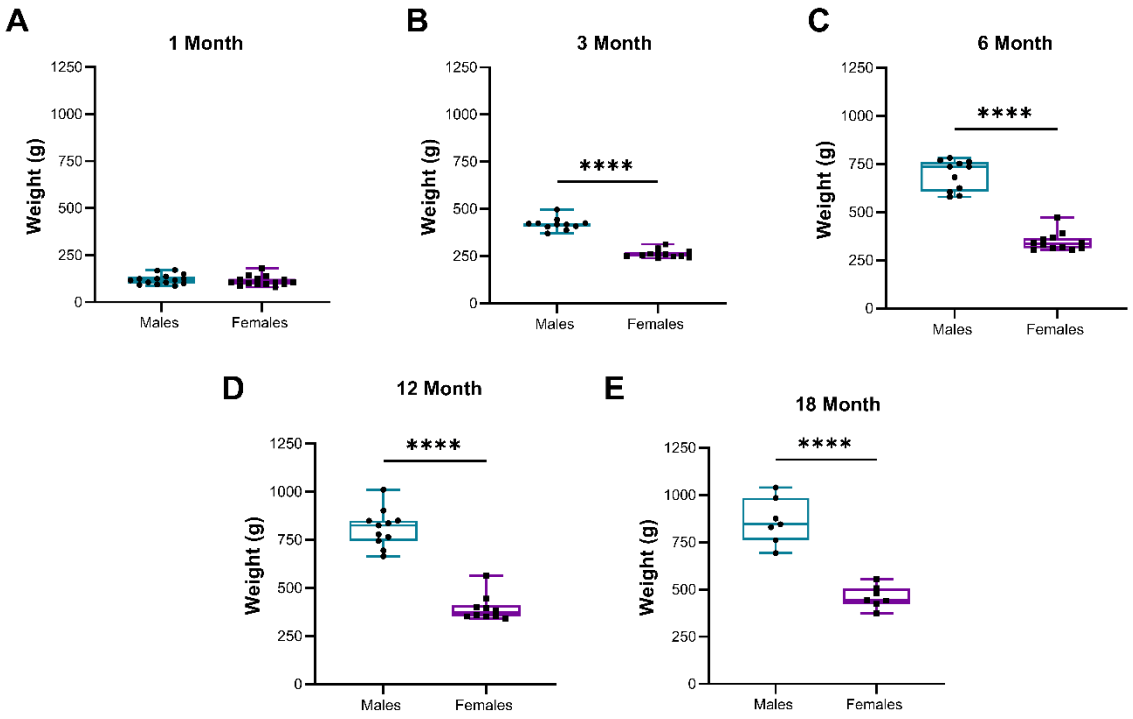

Figure 2. 3 Comparison of body weight by sex across aging timepoints. Body weight measurements were taken at each imagine time point: 1 month (A), 3 month (B), 6 month (C), 12 month (D) and 18 month (E). Results reported as min to max rangemin to max range, n=7-14 males and n=7-14 females; p values were obtained using unpaired parametric students t-test when comparing two groups, ****p<0.0001

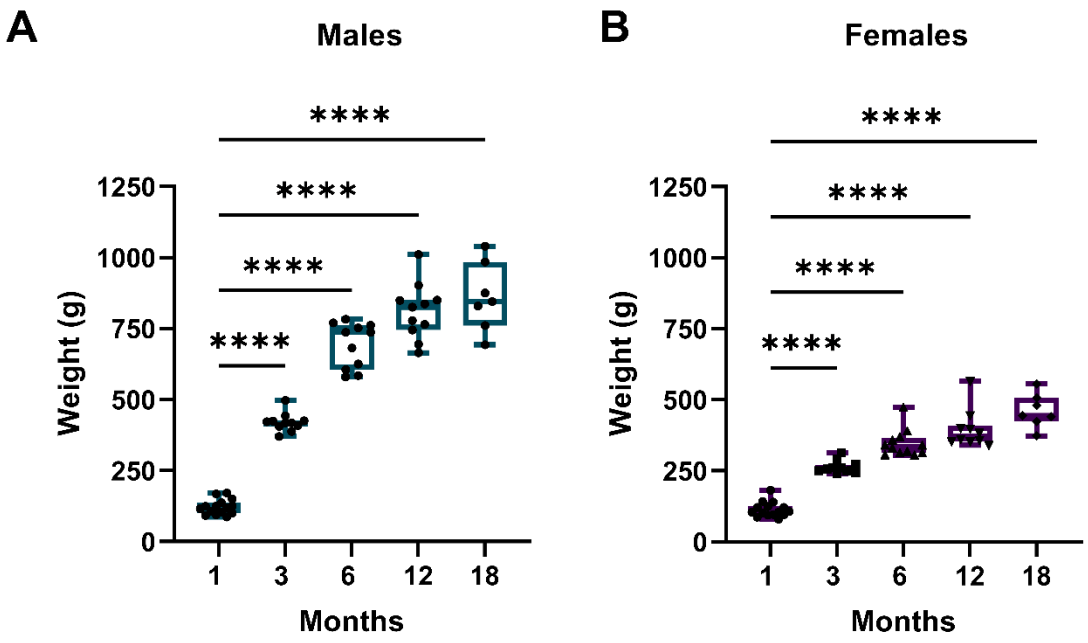

Figure 2. 4 Comparison of Body Weight by Sex Across Aging Timepoints. Longitudinal changes in males (A) and females (B) body weight measurement over 18 months. Results reported as min to max rangemin to max range, n=7-14 males and n=7-14 females; p values were obtained a one-way ANOVA and Dunnet's post hoc-test when comparing longitudinal data to the first timepoint. ****p<0.0001

2.3.3 Frailty significantly increases after one year of age regardless of sex

Frailty was measured based a strict set of criteria outlined in section 2.2.2, to understand how the overall body condition of the cohort changed over time. Males and females showed no significant sex differences in FI over time, as shown in Figure 2.5. Males and females were found to have very little indication of frailty at both 3 months (males: 0.01 ± 0.01; females: 0.00 ± 0; p=0.08) and 6 months (males: 0.01 ± 0.01; females: 0.01 ± 0.03; p=0.21) of age. Aging was found to have a significant impact on frailty in both males and females as shown in Figure 2.6 with males and females showing an increased FI score at 12 months, with over half of the group showing increased frailty, however, many of the cohort remained at low scores. Females showed a significant increase in frailty (0.03 ± 0.03) at 12 months, with males showing a similar trend (0.03 ± 0.04) but not significant (p=0.85). At 18 months, all animals in the cohort showed signs of increased frailty (males: 0.12 ± 0.03; females: 0.14 ± 0.07) which were significantly increased (males: p=0.001; females: p=0.005) in both males and females

from the baseline measurements. These results indicate that aging caused significant increases in FI scores suggesting their body condition deteriorated over the course of the experiment, however, there was no observable difference in male versus female frailty.

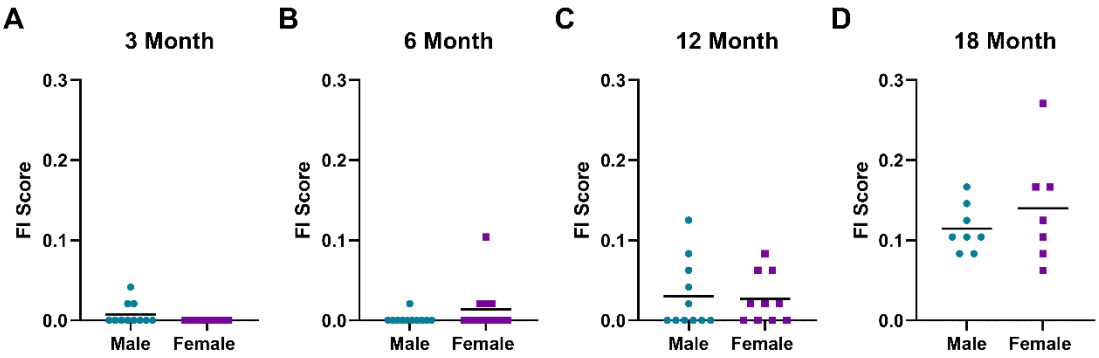

Figure 2. 5 Comparison of FI between sexes across aging timepoints. Frailty measurements were taken at each imagine time point: 3 month (A), 6 month (B), 12 month (C) and 18 month (D). Results reported as min to max rangemin to max range, n=7-14 males and n=7-14 females

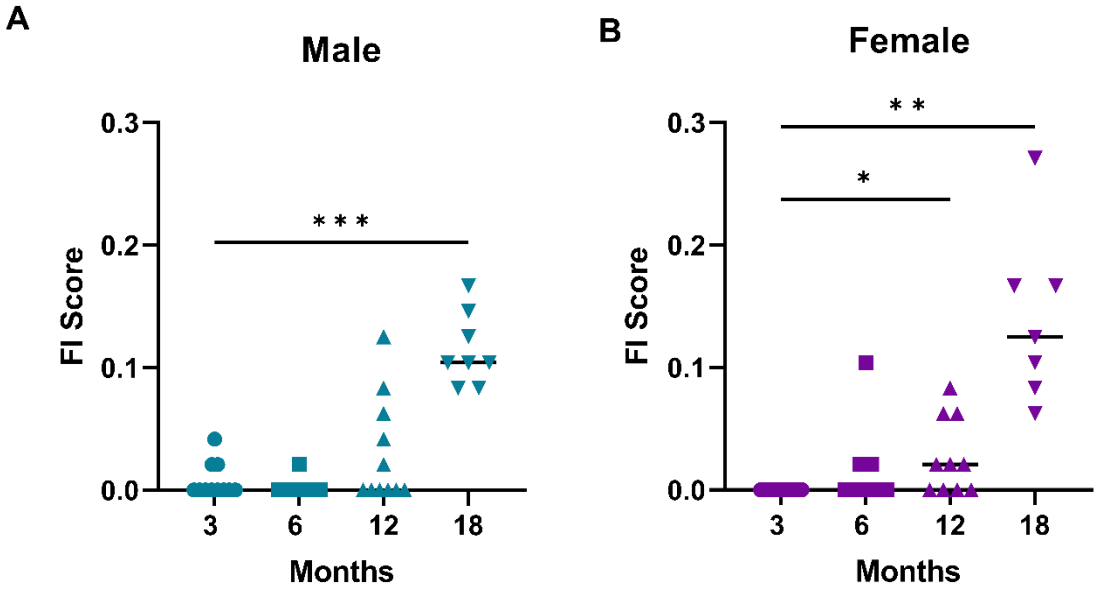

Figure 2. 6 Comparison of FI by sex across aging timepoints. Longitudinal changes in males (A) and females (B) frailty measurement over 18 months. Results reported as min to max range, n=7-14 males and n=7-14 females; p values were obtained by a Mixed-effects analysis and Dunnet's post hoc-test when comparing longitudinal data to the first timepoint. *p<0.05; **p<0.01; ***p<0.001

2.3.4 Cardiac volume significantly increases with age, with greater increases observed in the males

Similar to the other physiological parameters assessed over time, no differences were observed between CT derived cardiac volume of males (1.24 ± 0.26ml) and females (1.2 ± 0.31ml) at 1 month of age (Figure 2.7 A). Following 3 months of age, the males consistently showed significantly higher (p= <0.0001) cardiac volume likely due to the increase body weight (Figure 2.7 B-C). At 3 months, male cardiac volume was higher (p= <0.0001) than females with males having an average cardiac volume of 2.9 ± 0.27ml whilst the average cardiac volume for females was 1.9 ± 0.24ml. Both males and females showed age-related changes in cardiac volumes. Overall, the male cardiac volume increased on average by 234% over 18 months, showing a significant age-related increase cardiac volume (p= 0.0003) (Figure 2.8 A). A similar significant increase (p= 0.01) was observed in females with on average an increase of 151% over 18 months (Figure 2.8 B), however the volume increase was greater in the male cohort. These results show a direct effect of age and sex on cardiac volume, causing an increase in both males and females.

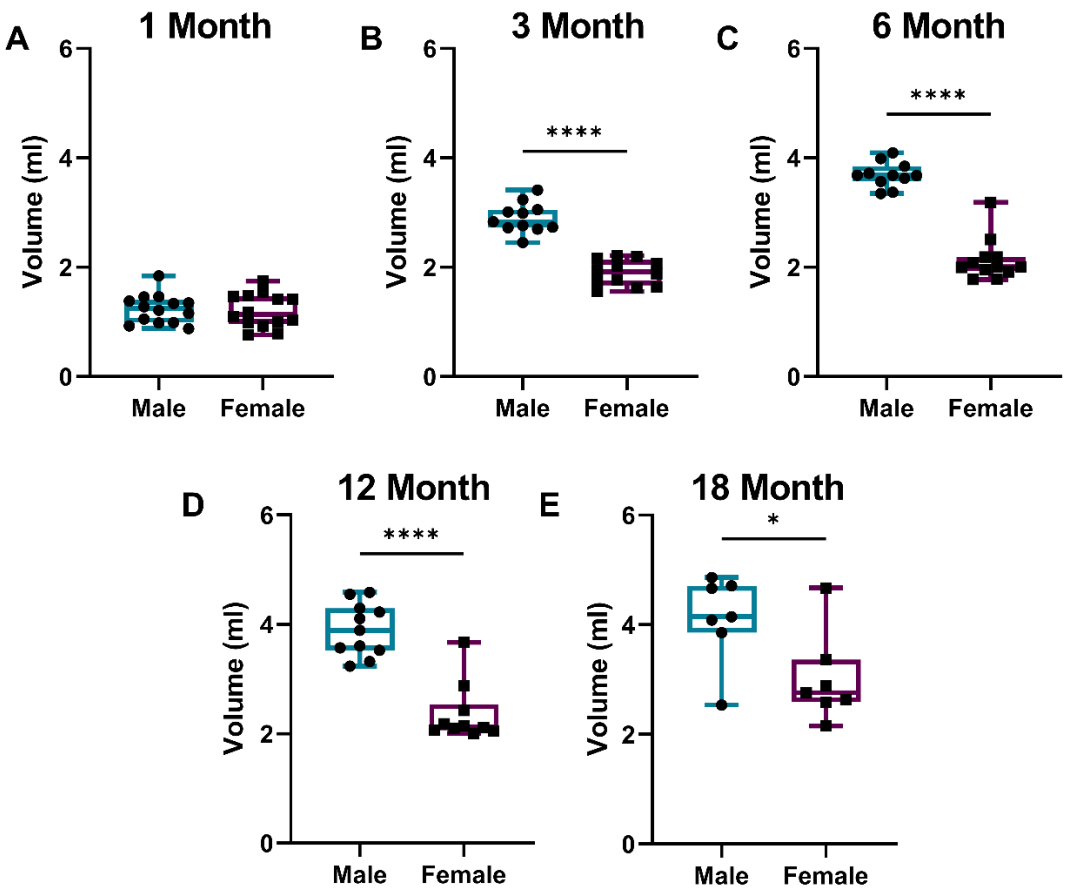

Figure 2. 7 Comparison of cardiac volume between sexes across aging timepoints. Cardiac volume measurements were taken at each imagine time point: 1 month (A), 3 month (B), 6 month (C), 12 month (D) and 18 month (E). Results reported as min to max range, n=7-14 males and n=7-14 females; p values were obtained using unpaired parametric students t-test when comparing two groups *p<0.05 and ****p<0.0001

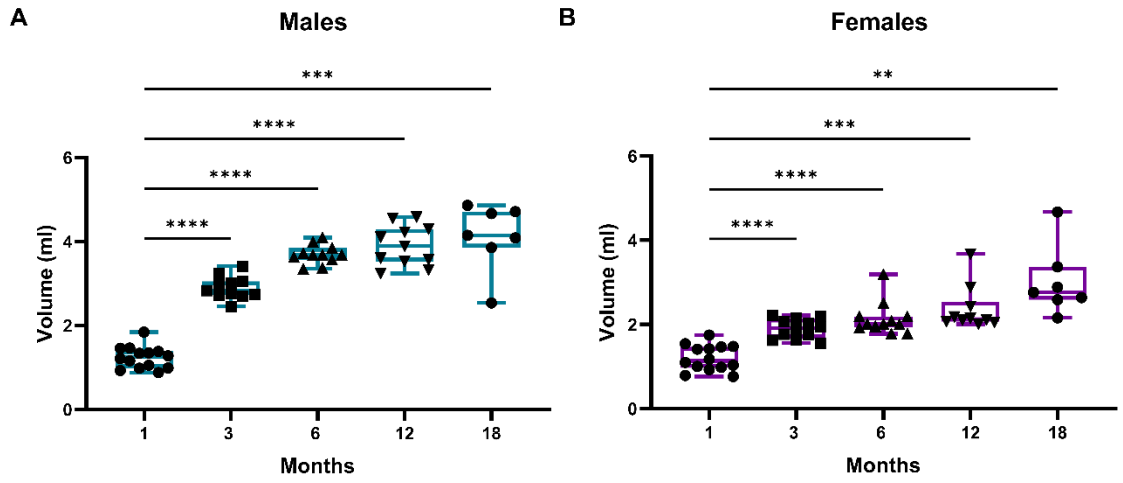

Figure 2. 8 Comparison of cardiac volume by sex across aging timepoints. Longitudinal changes in males (A) and females (B) cardiac volume measurement over 18 months. Results reported as min to max range, n=7-14 males and n=7-14 females; p values were obtained a Mixed-effects Analysis and Dunnet's Post-hoc test when comparing longitudinal data to the first timepoint. **p<0.01; ***p<0.001; and ****p<0.0001

Normalised cardiac volume showed significant sex-differences in cardiac volume from 6 months of age with no sex differences observed at 1 month or 3 months of age (Figure 2.9). All normalised cardiac volume measurements appeared to be within similar ranges except at the 1-month timepoint where values were higher with males on average 10.23 ± 1.31 ml/kg and females on average 10.37 ± 1.58 ml/kg. Relative to body weight females showed significantly higher cardiac volume (6.17 ± 0.51 ml/kg) compared to males (5.38 ± 0.58 ml/kg) (p= <0.0001) at 6 months of age. This significant difference is also observed at 12 months (p= <0.0001) and 18 months (p= 0.02). Aging was found to decrease cardiac volume normalized to body weight in both males and females, as illustrated in Figure 2.10. This indicates that the heart expands proportionally to changes in body weight, provided the first time point is excluded. The normalised data confirms the findings in the raw data that cardiac volume is affected by both age and sex.

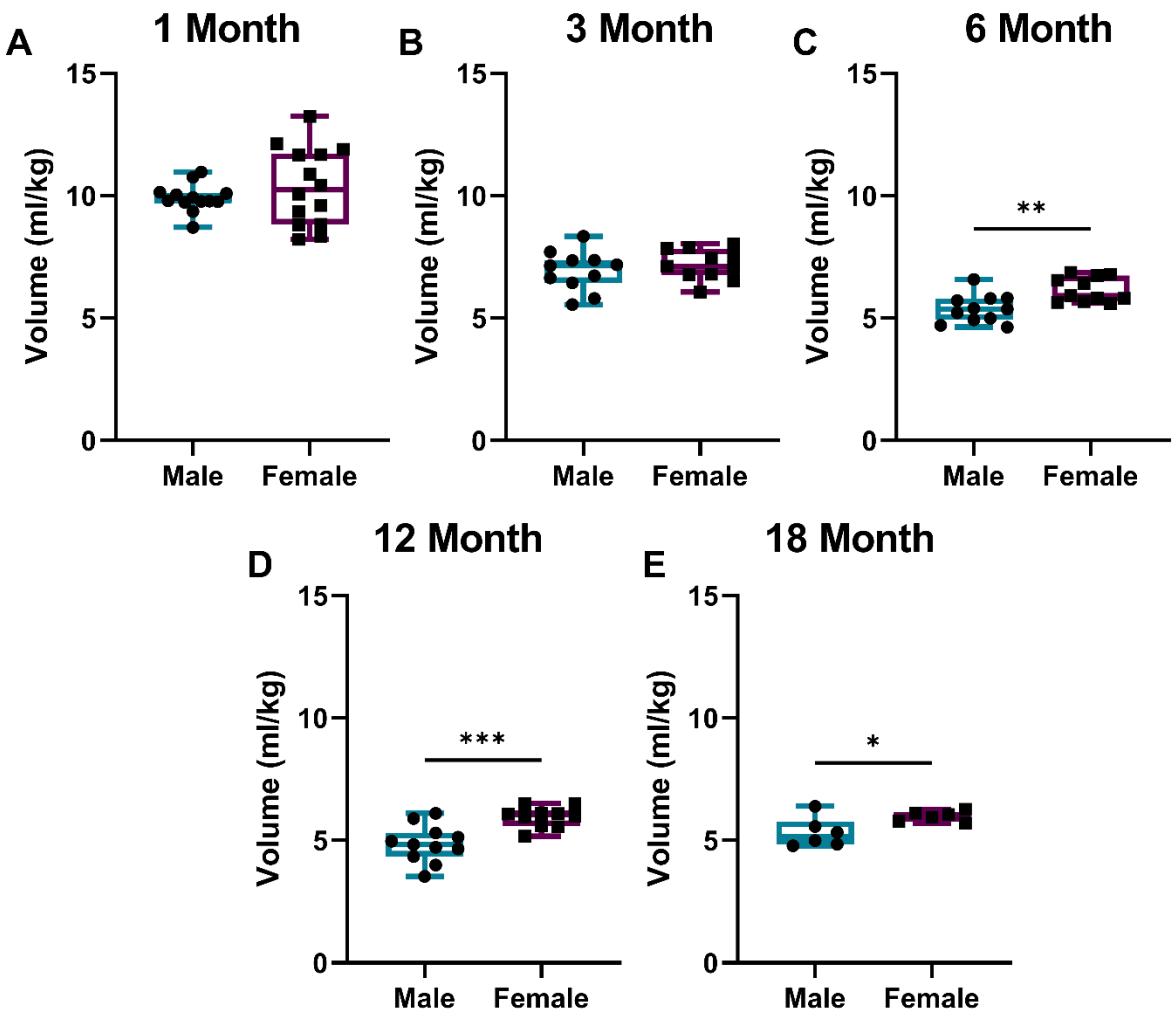

Figure 2. 9 Comparison of cardiac volume normalised to body weight between sex across aging timepoints. Cardiac volume normalised to body weight measurements were taken at each imagine time point: 1 month (A), 3 month (B), 6 month (C), 12 month (D) and 18 month (E). Results reported as min to max range, n=7-14 males and n=7-14 females; p values were obtained using unpaired parametric students t-test when comparing two groups; *p<0.05; **p<0.01; ***p<0.001

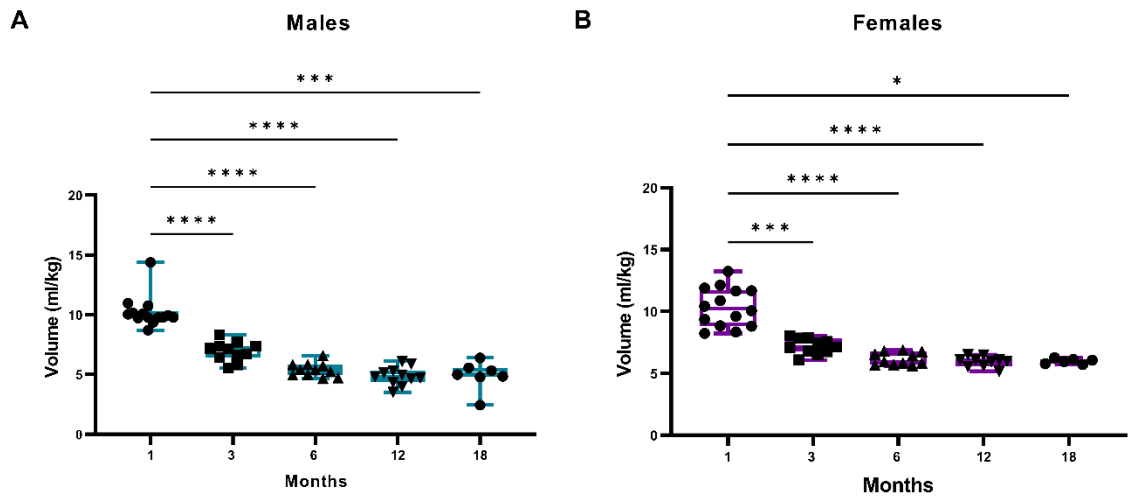

Figure 2. 10 Comparison of cardiac volume normalised to body weight by sex across aging timepoints. Longitudinal changes in males (A) and females (B) cardiac volume measurement normalised to body weight over 18months. Results reported as min to max range, n=7-14 males and n=7-14 females; p values were obtained a Mixed-effects Analysis and Dunnett's Post-hoc test when comparing longitudinal data to the first timepoint. *p<0.05; ***p<0.001; and ****p<0.0001

2.3.5 Age and sex do not influence blood pressure

Systolic and diastolic BP were measured by tail-cuff plethysmography to assess the impact of aging and sex on cardiac and vascular function. No sex differences were observed at each time point in systolic BP, as shown in Figure 2.11. Diastolic BP was significantly lower (p=0.03) in 1-month females (83 ± 14 mmHg) compared to 1-month males (97 ±14 mmHg), as seen in Figure 2.12.

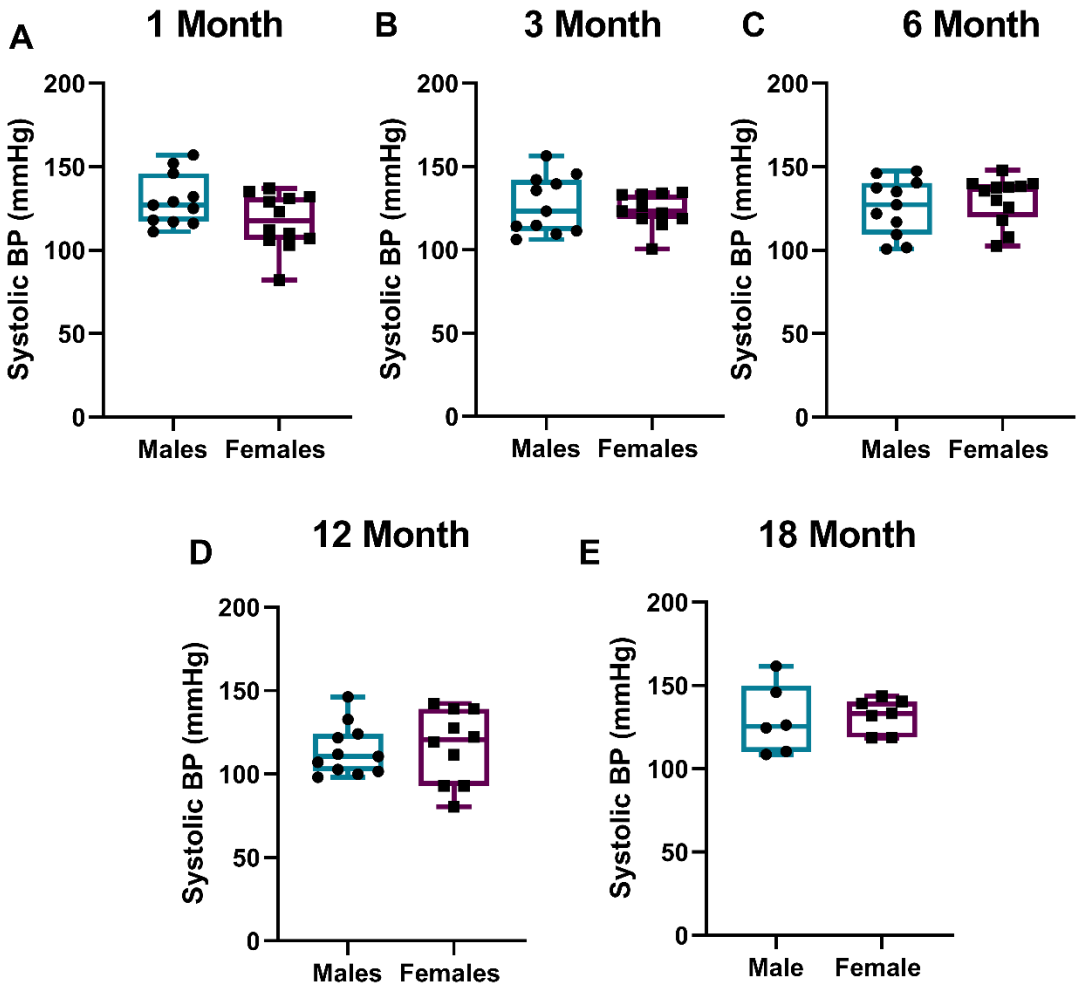

Figure 2. 11 Comparison of systolic blood pressure between sexes across different ages. Systolic blood pressure measurements were taken at each imagine time point: 1 month (A), 3 month (B), 6 month (C), 12 month (D) and 18 months (E). Results reported as min to max range, n=7-14 males and n=7-14 females. Changes were assessed using a Student's t-test; results were not statistically significant.

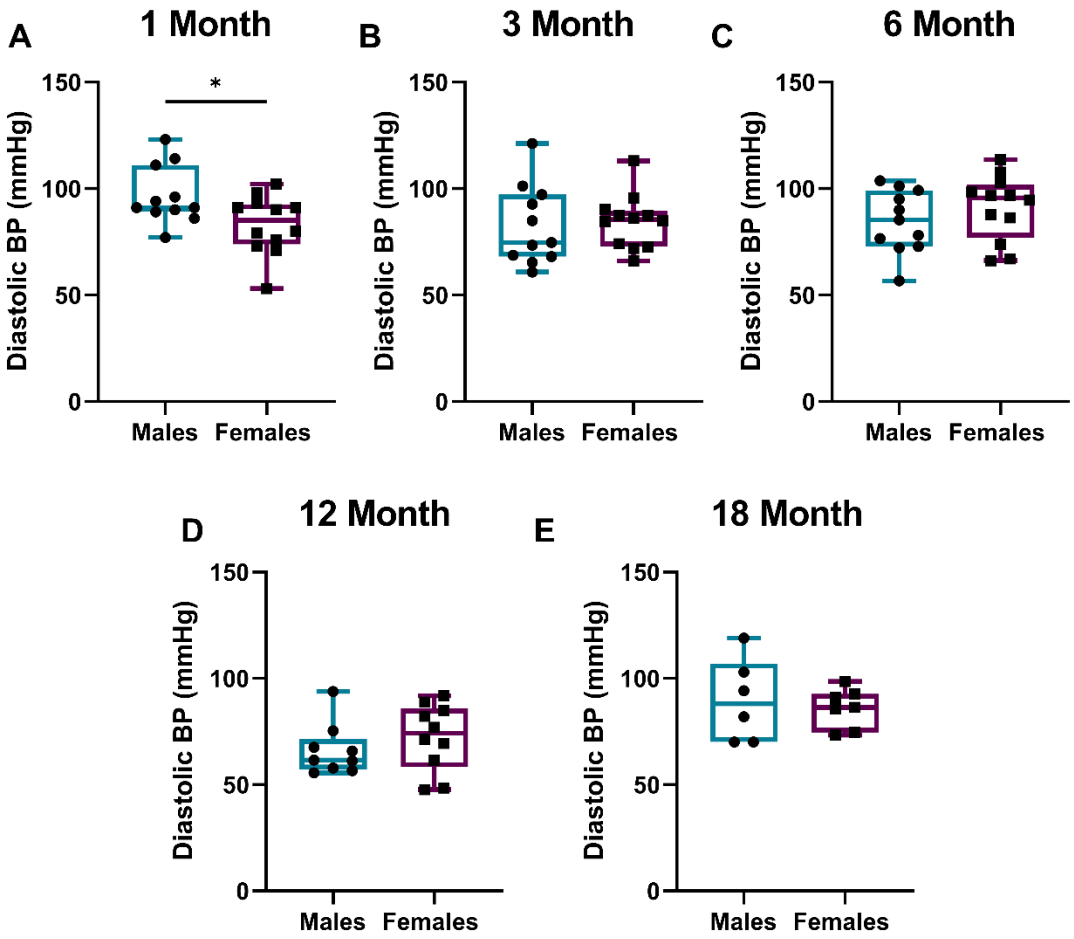

Figure 2. 12 Comparison of diastolic blood pressure between sexes across different ages. Diastolic blood pressure measurements were taken at each imagine time point: 1 month (A), 3 month (B), 6 month (C), 12 month (D) and 18 month (E). Results reported as min to max range, n=7-14 males and n=7-14 females; p values were obtained using unpaired students t-test when comparing two groups; *p<0.05

Males showed consistent average systolic BP throughout the study with an average of 130 ± 15 mmHg at 1 month and at 18 months an average of 130 ± 21 mmHg suggesting that aging had no effect on BP (Fig. 2.13 A). Similarly, females maintained systolic BP with age, however a significant increase in systolic BP (p=0.04) was observed at 18 months with an average of 132 ± 10 mmHg compared to 117 ± 17 mmHg at 1 month (Fig. 2.13 B). However, it is important to note that there is a high level of variability across each timepoint, making it challenging to assess what the true age-related changes in systolic BP.

Diastolic BP in the males showed a significant decline at 12 months with an average diastolic BP of 66 ± 12 mmHg compared to 1 month which had an average diastolic BP of 96 ± 13 mmHg (p= 0.0027), as

shown in Figure 2.14 C. In females, no significant effect of age was observed on diastolic BP with an average of 83 ± 14 mmHg at 1 months and no observable change at 18 months with a diastolic BP of 85 ± 9 mmHg as seen in Figure 2.14 D.

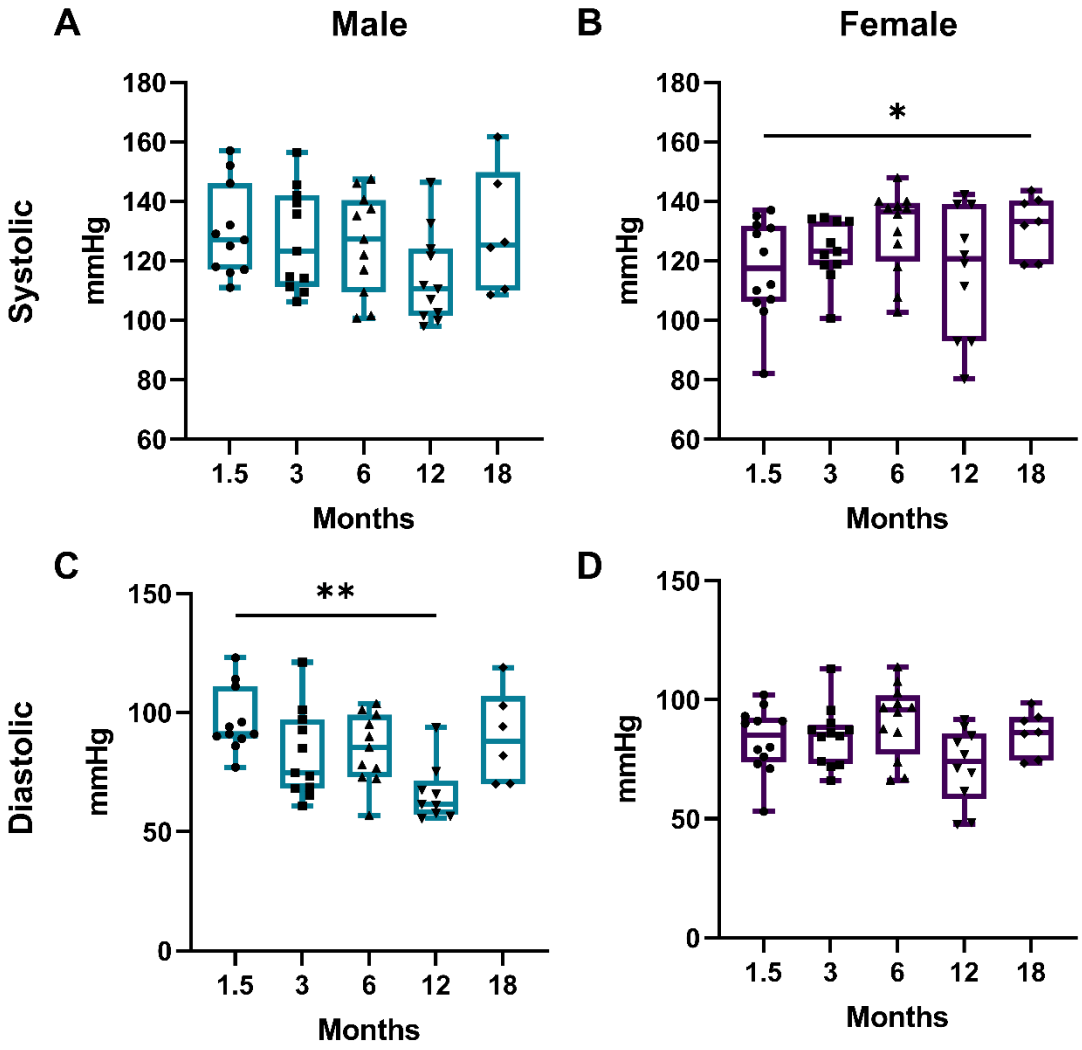

Figure 2. 13 Comparison of the effect of age on systolic and diastolic BP in male and female rats. Longitudinal changes in males (A+C) and females (B+D) Systolic (A+B) and diastolic (C+D) over 18months. Results reported as min to max range, n=7-14 males and n=7-14 females; p values were obtained a Mixed-effects Analysis and Dunnett's Post-host test when comparing longitudinal data to the first timepoint.; *p<0.05; **p<0.01

Mean arterial pressure (MAP) was calculated to understand the average BP throughout the cardiac cycle and is a key parameter for understand haemodynamic stability of the cohort. MAP measurements showed no sex differences throughout the different aging timepoints, suggesting that BP is not affected by sex (Figure 2.14). Similarly, no age effect was observed in MAP in either sex (Figure 2.15).

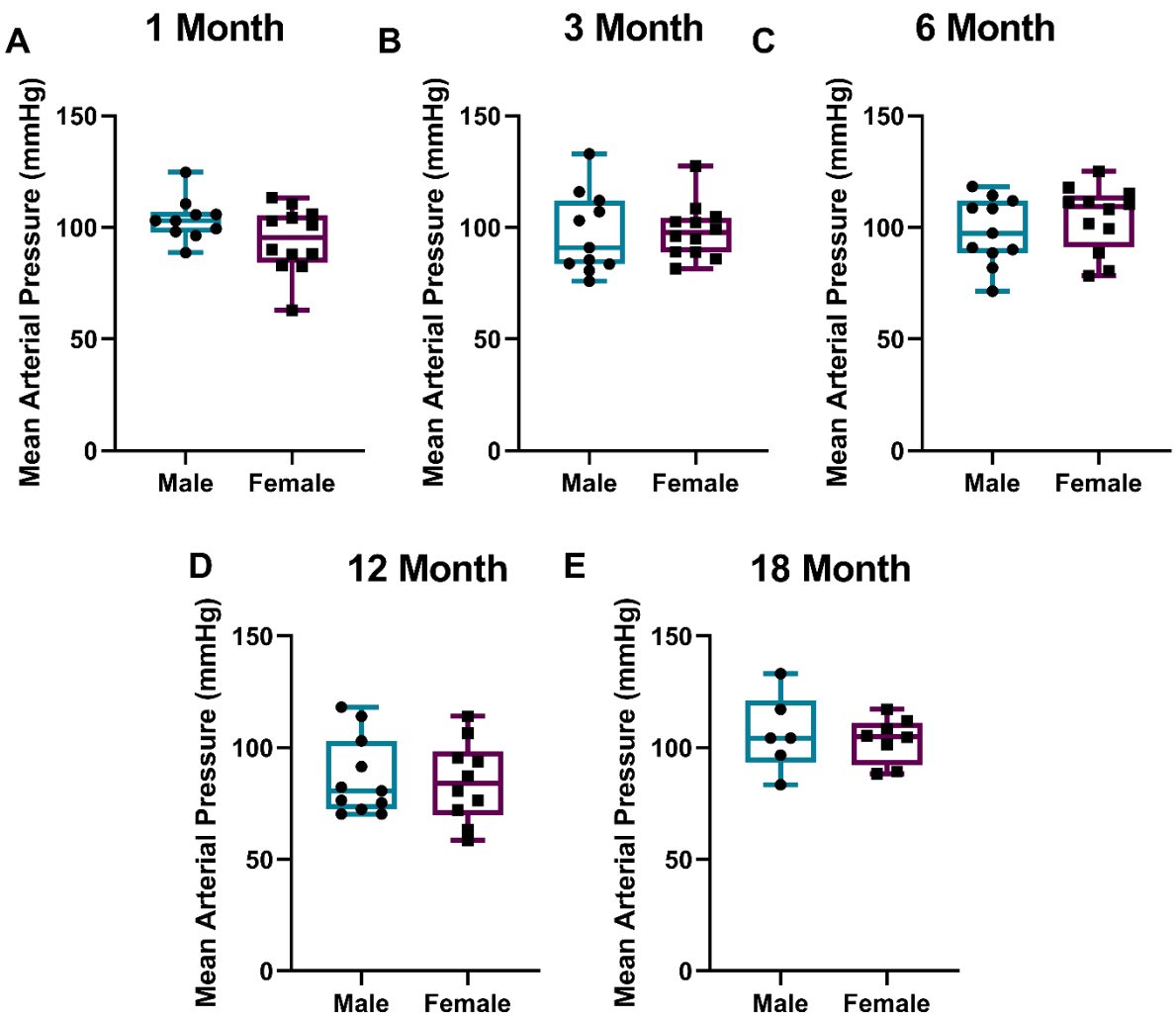

Figure 2. 14 Comparison of MAP between sexes across different aging timepoints. MAP measurements were taken at each imagine time point: 1 month (A), 3 month (B), 6 month (C), 12 month (D) and 18 months (E). Results reported as min to max range, n=7-14 males and n=7-14 females; Changes were assessed using a student's t-test; results were not statistically significant.

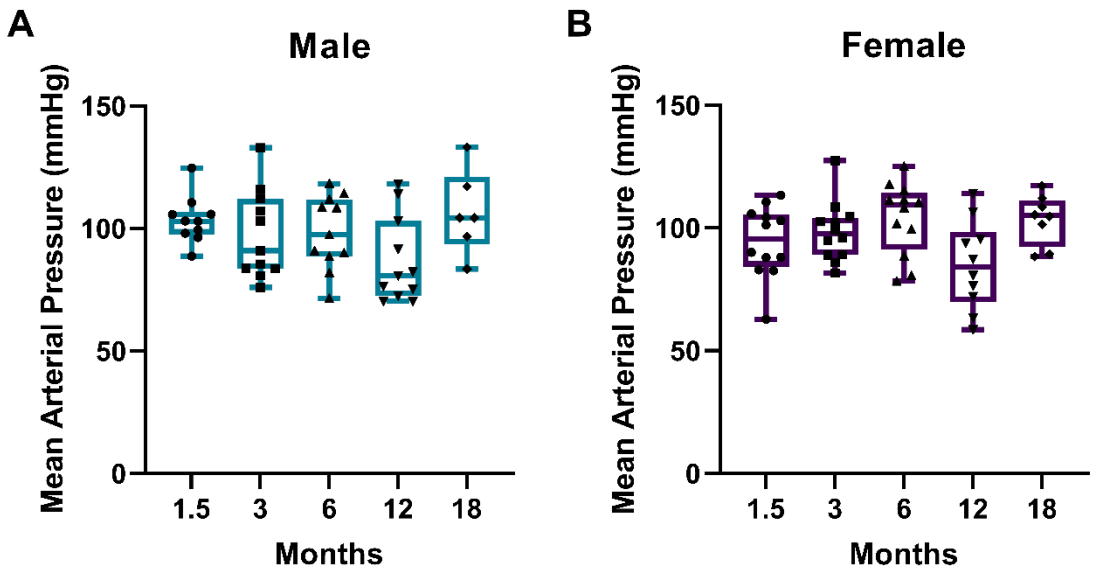

Figure 2. 15 Comparison of MAP by sexes across different aging timepoints. Longitudinal changes in males (A) and females (B) MAP over 18months. Results reported as min to max range, n=7-14 males and n=7-14 females; Changes were assessed using a Mixed-effects Analysis and Dunnett's Post-hoc test; results were not statistically significant

2.3.6 Ultrasound echocardiography reveals maintained cardiac function in aged animals, with significantly lower function in aged males

Structural and functional cardiac parameters were measured at the terminal aging timepoint only. Several parameters were measured including: Heart Rate (HR), LV mass, End-systolic Area (ESA) End-Systolic Volume (ESV), End-Diastolic Volume (EDV), End-Diastolic Area (EDA) and Ejection fraction (EF) as shown in Figure 2.16. Cardiac output, Fractional Shortening and stroke volume were also assessed, see Appendix Figure 7.1. Data was normalised to body weight as is standard practise, however, raw data can be seen in Appendix Figure 7.2. HR measurements in beats per minute (BPM) were compared between 18-month males and females, whilst no significant difference was observed, females showed a general trend towards higher HR than their male counterparts with an average 320 ± 25 BPM compared to male 300 ± 14 BPM (Figure 2.3.16 A). Males had a larger predicted LV mass (2010 ± 278 mg) compared to females (1433 ± 273 mg). ESV normalised to body weight showed no significant difference between males (0.33 ± 0.04 ml/kg) and females (0.33 ± 0.04 ml/kg) suggesting that, relative to body mass, sex did not affect ESV (Figure 2.16 B). Interestingly, EDV relative to body weight was significantly higher in females (1.10 ±0.12 ml/kg) compared to males (0.89 ± 0.14 ml/kg; p=0.002). Cardiac function was assessed based on EF, with all animals on study showing EF of between 60-75% at 18 months of age (Figure 2.16 E). Whilst function was maintained in older males with an average EF of 63 ± 2 %, females were found to have a significantly higher EF of on average 70 ± 4%, (p=0.004).

This suggests that females have better function than males at 18 months, with a potential decline in males with age. However, this study cannot validate whether this decline is present as all echocardiography measurements were only obtained at the terminal timepoint.

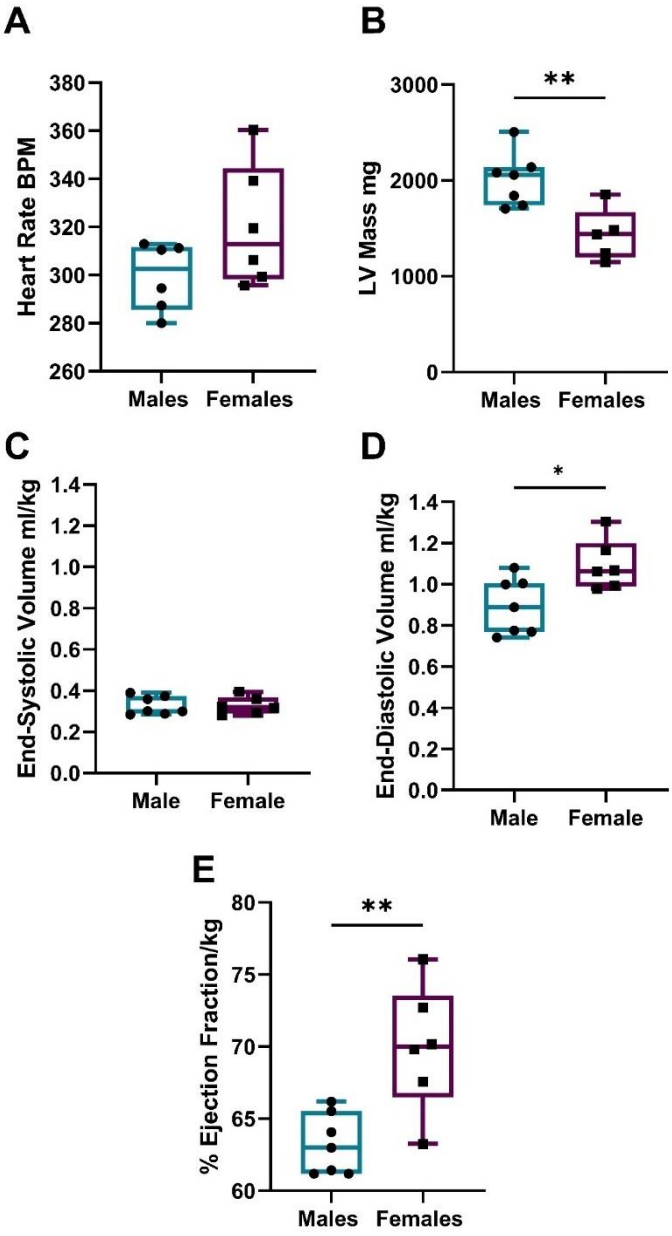

Figure 2. 16 Echocardiographic analysis of cardiac structure and function at the 18-month endpoint relative to body weight. Echocardiography measurements were taken at the terminal timepoints (18 months). Heart rate (A), LV mass (B), end-systolic volume (C), end-diastolic volume (D) and ejection fraction was assessed in both aged males and females. Results reported as min to max range, axis range was decided based on the physiologically 'healthy' ranges, n=7-14 males and n=7-14 females; p values were obtained using unpaired Students t-test when comparing two groups; *p<0.05; **p<0.01

2.4 Discussion

This second thesis chapter aimed to investigate the effects of natural aging on whole-body condition, frailty, and cardiovascular physiology in a Sprague Dawley rat model, with a particular focus on sex-specific differences. Based on our hypotheses, we expected a decline in survival rates and overall health with age, with male rats experiencing a greater reduction in survival and health compared to females. Additionally, we hypothesized that cardiovascular health would deteriorate more significantly in male rats as they age. To address these hypotheses, the aims of this chapter were threefold: (1) to examine the impact of aging on survival rates and assess potential sex differences, (2) to evaluate frailty and how it is affected by both aging and sex, and (3) to explore how natural aging and sex influence cardiac structure and function. Furthermore, this chapter sought to identify any underlying dysfunction in our model that may explain or contribute to observed outcomes. Our main findings related to natural aging are summarized in Figure 2.4.1.

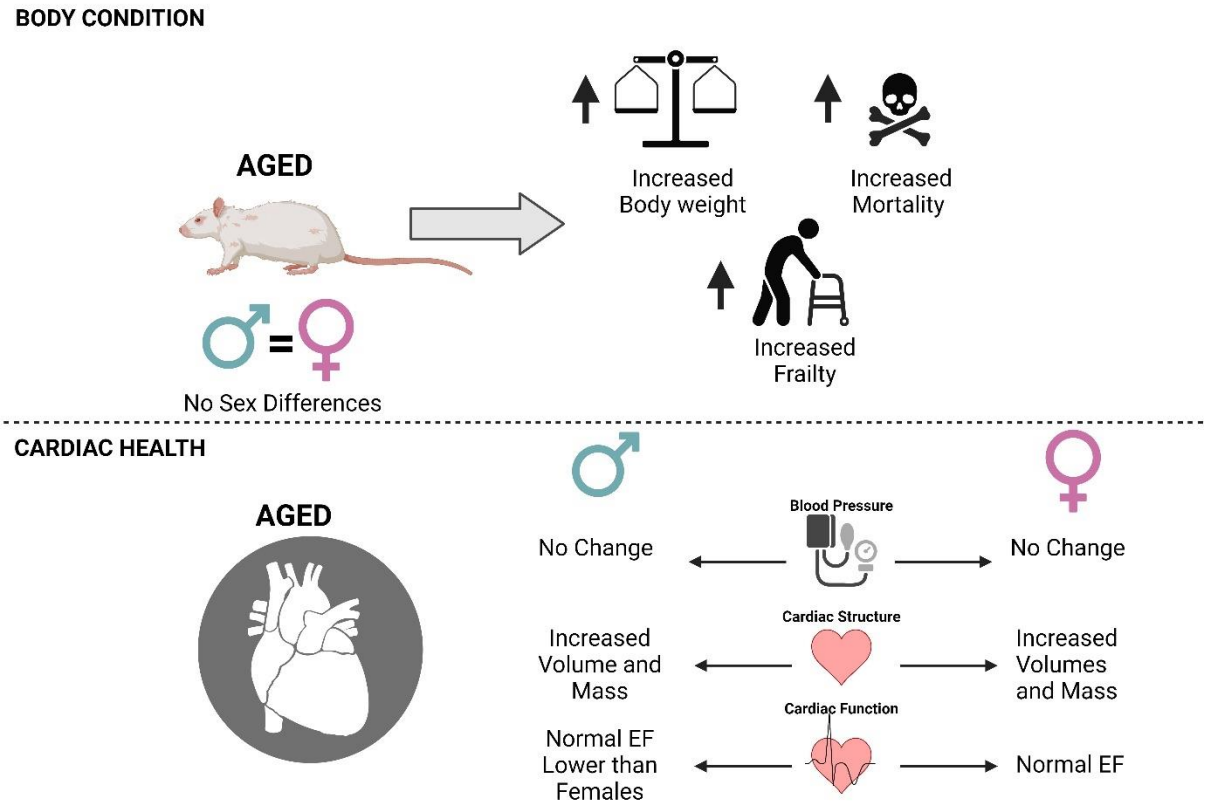

Figure 2. 17 Overview of key research findings from Chapter 2. Figure created using Biorender.

2.4.1 Natural aging leads to increased mortality from one year of age

Sprague-Dawley male and female rats showed increased mortality after 12 months of age, with many being culled for welfare-related health concerns. This led to the implementation of humane endpoints or sudden deaths increasing considerably after 12 months. In females, the incidence of mammary tumours greatly increased after 12 months and this is consistent with studies identifying that control female Sprague-Dawley rats have a higher incidence of mammary fibroadenomas than other rat strains (184). Similarly, other studies report a 57% tumour incidence in Sprague-Dawley females, of which 95% were mammary gland tumours (185).

Previous data suggests that a 90% survival rate is expected at around 20-21 months for control Sprague-Dawley rats (186). However, our study observed a lower survival rate of 61% at 18 months. This discrepancy may reflect the stringent welfare guidelines followed to prevent suffering in our study and the cumulative impact of interventions such as repeated imaging sessions, BP measurements and FI scoring. It is also important to acknowledge that the large reduction in animal numbers at the final timepoint could potentially have led to our study being underpowered and likely affecting the interpretation of results.

Interestingly, research suggests that the lifespan of laboratory rats is around 2-3.5 years, with some papers suggesting that one month for rats is equivalent to 2.5-3 human years (175). These findings imply that the human equivalent age of our final timepoint would be between 45-54 years, indicating that this study may be exploring early age-related changes rather than advanced aging. Other studies report the life expectancy of this strain to be closer to 2-2.5 years, suggesting a human equivalent age of around 65 years. This variation in the literature can complicate the interpretation of aging rodent studies, indicating that relying solely on chronological age as a marker of aging in rodents may not be the most appropriate metric (187, 188). Furthermore, life expectancy is significantly influenced by environmental factors such as cage size and enrichment. For instance, a study in mice found that acoustic environmental enrichment extended lifespans by 17% (189). Another factor to be considered is that studies suggest that the lifespan of commercially available laboratory rats have been declining (190). Similarly, in humans, chronological age often does not align with biological age, as research suggests that biological aging offers greater prognostic value (191). This discrepancy reflects differences in internal capacity, where individuals of the same chronological age may exhibit varying degrees of physiological function and resilience. Frailty, in particular, is increasingly recognized as a key marker of biological aging, offering insights into the internal capacity and overall health status of patients beyond their chronological years (191). These findings suggest that chronological age in

rodents and humans does not adequately represent the biological aging. Therefore, more in-depth measurements of frailty are necessary to better understand the impact of aging.

2.4.2 Natural aging leads to increased body weight and potential metabolic phenotype

This study identified that both male and female Sprague-Dawley rats showed significant increases in body weight over 18 months, the increase was greatest from 1 month to 3 months consistent with puberty related growth identified in the literature (192). As the animals aged, their body weight increased, but after 12 months, the rate of increase began to slow down and appeared to plateau around 18 months, as previously described (186, 188). Interestingly, studies have reported that peak body weight in Sprague Dawley rats is approximately 365g in females and 597g in male rodents compared to 460g in females and 861g in males in our study (175, 186). These findings when compared to those obtained within our study cohort may suggest that rats in our study have obesity phenotype with much higher average body weights in both male and female rodents. Furthermore, studies have suggested Charles River (CRL) Sprague Dawley have around 49% higher body fat compared to Harlan Laboratories (HAR) rats, suggesting they may have a very different metabolic profile compared to other strains such as fisher rats which may alter their physiological response to aging (192). Further studies would be required to validate this further utilising techniques such as promethion metabolic cages to compare differences in body mass, food and water consumption and physical activity amongst strains to fully understand strain variability on metabolic phenotype (193). Another potential cause for this high body weight could be due to the employment of *ad libitium* feeding which has been shown to increase body weight compared to more controlled feeding and is associated with increased heart weight, LV myocardial fibrosis, cardiac myopathy and renal abnormalities such as interstitial fibrosis (194). Although ad libitum feeding is common practice in many research studies, the sedentary nature of the rodents' lifestyle can promote obesity, which, while relatable to other studies, hinders a clear understanding of 'healthy' aging. Although our study did not delve further into this metabolic phenotype, it is important to consider its impact because of the strong, established link between obesity and the development of cardiovascular disease (195). Moreover, high adipose tissue prevalence has been associated with systemic inflammation and cancer development (192, 196). This problem isn't unique to Sprague Dawley rats occuring in other strains as well, where cardiovascular metrics are often unmonitored (190, 197). Growing concerns suggest that obesity may obscure disease mechanisms, reducing clarity in cardiovascular research (190, 197). Alternatively, some may argue that obesity in cardiac aging models may be beneficial given the known association of obesity and CVD development, however in the case of ‘healthy’ aging it reduces clarity of intrinsic aging mechanisms. Therefore, this study outcomes must be considered in conjunction with the impact of

Sprague Dawley genetic background on fat metabolism and its implication on natural aging mechanisms on a whole organism level as well in terms of cardiac health.

2.4.3 Increased frailty in cohort suggests advanced biological aging in cohort

Frailty has been defined as the presence of increased vulnerability to adverse health consequences (198). FI have been utilised in aging research due to the high variability in preclinical animal model lifespans and the need for a greater metric of biological age, as described previously. This study identified that both male and female Sprague Dawley rats showed significant increases in frailty at 18 months of age. This suggests that the increased frailty observed in our aging animals' points to advanced aging with an increased risk in mortality. This study is the first to utilize FI scores in healthy aging Sprague-Dawley rats, and therefore, there is limited information available for direct comparison with our results. Although some progress has been made in frailty assessments of rats, the value is limited by the lack of research in this area and the simplified criteria used for aging rats compared to human clinical frailty indexes (199, 200). Its relevance to the human condition is not yet fully understood; however, it is evident that higher FI scores are associated with accelerated aging and a heightened risk of death (200). It is important to note that most frailty assessments in preclinical research have focused on characterising natural aging in mice through adaptation of clinically utilised assessments (200). These studies have identified that mice show increased frailty at a similar rate to humans providing key context to aging studies, whilst little is understood about the equivalent in rats (179). Further developments have been made to allow for more clinically relevant FI measurements in rats through a more comprehensive set of criteria looking at strength using wire suspension challenges, speed using rotarod assessments, physical activity through open field assessment and endurance with an inclined screen (201). These measurements offer a more stringent criterion for assessing frailty through quantitative measures of physiological function, which were not assessed in this project due to their high technical and time demands. It is also important to acknowledge that the FI used here might be considered more subjective, given its qualitative nature and the potential for assessor bias. To mitigate this, all measurements were conducted by the same individual, ensuring consistency. Future aging studies should incorporate these quantitative measures to improve frailty assessments, which is essential as rats remain central to aging research (25). Finally, frailty has been identified to correlate with cardiac function in a sex-specific manner when comparing parameters such as EF, which were found to increase in male mice with increasing frailty but have no effect in females when measured using echocardiography (202). Frailty has been shown to promote maladaptive remodelling in both chamber types in the heart, increasing cardiac vulnerability to CVDs as

summarised in this review by Bisset et al., (203). Together, this study suggests that at 18 months Sprague Dawley rats exhibit clear signs of advanced aging with significantly increased frailty.

2.4.4 No underlying hypertension observed and therefore age-related changes are likely due to intrinsic aging mechanisms

Hypertension has long been linked to age-related cardiac hypertrophy and fibrosis, with aging causing vascular stiffening which contributes to the increased BP (159). Therefore, our study aimed to characterise whether our cohort developed longitudinal age-related changes in BP which may contribute to our later findings. Over 18 months, both males and females exhibited no significant change in MAP. This suggests that aging has no impact on BP in our cohorts. This lack of change in MAP has been reported in control animals up to 12 months where BP was measured using radiotelemetry, however no sex was specified in this study (204, 205). Similarly, MAP measurements in anaesthetised animals showed no significant effect of age between rats up to 24 months (206). Contrastingly, many studies have identified that MAP increases with age in a range of preclinical models such as sheep, rabbits, rats and mice (207, 208). In mice, MAP was found to increase in males at 14 months and plateau, where as in females MAP significantly increased at 18 months (207). This suggests that our study may not have identified the clear age-related changes observed in other studies, potentially due to the technique utilised and the loss of animals across the study. However, fully contextualizing our results remains challenging due to the scarcity of studies focusing exclusively on aging. Consequently, there is little literature on BP in healthy aging to provide reference values, despite the increasing interest in understanding aging mechanisms. Furthermore, studies that include aged controls in disease research often use only a single time point, resulting in very few longitudinal comparisons of changing BP values and strain specific information. In humans, aging was thought to lead to an inevitable increase in BP however, in some populations it is not observed highlighting that lifestyle and environment influence BP, causing it to increase with age (209).

In our study, males showed a relative decrease in diastolic BP at 12 months, while females experienced a significant increase in systolic BP at 18 months. However, our results clearly show that our animals do not exhibit overt hypertension, as all values fall within ‘normotensive’ ranges, defined in the literature with systolic BPs falling below 140 mmHg (204). This has been observed previously with studies in Sprague Dawley rats, where systolic BP increased from 1 month – 12 months but animals remained normotensive suggesting that our animals do not have any overt vascular dysfunction at 18 months (204). This provides key context for the following imaging studies in Chapter 3 and Chapter 4 as some studies suggest that the underlying cause of age-dependent fibrosis is hypertension (60, 210).

However, in this study we can assume that all changes are independent of BP changes. No notable sex differences were observed in MAP, systolic or diastolic BP in this study. In Long-Evans rats sex differences have been observed with females having lower BPs than age-matched males till 14 months, following this point advanced aging showed this sex specific advantage is lost suggesting that the reproductive lifespan of a female rat influences BP. This was also observed in Sprague Dawley rats up 20 months of age (211). Similarly, studies reported elevated MAP was observed in 5 month males with one study in C57BL/6 mice compared to female counterparts, though both sexes were normotensive (204). Furthermore, lower arterial pressure has been observed in adult females across species such normotensive dogs, sheep and rabbits (212). Interestingly, a study completed by Deschepper et al., in 13 different mouse strains identified sex differences in systolic blood pressure in only 4 strains suggesting that strain should be considered when attempting to recapitulate human aging (213). In human aging both sexes show increased BP, however, following menopause females were identified to have a rapid increase in BP compared to male counterparts, with the incidence of hypertension greater in aged females than aged males and pre-menopausal women suggesting that advanced aging influences female specific changes in BP (214). Given the known protective nature of E2 on cardiovascular health as described in Chapter 1, research has suggested that loss of E2 may contribute to hypertension development (215). Interestingly, in Sprague Dawley rats of menopausal age (450-600 days) were not found to have menopause associated BP increases, highlighting key species specific physiological differences (207, 212). Considering that the majority of our rats were, or could have been, premenopausal, it is relevant to discuss how this may have influenced our findings, particularly regarding the absence of menopause-related cardiovascular changes. This raises important considerations about the timing of physiological transitions and their potential impact on our study outcomes.

It is important to note that the significant changes we observe in male diastolic BP at 12 months and female systolic BP at 18 months should be interpreted with caution. This is primarily due to the high level of variation observed throughout the study due to low numbers, as described previously. The variation can also be attributed to the technique used as tail-cuff measurements can induce a stress response in spite of carefully carried out acclimatisation and measurement is also greatly affected by the environment (216). As set out by the editors of Hypertension, differences in non-invasive tail-cuff measurements should be only considered if they exceed 15 to 20mmHg, this suggests that the significant changes observed in this study should be considered with caution (216). Some researchers suggest that invasive radiotelemetry measurements are a much more robust method of blood pressure measurement due to the constant and direct measure of BP which leads to much less intra-group experimental variability (216). Studies comparing the two methods found significant differences

with one-off measurements, but when repeated measures were taken, the values showed moderate correlation (217). Considering the longitudinal nature, whilst radiotelemetry would have provided a more accurate and less variable BP measurements, tail-cuff can be seen as more appropriate as the animals underwent several interventions at each timepoint and therefore introducing an invasive surgery could have compromised the experiment. Taking these factors into account alongside the long-term nature of the study, the high running cost of telemetry experiments and the variation observed, tail cuff was still the appropriate method of assessment to understand average pressure over a longer period of time.

2.4.5 Preserved function overall, but males exhibit slightly reduced function and greater increases in cardiac volume compared to females

This project focused on the effect of aging on the cardiovascular system, therefore, the overall structure and function of the heart was assessed over 18 months. In this study, cardiac volume was evaluated using CT imaging. Both male and female Sprague Dawley rats exhibited significant increases in cardiac volume at each time point over 18 months. This has been observed in many aging studies with both male and females showing increased LV volume and mass increases with aging (81, 211). In humans, normalised cardiac mass is found to be 4-9% larger than females (218). However, this large difference observed in cardiac volume in aging can be attributed to not just body weight but also due to adverse cardiac remodelling which is much more prevalent in males (207). It is also worth noting that our measurement provides a general estimate of heart size, but it has limitations. For instance, the CT scan does not isolate measurements taken at diastole or systole but rather captures a composite view that includes both phases. Additionally, results are presented as both raw and normalized values. Normalizing geometric parameters to body weight is a common practice in both clinical and preclinical analysis (183). However, this normalization assumes isometric growth, which may not apply in cases of obesity (183). In such scenarios, an allometric approach might be more appropriate. This could be particularly relevant for this group of rodents, given that the average body weight of a Sprague Dawley rat varies significantly and our cohort contains the possibility of a metabolic phenotype (183).

It is well understood that the cardiovascular system undergoes various structural and functional changes with increased age (53). Therefore, we aimed to characterize cardiac structure and function at the terminal time point. Both aged males and females exhibited average heart rates above 300 BPM, indicating that the anaesthetic did not excessively depress cardiac function. This is vital as many studies have identified that anaesthetic such as isoflurane, xylazine and ketamine can depress cardiac

function (219). However, a study conducted by Murakami et al. confirmed that compared to other anaesthetic agents isoflurane has the least effect on cardiac function and is more stable (220). These heart rates are comparable to those found in healthy 4-20 week Sprague Dawley rats, suggesting that cardiac function remained within physiologically 'healthy' ranges in our cohort (211). Previous research has shown that 12-month-old control rats had higher heart rates (354±27 BPM) via radiotelemetry compared to our study (205). Although aging is associated with a decline in heart rate, cardiac health is often maintained despite this decrease (221). In our study, 18-month-old females had significantly higher heart rates than males, a pattern observed in Sprague Dawley rats up to 25 months of age (221). While this difference may be due to smaller body weight, sex-specific autonomic regulation of the heart could also play a role. Importantly, both sexes remained within healthy reference ranges.

Our study found that aged male rats had decreased EDV compared to their female counterparts, while no significant difference was observed in ESV. This aligns with some studies reporting that aged males have higher EDV and cardiac output than females(211). However, other research shows a decline in end-diastolic volume in aging males(53). In wild-type mice, both end-systolic and diastolic volumes increase with age in both sexes (222). The variability in findings may be due to the fact that many preclinical studies focus solely on males, highlighting the need for more research that includes females—especially in aging studies where sex differences in clinical outcomes are evident.

In terms of cardiac function, our study showed that aged males had a lower EF compared to females. This suggests a slight decline in cardiac function in males, despite both sexes maintaining healthy ejection fractions within the 60-75% range (223). While the literature is inconsistent, with some studies reporting no sex differences in EF or fractional shortening in aging rats (211), others report a decline in EF with age in males (53). In aging humans, this trend is also observed, with females generally having higher EF than males (224). The reduced function seen in males may be attributed to several factors. Some studies suggest that age-associated declines are linked to ECM deposition and cardiomyocyte hypertrophy, leading to increased LV stiffness and reduced contractility (190). Other studies propose that females may naturally have higher baseline EF, as evidenced in human MRI studies (225). Additionally, disrupted calcium regulation and increased oxidative stress have been implicated in the decline in male cardiac function (53, 226, 227). Overall, our findings indicate that while both cardiac structure and function are generally preserved in aging rats, males exhibit a slight impairment in function—characterized by decreased EF and lower end-diastolic volume—compared to females. This reflects trends observed in human aging, where similar sex differences in cardiac function are evident.

The interpretation of the effects of aging on cardiac function in this study is somewhat limited because imaging was conducted only at the final timepoint. This decision was made due to the high cost of imaging and to avoid repetitive prolonged sessions of anaesthesia, as this animal cohort also underwent 10 PET/CT imaging sessions under anaesthetic. Therefore, minimising prolonged exposure was essential to reducing the chronic cardiac, respiratory and neurological effects of repeated anaesthesia (228). The absence of longitudinal data makes it difficult to assess whether cardiac function is declining over time. Additionally, while there are previously described values, the data was not always be comparable due to the underrepresentation of females in studies or the absence of age and sex-specific analyses. However, echocardiography is a well-established and reproducible technique, which allows for a reliable understanding of generally healthy physiological values (211). Another factor that may influence the accuracy of the echocardiographic measurements is the large body weight of the animals, which led to difficulties in producing a clear visualization of the hearts due to image artifacts created by the lungs. Consequently, we were unable to perform Doppler analysis and strain analysis, which would have provided more detailed information regarding potential damage to the hearts in aged animals. Many of our measurements were obtained using the M-mode function, which can be prone to error, as it captures data from a single plane and may miss variations in the myocardium above and below the imaged slice (222). This is a limitation of our study, however considering the large size of the animals, imaging artifacts caused by the lungs, and the limitations of the ultrasound probe made this the only viable approach for our cohort. However, despite these limitations, the echocardiography approach used was the best possible option given the constraints related to animal welfare, the cost of scanning, and the lack of availability of ultrasound probes suited for larger animals.

2.4.6 Conclusion

In this chapter, we discussed the impact of aging on wild-type Sprague Dawley rats to characterize the effects of natural aging and examine whether sex influenced the severity of changes in survival and frailty. We found that aging leads to a deterioration in body condition and subsequent survival on a whole-organism level, and that this is not influenced by sex up to 18 months of age. This partially supports our hypothesis that age causes a decline in physiological health; however, males did not show a greater decline in overall body condition than females.

In this chapter, we explored the effects of natural aging on cardiac structure and function in Sprague Dawley rats, with a focus on sex differences. While the overall trajectory of cardiovascular aging was

similar between sexes, notable differences emerged in cardiac volume, end-diastolic volume, and ejection fraction. Specifically, aged males exhibited lower cardiac function compared to females, which supports part of our hypothesis that male rats would experience a greater decline in cardiovascular health with age. However, despite these differences, all measured cardiac parameters remained within ranges consistent with efficient function, suggesting that while males may experience a slight reduction, function is still largely preserved. This partially supports our hypothesis that cardiovascular health declines with age, but the extent of decline in males was less severe than anticipated.

These findings highlight the need for more detailed studies investigating sex-specific strain differences in aging models. Additionally, they underscore the importance of carefully characterizing aging cohorts in each experimental setup to distinguish changes driven by biological aging from those influenced by chronological age. Future research should aim to better understand how these sex-specific differences in cardiovascular function manifest and the underlying mechanisms responsible for them, particularly in the context of healthy aging.

Overall, this study also partially supports our hypothesis that aging would cause a more significant decline in health in males than in females, but our findings indicate that this difference was more pronounced in cardiac function than in overall survival or body condition. While we observed lower cardiac function in aged males, survival and frailty outcomes did not show a greater decline in males compared to females up to 18 months of age. Therefore, the results point to a need for more sex-specific investigations to fully understand the role of sex in aging-related physiological changes.

In the next chapter we looked to explore the effect of age and sex on cardiac collagen metabolism, assessing both *in vivo* and *ex vivo* collagen synthesis and metabolism respectively.

Chapter 3 – *The Impact of Age and Sex on Ventricular Collagen Metabolism*

3.1 Introduction

As individuals age, the risk of heart disease increases, and this progression often differs between men and women due to sex-specific physiological changes. One key factor in this process is collagen metabolism, which is vital for maintaining the structure and function of the heart. With aging, the ventricular ECM undergoes significant remodelling, leading to increased collagen deposition and crosslinking. This excessive collagen accumulation disrupts normal cardiac function and contributes to the stiffening of the heart. Research indicates that aged males typically experience greater collagen build up than females, though this sex difference diminishes following menopause (88). Despite these findings, many aspects of how aging influences collagen metabolism and its impact on heart disease, particularly in relation to sex differences, remain poorly understood, presenting a critical gap in the literature (88).

This third thesis chapter aims to elucidate the effects of aging on collagen metabolism in the LV and RV. The primary focus is on the quantitative analysis of ventricular collagen synthesis, which has not been assessed longitudinally in the context of cardiac aging. Current methods for evaluating collagen synthesis heavily rely on gene expression analysis and specific procollagen proteins. However, these approaches offer only a limited perspective, as mRNA levels do not consistently correlate with protein expression (229). Protein synthesis often lags behind mRNA synthesis, and post-translational modifications can further disrupt this correlation, rendering many mRNA findings less informative or even redundant (229). Furthermore, focusing on procollagen subtypes like PIP provides a limited view of the complex changes in collagen metabolism (103). Clinically, these markers are measurable only in serum, serving as indirect indicators of collagen synthesis rather than specifically reflecting cardiac collagen synthesis (103).

This thesis chapter will evaluate hydroxylated (structural) and unhydroxylated (interstitial) collagen synthesis and compare these findings with established *ex vivo* methods of collagen quantification. These two collagen types play essential roles in scar formation after injury, with hydroxylated collagen generally associated with replacement fibrosis and unhydroxylated collagen linked to reactive fibrosis (162). Previous research has demonstrated differential changes in hydroxylated and unhydroxylated collagen synthesis across cardiac injury models, such as MI and angiotensin II-induced pressure

overload (162, 165). With MI causing temporal changes in the both forms of collagen synthesis whilst in pressure overload greater changes were observed in hydroxylated collagen synthesis which suggest that more replacement like fibrosis occurs in this model but little reactive fibrosis (162, 165).

In aging, however, the distinct forms of fibrosis have yet to be examined *in vivo*, leaving it unclear whether these mechanisms occur in age-related fibrosis. Therefore, assessing both types of collagen synthesis in this study will provide valuable insight into the specific fibrotic mechanisms associated with aging.

Hypotheses:

- Ventricular cardiac collagen accumulation increases *in vivo* with age with a higher rate of deposition observed in male rats compared to female rats.
- Over the course of natural aging the rate of ventricular cardiac collagen synthesis declines *in vivo* with age in rats.
- A higher rate of cardiac collagen synthesis will be observed in male rats compared to female rats.
- Ventricular collagen synthesis can serve as a valuable prognostic indicator for predicting age-related changes in ejection fraction.
- Changes in collagen synthesis correlate with collagen deposition in the myocardium.

The aims of this chapter are as follows: 1) To investigate the effect of age and sex on ventricular collagen synthesis *in vivo*, 2) To determine whether age-related ventricular collagen synthesis changes in a sex-dependent manner, 3) To assess whether ventricular collagen deposition increases in an age- or sex-dependent manner, 4) To compare these two processes to determine if changes in synthesis correlate with collagen deposition in the tissue and 5) To assess whether collagen synthesis rates can serve as predictors of cardiac function during aging, offering potential prognostic value in the case of age-related CF.

3.2 Materials & methods

To address the study aims and hypotheses, a longitudinal *in vivo* study was designed involving serial PET/CT scans using the proline amino acid-based tracers *cis*- and *trans*-4-[^{18}F]fluoro-*L*-proline as illustrated in Figure 3.1. In a separate set of experiments, rodents were sacrificed at identical time points for tissue collection and analysis. This study aimed to comprehensively quantify and assess each stage of the collagen cascade, including procollagen, soluble collagen, insoluble collagen, hydroxyproline content, and total collagen deposition.

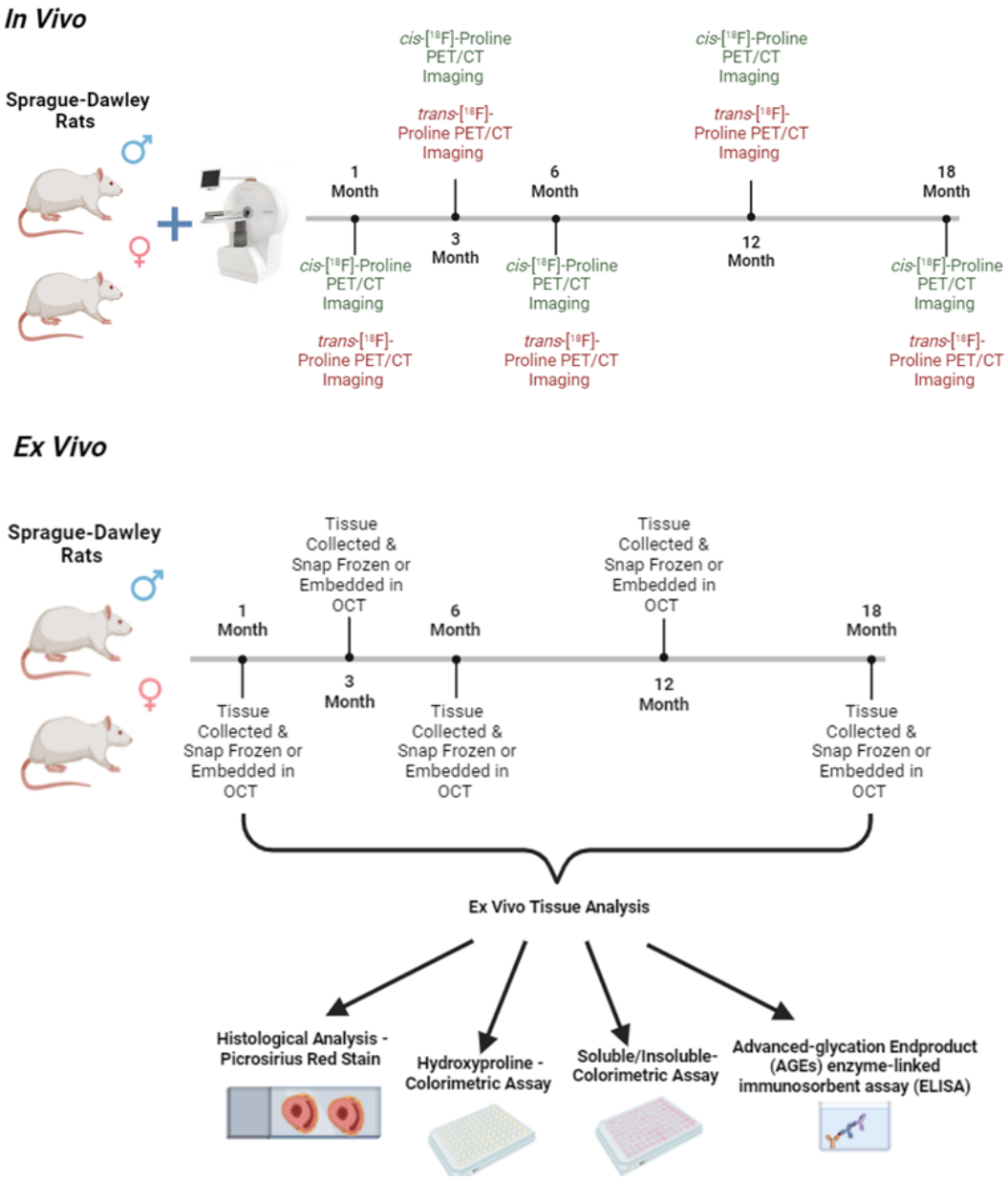

Figure 3. 1 Schematic of *in vivo* and *ex vivo* study design for assessing collagen synthesis and accumulation over an 18-month period. Figure created using Biorender.

3.2.1 Animal care and experimental handling

All *in vivo* experiments were carried out in accordance with the Home Office Animals (Scientific Procedures) Act 1986 and experimental plans were approved by the University of Edinburgh animal welfare and ethical review committee. All *in vivo* data is reporter according to the ARRIVE recommended criteria (182). Animals used for *in vivo* study were 3 week old Sprague-Dawley rats (Charles River, Tranent) and were given 1 week to acclimatise. . Animals were housed initially housed on cages of 2-3 however at later stages (12-18 months) due to loss of animals some animals were single housed. Animals were housed under standard conditions with a 12 h light: 12h dark cycle (7am – 7pm lights) at 22±2◦C and 55% humidity. Animals were provided weekly with enrichment such as wooden balls, tunnels and sizzle nest. Sample sizes were calculated based on power calculations, completed prior to commencement of study. The animals in this study (males: n=14, females: n=13) were the same as those in Chapter 2, enabling comparison of PET and physiological outcomes. Due to technical challenges (e.g., deaths during scans, failed reconstructions), not all scans were included in the final dataset (Table 3.1). Longitudinal assessments were conducted from 4 weeks onward, with average ages detailed in Table 3.2.At each timepoint bodyweights were collected. It should be noted due to the increased prevalence of foot pressure sores as a result of sedentary behaviour from 12 months animals were exercised for 15 mins, twice a week for the remainder of the study.

Table 3. 1 Longitudinal imaging aging study animal numbers per radiotracer.

	Number of Animals Studied					
	SEX	**1 Month**	**3 Month**	**6 Month**	**12 Month**	**18 Month**
cis-[18F]-Pro	**Males**	14	11	11	11	7
	Females	13	12	12	9	7
trans-[18F]-Pro	**Males**	11	10	11	11	7
	Females	12	12	11	9	7

Table 3. 2 Average age of animals for each imaging timepoint

	Average age (weeks ± SD)					
	SEX	**1 Month**	**3 Month**	**6 Month**	**12 Month**	**18 Months**
***cis*-[^{18}F]-Pro**	Males	5.2 ± 0.6	10.0 ± 0.5	25.4 ± 2.6	47.0± 2.4	66.7 ± 6.3
	Females	5.1 ± 0.6	11.2 ± 0.7	27.4 ± 2.5	52.2 ± 0.3	75.7 ± 4.6
***trans*-[^{18}F]-Pro**	Males	5.3 ± 0.8	10.3 ± 0.4	25.3 ± 3.0	47.7 ± 0.9	67 ± 4.7
	Females	5.7 ± 0.8	11.4 ± 0.6	28.3 ± 2.9	52.7 ± 0.3	74.6 ± 6.7

3.2.2 Radiosynthesis of *cis*- and *trans*-4-[^{18}F]fluoro-*L*-proline

Precursors were obtained from Prof Andrew Sutherland's research group, University of Glasgow and the method of synthesis for each radiotracer has previously been described by Morgan et al., (161). Radiosynthesis of *cis*- and *trans*-4-[^{18}F]fluoro-*L*-proline was carried out on the TRACERlab FX_{FN} synthesiser (GE Healthcare Technologies, Inc, Chicago). [^{18}F]Fluoride was generated following cyclotron irradiation of a [^{18}O]water target via the $^{18}O(p,n)^{18}F$ nuclear reaction. Following, trapping of the activity onto a Sep-Pak® QMA Carbonate Plus Light cartridge (Waters, Ireland) preconditioned with 10 mL water (sterile water for injections, ABX, Germany), a solution of Kryptofix® 222 (15 mg) (Merck KGaA, Germany) and potassium carbonate (2.4 mg) (Sigma- Aldrich, Spain) in acetonitrile (0.8 mL) (>99.9% pure, Acros Organics, USA) in 0.8ml if acetonitrile (>99.9% pure, Acros Organics, USA) and water (0.4 mL) was used to wash out activity. The solution was mixed for 2 minutes at 100◦C under vacuum and helium gas steam to dry and washed with acetonitrile, this step was repeated twice. The [^{18}F]Fluoride was dried using a full vacuum and then the precursor di-tert-butyl(2S,4R)-4-(tosyloxy)pyrrolidine-1,2-dicarboxylate (5 mg) for *cis*- 4-[^{18}F]fluoro-*L*-proline or di-tert-butyl (2S,4S)-4-(tosyloxy)-pyrrolidine-1,2-dicarboxylate for *trans*- 4-[^{18}F]fluoro-*L*-proline was added to 1 ml of acetonitrile and heated to 110◦C for 15 min with continuous mixing. The reaction was cooled to 60◦C and then 4M hydrochloric acid (HCl) (1.0ml) was added at a final concentration of 2M HCl. The reaction was mixed for 5 min at 60◦C and concentrated using a stream of helium under vacuum and then cooled to 30◦C and diluted using 50% aqueous acetonitrile solution (2ml). The reaction mixture was run through a high-performance liquid chromatography (HPLC) injector loop for purification using the semipreparative HPLC with SYKMN S1122 solvent delivery system using a Luna 5µm NH_2 100 Å, 250 × 10 mm column (00G-4378-N0, Phenomenex, USA). The mobile phase was comprised of 60% acetonitrile solution (>99.9% HPLC grade, Fisher Scientific, Belgium) in water (filtered deionised water with Millipore Direct Q pump, Germany) and released at a flow rate of 4ml min^{-1}. The radiolabelled

compound was detected via HPLC gamma-detector and collected at 9 minutes for *cis*- 4-[^{18}F]fluoro-*L*-proline or 7 minutes for *trans*- 4-[^{18}F]fluoro-*L*-proline. The radiotracers were transferred to the collection flask which contained 20ml of sterile water and transferred onto an Oasis MCX Plus Short cartridge (Waters, Ireland) which was prepared with ethanol (5 mL) (Rotem Industries, Israel) and then with water (10 mL). The product was pH adjusted and analysed using a Luna 5 µm NH_2 100 Å, 250 × 4.6 mm column (00G-4378-E0, Phenomenex, USA), the mobile phase used was 60% acetonitrile solution in water at a flow rate of 1ml min^{-1}. Product detection occurred using HPLC gamma counter and a UV wavelength of 210nm together with nonradioactive standards. The product was assessed to have a radiochemical purity of over 95% and a high molar activity as reported previously (*cis*-[^{18}F]-fluoro-*L*-Proline; >0.641 GBq µmol–1; *trans*-[^{18}F]-fluoro-*L*-Proline: >0.320 GBq µmol–1)(161)

3.2.3 PET/CT imaging

Male and female rats underwent longitudinal *in vivo* imaging at 1, 3, 6, 12 and 18 months of age. For all imaging sessions, anaesthesia was induced and maintained with 1.5–2.5% isoflurane (50/50 oxygen/nitrous oxide, 1 l/min). Heart rate and respiration rate were monitored throughout using monitoring probes from the PET/CT scanner. An intravenous (i.v.) line was established in the tail vein for bolus PET radiotracer injection. Body temperature was maintained at 37°C and monitored by rectal thermometer.

Following induction of anaesthesia, *cis*-4-[^{18}F]fluoro-*L*-proline (bolus i.v. tail, 150-300 µL) was administered and 90 min dynamic PET acquired before animals were recovered. At 48-72 hours post recovery, animals were anaesthetised and imaged for 90 min (starting from t=0) following administration of *trans*-4-[^{18}F]fluoro-*L*-proline (bolus i.v. tail, 200-500 µL). Immediately after each PET imaging acquisition, CT images were acquired within the selected field of view. Average injected doses of each tracer are summarised in Table 3.3.

Table 3. 3 Average injected dose of cis- and trans-4-[^{18}F]fluoro-L-proline at each scanning time point.

	Average Injected Dose (MBq/mL Injected ± SD)					
	SEX	**1 Month**	**3 Month**	**6 Month**	**12 Month**	**18 Month**
***cis*-[^{18}F]-Pro**	**Males**	26.9 ± 8.53	26.8 ± 8.9	28.7 ± 5.9	27.5 ± 5.2	29.1 ± 6.0
	Females	26.6 ± 8.2	25.4 ± 7.5	26.8 ± 7.7	23.3 ± 5.1	25.4 ± 5.9
***trans*-[^{18}F]-Pro**	**Males**	24.0 ± 8.33	26.8 ± 8.9	29.5 ± 4.1	27.8 ± 5.4	25.5 ± 8.7
	Females	24.8 ± 6.2	25.4 ± 7.5	25.2 ± 7.4	27.8 ± 3.3	22.3 ± 7.7

PET data was acquired using a small animal PET/CT scanner (nanoPET/CT, Mediso, Hungary). A CT scan (semi-circular full trajectory, maximum field of view, 360 or 480 projections, 50 kVp, 300 ms and 1:4 binning) was acquired for attenuation correction. Following radiotracer administration, a 90-minute dynamic scan was obtained using 3-dimentional 1:5 mode and re-binned as follows: 18×10 sec; 2×30 sec; 1×60 sec; 2×2 min; 10×5 min; 6×10 min. Animals at the final imaging timepoint underwent ultrasound echocardiography imaging (see section 2.2.4, previous chapter) prior to PET/CT imaging and were finally culled using an overdose of 5% isoflurane with death confirmed via cervical dislocation. Cardiac section was completed post-cull.

PET data were corrected for randoms, scatter and attenuation and reconstructed using Mediso's iterative Tera-Tomo 3D reconstruction algorithm using the following settings: 4 iterations, 6 subsets, full detector model, low regularization, spike filter on, voxel size 0.4 mm in all 3 dimensions and 400-600 keV energy window. CT data was reconstructed using filter back projection: voxel size 250x250x250 µm, 40x40x40 volume size, and 100% cut off. For the CT scans, a semi-circular scan method was used, capturing images across 360 projections to achieve comprehensive visualization of the sample. Scans were performed at maximum field of view (12 cm) to ensure full coverage. The tube voltage was set to 50 kVp to optimize imaging quality, and exposure time for each projection was set to 300 ms to enhance resolution. Binning was applied at a ratio of 1:4, which aided in reducing noise while preserving detail.

3.2.4 Cardiac template development

A bespoke cardiac template was created through the *ex vivo* high-resolution CT imaging of a 6 month old male Sprague-dawley model rat heart. Tissue was obtained following perfusion fixation through the left ventricle using 1ml of heparin/PBS (100U/ml) (LEO Laboratories Limited, Denmark) followed by 1ml of cadmium chloride (100mM) (Sigma-Aldrich, Germany) to arrest the heart in diastole. The heart was then dissected and placed in 4% PFA (Epredia, US). The heart was subsequently imaged using high-resolution CT settings: Zigzag scan method, side view, maximum zoom, 720 projections, and exposure time per projection of 450ms. The image was then imported into PMOD 3.7 (PMOD Technologies, Switzerland), cropped and masked using pixel replacement techniques of -1000 HU voxels to 0 HU. The heart was then orientated to conform to the American Heart Association recommended orientation(230). Volumes of interest (VOIs) were manually drawn slice-by-slice to define each heart chamber: left ventricle (LV), right ventricle (RV) left atrium (LA) and right atrium (RA) and a VOI was placed in the LV-blood pool (LV-BP) – representative images of the high-resolution CT and cardiac template are shown in Figure 3.2.

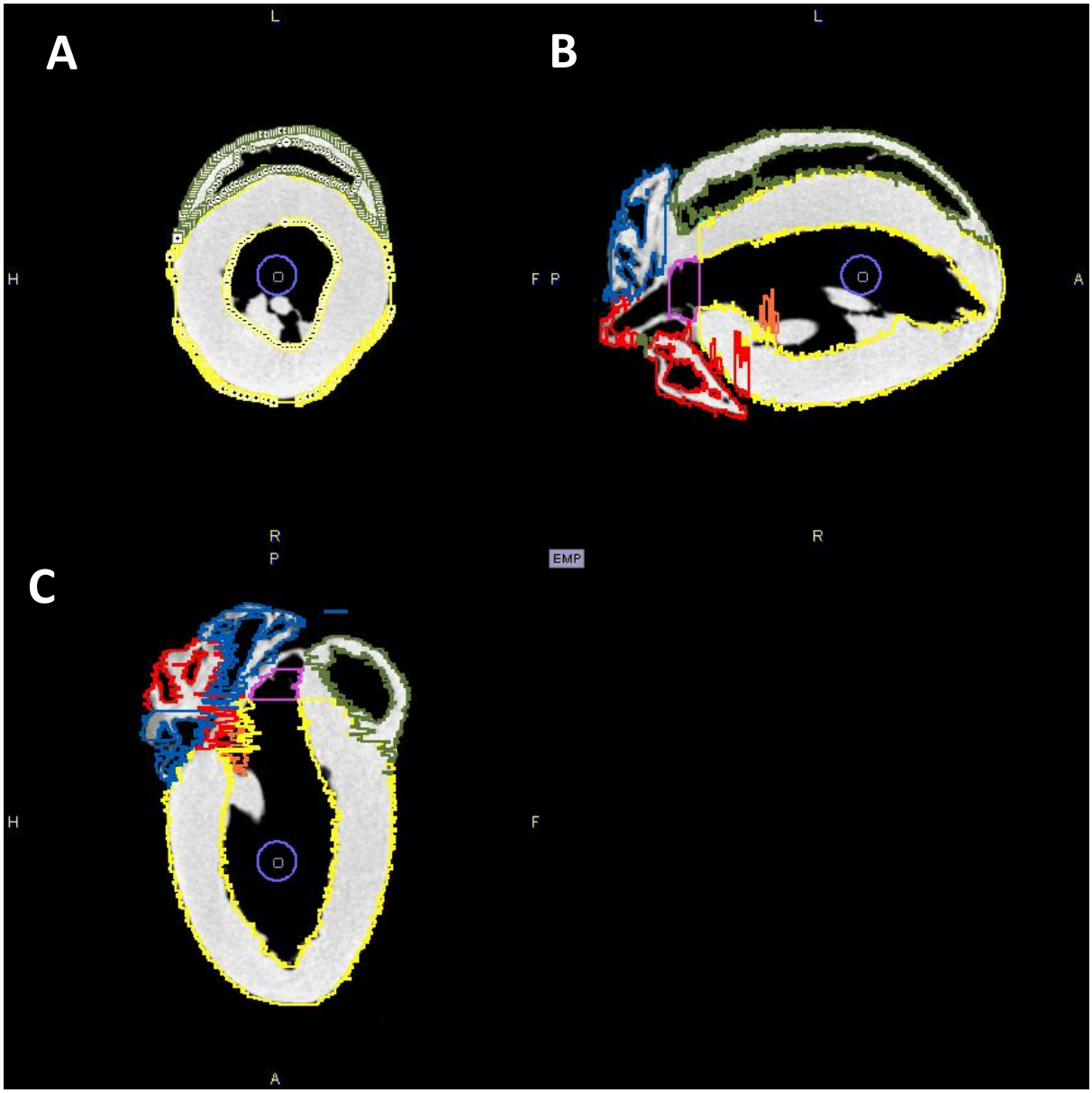

Figure 3. 2 Representative image of high-resolution CT and cardiac VOI template. *Ex vivo* high-resolution CT imaging was carried out cadmium enhanced PFA perfused heart and VOIs are outlined based on this image. Image shows the VOIs in transverse (A), coronal (B) and sagittal (C) planes. Yellow: LV; Green: RV; Red: LA; Blue: RA; Blue Circle VOI: Blood pool; Purple: Valve.

3.2.5 *In vivo* image processing and analysis

Image analysis was carried out blinded. Reconstructed *cis*- and *trans*-4-[^{18}F]fluoro-*L*-proline PET images were time-corrected, cropped and averaged across the last three frames (60-90mins) using PMOD version 3.7 (PMOD Technologies, Switzerland). Then, CT images were transformed to match in-house developed high-contrast cadmium enhance CT cardiac template (described in section 3.2.5) and the transformation was saved. The transformation was applied onto the PET image and the heart Volumes of interest (VOIs) template was applied to define each heart chamber, LV-BP, the aortic valve

and two tricuspid valves. Statistical data was then extracted for both PET and CT datasets. The average (from the last three frames) PET values were then normalised to the injected dose and animal weight to derive standard uptake values (SUV). SUV ratio (SUV_r) values were calculated based on the SUV of each cardiac VOI divided by the SUV of the LV-BP.

3.2.6 Tissue collection and freezing

Parallel to the longitudinal imaging aging cohort, male and female Sprague-Dawley rats (n=6-12/timepoint) were aged and sacrificed at 1, 3, 6, 12 and 18 months (from the imaging study) to match each equivalent imaging timepoint for *ex vivo* analysis. Animals were culled within two weeks of the targeted timepoint using overdose of isoflurane via inhalation method and death was confirmed using either cervical dislocation or decapitation. Blood and tissue samples (heart, kidneys, adrenals, liver, brains, pancreas, ovaries/testis, lungs and liver) were collected. Blood was collected via the vena cava using a syringe pre-rinsed with heparin (20 IU/ mL in saline; B. Braun Medical Inc., UK) and placed in blood collection tubes also precoated in heparin and spun at 2000g for 3 mins at 4◦C. Plasma (supernatant) was collected and place into Eppendorf tubes and stored at -80◦C.

The heart was dissected, kept on ice and then washed using PBS to remove remaining blood. The hearts were orientated with atria facing forward and sliced as described in Figure 3.3. The major blood vessels were removed and discarded. A blade was placed to divide the atria from the ventricles and then two 1-2mm sections were cut of the atria. The top section was placed in Optima cutting temperature (OCT) compound (CellPath UK Ltd, UK) and then snap frozen in isopentane (Merck Life Sciences, UK) and kept on dry ice at -40°C for snap freezing. The second atrial section was snap frozen using isopentane on dry ice at -40°C. Due to the smaller size of atrial tissue in the younger (1, 3 and 6 months) groups, whole atria were dissected and either placed in OCT or snap frozen. The ventricles were sectioned into three 2-3mm sections. The apex, the top section, was placed in OCT compound and then into isopentane kept on dry ice at -40°C for snap freezing. The next two ventricle sections were snap frozen using isopentane kept on dry ice at -40°C. The remaining organs were all snap frozen in isopentane and kept on dry ice at -40°C for snap freezing. All samples were then stored at -80◦C until ready to be utilised.

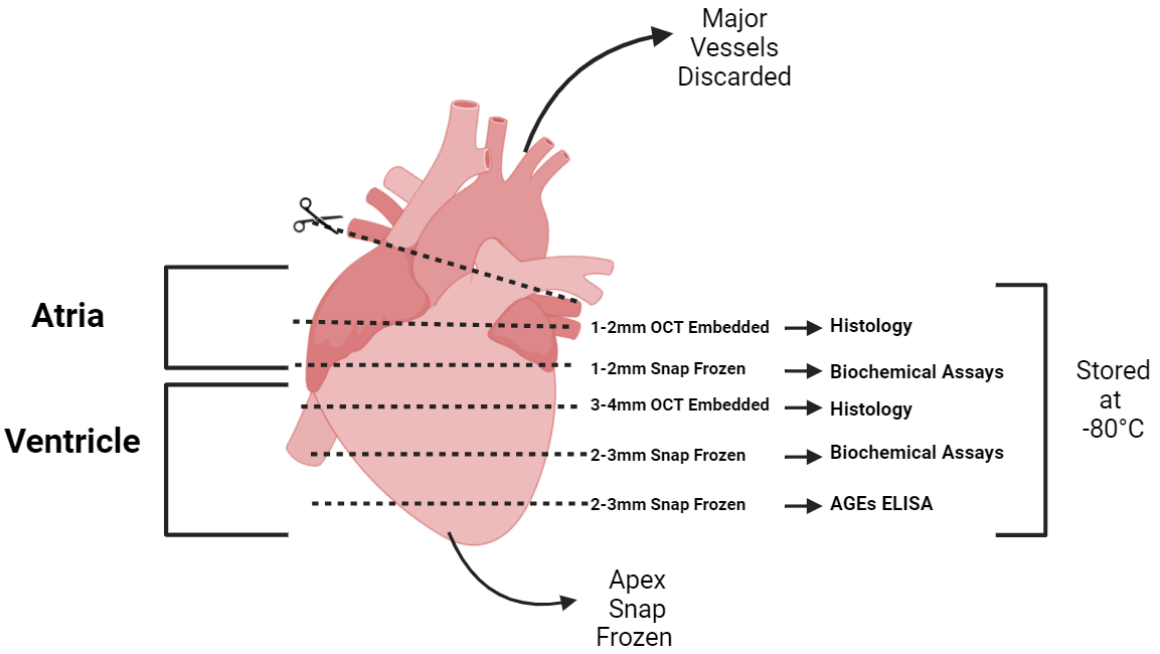

Figure 3. 3 Sectioning and processing of whole hearts for *ex vivo* analysis. Figure created using Biorender.

3.2.7 Cryosectioning

Tissue frozen in OCT was cryosectioned for histological analysis of total collagen content. Cryosectioning was carried out using a cryostat machine (CryoStar NX50, Thermoscientific, USA) at -18 °C to - 20°C and cryostat blades (MB35 Premier Microtome Blade, Epredia, UK) for each timepoint group. A guide plate (Glass anti-roll 69.5mm, Scientific Laboratory Supplies, UK) was utilised to ensure the cut tissue remained in place prior to adherence to slide. Tissue sections of 10µm thickness were cut and adhered to histological slides (two sections/slide) (Superfrost, Epredia, UK) for further analysis. A total of 114 samples were sectioned and stored at -80°C for subsequent use (Table 3.4).

Table 3. 4 Sample numbers for ventricular histological analysis.

Sex	Sample Numbers				
	1 Month	3 Month	6 Month	12 Month	18 Month
Male	6	6	6	6	6
Female	6	6	6	8	7

3.2.8 Picrosirius red histological staining

Picrosirius red (PSR) staining was performed on fresh frozen OCT embedded sections to assess total collagen. Optimisation of staining incubation was carried to ensure adequate staining that was comparable between the ventricles and atria without oversaturation of samples. A test cardiac sample from a 12-month male was utilized to assess different incubation time points: 15min, 30 min, 45 min and 60 min. Optimal incubation time was qualitatively assessed with 15min incubation (Fig. 3.4) showing best contrast of PSR positive (+PSR) staining in red compared to background (yellow) in both atria and ventricles.

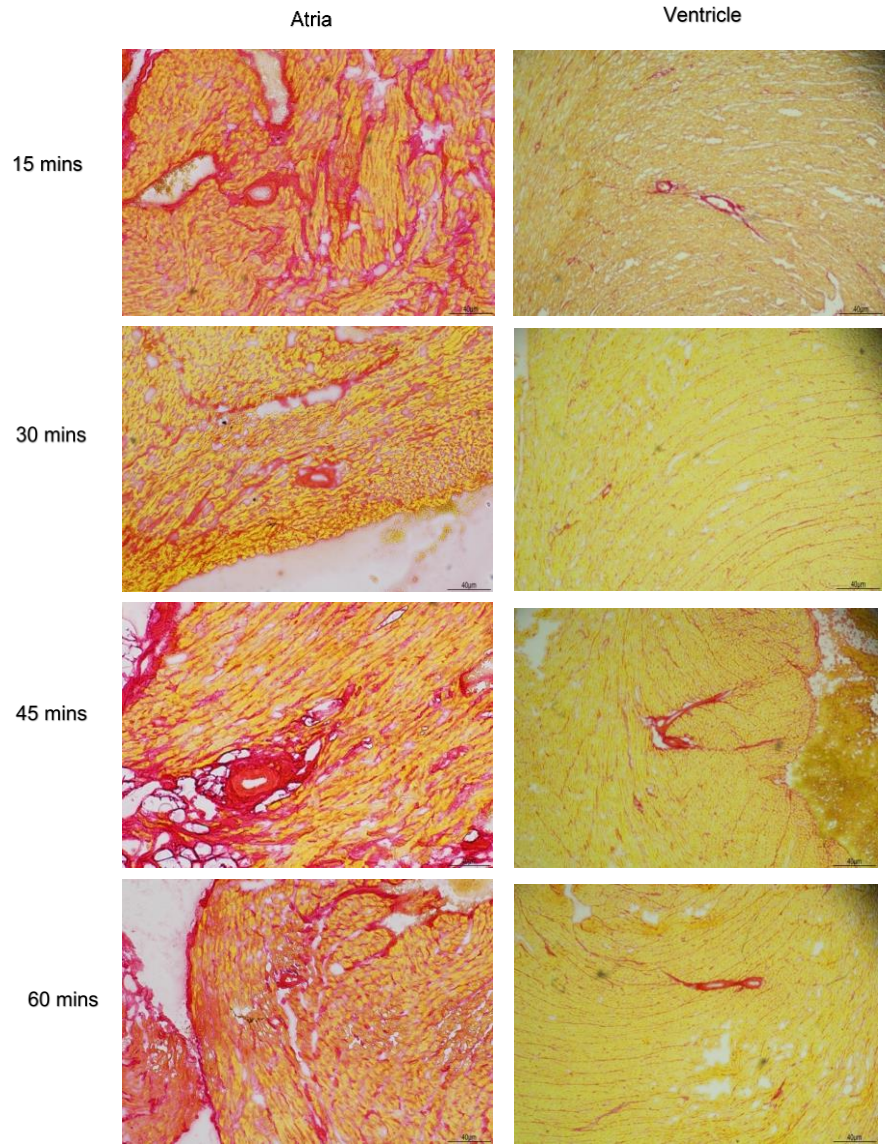

Figure 3. 4 Optimization of PSR Stain dye incubation. Cross-sectional images of the atria and ventricles from a 12-month-old rat heart, displaying intensity variations according to PSR staining durations (15, 30, 45, and 60 minutes). Images were acquired with a NIKON Brightfield Microscope and DS-L4 imaging software.

Frozen sections were air dried for a minimum of 30 min prior to commencement of the staining protocol. Once slides were dry, sections were placed in 100% EtOH for 4 minutes. Samples were then rehydrated by placing sections in 80% EtOH for 20 seconds, followed by 40% EtOH for 20 seconds to ensure removal of remaining OCT from slides. Slides were washed by placing sections in distilled water for 2 mins and shaking slide rack gently. Slides were fixed in 4% buffered formalin (4% Paraformaldehyde, Cambridge Bioscience, UK) for 30 minutes. Slides were again washed by placing sections in distilled water for 2 mins and shaking slide rack gently. Samples were placed into PSR dye (Picrosirius Red Solution, Abcam, UK) for 15 minutes in the dark based on optimisation outlined above. Samples were washed using 0.05% acetic acid solution (glacial acetic acid, Scientific Laboratory Supplies, UK) for 10 seconds whilst shaking slide rack gently to remove excess dye, twice. Slides were dehydrated using two washes in 100% EtOH for 2 minutes. Slides were transferred to xylene for three changes, slides were mounted using coverslips (Menzel-Gläser cover slips: 22x60x1.5mm, Epredia, UK) using Pertex mounting medium (Histolab Products AB, Sweden) and left to dry overnight in a fume hood. Once dry, slides were imaged using a brightfield profile on a Axio Scan Z1 slide scanner (Zeiss, Germany).

Histological analysis was performed using QuPath version 5.0.1 (Queen's University Belfast, UK) for quantification of positive (red) PSR staining (PSR+ %) (231). Tissue images were imported into QuPath and then tissue detection thresholder was created through the creation of LV, RV and whole tissue classifications. A threshold-based approach was utilised to detect tissue at a high resolution, thresholds were set as above threshold to ignore values and below threshold to mark as tissue, a Gaussian prefilter was selected and a threshold value of 200 was selected based on values observed on tissue – this classifier was named WT_1. This classifier was tested on several separate sections to ensure adequate tissue detection was occurring. Another pixel classifier was carried out by drawing regions of interest (ROIs) highlighting PSR positive stains, PSR negative areas on a section and regions to ignore such as artefacts/blood cells. For this classifier a random trees classification at a high resolution was utilised and Gaussian and Laplacian features were selected. The classifier was then trained and its accuracy to detect positive PSR stain was assessed across several sections. Batch analysis was carried out by manually defining LV, RV (see figure 3.5) to ensure that non-cardiac areas were not included and then applying both the tissue detection classifier and PSR stain trained classifier to these regions. This provided average intensity values for PSR positive areas and PSR negative areas across samples.

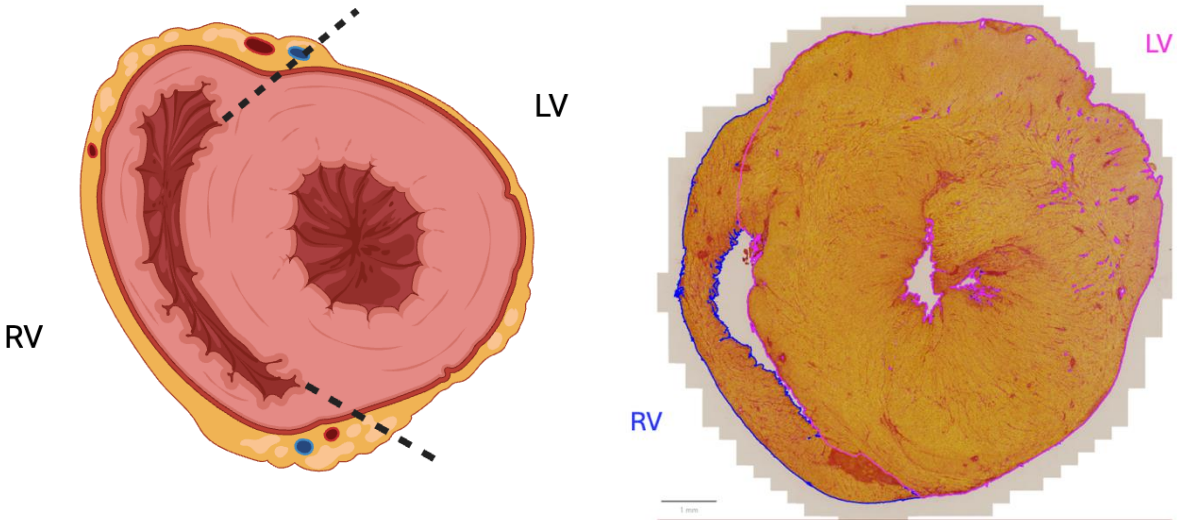

Figure 3. 5 Schematic (left) and representative image (right) showing the separation of left and right ventricles for subsequent analysis. Figure created using Biorender.

3.2.9 Hydroxyproline colorimetric assay

Tissue homogenisation was carried out to prepare samples for hydroxyproline assay, samples are shown in Table 3.5. Samples were defrosted on ice and then weighed and diluted in deionised (DI) water at 1:10 or 100 µl/10mg. Samples were cut into smaller sections using scissors and then the tissue was mechanically homogenised using an Ultra-Turrax ® homogeniser (T 10 basic Disperser, IKA, UK) on ice in 10sec bursts to prevent overheating of samples. Tissue homogenisation continued till a uniform suspension observed. Samples were aliquoted into 110 µl to prevent repeated freeze-thaw cycles and placed in - 80◦C for storage till analysis.

Table 3. 5 Sample numbers for hydroxyproline colorimetric assay

Sex	Sample Numbers				
	1 Month	3 Month	6 Month	12 Month	18 Month
Male	6	6	6	6	6
Female	5	5	5	6	6

A colorimetric assay kit (Abcam; Cambridge,UK) was used to measure the total hydroxyproline content in the LV, RV and atria as described in figure 3.6. Samples were defrosted on ice and then 100 µl of sample homogenate was transferred into a screw-capped polypropylene tube and then equal volumes (100 µl) of 10N concentrated NaOH was added and then sample was heated at 120◦C on a heat block

for 1 hour. Following incubation, samples were cooled on ice and then samples were neutralised using 100 µl of 10N of concentrated from HCl (diluted from VMR concentrated chemical). Samples were vortexed and centrifuged for 5 mins at 10,000g at 4◦C. The supernatant was collected and kept on ice, ready for the assay to begin.

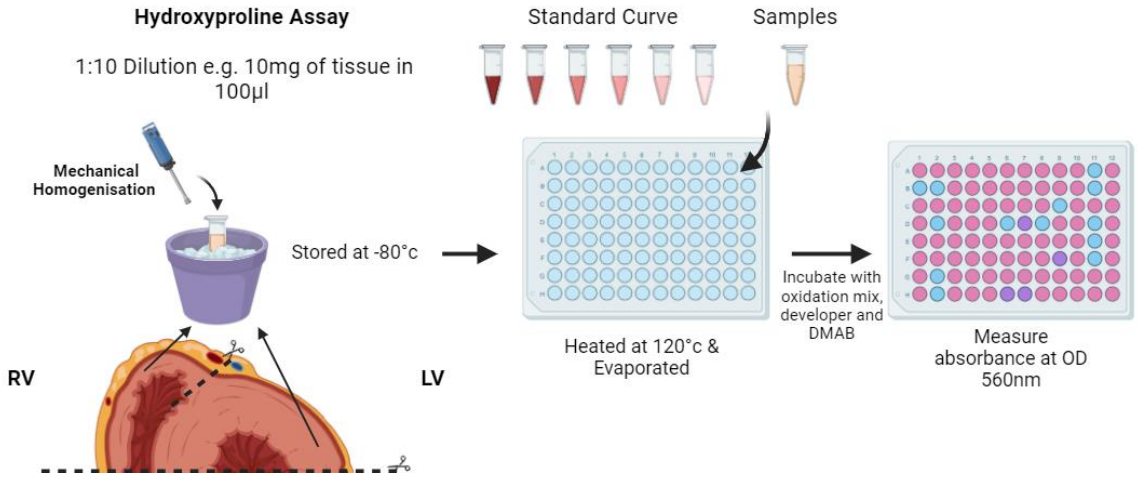

Figure 3. 6. Hydroxyproline assay protocol in *ex vivo* tissue samples. Figure created using Biorender.

Hydroxyproline standards were prepared according the kit protocol and then 10 µl of each standard was placed in duplicate into the 96-well plate. Then 10 µl of each sample was placed in duplicate into the 96-well plate. The plate was placed on heating block at 65◦C to allow for samples to evaporate for a minimum of 45 minutes. Oxidation mix (94 µl of oxidation buffer and 6 µl chloramine T concentrate per sample) provided in the kit was added to each well and then the plate was incubated at room temperature (RT) for 20 minutes in the dark. Following incubation, 50 µl of developer was added to the reaction and incubated at 37◦C for 5 minutes. Next, 50 µl DMAB concentrate was added to the plate and the plate was gently mixed and sealed using the plate seal supplied by the kit. The plate was incubated at 65◦C for 45 minutes. The plate was read using a microplate reader within 10 minutes of the incubation completion, an absorbance at OD 560 nm was used.

Total hydroxyproline content was calculated in Microsoft Excel Version 16.0 and was based on the standard curve generated by plotting the average of each duplicated standard minus the background (calculated from the blank). The background was subtracted from the unknown samples and then values were averaged. A best-fit linear trend line was calculated and the equation was used to calculate the total amount of hydrolysed hydroxyproline in each sample. To calculate the concentration of hydroxyproline in each well (µg/mg) the identified value was divided by the sample

volume (10 µl) and then multiplied by a factor of 3 and a factor of 10 to account for dilution occurring during preparation.

3.2.10 Soluble/Insoluble colorimetric assay

Tissue homogenisation was carried out to prepare samples for Sircol soluble/insoluble collagen assay (Biocolor, UK) samples numbers are shown in Table 3.6. Samples were defrosted on ice and then weighed and diluted in Acetic (0.5M) Pepsin (sigma-aldrich, USA) 0.1mg/ml at 1:10 or 100 µl/10mg and left overnight (18 hours) at 4◦C as detailed in Figure 3.2.6. Samples were then spun at 3000g for 10 minutes at 4◦C and then the supernatant containing the soluble collagen was collected and frozen at -20◦C. The pellet containing insoluble collagen was collected and frozen at -20◦C.

Table 3. 6 Ventricle sample numbers for insoluble/soluble colorimetric assay.

Sex	Sample Numbers				
	1 Month	3 Month	6 Month	12 Month	18 Month
Male	6	6	5	6	6
Female	6	6	6	6	6

Soluble and insoluble collagen content was assayed in separate runs due to differences in assay protocol. Soluble samples were defrosted on ice. Whilst samples were defrosting, soluble collagen standards (provided in the assay kit) were made up ranging from 1.25µg - 50µg in 100 µl volumes. Once samples were defrosted, 10 µl of each sample was transferred and made up to 100 µl using DI water. Following sample preparation, 1 ml of Sircol Dye (provided in the assay kit) was added to each standard and sample tube to fully saturate the collagen molecules in the volume, tubes were then inverted. Samples were incubated at RT for 30 minutes on a mechanical shaker at a gentle speed. Tubes were then centrifuged at 13000g for 10 minutes at 4◦C and supernatant was discarded. Samples were then washed with 750 µl of acid-salt wash reagent to remove unbound dye from the pellet and tube. Samples were then centrifuged at 13000g for 10 minutes at 4◦°C and supernatant was discarded. Finally, 1ml of alkali reagent was added to all standards and samples, which were vortexed and incubated for 5 minutes to allow for bound dye to dissolve. In duplicate, standards and samples were placed into a 96 well plate. The plate was read using a microplate reader within 2 hours of assay completion with an absorbance at OD 556nm.

Insoluble samples were defrosted on ice. Fragmentation reagent was added to each sample (50µl/mg of tissue) and the sample was placed onto a heatblock at 65◦C for 2 hours in screw capped round

bottom 2 ml digestion tubes. Samples were then centrifuged at 13000g for 10 minutes at 4◦C. The remainder of the assay was run as described in the previous paragraph and in Figure 3.7.

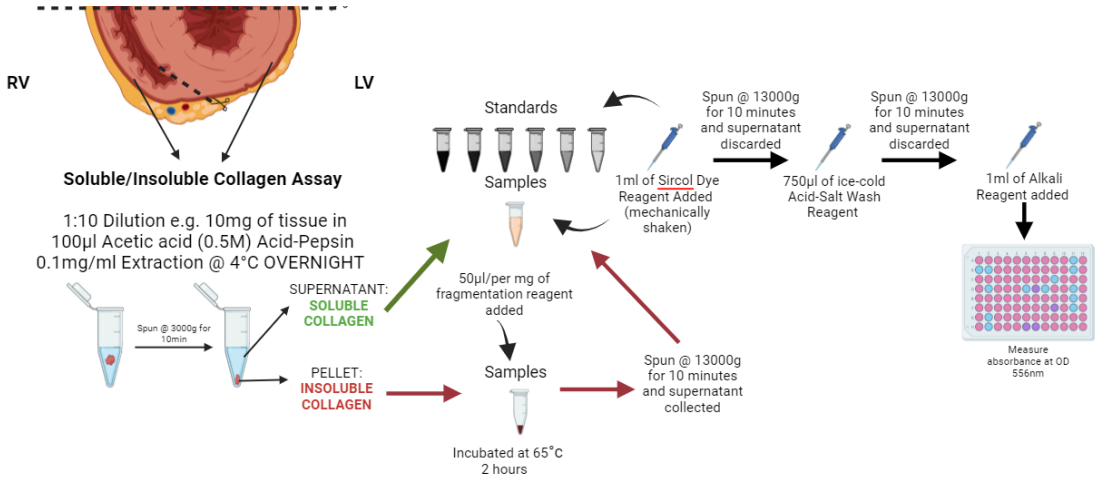

Figure 3. 7 Soluble and insoluble collagen assay protocol in *ex vivo* tissue samples. Figure created using Biorender.

Total soluble and insoluble content was calculated on Microsoft Excel and was based on the standard curve generated by plotting the average of each duplicated standard minus the background (calculated from the blank). The background was subtracted from the samples and then valued were averaged. A best-fit linear trend line was calculated and the equation was used to calculate the total amount of hydrolysed hydroxyproline in each sample. To calculate the concentration of soluble and insoluble content in each well (µg/µl) the identified value was then multiplied by a factor of 10 or 2 for soluble and insoluble respectively, to account for dilution occurring during preparation.

3.2.10 Advanced glycation end product enzyme-linked immunosorbent assay (ELISA)

Tissue homogenisation was carried out to prepare samples for the AGEs rat ELISA kit (MyBioSource, USA), samples are shown in Table 3.7. Optimization of the most suitable tissue homogenization method and the dilution of the homogenized tissue substrate. Two substrates were investigated: normal saline (NS) and tissue protein extraction reagent (ph7.4,0.01mol/L Tris-HCL, 0.0001MOL/LEDTA-2Na,0.01mol/L sucrose 0.8 % NaCl); and three tissue dilutions were tested 1:10,1:25, 1:50 and 1:100 for the assay based on known concentrations of AGEs present in the tissue. The optimisation identified that NS and tissue protein extraction reagent showed similar levels of efficiency during homogenisation and for ease of sample preparation NS was selected. Based on the standard curve as a dilution of 1:50 was selected due to its positioning along the standard curve.

Samples were defrosted on ice and then weighed and diluted in NS at 1:50. Samples cut into smaller sections using scissors and then tissue was mechanically homogenised using an Ultra-Turrax ® homogeniser (T 10 basic Disperser, IKA, UK) on ice in 10sec bursts to prevent overheating of samples. Tissue homogenisation continued till a uniform suspension observed. The samples were then centrifuged at 10000rpm for 10 min at 4◦C and supernatant was collected. Samples were aliquoted into 100µl volumes to prevent repeated freeze-thaw cycles and placed in - 80◦C for storage till analysis. Only LV samples were assessed due to the low tissue availability and cost of ELISA kit of both RV and atria and therefore other assays were prioritised.

Table 3. 7 Sample numbers for AGEs ELISA.

Sex	Sample Numbers				
	1 Month	3 Month	6 Month	12 Month	18 Month
Male	6	6	6	6	3
Female	6	6	6	8	5

ELISA kit was removed from -20◦C storage and brought to RT (approx. 1.5 hours), including well strips needed for the assay. Washing buffer was reconstituted in DI water at 1:25 dilution. Standard was constituted in 1ml of standard diluent and allowed to sit for 30 mins to allow for complete dissolvement. Standards concentration ranged from 5ng/ml to 500ng/ml as recommended by the kit protocol. Standards were made up via serial dilution where 7 tubes were labelled and 300µl of standard diluent was transferred into each tube. From the standard stock 300µl was transferred into the first tube and the standard was vortexed. This was repeated through the next 5 tubes and the final tube remained as a blank.

Following acclimatisation of the kit, 100µl of standards and samples were transferred to the 96 well plate, in duplicate. The plates were sealed using adhesive tape strip and incubated at 37◦C for 90 minutes. During the incubation (30 minutes prior to completion of step) the biotinylated antibody was prepared by dilution the biotinylated antibody solution 1:100 using the antibody diluent. Following completion of incubation, the remaining samples was discarded and the ELISA plate was washed twice manually, using the multichannel pipette and washing buffer. The biotinylated antibody (100µl/well) was added and the plate was sealed and incubated at 37◦C for 60 minutes. Enzyme conjugate was prepared by diluting the enzyme conjugate solution 1:100 with enzyme diluent and allowed to dissolve for 30 min. Following completion of the antibody incubation, the ELISA plate was manually washed thrice and then the enzyme conjugate was applied (100µl/well). The plate was sealed and incubated at 37◦C for 30 minutes. During incubation, colour reagent was prepared through combination of colour

reagent A and colour reagent B in a 9:1 proportion and left to rest for 30 minutes. Following incubation, ELISA plate was manually washed five times. Colour reagent was added to the plate (100µl/well), the plate was then incubated in the dark at 37◦C for 24 minutes. Colour reagent C (stopping agent) was added to each well (100µl/well) and the plate was read using a microplate reader at an absorbance OD 450nm, within 10 minutes of assay completion.

AGEs concentrations were calculated on Microsoft Excel Version 16.0 and was based on the standard curve generated by plotting the average of each duplicated standard minus the background (calculated from the blank). The background was subtracted from the samples and then valued were averaged. A best-fit linear trend line was calculated and the equation was used to calculate the total amount of hydrolysed hydroxyproline in each sample. To calculate the concentration of AGES in each well (µg/µl) the identified value was then multiplied by a factor of 50 to account for dilution occurring during preparation.

3.2.11 Data analysis

Data fitting, statistical analysis and production of graphs were completed using GraphPad Prism version 9 (GraphPad Software Inc., USA). Normality of the data was assessed for each group and paired or unpaired student T tests were used to statistically compare two groups. Where data was not normally distributed data was analysed with a non-parametric test was utilised. Comparison of multiple groups was completed using ANOVA or mixed effect models plus post-hoc tests as indicated within the relevant figure legends. Values are expressed as min to max range and the threshold for statistical significance is $p<0.05$.

Correlation analysis was completed to compare the techniques used to assess collagen deposition and collagen synthesis. The averages of different assays were compared using Pearson correlation analysis. Assays including PET imaging, hydroxyproline assay, soluble assay, insoluble assay, AGEs ELISA, PSR histology staining were compared alongside structural/functional age-related changes identified in Chapter 2. Pearson correlation coefficients (r) were calculated to evaluate the linear relationships between the assay averages, with r values ranging from -1 to +1, indicating the strength and direction of the relationships. The dataset was imported into GraphPad Prism, and a correlation matrix was generated to visualize and quantify the relationships between the assays. Analysis of males and females were conducted separately.

To allow for further interpretation, this study compared the averages of different assays across male and female subjects using Pearson correlation analysis and Morpheus

(https://software.broadinstitute.org/morpheus/) heat map visualization (232). Data was imported into Morpheus, creating heat maps with dendrograms to identify patterns. Morpheus allowed the import of matrices from various formats and customized colour schemes. Row/column annotations, filtering, and hierarchical clustering were applied to enhance data interpretation using its Kmeans function. All data is available upon request.

3.3 Results

This study aimed to assess the effects of aging and sex on cardiac collagen metabolism specifically collagen synthesis and deposition in the ventricles of Sprague Dawley rats up to 18 months of age. Additionally, we sought to characterize how sex and age influence ventricular collagen deposition *ex vivo*. Finally, we aimed to compare these two processes to determine if changes in synthesis correlate with collagen deposition in the tissue. These findings will provide a comprehensive understanding of changes in collagen synthesis and deposition, both *in vivo* and *ex vivo*.

3.3.1 Age-Related decline in LV *cis*-4-[^{18}F]fluoro-*L*-proline uptake, unaffected by sex

LV unhydroxylated collagen synthesis was measured using *cis*-4-[^{18}F]fluoro-*L*-proline *in vivo.* Uptake of the tracer was first assessed between males and females at each timepoint, to measure the effect of sex on unhydroxylated collagen synthesis as shown in one animal in Figure 3.8 and Figure 3.9. No sex differences were observed in the LV throughout the course of the study, with 1-month males having an average uptake of 0.94 ± 0.03 SUVr compared to females with an average of 0.92 ± 0.07 SUVr. This remained similar at 18 months with males averaging 0.90 ± 0.05 SUVr and females averaged an uptake of 0.89 ± 0.05 SUVr.

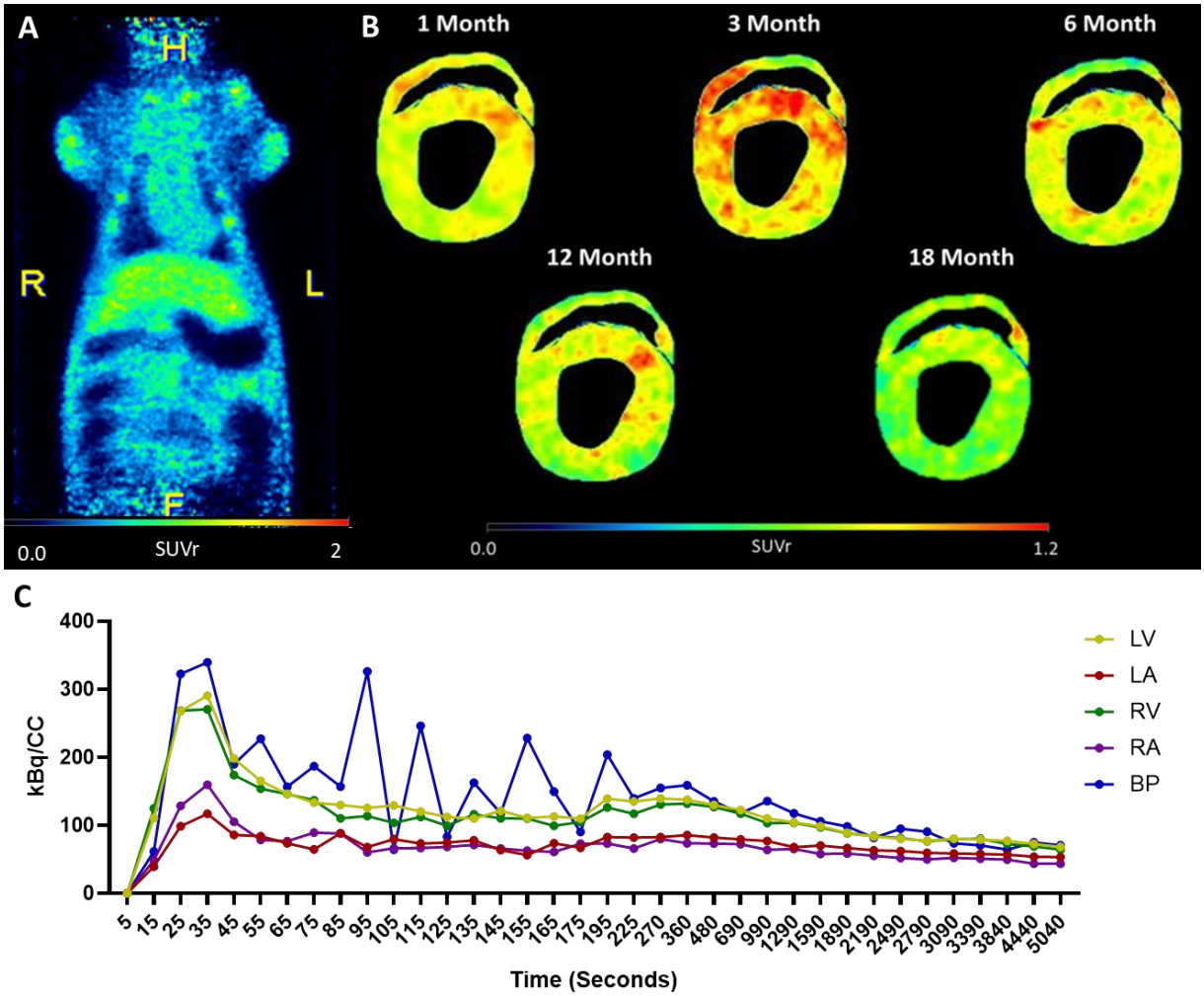

Figure 3. 8 Representative images of *cis*-4-[^{18}F]fluoro-*L*-proline Uptake (SUVr) and time-activity curves. A) Whole body images of *cis*-4-[^{18}F]fluoro-*L*-proline Uptake (SUVr) (male 6 month of age). B) Representative images of cardiac PET images over 18 months. C) Representative time activity curve from 6 month male rodent *cis*-4-[^{18}F]fluoro-*L*-proline scan.

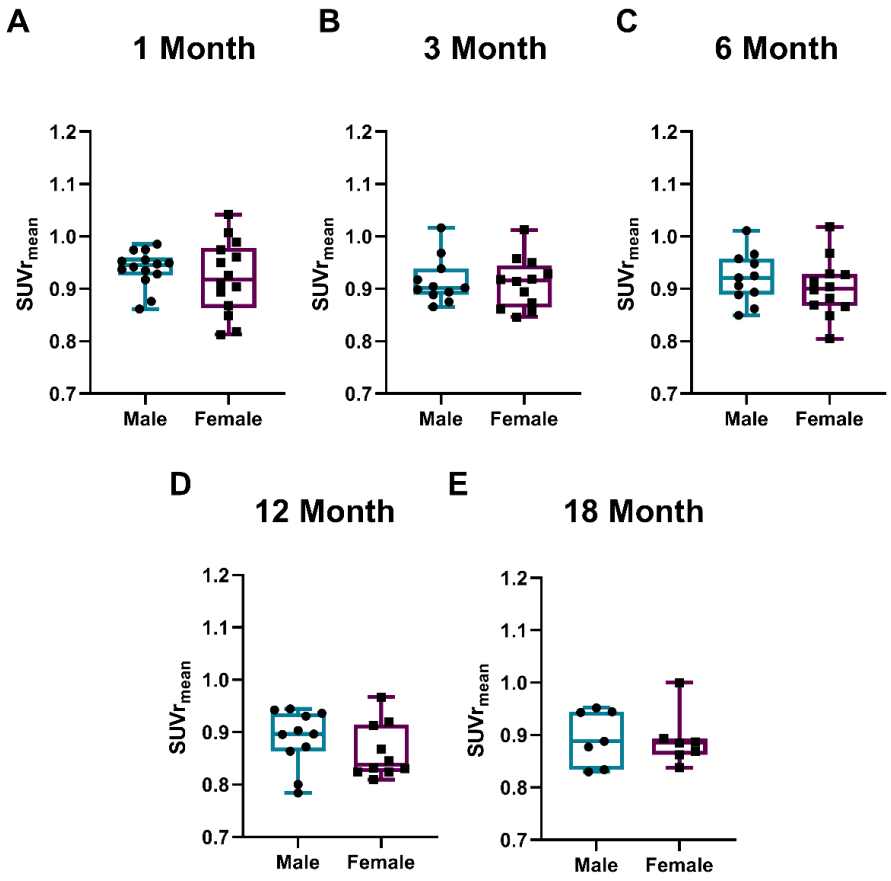

Figure 3. 9 Evaluating the impact of sex on LV *cis*-4-[^{18}F]fluoro-*L*-proline uptake across timepoints. *cis*-4-[^{18}F]fluoro-*L*-proline uptake was measured in the LV at each imaging time point: 1 month (A), 3 month (B), 6 month (C), 12 month (D) and 18 month (E). Results reported as min to max range, n=7-14 males and n=7-14 females; Changes were assessed using a Student's t-test; results were not statistically significant.

The effect of aging on *cis*-4-[^{18}F]fluoro-*L*-proline uptake was assessed in the LV of both sexes, with no significant differences observed over 18 months, as shown in Figure 3.10. Comparing the baseline at 1 month to 12 months, there was a trend toward decline, with a 5.4% decrease in males (p=0.13) and a 6.4% decrease in females (p=0.25), although this reduction was less pronounced at 18 months. Since no sex differences were noted, data from both sexes were combined to assess the effect of age on unhydroxylated collagen synthesis, as shown in Figure 3.11. With increased statistical power we observed a significant decrease (p=0.03) in *cis*-4-[^{18}F]fluoro-*L*-proline uptake, with a 5.8% decline at 12 months. A rebound of 1.9% was observed at 18 months. We completed an analysis removing animals lost during study to assess if survival bias impacted our findings (see Appendix Figure 7.3). The trend remained, but significance was lost, likely due to reduced overall power. These findings suggest that unhydroxylated collagen synthesis is unaffected by sex but decreases with aging at 12 months, indicating that collagen synthesis is a dynamic process.

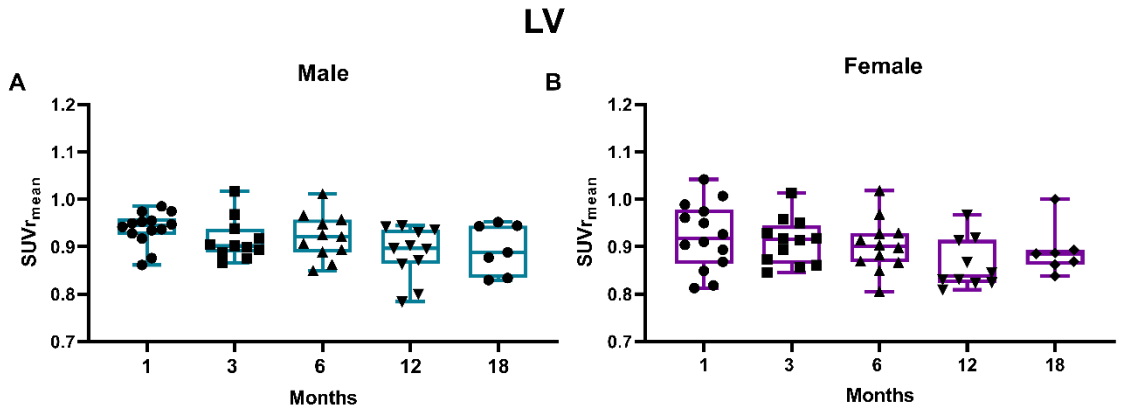

Figure 3. 10 Evaluating the impact of age on LV *cis*-4-[^{18}F]fluoro-*L*-proline in both sexes. Longitudinal changes in males (A) and females (B) *cis*-4-[^{18}F]fluoro-*L*-proline uptake in the LV over 18 months. Results reported as min to max range, n=7-14 males and n=7-14 females; Changes were assessed using a Mixed-effects Analysis and Dunnett's Post-hoc test; results were not statistically significant.

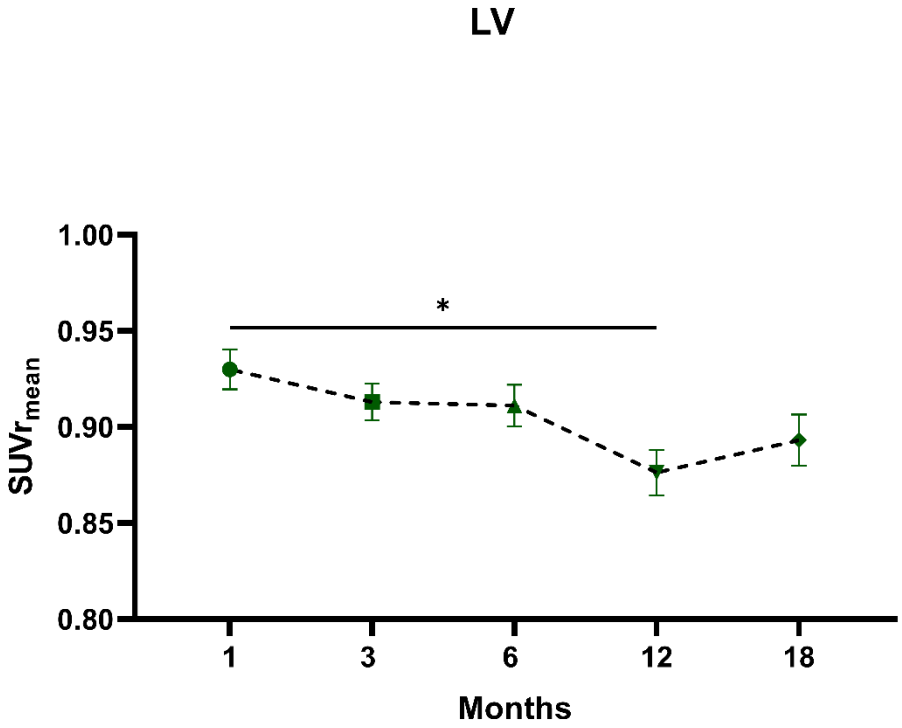

Figure 3. 11 Assessing the longitudinal effect of age in on LV *cis*-4-[^{18}F]fluoro-*L*-proline uptake. Longitudinal changes in *cis*-4-[^{18}F]fluoro-*L*-proline uptake in the LV over 18 months. Results reported as min to max range, n=7-14 males and n=7-14 females; p values were obtained a Mixed-effects Analysis and Dunnett's Post hoc test when comparing longitudinal data to the first timepoint. *p<0.05

3.3.2 Age-related decline in LV *trans*-4-[^{18}F]fluoro-*L*-proline uptake, unaffected by sex

LV hydroxylated collagen synthesis was measured using *trans*-4-[^{18}F]fluoro-*L*-proline over 18 months. Similar to unhydroxylated collagen synthesis, hydroxylated collagen synthesis showed no sex differences over 18 months, as seen in Figure 3.12 and Figure 3.13. Both sexes remained comparable from 1 month with males averaging around 0.96 ± 0.06 SUVr and females averaging around 0.96 ± 0.04 SUVr and this was maintained till 18 months with males averaging 0.95 ± 0.06 SUVr and females averaging 0.94 ± 0.05 SUVr mean.

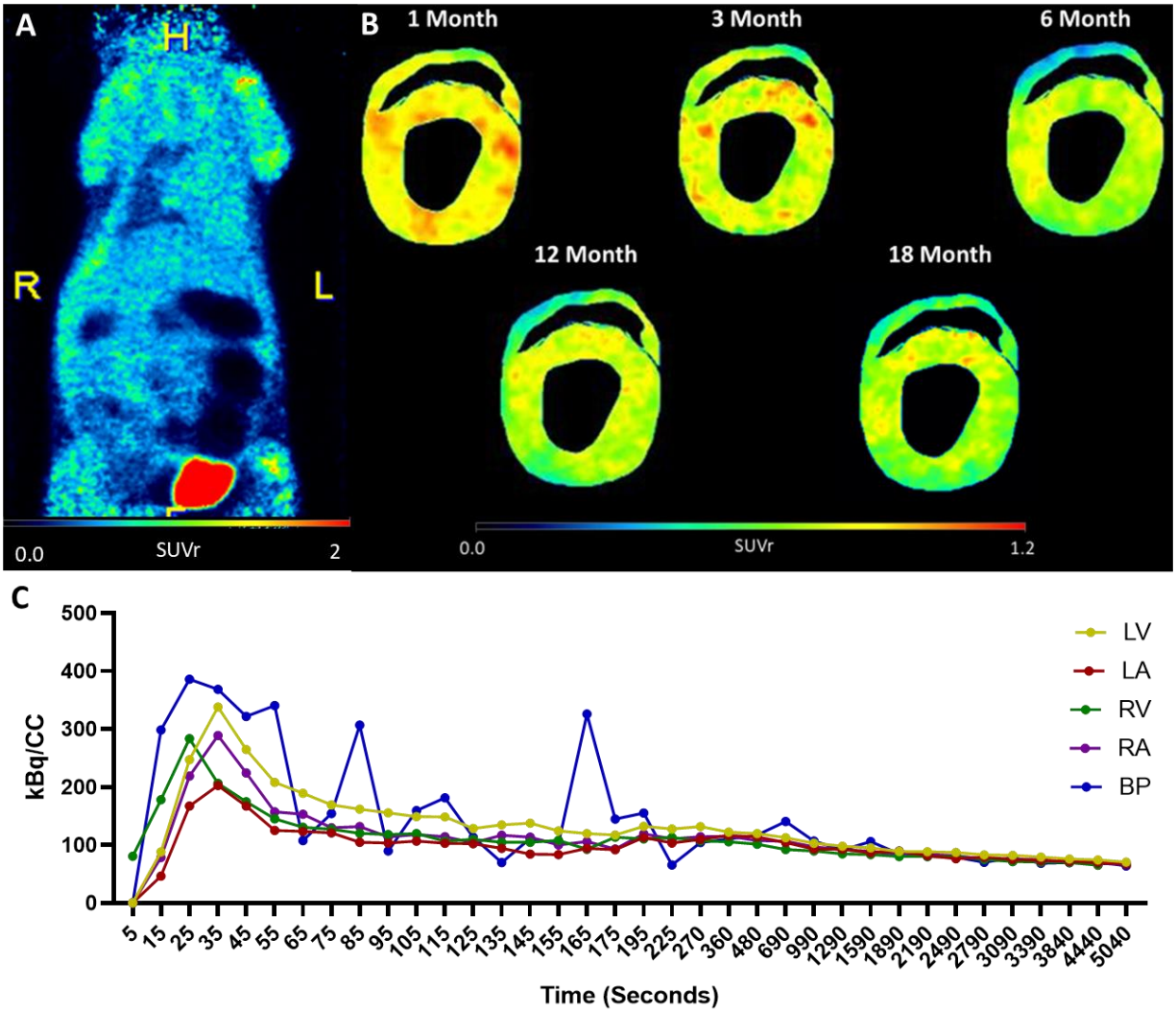

Figure 3. 12 Representative images of ventricular *trans*-4-[^{18}F]fluoro-*L*-proline Uptake (SUVr) over 18 months. A) Whole body images of *trans*-4-[^{18}F]fluoro-*L*-proline Uptake (SUVr) (male 6 month of age). B) Representative images of cardiac PET images over 18 months. C) Representative time activity curve from 6 month male rodent *trans*-4-[^{18}F]fluoro-*L*-proline scan.

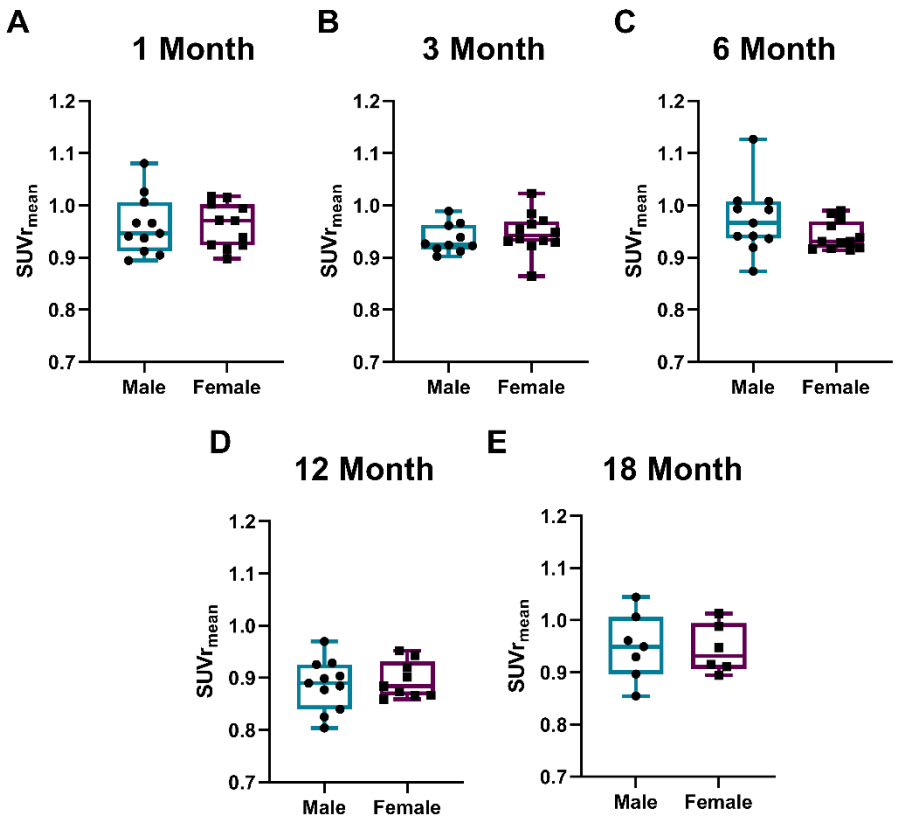

Figure 3. 13 Evaluating the impact of sex on LV *trans*-4-[^{18}F]fluoro-*L*-proline uptake across Timepoints. *trans*-4-[^{18}F]fluoro-*L*-proline uptake was measured in the LV at each imaging time point: 1 month (A), 3 month (B), 6 month (C), 12 month (D) and 18 month (E). Results reported as min to max range, n=7-14 males and n=7-14 females; Changes were assessed using a Student's t-test; results were not statistically significant.

Longitudinal assessment of *trans*-4-[^{18}F]fluoro-*L*-proline uptake in the LV was carried out over 18 months. Both males and females showed a significant decline in *trans*-4-[^{18}F]fluoro-*L*-proline at 12 months of age, as seen in Figure 3.14. Males showed on average a 7.9% decrease (p=0.001) at 12 months of age (0.88 ± 0.05 SUVr), which was followed by an increase of 7.1% at 18 months. Females showed on average a 6.8% decrease (p=0.03) at 12 months compared to 1 month of age, this was followed by a similar increase of 5.4% at 18 months. Once again, the overall effect of age was assessed in both sexes together to understand the effect of aging on the whole cohort. This showed a significant decline of 7.4% at 12 months (p<0.0001), followed by a 6.3% increase at 18 months. We assessed whether our findings were influenced by survival bias and whether this was driving the changes observed at 18 months, see appendix Figure 7.3. The trend remained the same but the significance was reduced, likely due to the reduction in overall power. Together these findings, suggest that

hydroxylated collagen synthesis is unaffected by sex but is reduced at 12 months with aging, this highlights that hydroxylated collagen synthesis is altered greatly indicated at 12 months and suggests there is key alterations in collagen metabolism at this timepoint (Figure 3.15). This highlights that within the LV similar declines in uptake were observed between *trans*-4-[^{18}F]fluoro-*L*-proline and *cis*-4-[^{18}F]fluoro-*L*-proline suggesting that in aging both collagen synthesis types decline. The observed increase at 18 months is challenging to interpret due to reduced statistical power at this time point. However, it may suggest that more advanced aging could lead to additional changes.

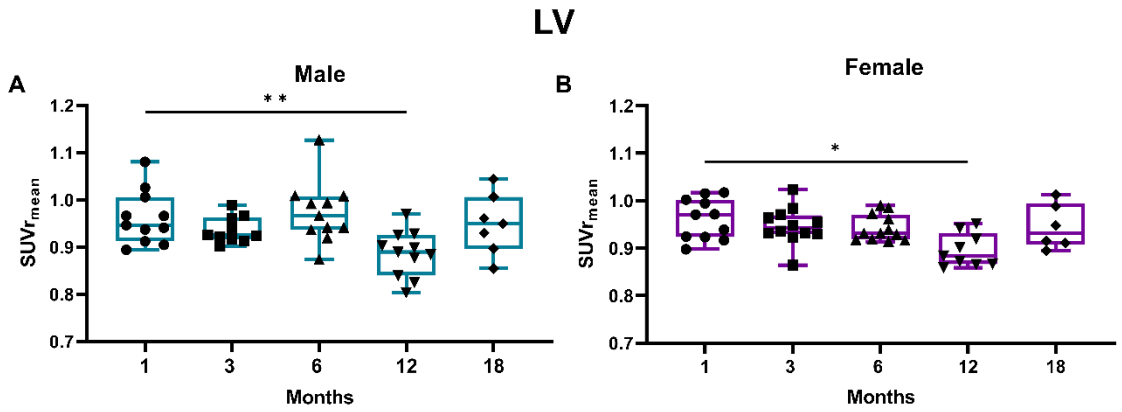

Figure 3. 14 Evaluating the impact of age on LV *trans*-4-[^{18}F]fluoro-*L*-proline in both sexes. Longitudinal changes in males (A) and females (B) *trans*-4-[^{18}F]fluoro-*L*-proline uptake in the LV over 18 months. Results reported as min to max range, n=7-14 males and n=7-14 females; p values were obtained a Mixed-effects Analysis with Dunnett's Post-hoc test when comparing longitudinal data to the first timepoint. *p<0.05; **p<0.01;

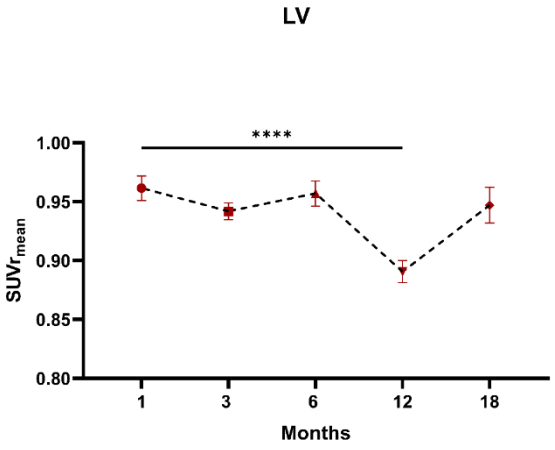

Figure 3. 15 Assessing the longitudinal effect of age in on LV *trans*-4-[^{18}F]fluoro-*L*-proline uptake. Longitudinal changes in *trans*-4-[^{18}F]fluoro-*L*-proline uptake in the LV over 18 months. Results reported as min to max range, n=7-14 males and n=7-14 females; p values were obtained a Mixed-effects Analysis with Dunnett's Post-hoc test when comparing longitudinal data to the first timepoint. ****p<0.0001

3.3.3 Accumulation of total deposited collagen in adulthood, followed by decline at 18 months in the LV

Total deposited collagen was measured using PSR histological staining, which stains collagen fibres red. The percentage of positive PSR stain was measured and assessed over 18 months. Within the LV, no sex differences were apparent at 1 month and 3 months, though there was a trend toward females having higher total collagen at both time points. At 1 month, males averaged 6.0 ± 1.6%, while females had an average of 9.0 ± 2.7%, as seen in Figure 3.16 A & B. Similarly, at 3 months, males had an average staining of 10.0 ± 2.6%, while females averaged 13.0 ± 2.3%. Significant differences between the sexes emerged at 6 months, with females having higher total collagen staining (14.0 ± 3.6%) (p=0.04) compared to males (9.7 ± 3.5%), as shown in Figure 3.16 C. At 12 months, collagen deposition was similar between both sexes (Figure 3.16 D). Finally, at 18 months, females (8.4 ± 2.6%) (p=0.03) were found to have significantly higher collagen deposition in the LV than aged males (5.5 ± 1.3%) (Figure 3.16 E). It is important to note that females generally higher collagen content throughout the study compared to males with fewer significant changes over time.

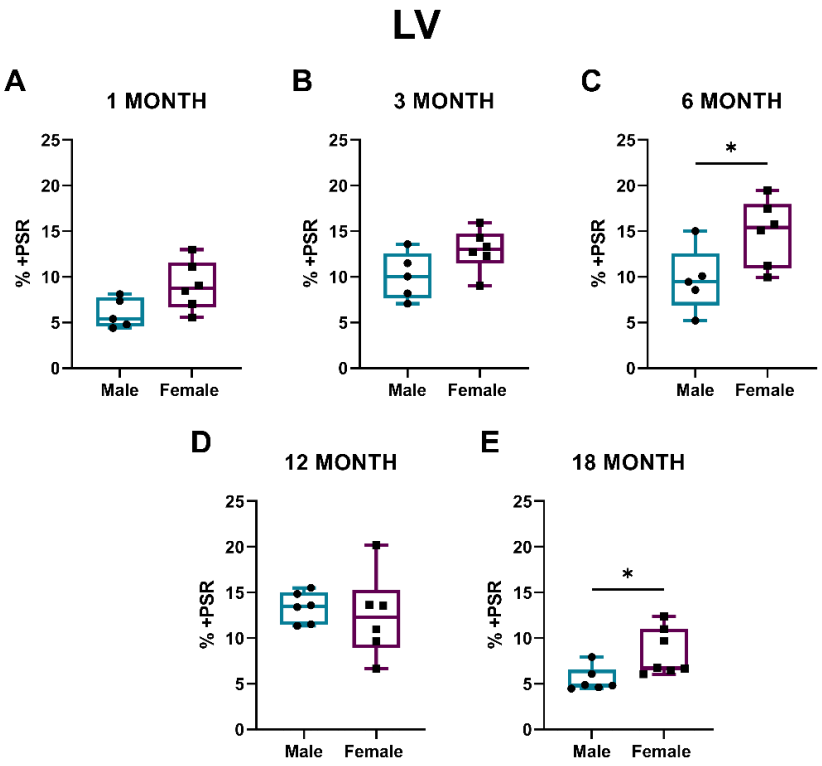

Figure 3. 16 Evaluating the impact of sex on total LV collagen deposition across timepoints. % Positive PSR stain (%+PSR) was measured in the LV at each imaging time point: 1 month (A), 3 month (B), 6 month (C), 12 month (D) and 18 month (E). Results reported as min to max range, n=5-6 males and n=5-6 females; p values were obtained using unpaired parametric students t-test when comparing two groups; *p<0.05

The effect of age was assessed by comparing the longitudinal effects of age in both sexes. Both males and females exhibited age-related changes in total collagen over 18 months, as depicted in Figure 3.17. Males demonstrated significant increases in total collagen at 3 months (10.0 ± 2.6%; p=0.03) and 12 months (13.4 ± 1.7%; p<0.0001) compared to baseline at 1 month (6.0 ± 1.6%). Notably, males showed a 122% increase in total collagen at 12 months versus baseline at 1 month. A similar trend was observed at 6 months with a 61% increase (9.7 ± 3.5%; p=0.06) However, a significant decrease in total collagen was observed between 12 months and 18 months (p= <0.0001), with a total 59.1% reduction, returning to values comparable to those at 1 month. This suggests that collagen content is dynamic and varies with age. In females, a similar pattern of increased collagen content was observed, with the most significant increase occurring at 6 months (14.8±3.6%; p=0.016), resulting in an overall 64.41% increase. Additionally, a significant decrease in total collagen was observed between 6 months and 18 months (p= 0.01), with an overall 32.3% reduction. These findings indicate that both sexes exhibit dynamic changes in collagen content over time, implying that collagen accumulation is not constant throughout aging.

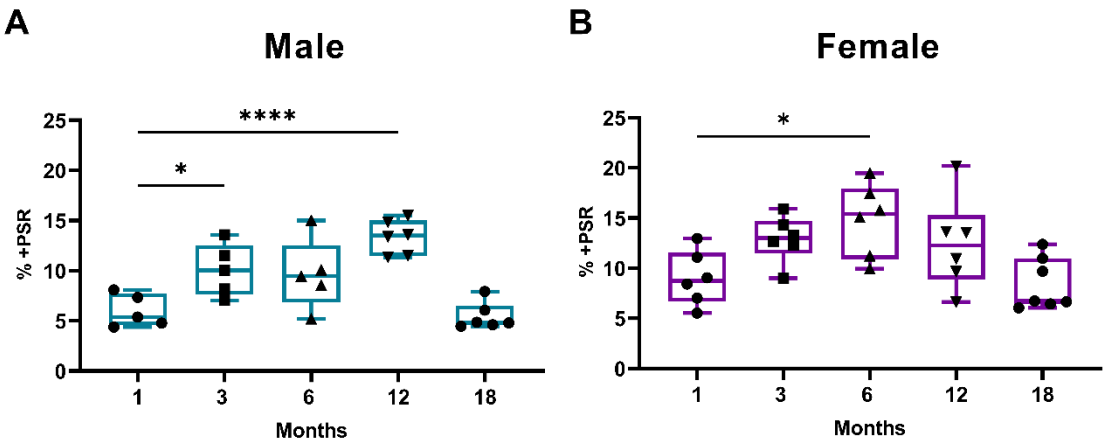

Figure 3. 17 Evaluating the impact of age on total collagen deposited in the LV in both sexes. Longitudinal changes in males (A) and females (B) % positive PSR stain (%+PSR) in the LV over 18 months. Results reported as min to max range, n=7-14 males and n=7-14 females; p values were obtained a Mixed-effects Analysis with Dunnett's Post-hoc test when comparing longitudinal data to the first timepoint. *p<0.05; ****p<0.0001

3.3.4 Hydroxyproline content remains stable in the LV in aging

Total hydroxyproline content was measured as an indicator of collagen quantity, capturing collagen at all stages post-hydroxylation. In our study, we first assessed hydroxyproline content changes between the sexes, as shown in Figure 3.18. No sex differences were identified across all timepoints over 18 months. Hydroxyproline content appeared consistent in both sexes, ranging from 1 month (males: 0.20 ± 0.08 µg/mg; females: 0.23 ± 0.06 µg/mg) to 18 months (males: 0.14 ± 0.06 µg/mg; females: 0.15 ± 0.09 µg/mg). This suggests that hydroxyproline content is not significantly influenced by sex.. The effect of age on total hydroxyproline content was assessed. Once again, no differences were observed in total hydroxyproline content in males or females as shown in Figure 3.19.

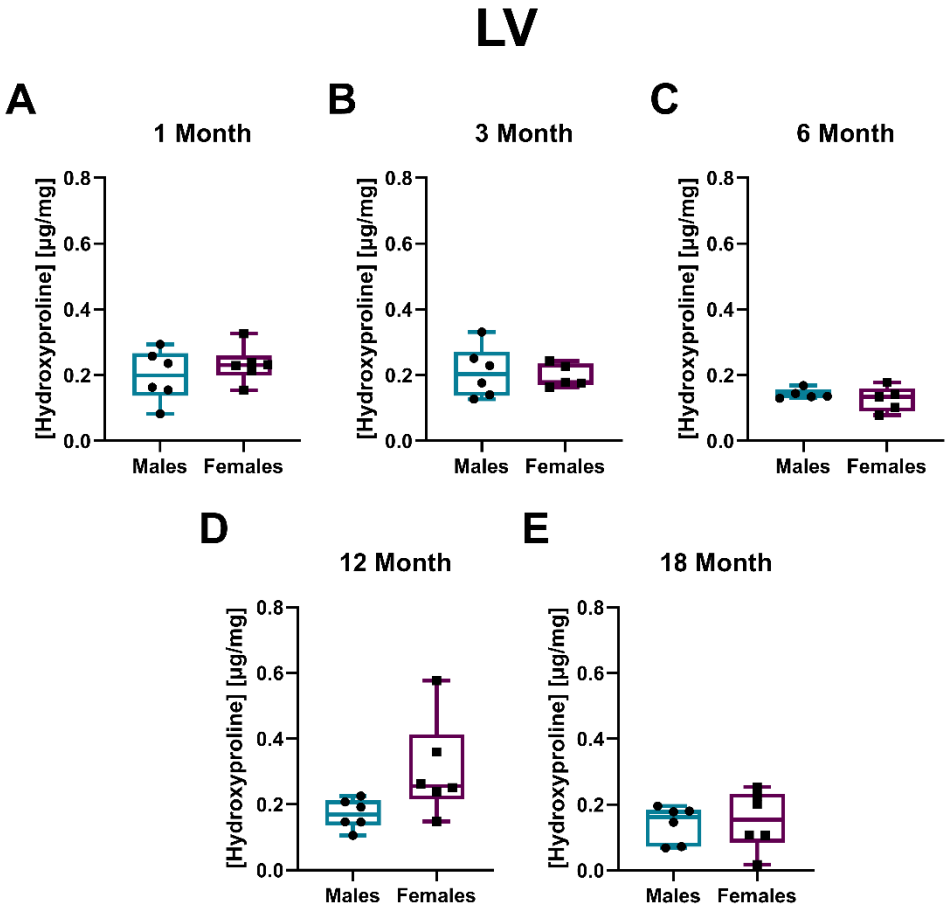

Figure 3. 18 Evaluating the impact of sex on total LV hydroxyproline content across timepoints. Hydroxyproline content (µg/mg) was measured in the LV at each imaging time point: 1 month (A), 3 month (B), 6 month (C), 12 month (D) and 18 months (E). Results reported as min to max range, n=5-6 males and n=5-6 females; p values were obtained using unpaired parametric students t-test when comparing two groups'

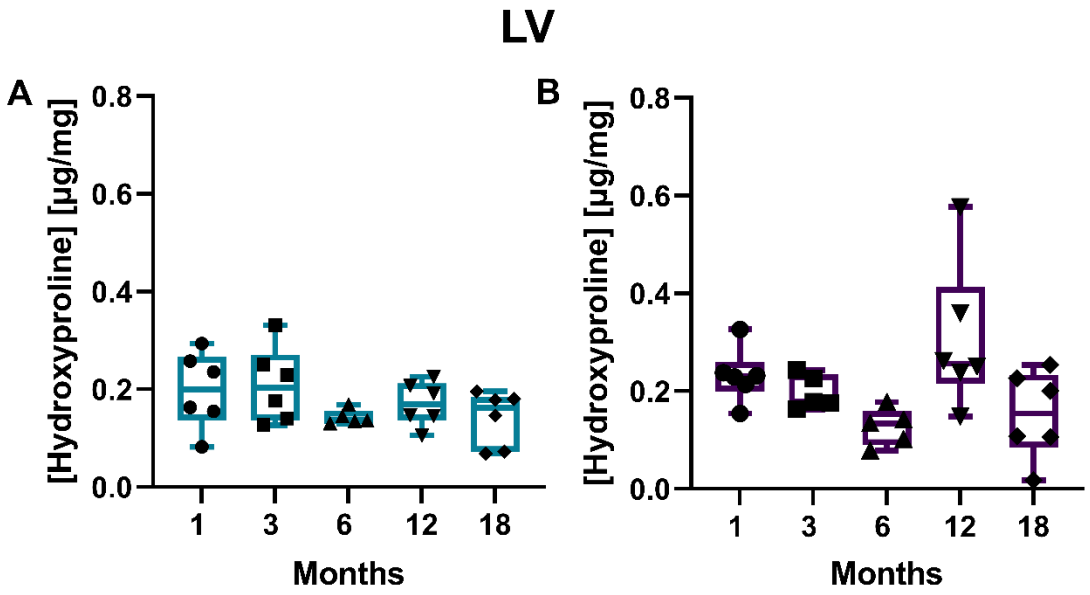

Figure 3. 19 Evaluating the impact of age on total LV hydroxyproline content in both sexes. Longitudinal changes in males (A) and females (B) Hydroxyproline content (µg/mg) uptake in the LV over 18 months. Results reported as min to max range, n=5-6 males and n=5-6 females; Changes were assessed using a one-way ANOVA and Dunnett's Post-hoc test; results were not statistically significant.

3.3.5 Male-specific age-related increase in soluble collagen, absent in females

Soluble collagen content was measured in both sexes over an 18-month period to assess the early stages of collagen synthesis and turnover, as it can indicate both increased synthesis and degradation. Typically, soluble collagen represents newly synthesized collagen that has not yet been cross-linked or is in the process of being degraded. The effect of sex on soluble collagen content was assessed, with females consistently exhibiting higher LV soluble collagen content at 1, 3, 6, and 12 months of age, as shown in Figure 3.20. At 1 month, females had a significantly higher average of 61221 ± 10,028 µg/µl compared to 38125 ± 7851 µg/µl in males (p=0.0005). This trend continued at 3 months (males: 62528 ± 8767 µg/µl; females: 77884 ± 14585 µg/µl; p=0.04), 6 months (males: 48026 ± 4489 µg/µl; females: 77884 ± 14585 µg/µl; p=0.01), and 12 months (males: 43524 ± 5,503 µg/µl; females: 77884 ± 14585 µg/µl; p=0.03). However, by 18 months, this sex difference was no longer observed, with males and females showing comparable levels of soluble collagen (males: 77733 ± 21317 µg/µl; females: 77884 ± 14585 µg/µl).

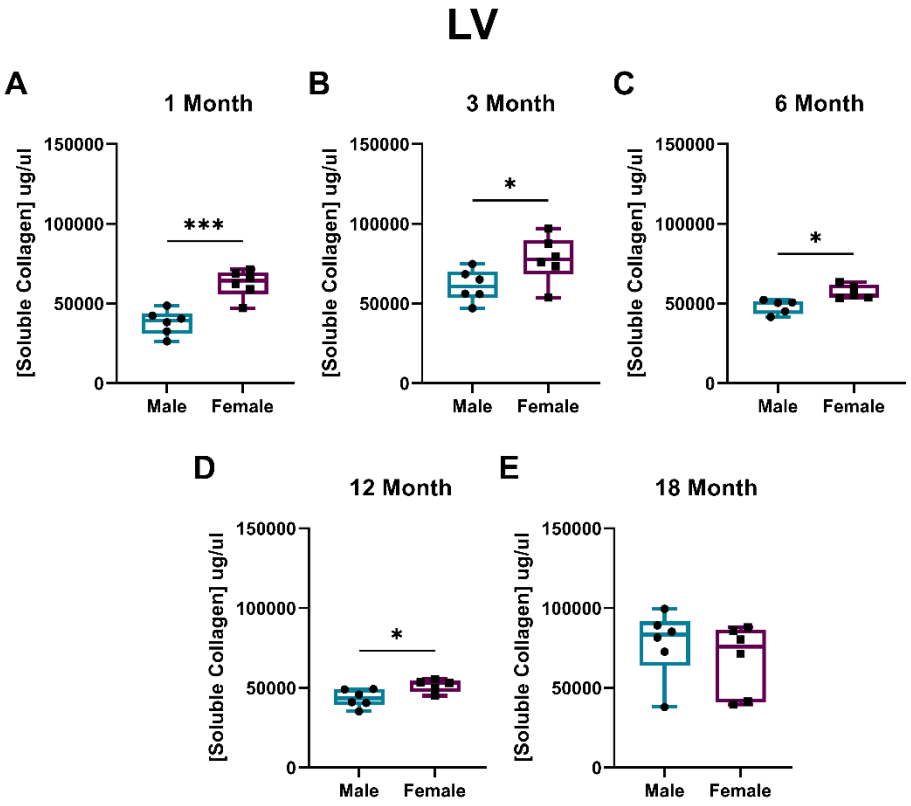

Figure 3. 20 Evaluating the impact of sex on total LV soluble collagen content across timepoints. Soluble collagen (µg/µl) was measured in the LV at each imaging time point: 1 month (A), 3 month (B), 6 month (C), 12 month (D) and 18 months (E). Results reported as min to max range, n=5-6 males and n=5-6 females; p values were obtained using unpaired parametric students t-test when comparing two groups' *p<0.05; ***p<0.001

The effect of aging on soluble collagen content was assessed in both sexes over an 18-month period. Males exhibited an age-associated increase in collagen, with peaks at 3 (p=0.004) and 18 months (p=<0.0001). At 3 months, males showed a 64% increase compared to baseline 1-month measurements, likely associated with LV growth (Figure 3.21 A). Soluble collagen levels in males were comparable to the 1-month time point at 6 and 12 months. At 18 months, males demonstrated a highly significant increase in soluble collagen content of 103.9%, indicating a higher level of soluble collagen at this age. Interestingly, females showed no significant changes in soluble collagen over the 18 months (Figure 3.21 B). While minor oscillations were present, they indicated no real changes in soluble collagen content in females. These findings identify a sex-specific effect in males, showing increased soluble collagen content in the LV with advanced aging.

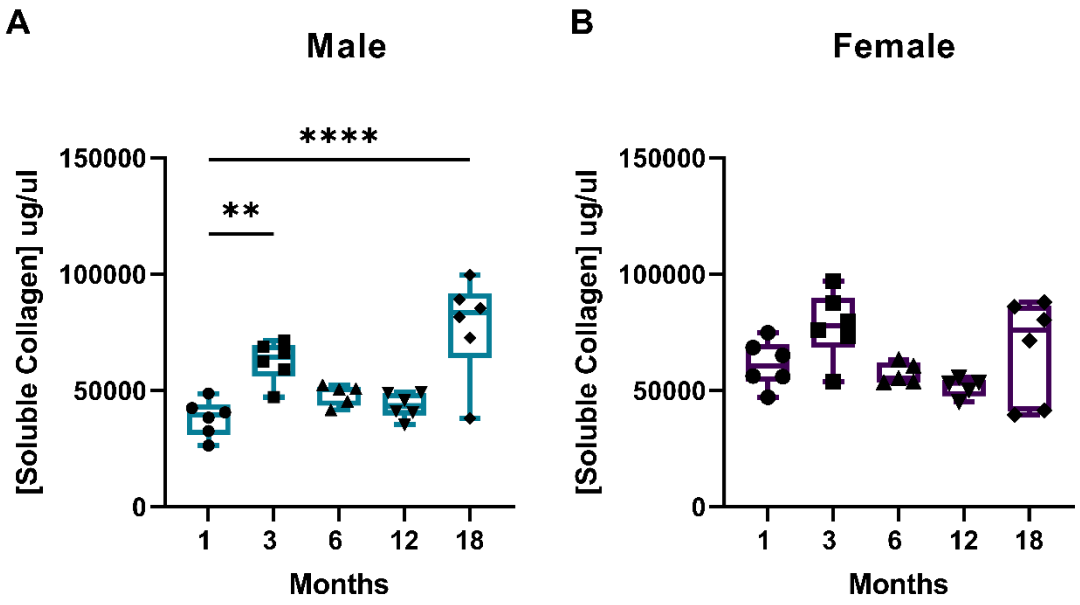

Figure 3. 21 Evaluating the impact of age on total LV soluble collagen content in both sexes. Longitudinal changes in males (A) and females (B) Soluble collagen (µg/µl) uptake in the LV over 18 months. Results reported as min to max range, n=5-6 males and n=5-6 females; p values were obtained a one-way ANOVA with Dunnett's Post hoc test when comparing longitudinal data to the first timepoint. **p<0.01 and ****p<0.0001

3.3.6 Male-specific age-related increase in insoluble collagen, absent in females

Insoluble collagen is a measure of mature, cross-linked collagen fibres that are crucial for maintaining the structure and function of the heart. These fibres are resistant to solubilization due to several post-translational modifications, such as hydroxylation and cross-linking. Sex differences in insoluble collagen content were assessed over 18 months. Differences were only observable at 1 month (p=0.012) and 3 months (p=0.02) of age, with females exhibiting higher collagen content (1 month: 3180 ± 728 µg/µl and 3 months: 1875 ± 718 µg/µl) compared to their male counterparts (1 month: 2112 ± 583.7 µg/µl and 3 months: 891.3 ± 126.8 µg/µl) (Figure 3.22). After 6 months, insoluble collagen content remained similar between males and females up to 18 months of age. No clear sex-specific association with insoluble collagen content was observed beyond the early time points.

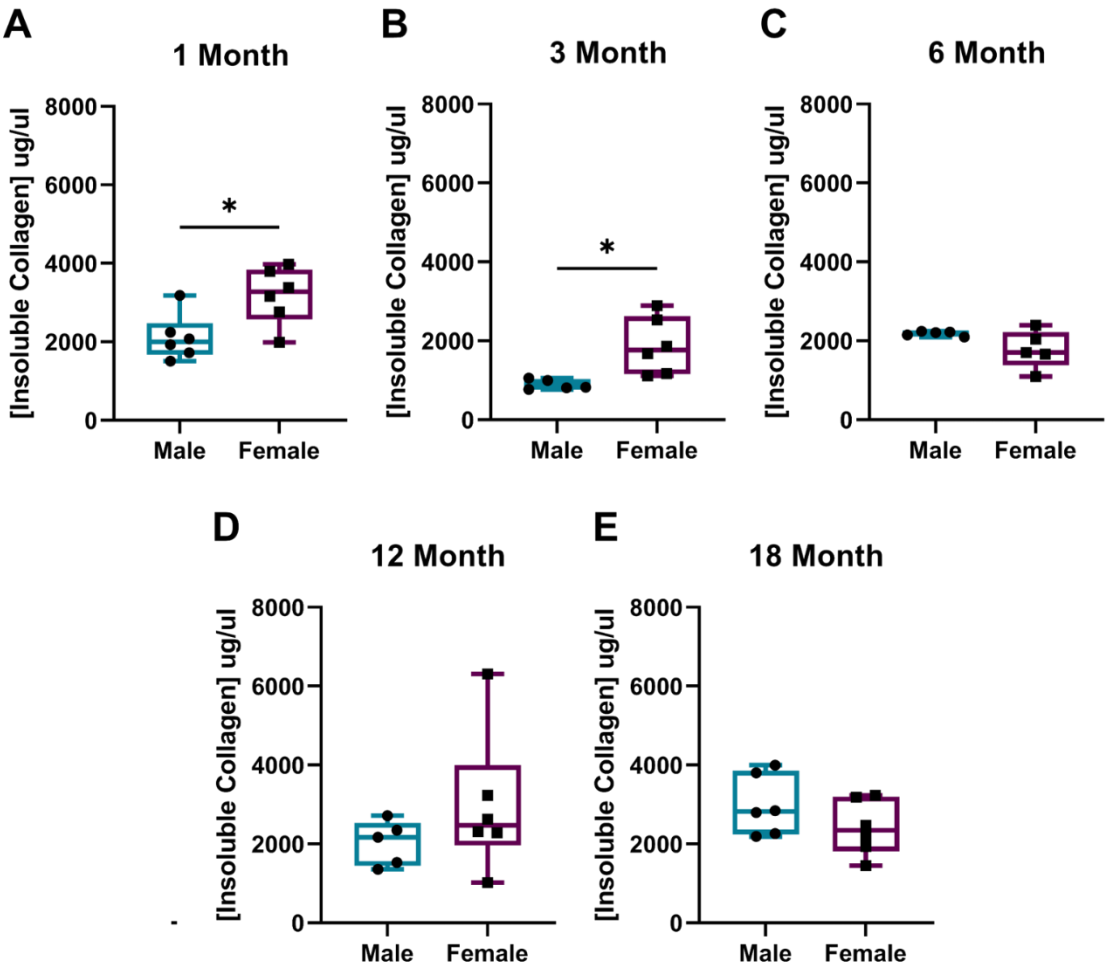

Figure 3. 22 Evaluating the impact of sex on total LV insoluble collagen content across timepoints. Insoluble collagen (µg/µl) was measured in the LV at each imaging time point: 1 month (A), 3 month (B), 6 month (C), 12 month (D) and 18 months (E). Results reported as min to max range, n=5-6 males and n=5-6 females; p values were obtained using unpaired parametric students t-test when comparing two groups' *p<0.05

The effect of aging on insoluble collagen content was assessed in both sexes, revealing a sex-specific increase in aged males. Males exhibited a significant decrease in insoluble collagen content, averaging 891 ± 12 µg/µl at 3 months (p=0.003) compared to 2112 ± 583.7 µg/µl at 1 month, representing an overall decrease of 57.8% (Figure 3.23 A). This reduction was followed by a recovery at 6 and 12 months, with levels comparable to baseline measurements. At 18 months, males showed a significant increase of 41.2% (p=0.03) in insoluble collagen. In contrast, females displayed no significant age-associated changes in insoluble collagen content, similar to the findings for soluble collagen (Figure 3.23 B). Although females exhibited a similar trend to males at 3 months, with a 41% decrease in insoluble collagen, there was greater variability in the data and trend wasn't significant (p=0.10).

Overall, insoluble collagen levels in females remained stable up to 18 months. These findings highlight an age-related increase in insoluble collagen expression in males compared to their female counterparts.

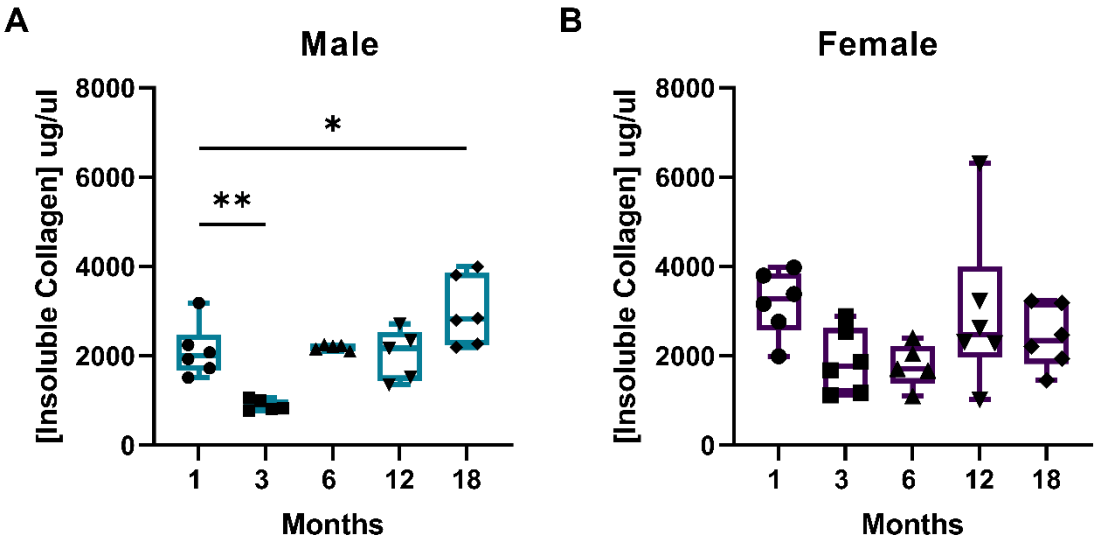

Figure 3. 23 Evaluating the impact of age on total LV insoluble collagen content in both sexes. Longitudinal changes in males (A) and females (B) Insoluble collagen (µg/µl) uptake in the LV over 18 months. Results reported as min to max range, n=5-6 males and n=5-6 females; p values were obtained a one-way ANOVA and Dunnett's Post hoc test when comparing longitudinal data to the first timepoint. *p<0.05 and **p<0.01

3.3.7 Soluble/Insoluble collagen ratio is not altered by age or sex

The insoluble-to-soluble collagen ratio was calculated as a measure of tissue integrity and function, providing insight into the balance between collagen synthesis and maturation. Sex was found to have no impact on the LV insoluble-to-soluble ratio over 18 months, suggesting that both males and females maintain a consistent balance between insoluble and soluble collagen throughout this period (Figure 3.24). Interestingly, age had a significant effect on the insoluble-to-soluble ratio in both males and females at 3 months (p=0.04) (Figure 3.25). This significant decline indicates an increased abundance of soluble collagen, which may reflect elevated collagen turnover and synthesis of soluble collagen that has not yet been cross-linked. No further changes were observed after 3 months, suggesting that this shift may be a key component of cardiac growth with age.

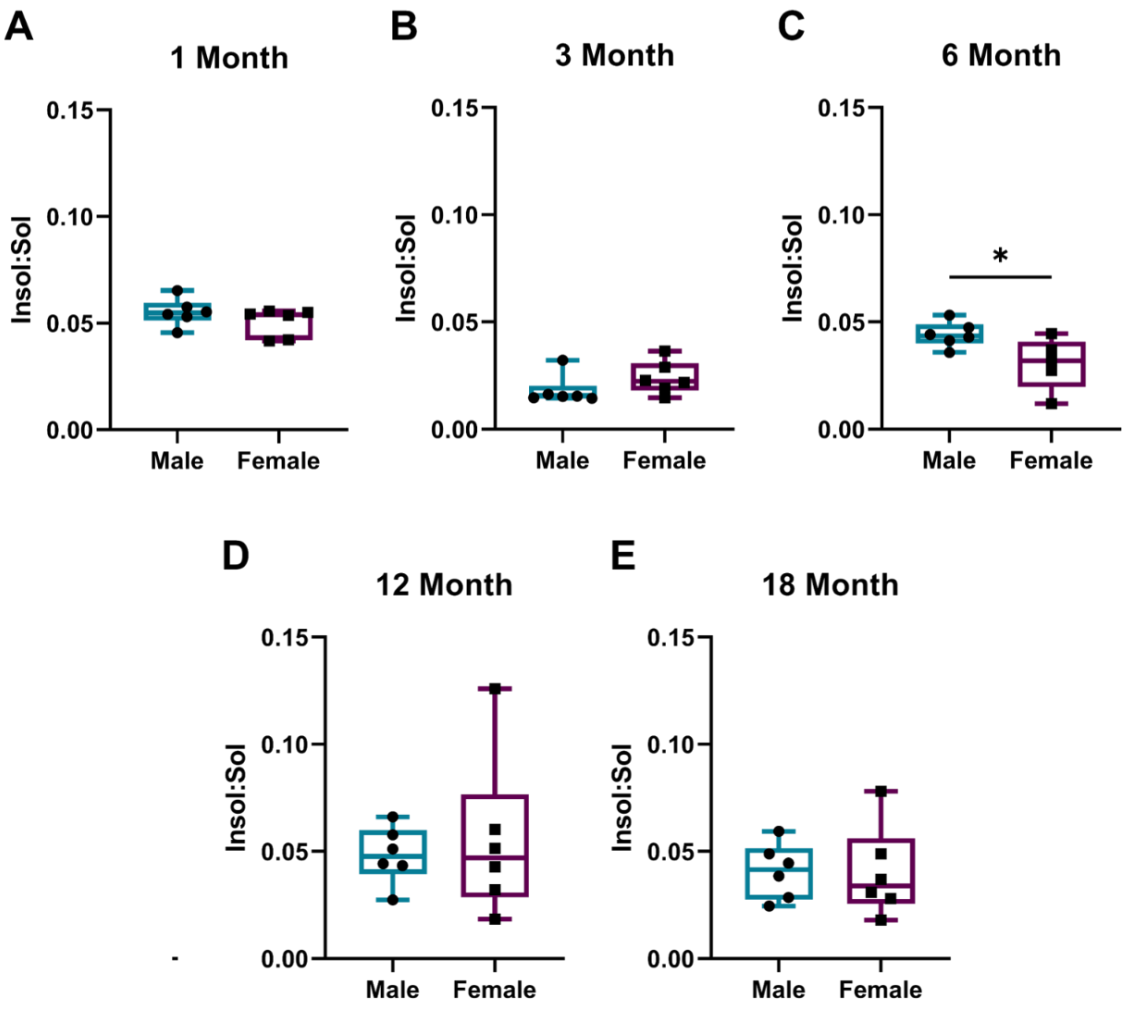

Figure 3. 24 Evaluating the impact of sex on total LV insoluble: soluble collagen content ratio across timepoints. Insoluble: soluble collagen ratio was calculated for the LV at each imaging time point: 1 month (A), 3 month (B), 6 month (C), 12 month (D) and 18 months (E). Results reported as min to max range, n=5-6 males and n=5-6 females; p values were obtained using unpaired parametric students t-test when comparing two groups' *p<0.05

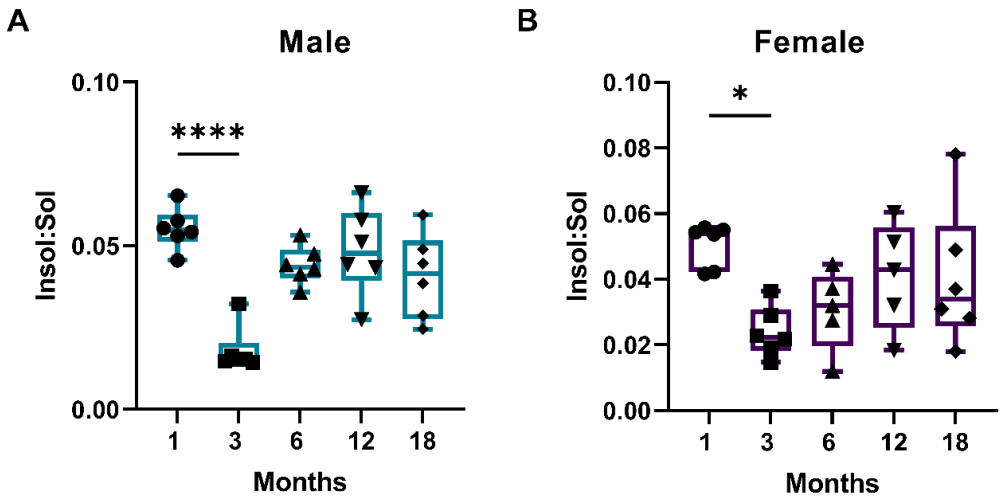

Figure 3. 25 Evaluating the impact of age on total LV insoluble: soluble collagen ratio in both sexes. Longitudinal changes in males (A) and females (B) insoluble: soluble collagen content ratio was calculated for the LV over 18 months. Results reported as min to max range, n=5-6 males and n=5-6 females; p values were obtained a one-way ANOVA and Dunnett's post hoc test when comparing longitudinal data to the first timepoint *p<0.05 and ****p<0.0001

3.3.8 Increased AGE crosslinking in aged males, absent in female in the LV

Aging-associated crosslinking proteins, AGEs, created through a non-enzymatic reaction between glucose and ECM proteins, were measured to assess the abundance of crosslinking and the impact of age and sex. AGEs crosslinking was compared between the sexes over 18 months, as shown in Figure 3.26. Males and females showed comparable levels of AGEs at all time points except at 6 months, where females exhibited around 20% higher crosslinking than their male counterparts. However, no sex differences were observed in advanced aging.

The effect of aging on AGEs crosslinking was assessed in both males and females over 18 months. Males exhibited significantly increased crosslinking at 3 months (112223 ± 1475 ng/ml; p=0.01), reflecting a 60% increase (Figure 3.27 A). This upward trend continued at 6 months (99530 ± 1719), with a 42% increase that approached significance (p=0.07). At 12 months, a significant 50% increase (p=0.03) in crosslinking was observed in males, suggesting that aging leads to increased AGEs crosslinking. However, no significant differences were noted at 18 months. In females, no significant changes were identified over the 18 months, though a similar trend was observed with a 33.8% increase between 1 month and 12 months, followed by a decline at 18 months (Figure 3.27 B). Interestingly, females generally exhibited higher levels of crosslinking with fewer fluctuations in AGEs concentration. These results indicate that males experience an age-associated increase in AGEs crosslinking that is not observable in females.

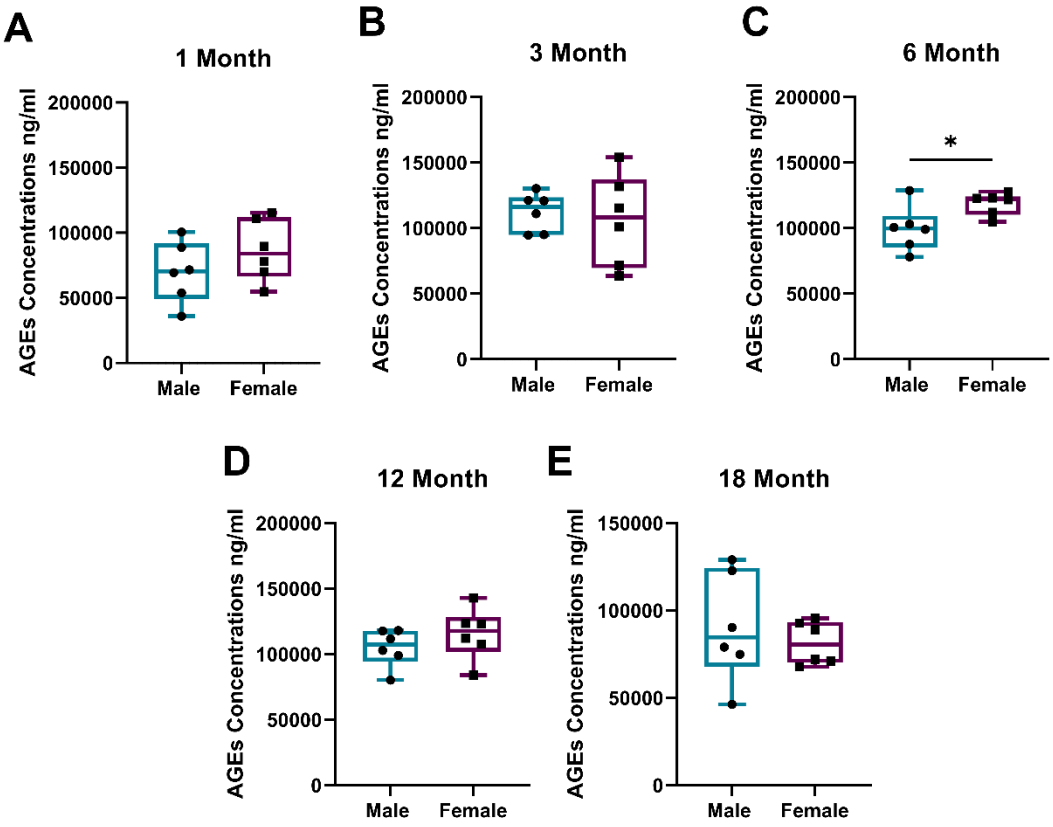

Figure 3. 26 Evaluating the impact of sex on AGEs concentration across 18 months. AGEs concentration was measured within the LV at each imaging time point: 1 month (A), 3 month (B), 6 month (C), 12 month (D) and 18 months (E). Results reported as min to max range, n=5-6 males and n=5-6 females; p values were obtained using unpaired parametric students t-test when comparing two groups' *p<0.05

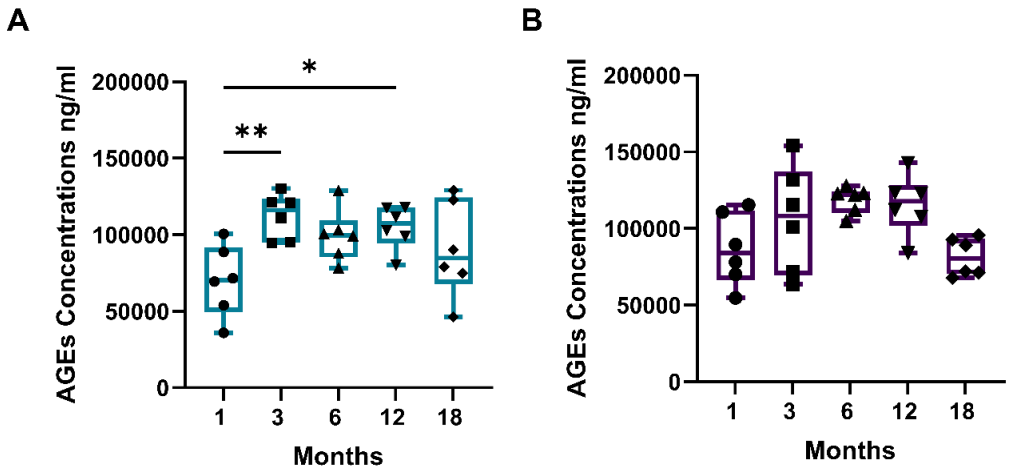

Figure 3. 27 Evaluating the impact of age on AGEs crosslinking in both sexes over 18 months. Longitudinal changes in males (A) and females (B) AGEs Crosslinking were measured for the LV over 18 months. Results reported as min to max range, n=5-6 males and n=5-6 females; p values were

obtained a one-way ANOVA and Dunnett's Post hoc test when comparing longitudinal data to the first timepoint. *p<0.05; **p<0.01

3.3.9 LV collagen synthesis outcomes may predict functional outcomes

Aged EF values (see Chapter 2, Section 3.6.) were compared with longitudinal measurements of *cis*-4-[^{18}F]fluoro-*L*-proline and *trans*-4-[^{18}F]fluoro-*L*-proline uptake to determine if either tracer or timepoint correlated with functional outcomes in aged animals. Non-linear regression analysis of *cis*-4-[^{18}F]fluoro-*L*-proline data revealed that no single time point was significantly associated with *in vivo* imaging results (Table 3.8). Similarly, LV *trans*-4-[^{18}F]fluoro-*L*-proline uptake showed no strong associations, although the 6-month measurements were significantly associated with 18-month ejection fraction. However, the R^2 value was low at 0.3071, indicating that no substantial association can be inferred from these results (Figure 3.28). This suggests that fluorproline PET measurements do not correlate well with functional outcomes in aging. It is important to note that the low sample numbers, as only animals that survived the entire study were included in the analysis, could lead to imprecise formulation.

Table 3. 8. Summary of linear regression analysis comparing *cis*-4-[^{18}F]fluoro-*L*-proline and *trans*-4-[^{18}F]fluoro-*L*-proline uptake in the LV at different time points during the course of natural aging and EF outcomes measured at 18 months of age. Dunnett's Post-hoc test corrected for multiple comparison.

Radiotracer	Outcome Measure	Months				
		1	3	6	12	18
***cis*-[^{18}F]-Pro**	**R Squared**	0.2485	0.0005542	0.1549	0.04347	0.07921
	P Value	0.0829	0.9392	0.1833	0.4942	0.3516
***trans*-[^{18}F]-Pro**	**R Squared**	0.01968	0.3015	0.3071	0.01423	0.03560
	P Value	0.6637	0.0644	0.0494	0.6979	0.5370

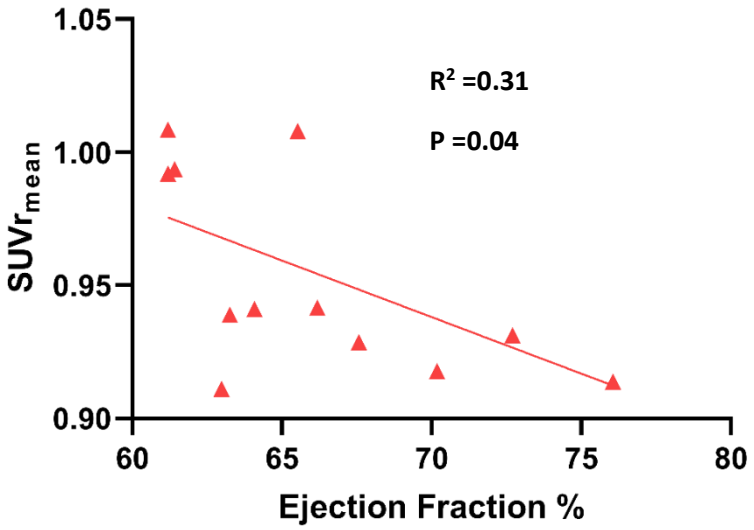

Figure 3. 28 Longitudinal correlation analysis of collagen synthesis and cardiac functional outcomes in the LV. *trans*-4-[^{18}F]fluoro-*L*-proline uptake at 6 months was found to significantly correlate with ejection fraction measures at 18 months of age. Results reported as min to max range, n=7 males and n=6 females; p values were obtained a non-linear regression analysis *p<0.05 and corrected for multiple comparisons.

3.3.10 Correlation analysis between LV collagen synthesis and deposition

Associations between collagen synthesis, collagen deposition, and cardiac functional outcomes were examined to determine whether different metrics of collagen metabolism yield consistent functional insights. Notably, PET outcomes revealed that males did not exhibit significant correlations between *cis*-4-[^{18}F]fluoro-*L*-proline and *trans*-4-[^{18}F]fluoro-*L*-proline measures, whereas females demonstrated a significant positive correlation between the two tracers (Figure 3.29). Both sexes showed a positive correlation between insoluble collagen and AGEs crosslinking, although this correlation was statistically significant only in females. However, no correlations were observed between any *ex vivo* collagen deposition measures and *in vivo* imaging outcomes, indicating that the *in vivo* radiotracers are capturing distinct processes from those measured by *ex vivo* methods.

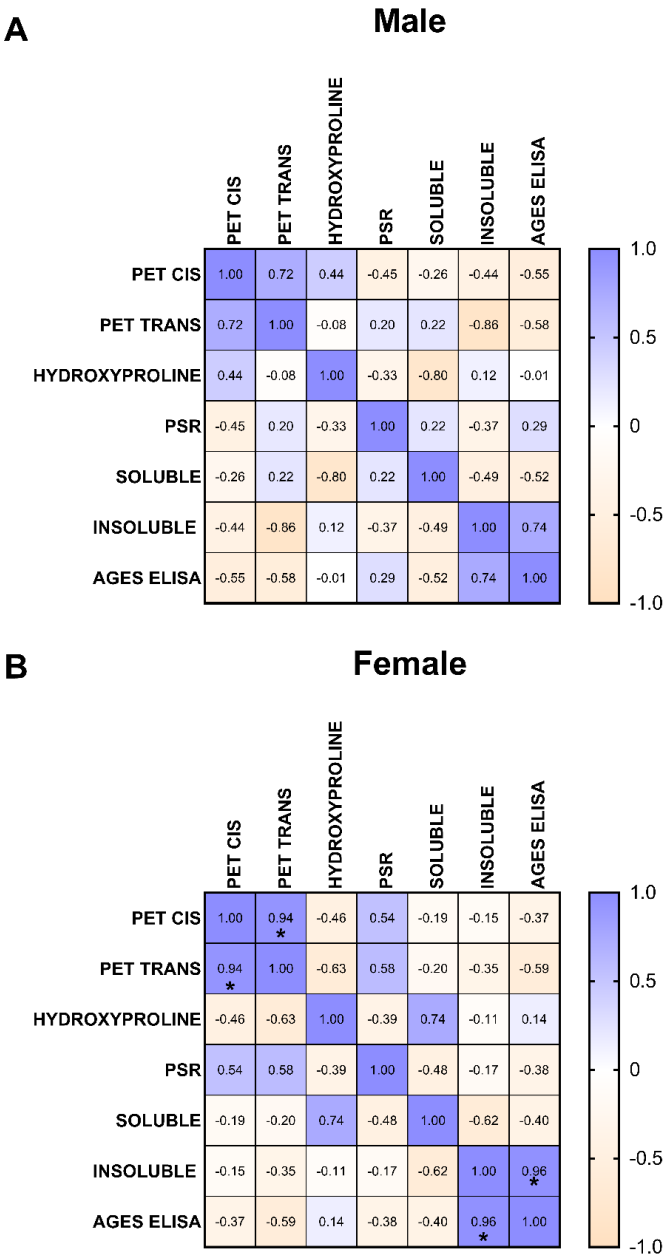

Figure 3. 29 – Correlation analysis of LV collagen synthesis and deposition outcomes. Correlation analysis was carried out comparing longitudinal collagen synthesis outcomes and longitudinal collagen deposition outcomes in males (A) and females (B) Correlation matrix analysis was performed using Pearson correlation to assess the relationships between various parameters. Statistical significance was determined Pearson rank correlation analysis. Significance levels are indicated as follows: *p<0.05 and corrected for multiple comparisons; Abbreviations: PET CIS: cis-4-[^{18}F]fluoro-*L*-proline; PET TRANS: *trans*-4-[^{18}F]fluoro-*L*-proline; PSR: Picrosirius RED staining; AGES ELISA: Advanced glycation end production enzyme linked immuoabsorbance assay.

In vivo imaging outcomes were compared with functional measures reported in the previous chapter 2. Notably, in males, *trans*-4-[^{18}F]fluoro-*L*-proline outcomes exhibited a strong positive correlation with both systolic and diastolic blood pressure, a correlation not observed in females (Figure 3.30). Additionally, frailty measures showed no correlation with PET outcomes or blood pressure measures.

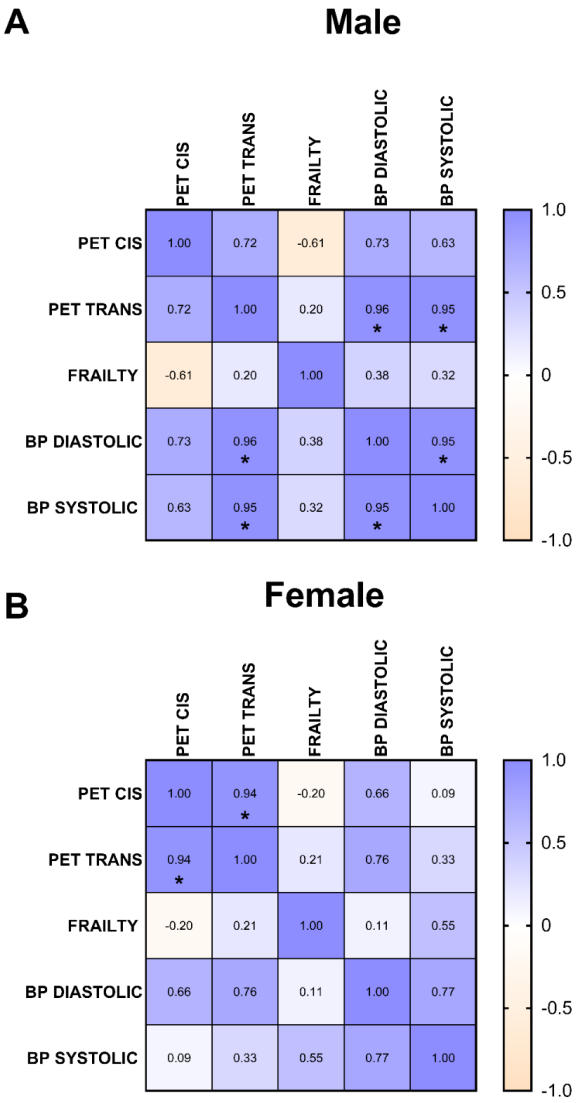

Figure 3. 30 Correlation analysis of LV collagen synthesis and cardiac functional outcomes. Correlation analysis was carried out comparing longitudinal collagen synthesis outcomes and longitudinal cardiac functional outcomes in males (A) and females (B) Correlation matrix analysis was performed using Pearson correlation to assess the relationships between various parameters. Statistical significance was determined Pearson rank correlation analysis. Significance levels are indicated as follows; *p<0.05 and corrected for multiple comparisons; Abbreviations: PET CIS: cis-4-[^{18}F]fluoro-*L*-proline; PET TRANS: *trans*-4-[^{18}F]fluoro-*L*-proline; PSR: Picrosirius RED staining; AGES ELISA: Advanced glycation end production enzyme linked immuoabsorbance assay.

3.3.11 Hierarchical clustering reveals age-related patterns in collagen synthesis and deposition in the LV, independent of sex

Hierarchical clustering was performed to investigate relationships between collagen synthesis and outcomes, as well as differences across time points and groups. The analysis showed no clear clustering by sex, indicating that sex does not influence collagen synthesis and deposition in this study (Figure 3.31). Outcome measures demonstrated distinct clustering: PET radiotracer measurements clustered with soluble collagen, reflecting newly synthesized, immature collagen, while the second main cluster was associated with mature collagen and crosslinking. This confirms that PET measurements are independent of collagen deposition measurements. Clustering of PET outcomes compared to functional measures, identified once again no clear clustering by sex, however, a clearer cluster by age with 12month and 18-month groups closely associated (Figure 3.32). The most notable finding was that frailty did not cluster with any other outcome.

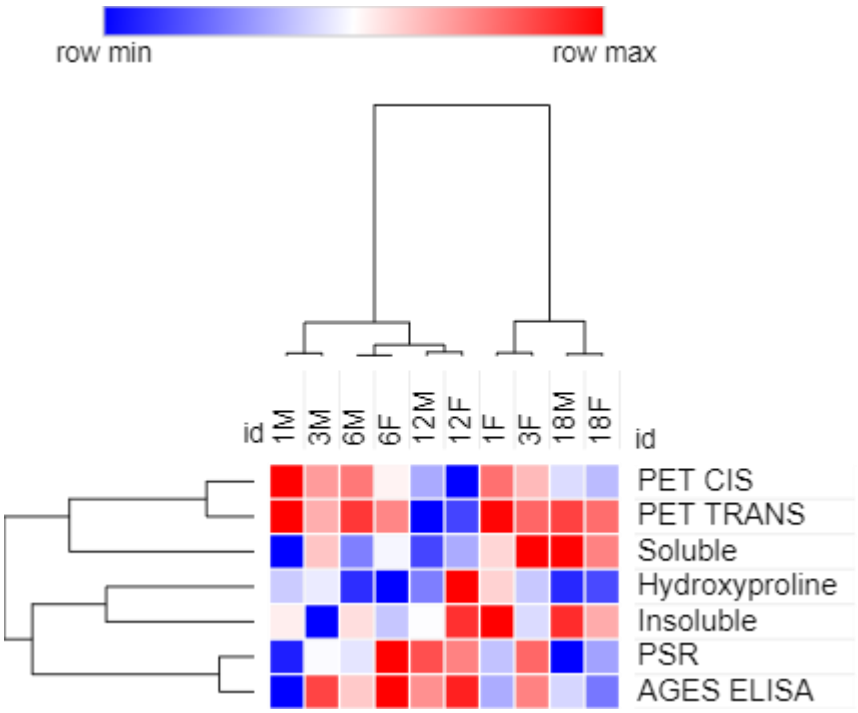

Figure 3. 31 Hierarchical clustering analysis of collagen synthesis and deposition in the LV. Hierarchical clustering using Morpheus was performed to compare collagen synthesis and deposition across different time points and sexes. The heatmap shows clustering patterns in male and female subjects at 1 month (1M, 1F), 3 months (3M, 3F), 6 months (6M, 6F), 12 months (12M, 12F), and 18 months (18M, 18F). The dendrogram indicates the relationships among groups, highlighting similarities and differences in collagen metabolism over time.

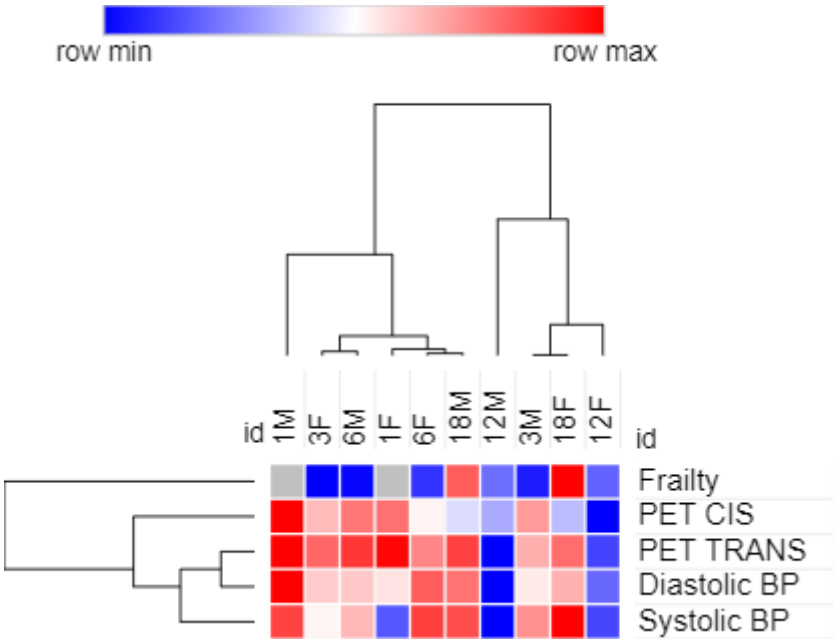

Figure 3. 32 Hierarchical clustering analysis of collagen synthesis and cardiac function. Hierarchical clustering using Morpheus was performed to compare collagen synthesis and cardiac function across different time points and sexes. The heatmap shows clustering patterns in male and female subjects at 1 month (1M, 1F), 3 months (3M, 3F), 6 months (6M, 6F), 12 months (12M, 12F), and 18 months (18M, 18F). The dendrogram indicates the relationships among groups, highlighting similarities and differences in collagen metabolism over time.

3.3.12 Age-related decline in RV *cis*-4-[^{18}F]fluoro-*L*-proline uptake is unaffected by sex

The effect of age and sex on RV unhydroxylated collagen synthesis was assessed *in vivo*. These collagen fibres do not form mature collagen and are less stable and more prone to degradation. No significant sex differences were observed in RV unhydroxylated collagen synthesis, with males and females showing comparable levels of uptake from 1 month (males: 0.96 ± 0.04; females: 0.94 ± 0.07) to 18 months (males: 0.92 ± 0.08; females: 0.89 ± 0.05) (figure 3.33).

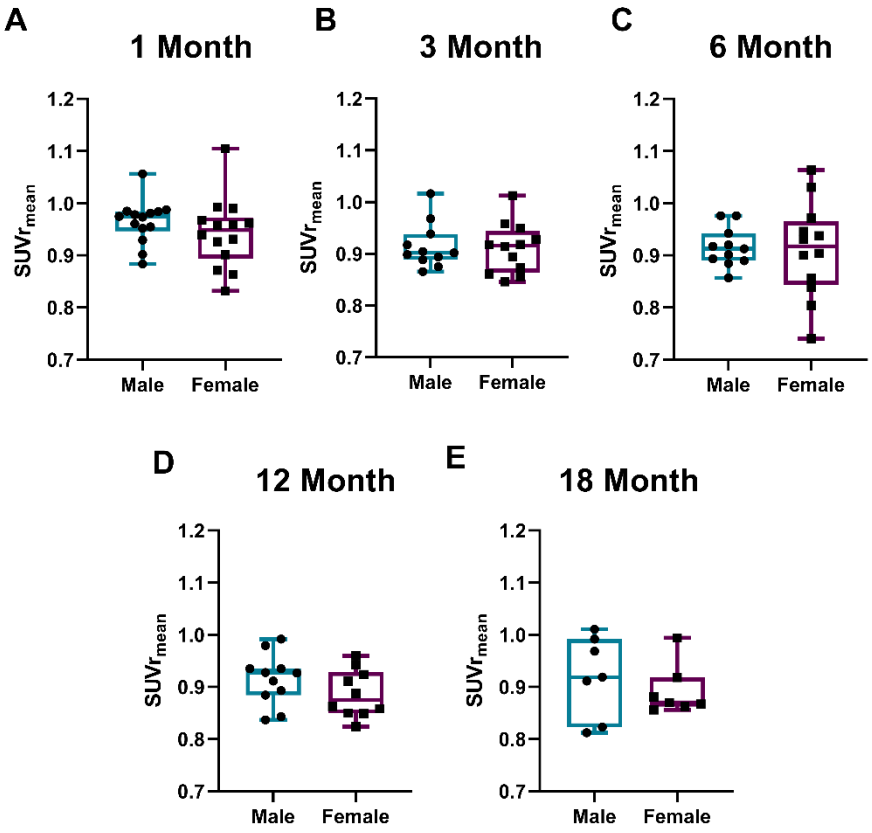

Figure 3. 33 Evaluating the impact of sex on RV *cis*-4-[^{18}F]fluoro-*L*-proline Uptake Across Timepoints. *cis*-4-[^{18}F]fluoro-*L*-proline uptake was measured in the RV at each imaging time point: 1 month (A), 3 month (B), 6 month (C), 12 month (D) and 18 month (E). Results reported as min to max range, n=7-14 males and n=7-14 females; Changes were assessed using a Student's t-test; results were not statistically significant.

The effect of age on RV unhydroxylated collagen synthesis was assessed in both males and females over 18 months. Males exhibited a significant decrease of 5% (p=0.012) between 1 and 6 months (Figure 3.34 A). This declining trend continued at 3 months with a 4.1% decrease (p=0.16), at 12 months with a 5.1% decrease (p=0.10), and at 18 months with a 4.6% decrease (p=0.34), although these were not statistically significant. This suggests that the uptake of the radiotracer and unhydroxylated collagen synthesis decline with age. In females, no significant changes were observed over the 18 months (Figure 3.34 B). However, a similar trend was noted, with a consistent decline in uptake over 18 months of 7.4%, though this may not be significant due to higher data variability.

Since no sex differences were observed in unhydroxylated collagen synthesis, the data from both groups were combined to assess the overall effect of aging. This analysis confirmed previous trends, showing significant declines of 3.5% at 3 months (0.92 ± 0.04 SUVr; p=0.04), 4.4% at 6 months (0.91 ±

0.07 SUVr; p=0.04), and 5.6% at 12 months (0.90 ± 0.05 SUVr; p=0.01) (Figure 3.35). A similar trend was observed at 18 months (0.90 ± 0.06 SUVr) with a 5.1% decline compared to baseline, although this decline did not reach statistical significance (p=0.07), likely due to the reduced sample size.

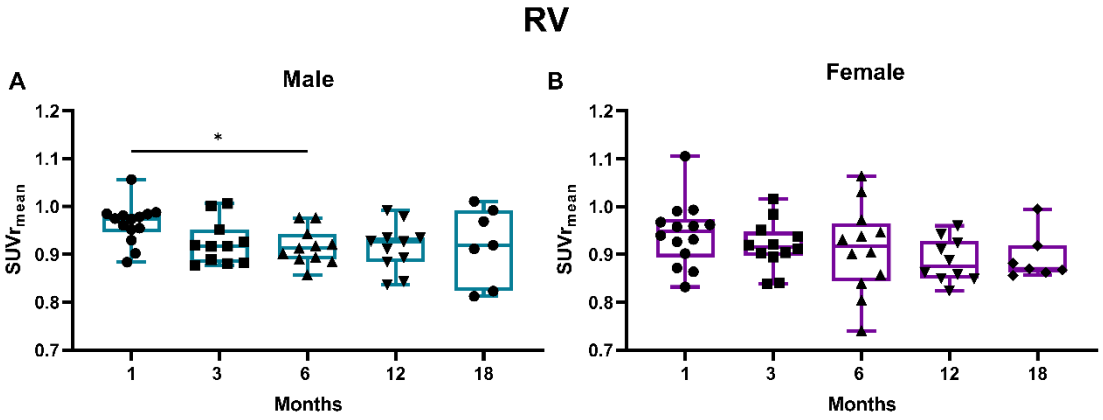

Figure 3. 34 Evaluating the impact of age on RV *cis*-4-[^{18}F]fluoro-*L*-proline in both sexes. Longitudinal changes in males (A) and females (B) *cis*-4-[^{18}F]fluoro-*L*-proline uptake in the RV over 18 months. Results reported as min to max range, n=7-14 males and n=7-14 females; p values were obtained a Mixed-effects Analysis and Post hoc Analysis when comparing longitudinal data to the first timepoint.; *p<0.05

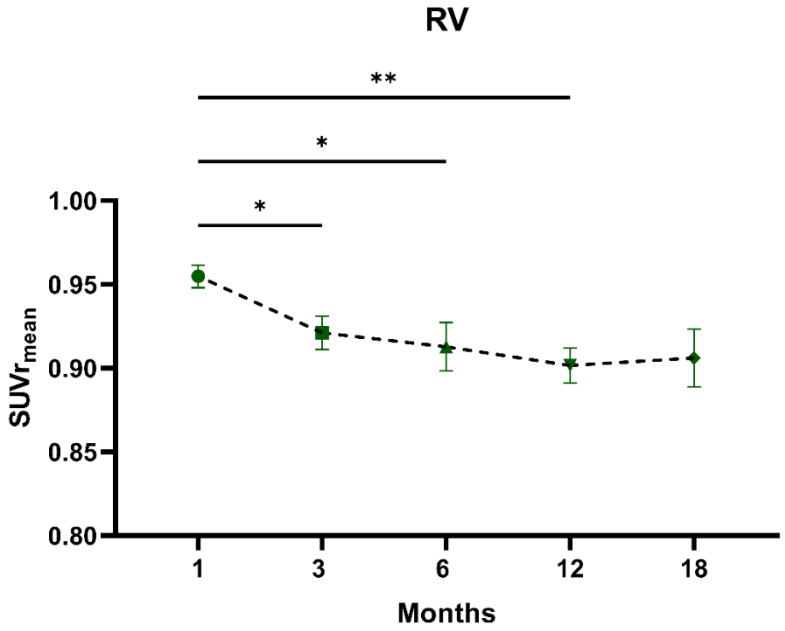

Figure 3. 35 Assessing the longitudinal effect of age in on RV *cis*-4-[^{18}F]fluoro-*L*-proline uptake. Longitudinal changes in *cis*-4-[^{18}F]fluoro-*L*-proline uptake in the RV over 18 months. Results reported as min to max range, n=7-14 males and n=7-14 females; p values were obtained a Mixed-effects Analysis and Post hoc Analysis when comparing longitudinal data to the first timepoint. *p<0.05; **p<0.01

3.3.13 Age-related decline in RV *trans*-4-[^{18}F]fluoro-*L*-proline uptake, unaffected by sex

RV hydroxylated collagen synthesis was assessed over 18 months using *trans*-4-[^{18}F]fluoro-*L*-proline. No significant sex differences were observed across the five time points, with males and females showing comparable levels (Figure 3.36). At 1 month, both males and females had similar SUVr values (males: 0.96 ± 0.05; females: 0.96 ± 0.05), which remained consistent at 18 months (males: 0.92 ± 0.08; females: 0.88 ± 0.04).

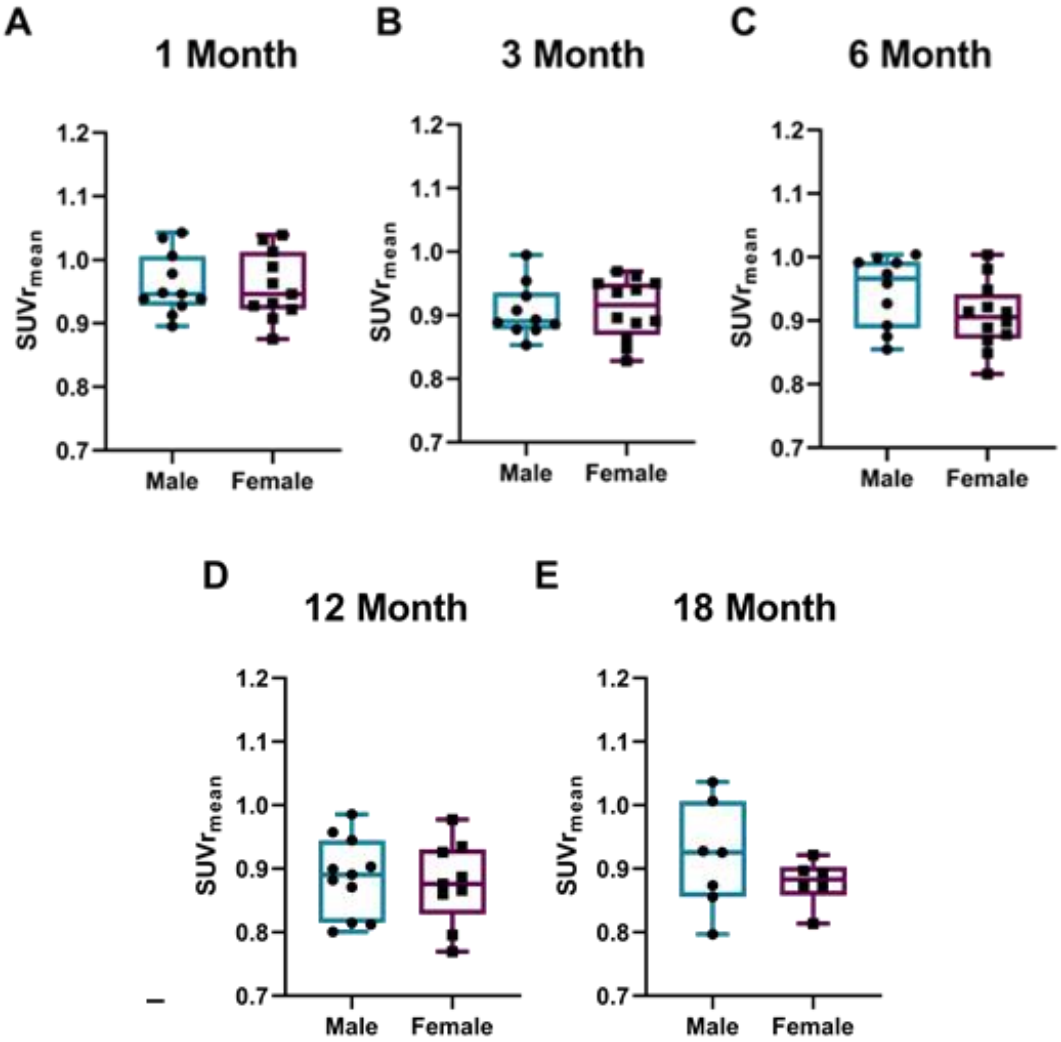

Figure 3. 36 Evaluating the impact of sex on RV *trans*-4-[^{18}F]fluoro-*L*-proline uptake across timepoints. *trans*-4-[^{18}F]fluoro-*L*-proline uptake was measured in the RV at each imaging time point: 1 month (A), 3 month (B), 6 month (C), 12 month (D) and 18 month (E). Results reported as min to max range, n=7-14 males and n=7-14 females; Changes were assessed using a Student's t-test; results were not statistically significant.

The effect of age on RV hydroxylated collagen synthesis was assessed in both males and females over an 18-month period. Males showed a significant decline in uptake between 1 and 3 months, with a 5.7% decrease at 3 months (p=0.03) (Figure 3.37). This trend continued with a non-significant decrease of 2.17% at 6 months. At 12 months, males exhibited a significant decline of approximately 7.64% (p=0.01) in collagen synthesis, indicating a reduction in RV unhydroxylated collagen synthesis at this time point. At 18 months, a non-significant increase of 4.5% was observed, suggesting a potential change in collagen synthesis with further aging. In females a significant decline in uptake observed at 3 months with a decrease of 5.1% (p=0.02) and at 18 months with a decrease of 8.4% (p=0.04).

As no sex differences were observed, the effect of aging on hydroxylated collagen synthesis was assessed in the entire cohort. A significant decline of 5.6% was observed at 3 months (0.91 ± 0.04 SUVr; p=0.01). This trend continued at 6 months (0.92 ± 0.056 SUVr; p=0.05), with a non-significant decline of 3.6% (Figure 3.38). At 12 months, a significant decline of 8% (p=0.01) was observed between 1 month (0.96 ± 0.05 SUVr) and 12 months (0.88 ± 0.06 SUVr). Furthermore, with increased statistical power, a significant decline of 6.2% was observed at 18 months (0.90 ± 0.07 SUVr; p=0.032), suggesting that hydroxylated collagen synthesis declines with aging.

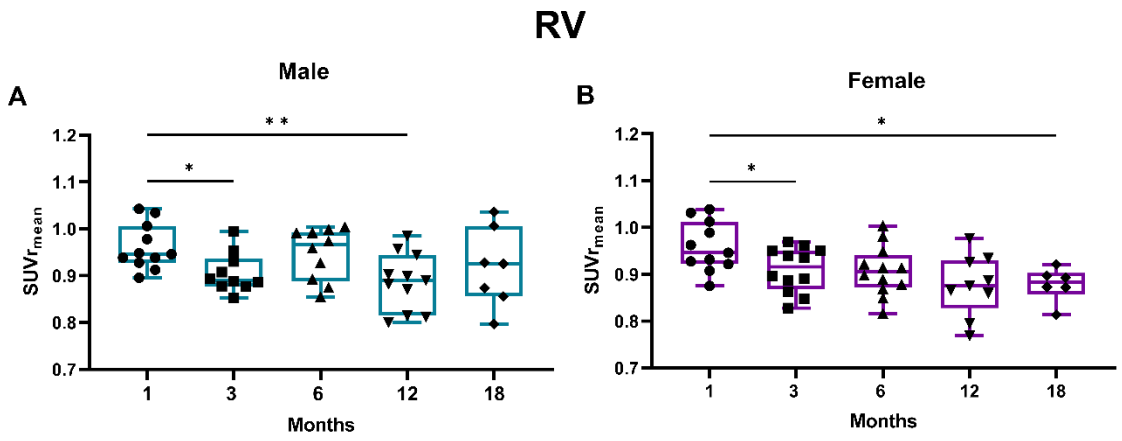

Figure 3. 37 Evaluating the impact of age on RV *trans*-4-[^{18}F]fluoro-*L*-proline in both sexes. Longitudinal changes in males (A) and females (B) *trans*-4-[^{18}F]fluoro-*L*-proline uptake in the RV over 18 months. Results reported as min to max range, n=7-14 males and n=7-14 females; p values were obtained a Mixed-effects Analysis and Dunnett's Post hoc test when comparing longitudinal data to the first timepoint. *p<0.05; **p<0.01;

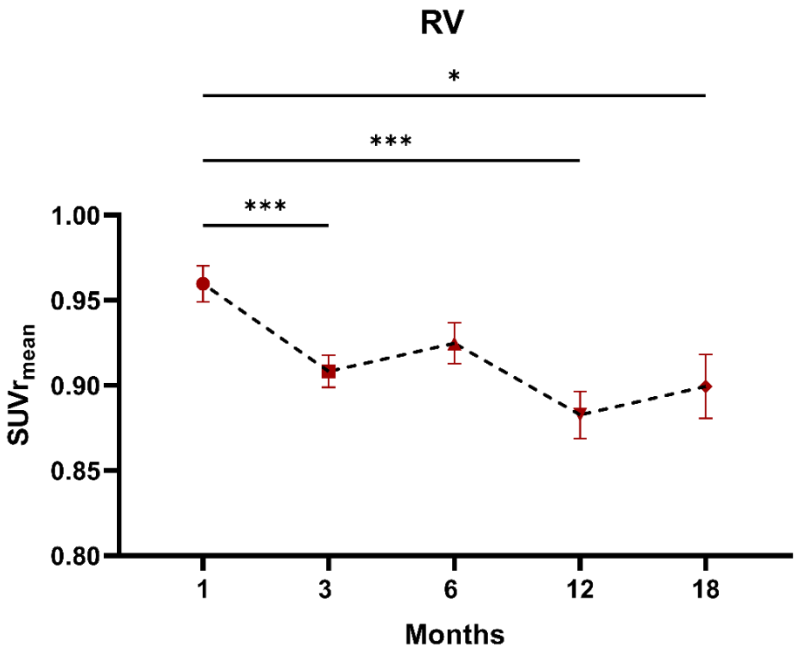

Figure 3. 38 Assessing the longitudinal effect of age in on RV *trans*-4-[^{18}F]fluoro-*L*-proline uptake. Longitudinal changes in *trans*-4-[^{18}F]fluoro-*L*-proline uptake in the RV over 18 months. Results reported as min to max range, n=7-14 males and n=7-14 females; p values were obtained a Mixed-effects Analysis and Dunnett's Post hoc test when comparing longitudinal data to the first timepoint. *p<0.05; **p<0.01; ***p<0.001

3.3.14 Accumulation of total deposited collagen in adulthood, followed by decline at 18 months in the RV

The total collagen content in the RV was assessed using PSR histological staining, following previously described methods. Both sexes exhibited similar percentages of positive PSR staining in the RV over 18 months (Figure 3.39). Males and females showed comparable levels of total collagen from 1 month (males: 10.2 ± 4%; females: 13.0 ± 1.6%) to 18 months (males: 10.2 ± 4.0%; females: 13.0 ± 1.6%). This suggests that the RV is less influenced by sex or that any differences are too subtle to be detected by the staining method used.

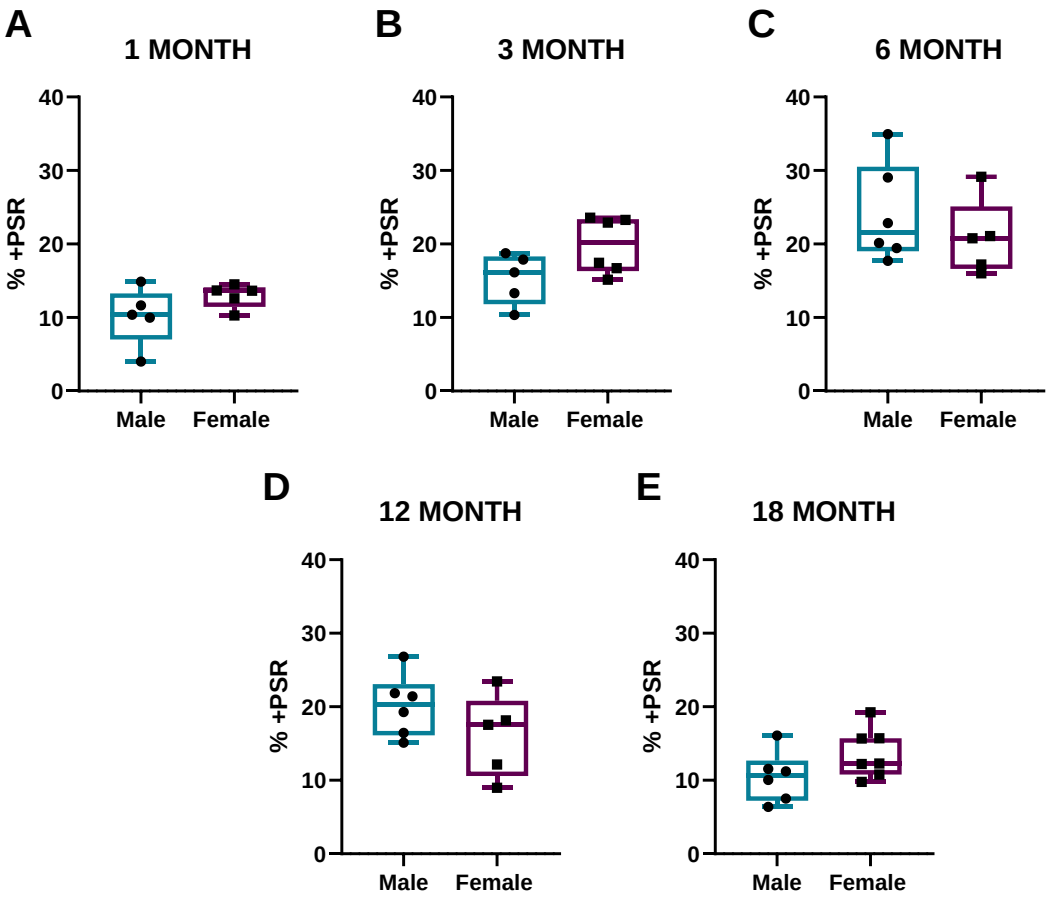

Figure 3. 39 Evaluating the impact of sex on total RV collagen deposition across timepoints. % positive PSR stain (%+PSR) was measured in the RV at each imaging time point: 1 month (A), 3 month (B), 6 month (C), 12 month (D) and 18 month (E). Results reported as min to max range, n=5-6 males and n=5-6 females; Changes were assessed using a Student's t-test; results were not statistically significant.

This study identified a cyclical pattern in collagen deposition for both sexes, with an initial increase followed by a decline at 18 months (Figure 3.40). In males, total collagen deposition increased from 1 month (10.2 ± 4.0%) to 12 months (20.2 ± 4.2%), with significant increases of 138% at 6 months (24.3 ± 7.4%; p=0.01) and 97% at 12 months (p=0.01) (Figure 3.40 A). A 50% increase was also observed at 3 months, although it was not significant (p=0.27). Interestingly, a significant decline of 48% in total deposited collagen was observed between 12 and 18 months, returning levels to baseline (p=0.99), indicating that aging does not cause unidirectional collagen accumulation. In females, a significant increase was observed at 3 months (19.8 ± 3.8%; p=0.04) of 53% (Figure 3.40 B). The peak total collagen in females was observed at 6 months (21.2 ± 5.2%; p=0.01) with a 63.8% increase, followed by a significant decline at 18 months (13.7 ± 3.3%) of 35.5%, returning to baseline levels. Both males

and females show significant age-related oscillations in total deposited collagen, but males exhibit much greater fluctuations.

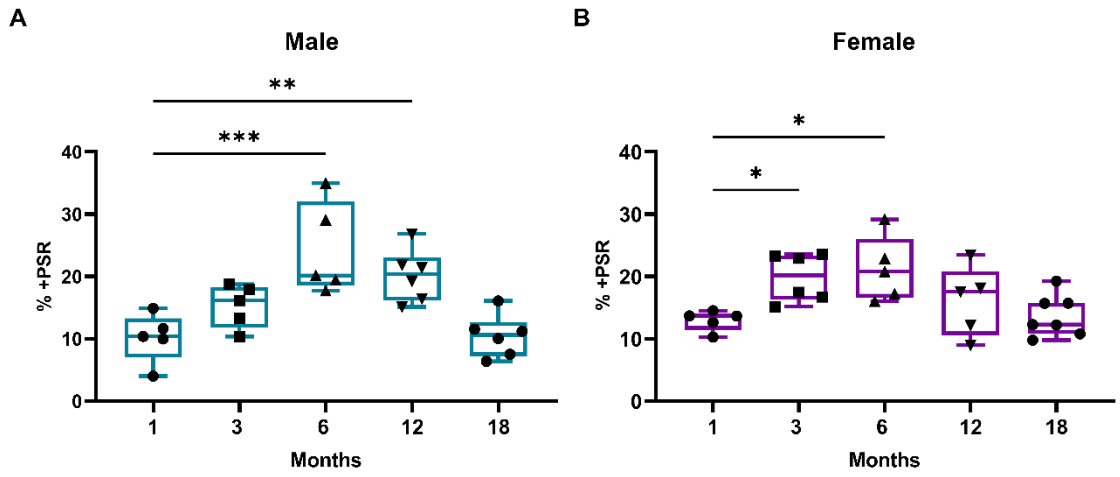

Figure 3. 40 Evaluating the impact of age on total RV collagen deposition in both sexes. Longitudinal changes in males (A) and females (B) % positive PSR stain (%+PSR) in the RV over 18 months. Results reported as min to max range, n=7-14 males and n=7-14 females; p values were obtained a Mixed-effects Analysis and Dunnett's Post hoc test when comparing longitudinal data to the first timepoint. *p<0.05; **p<0.01; ***p<0.001;

3.3.15 Hydroxyproline content increases at 12 months in the RV

Hydroxyproline content in the RV was measured as an indicator of total hydroxylated collagen and overall collagen abundance. Longitudinal comparisons of total hydroxyproline content between sexes revealed generally comparable levels at 1 month (males: 0.13 ± 0.08 µg/mg; females: 0.18 ± 0.08 µg/mg), 6 months (males: 0.17 ± 0.07 µg/mg; females: 0.10 ± 0.05 µg/mg), 12 months (males: 0.24 ± 0.07 µg/mg; females: 0.29 ± 0.05 µg/mg), and 18 months (males: 0.09 ± 0.08 µg/mg; females: 0.10 ± 0.37 µg/mg) (Figure 3.41). However, a significantly higher hydroxyproline content was observed at 3 months in females p=0.01), with a 159% higher hydroxyproline content compared to males at the same time point (Figure 3.41 B). This finding may indicate a sexually dimorphic developmental shift in cardiac structure between males and females.

The effect of aging on total hydroxyproline content over 18 months was studied in both sexes. In males, RV hydroxyproline content significantly increased from baseline at 1 month to 12 months by 82% (p=0.04) (Figure 3.42 A). This increase occurred gradually, with a 23.9% rise observed at 6 months, although this was not significant. A significant decline was noted between 12 and 18 months, suggesting that hydroxyproline content returns to baseline levels at 18 months. Similarly, females showed a significant increase in hydroxyproline content at 12 months, averaging 56.6% (p=0.03)

(Figure 3.42 B), followed by a significant decline between 12 and 18 months. It is important to acknowledge that this data set exhibits high variability, making interpretation challenging.

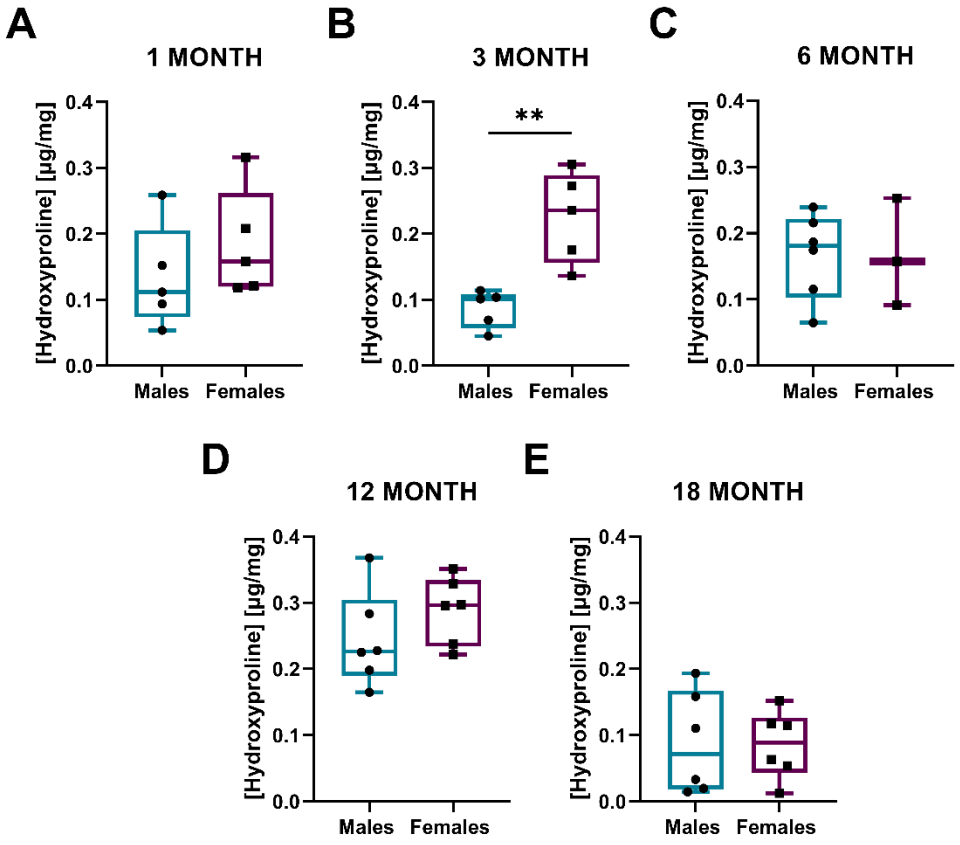

Figure 3. 41 Evaluating the impact of sex on total RV hydroxyproline content across timepoints. Hydroxyproline content (µg/mg) was measured in the RV at each imaging time point: 1 month (A), 3 month (B), 6 month (C), 12 month (D) and 18 months (E). Results reported as min to max range, n=5-6 males and n=5-6 females; p values were obtained using unpaired parametric students t-test when comparing two groups'; **p<0.01;

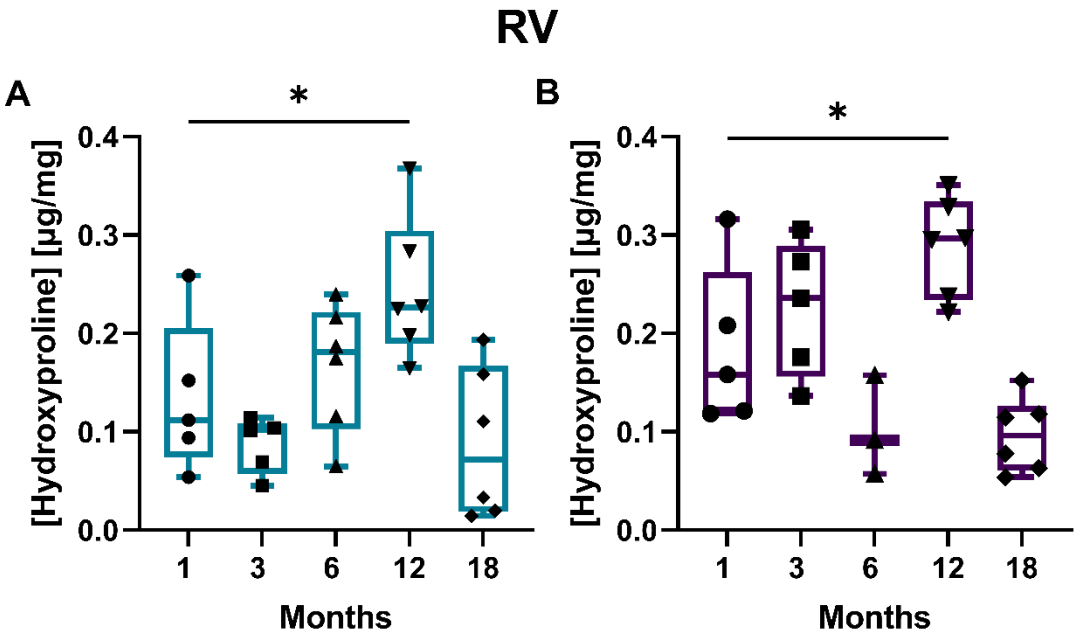

Figure 3. 42 Evaluating the impact of age on total RV hydroxyproline content in both sexes. Longitudinal changes in males (A) and females (B) Hydroxyproline content (µg/mg) uptake in the RV over 18 months. Results reported as min to max range, n=5-6 males and n=5-6 females; p values were obtained a Mixed-effects Analysis and Dunnett's Post hoc test when comparing longitudinal data to the first timepoint.; *p<0.05

3.3.16 Male-specific age-related increase in soluble collagen in the RV, absent in females

Soluble collagen was analysed to measure newly synthesized collagen in the RV. Sex differences were assessed, and no significant differences were identified over 18 months, suggesting that RV soluble collagen is not sexually dimorphic (Figure 3.43). Soluble collagen levels remained comparable between males and females from 1 month (males: 41745 ± 12458 µg/µl; females: 60504 ± 16033 µg/µl) to 18 months (males: 78610 ± 18926 µg/µl; females: 75153 ± 5529 µg/µl).

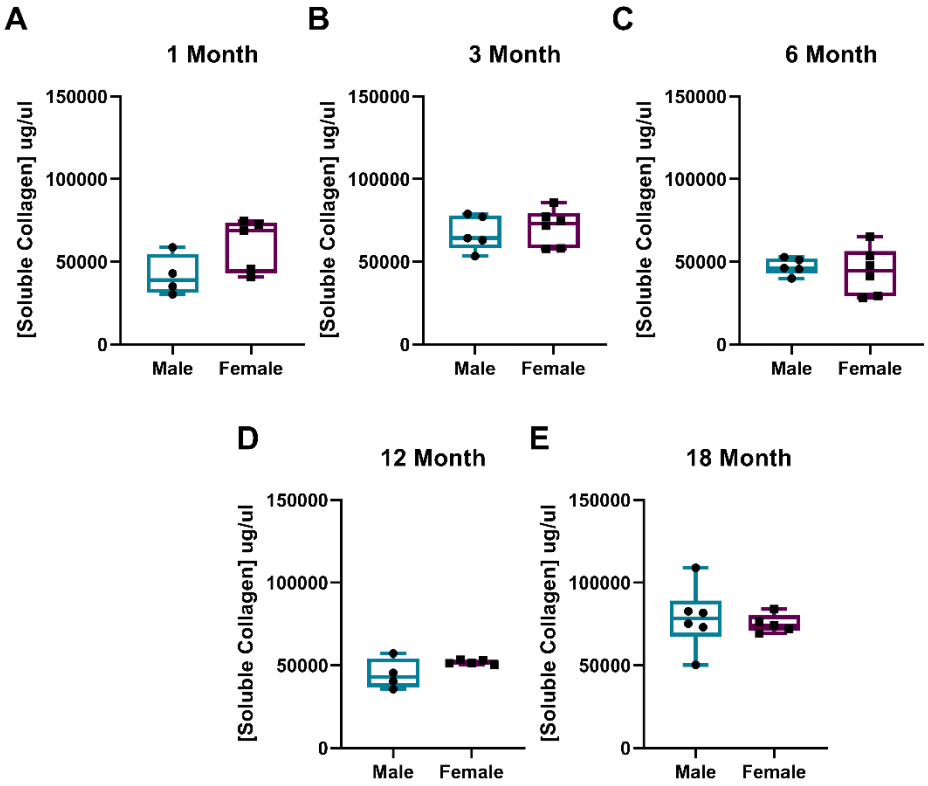

Figure 3. 43 Evaluating the impact of sex on total RV soluble collagen content across timepoints. Soluble collagen (µg/µl) was measured in the RV at each imaging time point: 1 month (A), 3 month (B), 6 month (C), 12 month (D) and 18 months (E). Results reported as min to max range, n=5-6 males and n=5-6 females; Changes were assessed using a Student's t-test; results were not statistically significant.

Aging caused a significant increase in soluble collagen in males but not in females. In males, there was a significant increase in soluble collagen at 3 months (67379 ± 10613 µg/µl; p=0.02) compared to baseline (41745 ± 12458 µg/µl), with a 61.4% increase observed (Figure 3.44 A). Soluble collagen levels returned to baseline at 6 and 12 months, followed by a highly significant increase at 18 months (78610 ± 18926 µg/µl; p=0.01), representing an 88.3% increase. In contrast, females showed no statistically significant changes. Two peaks were observed: at 3 months (70910 ± 11018 µg/µl; p=0.08), representing a 17.2% increase from baseline (60504 ± 16033 µg/µl), and at 18 months, with a 24% increase (75153 ± 5529 µg/µl; p=0.15). However, none of these peaks were significantly different, indicating that female soluble collagen levels remain relatively stable over 18 months compared to males.

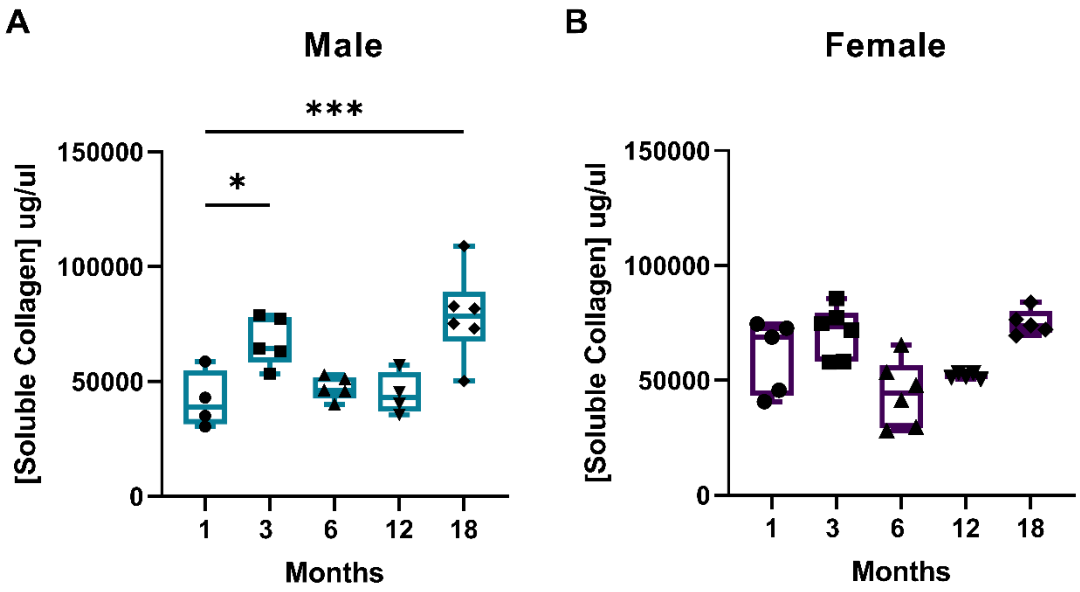

Figure 3. 44 Evaluating the impact of age on total RV soluble collagen content in both sexes. Longitudinal changes in males (A) and females (B) Soluble collagen (µg/µl) uptake in the RV over 18 months. Results reported as min to max range, n=5-6 males and n=5-6 females; p values were obtained a Mixed-effects Analysis and Dunnett's Post hoc test when comparing longitudinal data to the first timepoint. *p<0.05; ***p<0.001

3.3.17 Age and sex had no effect on soluble collagen in the RV

Insoluble collagen was measured to assess changes in mature collagen fibres over 18 months. No significant sex differences were observed, with males and females exhibiting comparable average levels of insoluble collagen (Figure 3.45). Similarly, no age-related effects on RV insoluble collagen deposition were identified in either sex (Figure 3.46). However, the assay showed high variability, potentially exacerbated by the low sample numbers due to the limited availability of RV tissue.

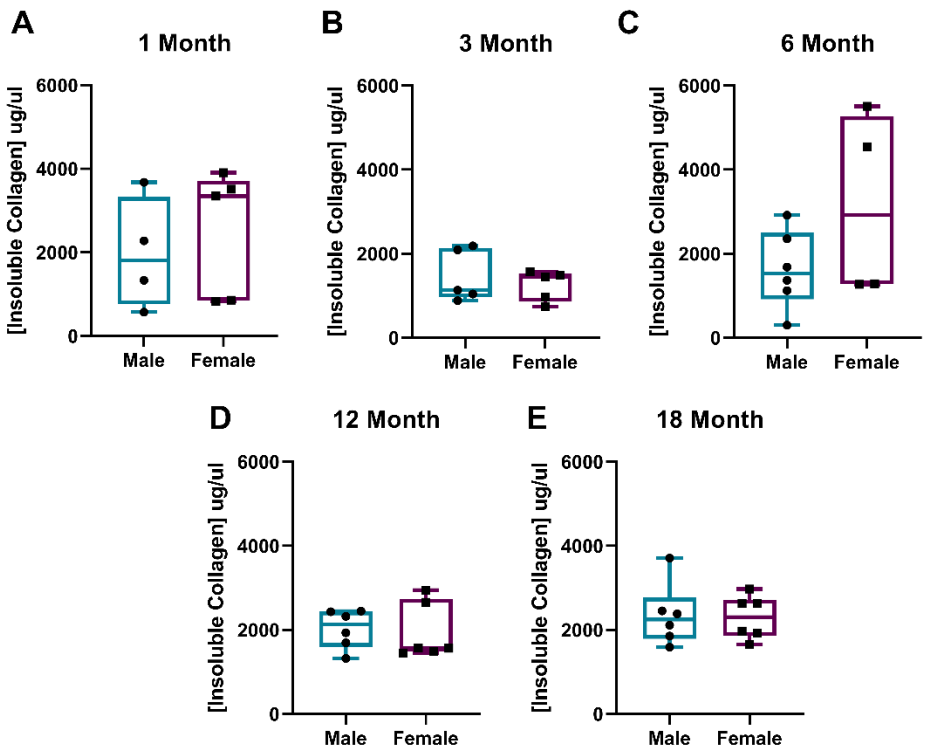

Figure 3. 45 Evaluating the impact of sex on total RV insoluble collagen content across timepoints. Insoluble collagen (µg/µl) was measured in the RV at each imaging time point: 1 month (A), 3 month (B), 6 month (C), 12 month (D) and 18 months (E). Results reported as min to max range, n=5-6 males and n=5-6 females; Changes were assessed using a Student's t-test; results were not statistically significant.

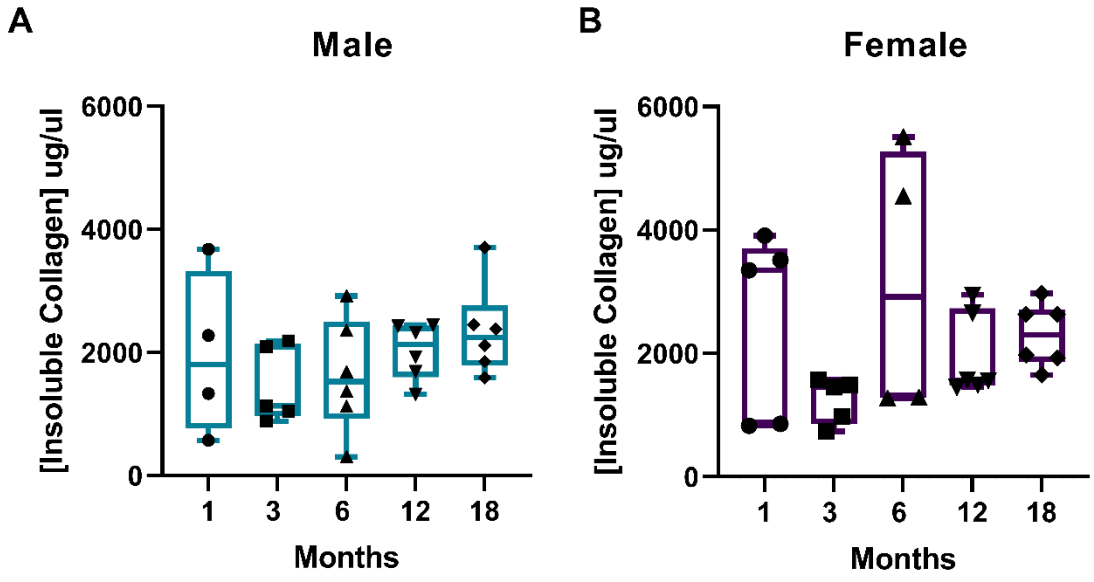

Figure 3. 46 Evaluating the impact of age on total RV insoluble collagen content in both sexes. Longitudinal changes in males (A) and females (B) insoluble collagen (µg/µl) uptake in the RV over 18 months. Results reported as min to max range, n=5-6 males and n=5-6 females; Changes were assessed using a one-way ANOVA and Dunnett's Post-hoc test; results were not statistically significant.

3.3.18 Soluble:Insoluble ratio does not alter with age and sex

The insoluble-to-soluble collagen ratio was calculated as a measure of tissue integrity and function, offering insight into the balance between collagen synthesis and maturation. No sex differences were observed, suggesting that the insoluble-to-soluble collagen ratio is maintained over 18 months (Figure 3.47). Additionally, the effect of age on this ratio was assessed, and no significant changes were observed over 18 months in either sex (Figure 3.48). While some fluctuations were noted, these are likely due to the high variability inherent in the ratio measurement.

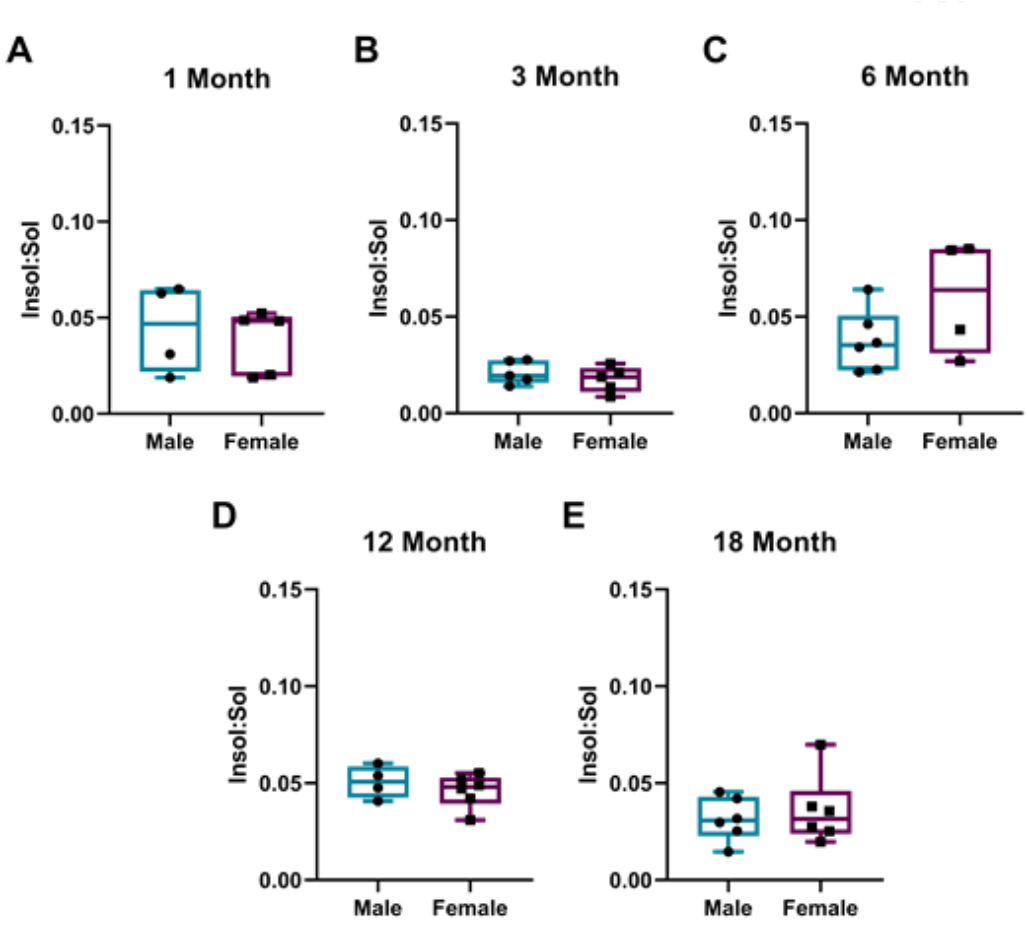

Figure 3. 47 Evaluating the impact of sex on total RV insoluble: soluble collagen content ratio across timepoints. Insoluble: soluble collagen ratio was calculated for the RV at each imaging time point: 1 month (A), 3 month (B), 6 month (C), 12 month (D) and 18 months (E). Results reported as min to max range, n=5-6 males and n=5-6 females; Changes were assessed using a Student's t-test; results were not statistically significant.

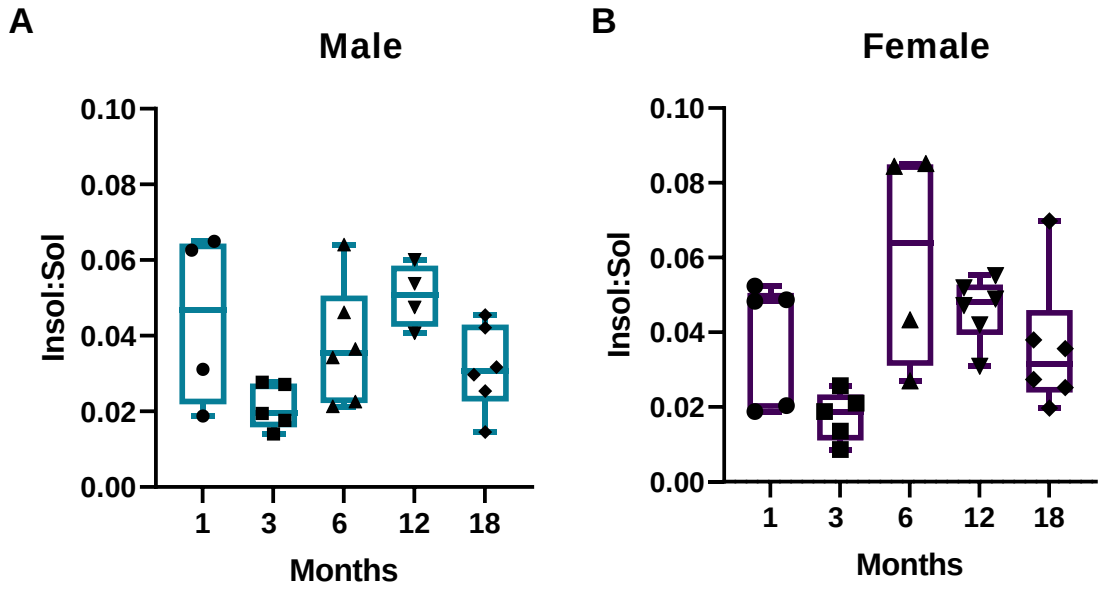

Figure 3. 48 Evaluating the impact of age on total RV insoluble:soluble collagen ratio in both sexes. Longitudinal changes in males (A) and females (B) insoluble:soluble collagen content ratio was calculated for the RV over 18 months. Results reported as min to max range, n=4-6 males and n=4-6 females; Changes were assessed using a one-way ANOVA and Dunnett's Post-hoc test; results were not statistically significant.

3.3.19 Correlation analysis between RV collagen synthesis and deposition and function

Correlation analysis was conducted to determine whether *in vivo* PET outcomes reflected *ex vivo* collagen deposition or functional outcomes. In males, no significant correlations were found between collagen synthesis and collagen deposition measures within the RV, suggesting that these processes occur independently and that synthesis does not directly contribute to deposition or accumulation (Figure 3.49 A). In females, the only significant correlation identified was between the two radiotracer measurements, with no significant correlation between synthesis measurements and deposition (Figure 3.49 B).

When functional outcomes were compared to PET outcomes, no significant associations were observed in females. In males, a correlation was found between diastolic blood pressure and *trans*-4-[^{18}F]fluoro-*L*-proline uptake (Figure 3.50).

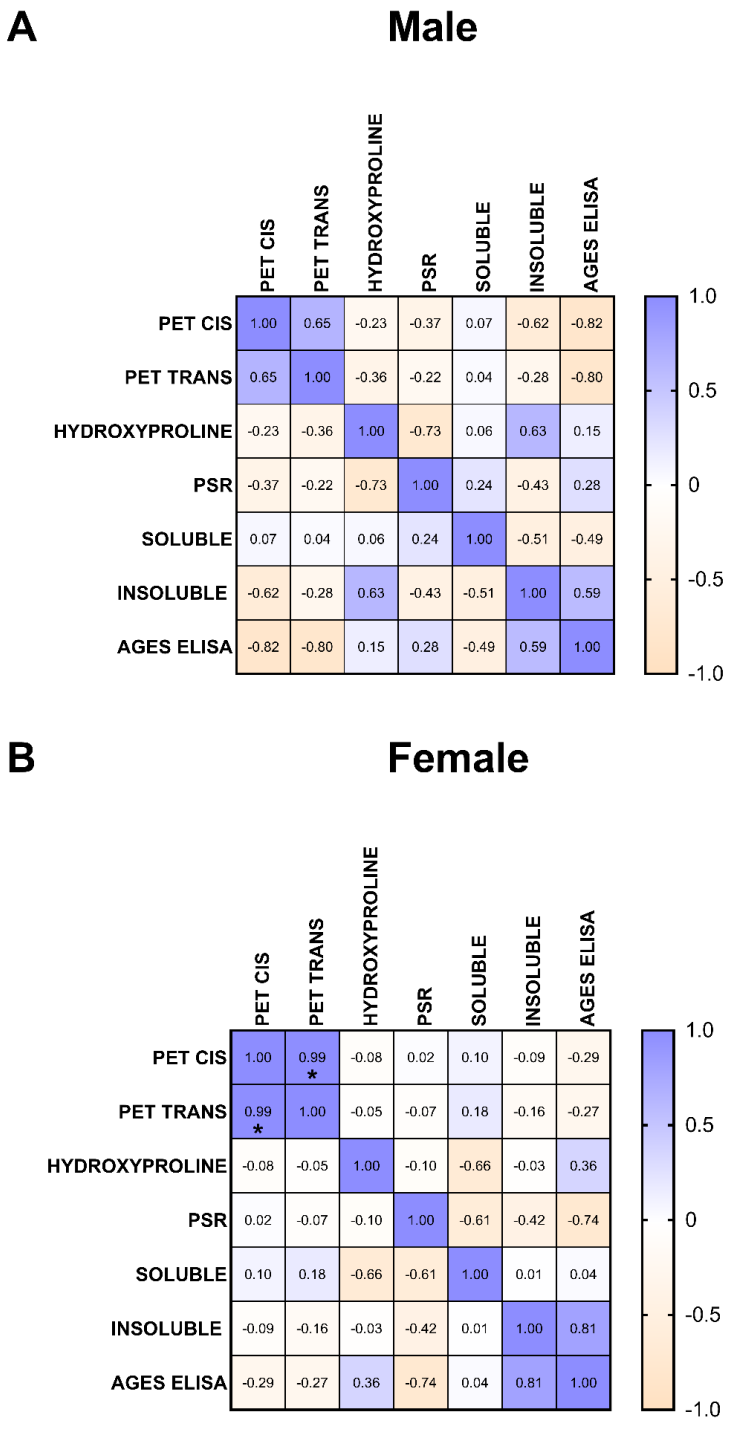

Figure 3. 49 Correlation analysis of RV collagen synthesis and deposition outcomes. Correlation analysis was carried out comparing longitudinal collagen synthesis outcomes and longitudinal collagen deposition outcomes in males (A) and females (B) Correlation matrix analysis was performed using Pearson correlation to assess the relationships between various parameters. Statistical significance was determined Pearson rank correlation analysis. Significance levels are indicated as follows: *p<0.05 and corrected for multiple comparisons; Abbreviations: PET CIS: cis-4-[^{18}F]fluoro-*L*-proline; PET TRANS: *trans*-4-[^{18}F]fluoro-*L*-proline; PSR: Picrosirius RED staining; AGES ELISA: Advanced glycation end production enzyme linked immuoabsorbance assay.

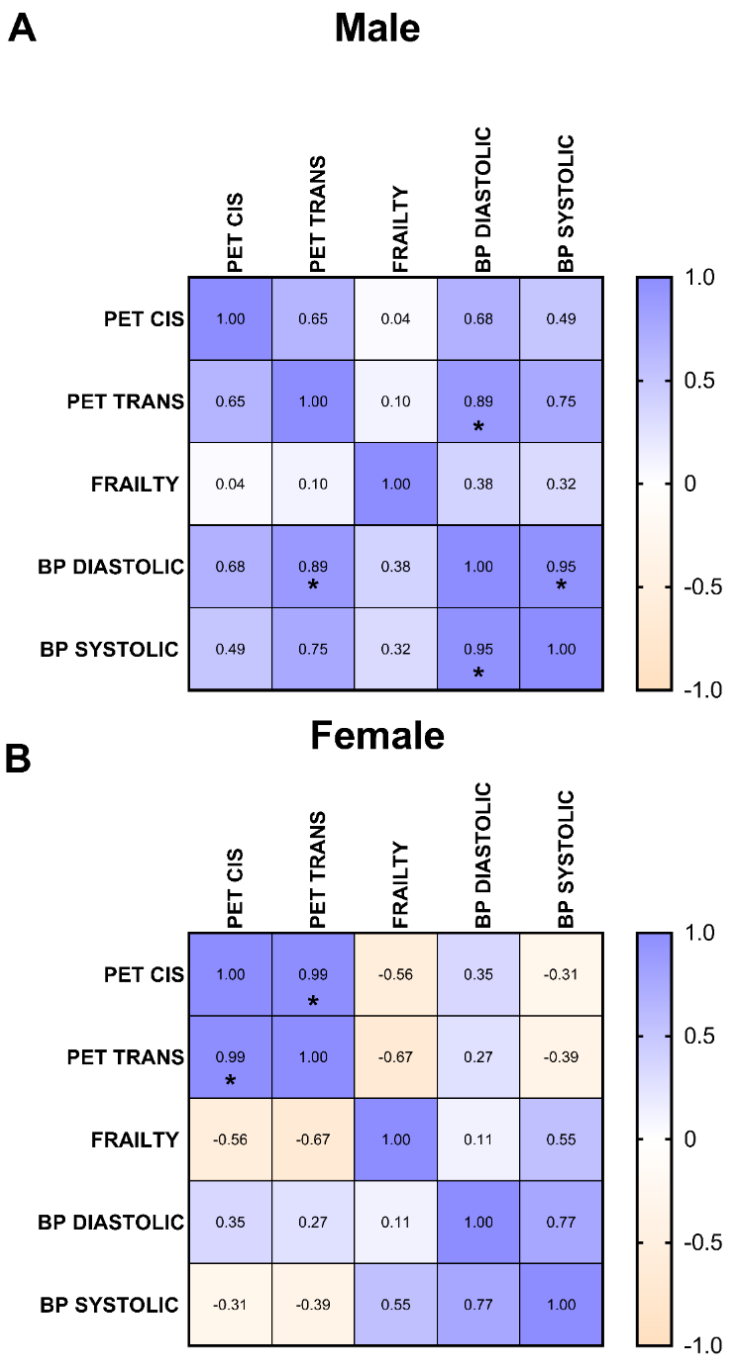

Figure 3. 50. Correlation analysis of RV collagen synthesis and cardiac functional outcomes. Correlation analysis was carried out comparing longitudinal collagen synthesis outcomes and longitudinal cardiac functional outcomes in males (A) and females (B) Correlation matrix analysis was performed using Pearson correlation to assess the relationships between various parameters. Statistical significance was determined Pearson rank correlation analysis Significance levels are indicated as follows: *p<0.05 and corrected for multiple comparisons; Abbreviations: PET CIS: cis-4-[^{18}F]fluoro-*L*-proline; PET TRANS: *trans*-4-[^{18}F]fluoro-*L*-proline; PSR: Picrosirius RED staining; AGES ELISA: Advanced glycation end production enzyme linked immuoabsorbance assay.

3.3.20 Hierarchical clustering reveals age-related patterns in collagen synthesis and deposition, independent of sex in the RV

Hierarchical clustering was performed to determine if distinct groupings could be observed between various groups and outcome measures. In the RV, no clear clustering was evident based on age or sex. The 12-month time points for both sexes clustered closely together, indicating similarities in collagen synthesis and deposition at this stage. Similarly, the 18-month time points for both sexes also formed a distinct, closely related cluster, suggesting comparable patterns between sexes at this later age (Figure 3.51 and Figure 3.52). This clustering suggests shared processes or conditions affecting both sexes at these time points in the RV. Additionally, the clustering analysis revealed that collagen metabolism outcomes can be categorized into distinct groups: PET outcomes, reflecting newly synthesized collagen, clustered together, while more mature collagen fibres, assessed by PSR and AGEs ELISA, formed a separate cluster. This hierarchical clustering is informative as it highlights the progression from newly synthesized to mature collagen, providing insight into the temporal dynamics and relationships of collagen metabolism within the RV and LV. Moreover, clustering of functional outcomes showed that the 12- and 18-month time points were the most similar for both males and females, with PET outcomes forming a cluster alongside the functional outcome cluster. These findings emphasize the value of hierarchical clustering in uncovering patterns and relationships within complex biological data, offering a comprehensive understanding of collagen metabolism and its impact on cardiac function.

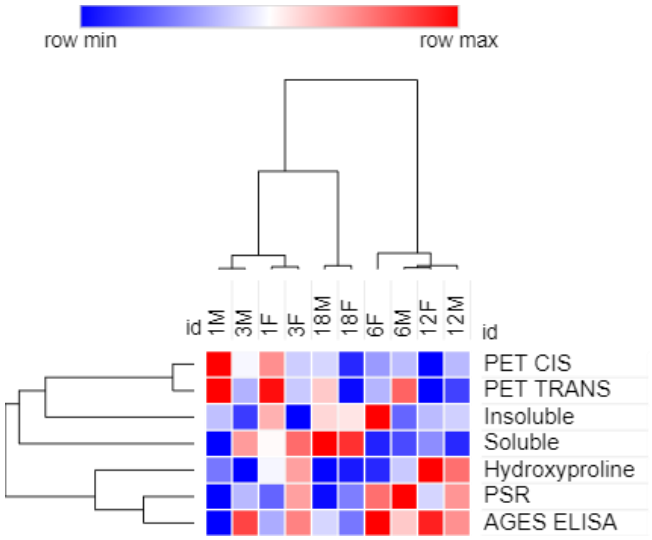

Figure 3. 51 Hierarchical clustering analysis of collagen synthesis and deposition in the RV. Hierarchical clustering using Morpheus was performed to compare collagen synthesis and deposition across different time points and sexes. The heatmap shows clustering patterns in male and female subjects at 1 month (1M, 1F), 3 months (3M, 3F), 6 months (6M, 6F), 12 months (12M, 12F), and 18 months (18M, 18F). The dendrogram indicates the relationships among groups, highlighting similarities and differences in collagen metabolism over time.

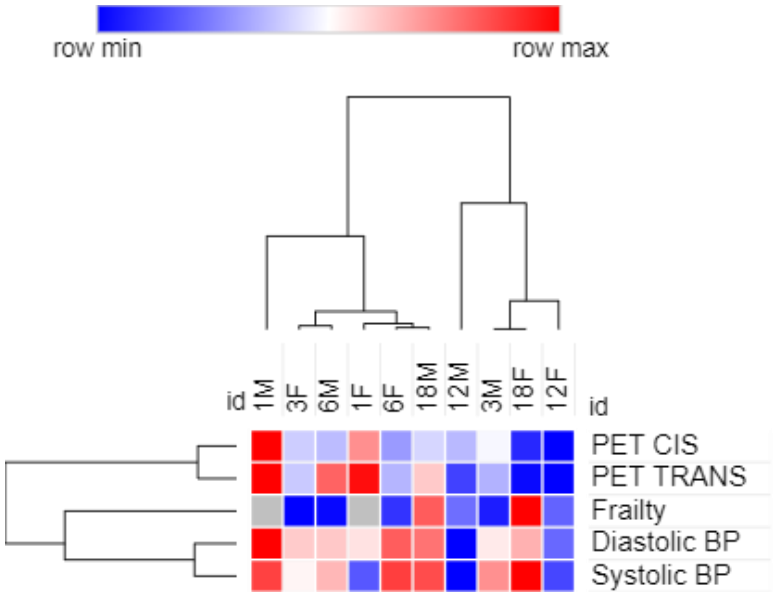

Figure 3. 52 Hierarchical clustering analysis of collagen synthesis and cardiac function in the RV. Hierarchical clustering using Morpheus was performed to compare collagen synthesis and cardiac function across different time points and sexes. The heatmap shows clustering patterns in male and female subjects at 1 month (1M, 1F), 3 months (3M, 3F), 6 months (6M, 6F), 12 months (12M, 12F), and 18 months (18M, 18F). The dendrogram indicates the relationships among groups, highlighting similarities and differences in collagen metabolism over time.

3.4 Discussion

This chapter examines the influence of aging and sex on ventricular collagen metabolism, focusing on cardiac collagen synthesis and deposition in the ventricles over an 18-month period. Specifically, it aimed to investigate whether ventricular cardiac collagen accumulation increased with age and if this occurred at a higher rate in male rats compared to females. Additionally, we explored whether age-related collagen synthesis declines over time, with a potential sex-based disparity that could reveal a higher rate of synthesis in males. Notably, ventricular collagen synthesis is also evaluated as a potential prognostic marker for predicting age-related changes in EF.

This research uniquely employs *cis*-4-[^{18}F]fluoro-*L*-proline and *trans*-4-[^{18}F]fluoro-*L*-proline radiotracers to quantify *in vivo* collagen synthesis, distinguishing between unhydroxylated and hydroxylated collagen forms, facilitating a novel assessment of collagen synthesis changes with age (162, 165). Collagen deposition is assessed via hydroxyproline quantification, PSR staining for total collagen deposition, and the analysis of soluble and insoluble collagen fractions. This dual approach provided an insight into whether changes in synthesis correlate with collagen deposition in the myocardium and can serve as indicators of cardiac functional decline with aging. Findings highlight the dysregulation between collagen synthesis and deposition as a function of age, offering valuable insight into the mechanisms driving age-related changes in cardiac structure and function. Key findings are summarized in Figure 3.53.

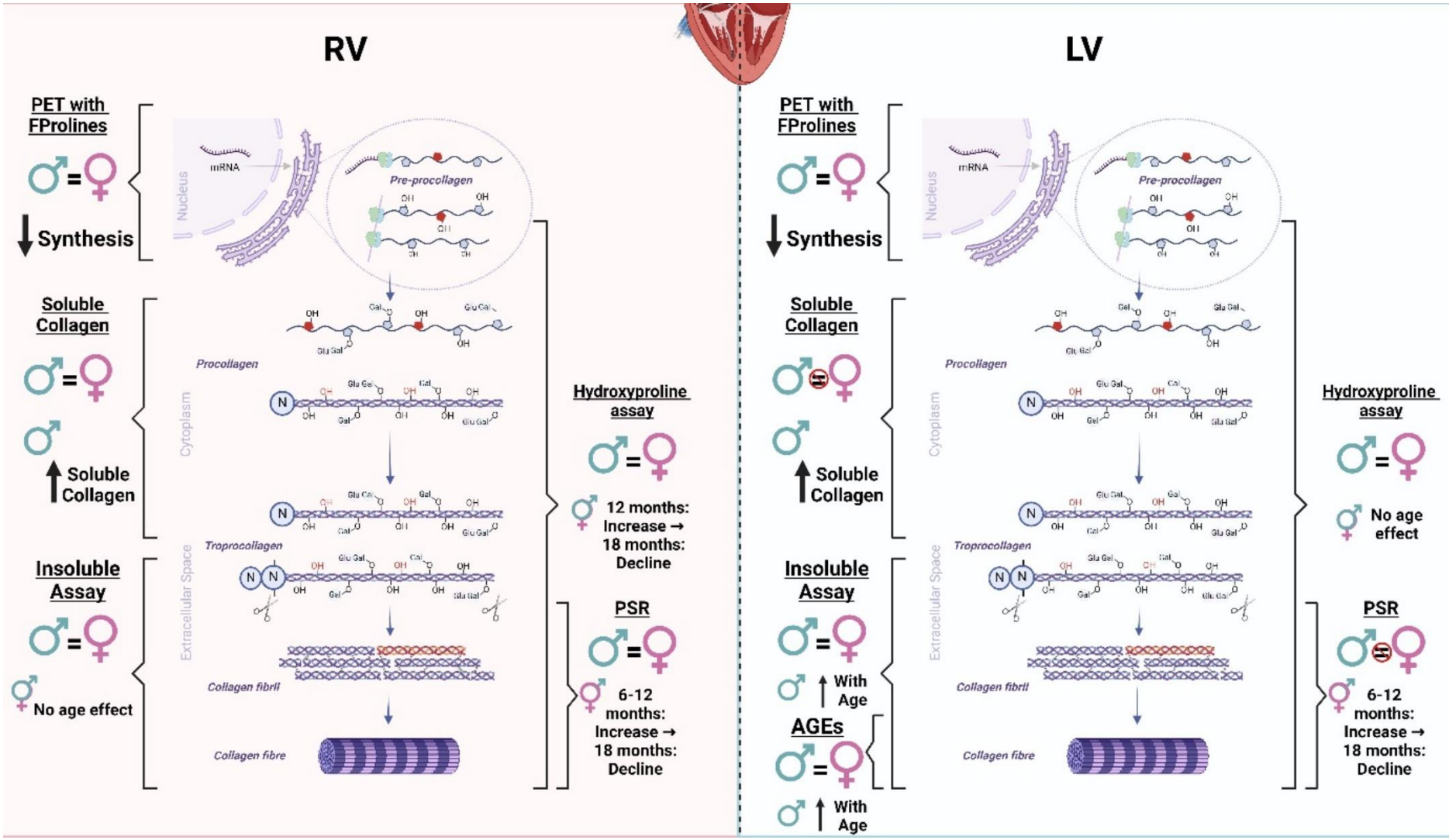

Figure 3. 53. Summary of findings regarding ventricular collagen metabolism in this study. Key changes in RV (left) and LV (right) collagen metabolism comprising of collagen synthesis and collagen accumulation outcomes. Abbreviations: PSR – Picrosirius red staining; AGES- Advanced Glycation End Products Crosslinking. Arrows indicate direction of change in metric with age. Figure created using Biorender.

3.4.1 Ventricular collagen synthesis is not influenced by sex

In this study, we assessed the effect of sex on collagen synthesis in the context of aging and found no significant influence of sex in either ventricle. This contrasts with studies suggesting that collagen synthesis is influenced by sex in cFbs using crystal violet assay (233). For example, previous transcriptomic analyses have revealed sex-specific differences in collagen synthesis. In female mice, collagen I mRNA expression remains elevated and sustained in adult life, only declining post-menopause in more advanced aging (234). Conversely, male mice exhibit a marked decrease in collagen I mRNA expression following adolescence, which is sustained in advanced aging (234). These differences are thought to be mediated by E2, as described in Chapter 1 (92). These findings suggest that the mechanisms of *de novo* collagen synthesis differ significantly between sexes due to variations in temporal profiles during the aging process. However, it is important to note that direct evidence from tracer studies measuring collagen synthesis using fluoroproline PET remains limited. Nonetheless, strong associations between collagen synthesis, as inferred from mRNA measurements, and liver fibrosis studies provide substantial support for our hypothesis regarding the mechanisms of action of these two tracers(235, 236).

Our study indicates that sex does not impact collagen synthesis when measuring total hydroxylated and unhydroxylated collagen synthesis by PET with the fluoroproline tracers. However, studies assessing the effect of sex on ventricular collagen synthesis are limited, with most utilising mRNA expression as a marker of collagen synthesis (88, 236). This makes understanding the influence of sex on collagen synthesis challenging and requires further exploration. It is important to note that *cis*-4-[^{18}F]fluoro-*L*-proline and *trans*-4-[^{18}F]fluoro-*L*-proline do not specifically measure the synthesis of individual collagen subtypes; instead, they assess the production of all collagen types collectively. This could result in the failure to observe sex differences, as the literature primarily discusses these differences concerning the expression and ratios of collagen types I and III but does not address the % contribution of other types on heart collagen to total collagen(92). This suggests that the rate of collagen synthesis across all types does not change with sex over 18 months in rats. However, it is possible that the synthesis of specific collagen types varies with sex, which might not be captured when assessing total collagen production. Additionally, differences across species and the various techniques used to measure collagen synthesis could influence these findings and should be considered in interpreting the results.

Another possible reason for not observing sex differences in collagen synthesis in this study could be the lack of cardiac dysfunction in the subjects. Cardiac dysfunction may lead to pronounced sex

differences in collagen synthesis as a response to injury, but without such dysfunction, these differences may not be evident. This is observed in humans with aortic stenosis; LV biopsies were taken to assess ECM-related sex differences, and this study identified that females had lower collagen I and III mRNA expression compared to male counterparts (237). Similarly, in mice with TAC, females were observed to have significantly lower collagen type III gene expression compared to males, due to E2-mediated reduction in collagen turnover in females (238).

The study had several limitations that are important to acknowledge. One key limitation is that this study did not control for the reproductive cycle during imaging sessions. This is significant because different phases of the reproductive cycle can impact collagen production in humans (239). This lack of control may have led to increased variation among female subjects, making it more difficult to distinguish sex differences. However, our imaging data generally showed low variability among individual values, suggesting that the reproductive cycle did not significantly impact our results. Though we did not directly compare the variability between the sexes. Another limitation is that we did not confirm the induction of reproductive senescence in the female group. Therefore, we cannot confidently attribute any observed effects to post-menopausal changes in collagen synthesis. Additionally, the study experienced a loss of animals at the final time point, which is crucial because detecting sex differences, particularly in the absence of dysfunction, often requires high statistical power. Underpowered studies assessing sex differences carry a high risk of false negatives (240). Despite these limitations, we believe our findings are reliable. Intragroup variability was carefully assessed against the expected collagen turnover within the imaging timeframe, supporting the robustness of our observations. The high sensitivity of PET imaging, combined with our radiotracers' ability to capture both hydroxylated and unhydroxylated collagen synthesis, provides confidence that no sex differences in collagen synthesis were detected in the left or right ventricles. As this field continues to evolve, further characterization will be essential to build on these findings.

3.4.2 Ventricular collagen synthesis declines with age

In this study, we observed a distinct age-related decline in both hydroxylated and unhydroxylated collagen synthesis by fluoroproline PET at 12 months of age. However, our findings also highlight the dynamic nature of collagen synthesis, with levels returning to baseline by 18 months. This suggests that, within this aging model, collagen synthesis does not contribute to the excessive collagen accumulation frequently reported in the literature in models of ageing.

Previous research utilised flooding doses of [^{14}C]Proline in 24-month-old Wistar rats and identified a tenfold reduction in collagen synthesis between 1 and 24 months, not only in the heart but also in the lungs and skeletal muscle (61). This study also reported significant, dynamic changes in whole-heart collagen synthesis: a substantial decline from 1 to 6 months, an increase at 15 months, and a dramatic decrease by 24 months (61). While these time points do not align exactly with those in our study, the observed parallels are noteworthy. It is crucial to recognize, however, that their study assessed the whole heart, whereas our study specifically examined the ventricles. Given that the ventricles constitute the majority of cardiac tissue, the findings from previous studies are unsurprisingly representative of our findings. This study was also limited by the fact that large flooding doses of proline can alter collagen synthesis rates (61). This is something our study using [^{18}F]Fluoroprolines avoided due to the radiotracer principle—that the radiotracer does not alter or perturb the biological processes assessed—ensuring that the system is not altered due to the tracer occupying a low level of the target (241).

Ensuring that the system remains unaltered is critical, as radiotracers are designed to be administered at levels far below those required to induce a pharmacological or biological response. Mass dose effects are often considered in radiotracer studies specifically for receptor-based imaging where minimal amounts of non-radioactive ligand can alter target occupancy and imaging accuracy. However, for fluoroproline PET these challenges are not observed due to the nature of collagen biosynthesis. Previously, studies utilising collagen inhibitors dehydroproline have demonstrated that collagen synthesis inhibition requires millimolar concentrations of inhibitors as described in studies conducted usin [^{3}H]Proline incorporation assays (242). Given that these inhibitory concentrations are orders of magnitude higher than the administered dose of [^{18}F]Fluoroprolines, the risk of self-blocking or mass dose effects on the process under investigation is negligible. Additionally, physiological proline concentrations in rat plasma samples have been reported at approximately 160 µM, corresponding to an estimated 16 µmol per rat, assuming a plasma volume of 100 mL(243). When compared to the mass dose of the administered tracer, the exogenous proline load introduced by [^{18}F] Fluoroprolines is negligible, further supporting the conclusion that the tracer does not disrupt endogenous proline metabolism(243).

Furthermore, a decline in cardiac collagen synthesis has also been observed between 2 and 19 months in male Sprague Dawley rats, with a decrease in pro-α1(I) mRNA expression in the LV and pro-α1(III) mRNA expression in the LV and RV (244). Conversely, other studies have reported that collagen mRNA is not altered in 'healthy' aging, as also observed in C57Bl/6 mice, which showed no change in PIP with

aging (24). Given that most studies rely on mRNA as a measure of collagen synthesis—a method that often shows poor correlation with protein synthesis—our study's approach offers a critical advancement. By longitudinally quantifying collagen protein synthesis and employing PET imaging, our study confirms previous findings and demonstrates that aging leads to a decline in ventricular collagen synthesis in both the LV and RV.

In contrast, common models of fibrosis, such as myocardial infarction or pressure overload, typically demonstrate that synthesis mechanisms contribute to increased collagen deposition and subsequent fibrosis (245, 246). For instance, studies on pressure overload in 18–24-month-old spontaneously hypertensive rats (SHR) have shown a fourfold increase in procollagen (pro-α1(I) and pro-α1(III)) mRNA expression compared to Wistar-Kyoto (WKY) rats (245, 246). Similarly, in humans, patients with heart failure have been found to have higher levels of PIP than normotensive individuals (247). Collagen synthesis play a crucial role in maintaining tissue structural integrity, especially in aging, where a decline could impact overall tissue stability. Tracking collagen synthesis with specific markers not only enhances our understanding of fibrotic processes but also supports the development of therapies by providing insight into upstream effects in the fibrotic cascade across multiple tissues—a critical factor when evaluating the safety and potential side effects of systemic anti-fibrotic treatments. These findings underscore that collagen synthesis is a key component of fibrotic mechanisms in both rodent models and humans, highlighting its relevance for therapeutic strategies in both cardiac disease and aging contexts. In cases of injury or stress-related fibrosis, targeting collagen synthesis with drugs like losartan has successfully reduced and reversed left ventricular fibrosis in SHR (246). However, these results underscore the unreliability of using mRNA measurements as an indicator of collagen synthesis, as mRNA levels remained unchanged despite reductions in collagen volume fraction and total deposited collagen, as evidenced by PSR staining (246). This discrepancy demonstrates the need for more sensitive measures of collagen synthesis, such as [^{18}F]Fluoroproline radiotracers. However, it is important to note that age-related fibrosis does not follow the same mechanisms as cardiac disease-related fibrosis. Therefore, age-related collagen accumulation must be evaluated from other perspectives, focusing closely on post-translational modifications, increased crosslinking, and collagen degradation as potential contributors. Our findings suggest that while collagen synthesis may not be a primary target for anti-fibrotic intervention in age-related fibrosis, monitoring collagen synthesis remains valuable for understanding tissue integrity and guiding the development of therapies that assess upstream effects across multiple tissues

Interestingly, our study does not reveal any longitudinal differences between the uptake of *cis*-4-[^{18}F]fluoro-*L*-proline and *trans*-4-[^{18}F]fluoro-*L*-proline, which are used to measure unhydroxylated and hydroxylated collagen synthesis, respectively. Both types of collagen synthesis appear to decline with age. Typically, fibrotic mechanisms are characterized by reactive fibrosis, which involves the expansion of collagen fibres, and replacement fibrosis, which is the deposition of newly synthesized collagen to replace lost myocytes (45). However, the decline in both types of collagen synthesis observed in this study may suggest a lack of replacement fibrosis and possibly the absence of reactive fibrosis. Alternatively, it could indicate an inhibition of de novo collagen synthesis due to reduced collagen degradation, which, while not definitive, warrants consideration as an alternative explanation. This pattern has been reported previously in patients with idiopathic dilated cardiomyopathy, where aging did not correlate with either type of fibrosis, although the impact of the disease on these findings should be considered (248). Other studies have suggested that reactive fibrosis is the main contributor to age-related fibrosis (249). Understanding these typical mechanisms of fibrosis is challenging, as aging appears to deviate from the traditional path of fibrosis development.

It is important to acknowledge several limitations and considerations in our imaging study. A significant loss of subjects occurred during the study, which complicated the interpretation of the final imaging timepoint. Despite assessing potential survival bias, our analysis indicates that it did not influence the overall results. Additionally, the choice of 18 months as the study's endpoint may not fully capture the entire aging process, as 18 months has been suggested as the onset of aging. However, due to time constraints and welfare concerns, this was deemed the most appropriate timepoint. Thus, our findings may not entirely reflect the later stages of aging. It is also important to recognize the limited understanding of human collagen synthesis, largely due to the scarcity of healthy control tissue and the challenge of isolating aging effects from dysfunction. This underscores the need for further research to determine whether the findings observed in this study are applicable to humans. The use of [^{18}F]Fluoroproline radiotracers offers a valuable opportunity to conduct *in vivo* assessments of collagen synthesis and explore aging processes in a human context.

3.4.3 Collagen accumulation appears to occur in both sexes with aged males showing increased levels of collagen accumulation compared to females

This study identifies that aging leads to increased collagen deposition in both sexes up to 12 months in both the LV and RV, as observed through PSR and hydroxyproline analysis. These findings are consistent with existing literature indicating that aging is associated with collagen accumulation in both sexes (45). This phenomenon has been observed across various animal models, such as in aged female sheep, where histological PSR analysis showed increased collagen content at 8 years of age (24). A similar increase has been reported in human healthy post-mortem cardiac tissue, where aged humans exhibited a 2% increase in collagen content (from 3.9% to 5.9%) (36). Hydroxyproline content measurements have also shown similar findings in rodents, with 24-26-month-old rats having significantly higher collagen content contributing to cardiac stiffening (58).

Interestingly, the majority of studies report a unidirectional collagen accumulation, with a consistent increase over time. However, our study depicted a more dynamic process, with collagen accumulation peaking in males at 12 months and in females at 6 months, followed by significant declines in both groups. This pattern has been reported previously in the aging female F344xBN rat heart, where peak collagen (measured using PSR staining) was identified at 6 months of age and was found to significantly decline at 26 and 30 months of age (250). Several factors may account for differences in collagen accumulation: 1) increased age-related dysfunction in these models, or 2) species-specific variations in cardiac collagen synthesis. For example, a study by Grilo et al. assessed the effects of aging on collagen metabolism in C57Bl/6 mice and identified a significant increase in diastolic blood pressure (3.4 mmHg) and mean arterial pressure (7.2 mmHg) in their aged control cohort(88). This suggests that vascular dysfunction was present in their model, a factor not observed in our study. As previously described, this physiological change has been shown to cause increased collagen deposition (210). Furthermore, species/strain differences in cardiac aging have been reported, with Sprague Dawley rats associated with “disease-free” aging (251). In contrast, strains such as the Fischer 344 rats develop spontaneous cardiomyopathy and exhibit myocardial degeneration and interstitial fibrosis with aging (252). This suggests that our model and findings may provide a greater indication of aging in the absence of overt dysfunction and may explain the increase in collagen accumulation and decline in collagen synthesis.

It is important to note that LV hydroxyproline measurements showed no significant increases in collagen content, which is inconsistent with the literature (88). This suggests that the assay may not have been sensitive enough to detect differences in aging, as the measured values remained at the

lower end of the standard curve despite extensive optimizations not shown in this thesis. Interestingly, significant changes were observed in the RV; however, this is unsurprising, as the RV is known to have a higher collagen content than the LV (253). Therefore, the assay may have had sufficient sensitivity to assess changes in the RV but not in the LV. Future measurements of hydroxyproline content should be made with more sensitive methodologies, such as liquid chromatography-mass spectrometry (LC-MS) or high-performance liquid chromatography (HPLC), which have proven to show more accurate measurements than many kit-based assays (254).

This study investigates the effects of aging and sex on established mature collagen fibres, with a specific focus on insoluble collagen fibres. Our research identified an increase in insoluble collagen content within the LV of male subjects up to 18 months of age; this was not observed in the RV. These findings align with existing literature that suggests age-related ECM accumulation is sex-dependent in rodents, with males exhibiting more pronounced fibrosis than females (255). This trend is also observed in human imaging studies, where significantly higher levels of myocardial fibrosis have been reported in aging males compared to their female counterparts (249, 256). This provides another potential explanation for the reduced EF observed in males at 18 months. However, studies specifically looking at insoluble collagen have observed a decline in insoluble collagen in aging CB6F1 male and female mice, although sex differences were not explored in that study (13). Females were also found to have higher type I and III collagen compared to males within the human LV (92). This contrasts with our study, as females were identified to have stable insoluble collagen levels in both ventricles, while males showed an increase. Interestingly, no changes in RV insoluble collagen were observed in males, which could be attributed to the RV's function of pumping blood solely to the lungs. This results in a lower cardiac burden and pressure compared to the LV, leading to a reduced fibrotic response.

Additionally, this study identified an increase in soluble collagen content in males in both the LV and RV up to 18 months of age. This observation was made in CB6F1 mice, which showed a significant increase in soluble collagen in the aged cohort (13). Soluble collagen reflects both newly synthesized and newly degraded collagen that has not yet been cross-linked or cleared, providing an indicator of collagen turnover (13). In males, this suggests a significant increase in collagen turnover is occurring. Based on the observed reduction in collagen synthesis at 12 months in this study, it appears that the increase in soluble collagen may indicate a change in collagen degradation. Furthermore, studies have suggested that increased soluble collagen content correlates with increased ventricular dimensions, indicating potential adverse remodelling of the heart (257).

3.4.4 LV crosslinking increases in males with age but not females

This study assessed the effect of age on ECM crosslinking in the LV of rats up to 18 months. It focused on how aging influences the formation of AGEs crosslinking, finding that aging causes a significant increase in AGEs in males at 3 and 12 months, an effect not observed in females. This suggests that males may experience more cardiac stiffening with age compared to females, potentially explaining the lower ejection fraction noted in Chapter 2. Previous research has shown that aging can increase myocardial stiffness due to enhanced ECM and collagen-specific crosslinking, even in the absence of increased collagen content, though often these studies are completed in males (80).

Post-translational modification of collagen fibres through glucose-mediated formation of AGEs has been directly attributed to increased cardiac stiffness in humans and has been closely associated with diastolic dysfunction development in aging (258). This has also been observed in canines, where AGEs accumulated in control-aged animals and treatment with AGEs breaker ALT711 reduced diastolic dysfunction and cardiac stiffening, indicating its role in age-associated fibrosis (259). Preclinically, very little longitudinal assessment of AGEs has been completed with little understanding of sex-specific changes over the lifespan of the rodent. Sex differences in ECM crosslinking proteins have been observed previously, with aged C57BL/6 female mice showing significantly higher levels of LOX in the LV at 18 months compared to male counterparts (88). Contrastingly, other studies have identified the opposite, with LOX found to increase in aged male mice (57). However, no study has yet examined the longitudinal effect of sex on cardiac AGE accumulation directly. Our study appears to be the first to characterize a male-specific accumulation of AGE crosslinking in Sprague Dawley rats over time, suggesting a potential level of resilience in females against maladaptive crosslinking. Similar sex differences have been observed in plasma AGE levels in males with Alzheimer's disease, another age-associated condition, suggesting the potential influence of sex on AGE accumulation across multiple organs (260).

This study has several limitations. The assessment of tissue AGEs was confined to the LV due to the limited availability of RV tissue, which is significantly less abundant. Given the distinct functional differences between the right and left ventricles, it is likely that aging may impact crosslinking differently in each chamber. However, studies assessing the impact of collagen crosslinking in the RV identified negligible differences in crosslinking in the RV compared to the LV (261). Moreover, this study focused on only AGEs, whereas other crosslinking proteins known to vary with age and sex have been identified. Consequently, our research does not offer a comprehensive understanding of the overall impact on collagen crosslinking.

3.4.5 Ventricular collagen metabolism appears to become dysregulated with age

This study found that aging results in decreased collagen synthesis in both ventricles. Despite this decline, collagen deposition increases with age up to 12 months in both males and females. These observations suggest a dysregulation in collagen metabolism, where collagen accumulation rises even though synthesis is reduced. Two potential explanations for this are: (1) Aging disrupts the mechanisms of collagen turnover, leading to a reduction in collagen degradation causing increased collagen accumulation, or (2) Increased collagen accumulation triggers a negative feedback response that further reduces collagen synthesis. The observations from this study could likely be explained by a combination of the two proposed mechanisms.

A dysregulation in collagen degradation mechanisms have been proposed as the main mechanism behind age-associated cardiac fibrosis. Studies have aimed to tease apart the mechanisms that underpin age-related fibrosis by assessing changes that occur in the expression of pro-fibrotic genes and anti-fibrotic gene expression in aged male and female C57BL/6 mice (234). Much like our study this transcriptomic identified a decline in profibrotic genes, specifically collagen I expression in both sexes at 18 months suggesting a down-regulation of collagen synthesis (234). Simultaneously, a significant decline in antifibrotic genes have been observed and likely may contribute to collagen accumulation observed in our study and others. This has further been explored through longitudinal assessments of MMPs (involved in collagen degradation), TIMPs (inhibitors of MMPs) and ECM crosslinking preventing collagen clearance. The current hypothesis in the field is that degradation mechanisms become dysregulated with many aging studies observing MMP downregulation (primarily, MMP-1, -2, -4 and -14) and the overexpression of TIMPs (primarily TIMP-1 and -4) (262, 263). The male-specific accumulation observed in our study has been observed previously, with studies assessing the effect of E2 on collagen degradation mechanisms and identifying that E2 improved the TIMP/MMP balance ensuring optimal collagen turnover and distribution in a model of volume overload in female Sprague Dawley rats (102). These findings underscore the critical role of impaired collagen degradation mechanisms in age-related cardiac fibrosis, indicating that interventions targeting the regulation of MMPs and TIMPs could be pivotal in mitigating collagen accumulation and its associated cardiac dysfunction.

A lesser discussed explanation for collagen synthesis decline is as part of a negative feedback mechanisms in response to age-associated collagen accumulation. This has only been described in the

context of dermal aging and collagen loss, however, studies suggest that high-molecular weight collagen fragments inhibit collagen synthesis leading to a decline with age (264). It has been proposed that increased abundance of collagen fragments or soluble collagen can drive oxidative stress and subsequent impairment of collagen metabolism (265). However, it is important to consider that this has only be assessed in the context of dermal aging and not in cardiac tissue.

3.4.6 Right ventricleand left ventricle ECM differences in aging

This study investigates the influence of age and sex on collagen metabolism in the LV and RV of the heart. Our findings indicate that collagen synthesis declines similarly with age in both ventricles. However, while collagen accumulation occurs in both the LV and RV, a specific increase in insoluble collagen was observed in the LV of male subjects, consistent with previous reports. Understanding the differences in extracellular matrix (ECM) changes between the RV and LV is crucial for identifying how aging affects cardiac collagen metabolism.

Predominantly, cardiac research is LV-centric, with most studies focusing on the impact of aging and disease on the LV due to many conditions affecting the LV in particular (266). Interestingly, although both ventricles show increased collagen deposition with aging, studies have reported greater fibrosis and collagen deposition in the RV (26). This is partly due to their distinct functions in blood circulation and the different embryonic origins of their fibroblasts: LV fibroblasts largely originate from the epicardium and endocardium, whereas RV fibroblasts stem only from the epicardium (267). Further studies have explored these differences by examining gene expression, identifying 25 genes expressed exclusively in the LV and 51 genes expressed only in the RV (268). Additionally, in aging, the RV has been found to exhibit higher pro-fibrotic gene expression (261). This suggests that the underlying mechanisms behind age-associated collagen accumulation in each ventricle are distinct.

The RV is largely neglected in aging and dysfunction research, and there is currently limited understanding of the impact of aging on collagen degradation mechanisms in the RV and limited data on crosslinking. By assessing these changes, we can better comprehend the structural and functional implications of aging on the heart, potentially leading to improved strategies for managing age-related cardiac conditions.

3.4.7. Ventricular collagen synthesis does not predict cardiac functional with age

This study aimed to assess whether collagen synthesis outcomes at each timepoint provided any prognostic value for aged cardiac function. Since the animals were all healthy, without evident dysfunction, no strong significant associations were identified between RV and LV collagen synthesis measurements from 1–18 months of age, reflecting only a narrow range of changes typical of healthy aging. This suggests that while both PET radiotracers provide sensitive measurement of hydroxylated and unhydroxylated collagen synthesis (based on previous unpublished data), they do not appear to hold clear prognostic value for cardiac function in the absence of disease. Additionally, metrics like frailty may offer more insight when correlated with *in vivo* and *ex vivo* collagen analysis, as they provide a broader view of physiological aging than collagen synthesis alone. Previous research investigating plasma PIP (a marker of collagen I synthesis) in heart failure patients did not identify a positive correlation with HF related death (269). Interestingly, a strong positive association was noted between HF and MMP-1, suggesting that collagen degradation markers may offer more prognostic value (269). Although our study focused on healthy animals, the findings align with studies in HF patients, supporting that collagen synthesis alone does not reliably indicate cardiac function outcomes with age. Studies combining markers of synthesis (PIP) and degradation (MMP-1) have shown good prognostic value in non-ischemic dilated cardiomyopathy, closely associating with reduced EF in patients(270). Understanding the balance between collagen synthesis and degradation remains crucial for clinical outcomes related to cardiac function.

3.4.7 Conclusion

In this chapter, we investigated how aging and sex influence ventricular collagen metabolism by assessing both *in vivo* collagen synthesis and *ex vivo* collagen accumulation in Sprague Dawley rats. Our results indicate that collagen synthesis declines with age in both ventricles, with no significant differences in hydroxylated or unhydroxylated collagen synthesis between sexes. These findings support our hypothesis that collagen synthesis decreases with age, while disproving our hypothesis regarding sex-based differences.

We observed that total collagen deposition increased with age in both sexes, although a notable decline occurred at 18 months. Interestingly, males exhibited significant increases in both soluble and insoluble collagen in the LV and soluble collagen in the RV, whereas collagen levels remained stable in females throughout the study. These results support our hypothesis that males show higher collagen accumulation across stages of the deposition process. Additionally, we identified increased LV crosslinking through AGEs specifically in males. This accumulation, along with increased collagen deposition, may explain the lower ejection fraction seen in males, as reported in the previous chapter.

Our findings suggest that collagen synthesis and deposition become increasingly dysregulated with aging. This desynchronization results in collagen accumulation despite reduced synthesis, likely due to a dysregulated collagen degradation pathway—an area warranting further investigation. This study assessed aging in a rat strain known for its resilience to cardiac dysfunction, offering a unique perspective on cardiac collagen changes under natural aging conditions. This context may account for the absence of consistent collagen accumulation reported in other preclinical studies.

The next chapter will expand on these findings by exploring the effect of aging on atrial collagen metabolism, an area essential to understanding many age-related cardiac dysfunctions but currently underexplored.

Chapter 4 - *The Impact of Age and Sex on Atrial Collagen Metabolism*

4.1 Introduction

Our current understanding of atrial aging remains limited, primarily due to the inherent challenges associated with aging research, including high costs and the complexities of long-term studies. However, it is increasingly evident that aging also plays a crucial role in atrial dysfunction. This is underscored by the rising incidence of atrial fibrillation (AFib), atrial fibrosis, and impaired atrial contractility observed in aging populations (17, 271, 272). Historically, cardiac research has predominantly focused on the ventricles, given their critical role in conditions such as myocardial infarction and pressure overload, which significantly impair ventricular function. Our understanding of ventricular fibrosis cannot be directly applied to atrial age-related fibrosis, as demonstrated by several animal studies (273, 274). For instance, in a mouse fibrosis model involving the overexpression of TGFβ1—a key regulator of collagen synthesis and cardiac fibroblast proliferation—atrial remodelling was observed exclusively, indicating that the atria and ventricles are affected differently (273). Furthermore this has been observed in a canine model of heart failure induced by rapid ventricular pacing which was found to cause cardiac fibrosis in the left atrial (LA) but not LV (275). This suggests that the mechanisms driving fibrosis in these two cardiac chambers may be distinct (276, 277) .

Despite the clear divergence in fibrosis mechanisms between the atria and ventricles, little to no research into the effect of aging and sex on atrial collagen metabolism has been conducted. Therefore, this fourth thesis chapter aims to assess the effects of aging on atrial collagen metabolism in the LA and right atria (RA). The primary focus of this chapter is the quantitative analysis of atrial collagen synthesis, an area that has yet to be thoroughly explored. Given the limited gene expression analysis of collagen synthesis in the atria, this remains a critical area of research. This study will evaluate both hydroxylated (structural collagen) and unhydroxylated (interstitial collagen) collagen synthesis and compare these findings with *ex vivo* established methods of collagen quantification.

In Chapter 3, ventricular collagen synthesis was shown to decline with aging, even as collagen deposition increased, suggesting that turnover, rather than production, may drive fibrotic remodelling in aging ventricles. This chapter extends the investigation to atrial collagen synthesis, aiming to determine whether a similar disconnect exists between synthesis and deposition in the atria. However,

considering distinct fibrotic patterns observed between the atria and ventricles, it is plausible that collagen metabolism in the atria may respond differently to aging.

Prior studies have indicated that atrial fibrosis increases with age, often independently of ventricular fibrosis, suggesting that the mechanisms regulating collagen turnover in the atria may not mirror those in the ventricles. Furthermore, aging is associated with an increased incidence of AFib, especially in males, where atrial fibrosis and its associated structural remodelling are more pronounced(278). This sex-based disparity in fibrotic burden suggests that collagen synthesis, deposition, or turnover may be higher in aging male atria compared to females, potentially contributing to the heightened AFib risk observed in older males (278).

Hypotheses:

- Over the course of natural aging, the rate of atrial cardiac collagen synthesis declines *in vivo* with age in rats.
- A higher rate of atrial collagen synthesis will be observed in male rats compared to female rats.
- The atrial cardiac collagen accumulation rate increases *in vivo* with age with a higher rate of deposition observed in males' rats compared to females' rats.

By investigating these hypotheses, this chapter seeks to clarify how aging and sex influence collagen metabolism in atrial tissue and whether atrial collagen dynamics contribute to fibrotic remodelling distinct from that observed in the ventricles. The objectives of this chapter are to: 1) examine the impact of age and sex on atrial collagen synthesis *in vivo*; 2) determine whether age-related changes in atrial collagen synthesis are influenced by sex; 3) evaluate the potential for increased atrial collagen deposition in relation to age and sex; and 4) To assess whether collagen synthesis rates can serve as predictors of cardiac function during aging, offering potential prognostic value in the case of age-related CF.

4.2 Materials & methods

The methods in this section largely mirror those described in Chapter 3.2. For ease of reference, only the elements unique to the atrial analysis are detailed here, including sample numbers and example images specific to this analysis. All *in vivo* data is reporter according to the ARRIVE recommended criteria (182). The study design remains consistent with previous chapters, except for differences in sample numbers, PSR analysis, as outlined in each relevant subsection.

4.2.1 Atrial PSR histological Staining

Sample numbers for PSR atrial staining are described in Table 4.1. Frozen sections were air dried for a minimum of 30 min prior to commencement of the staining protocol. Once slides were dry, sections were placed in 100% EtOH for 4 minutes. Samples were then rehydrated by placing sections in 80% EtOH for 20 seconds, followed by 40% EtOH for 20 seconds to ensure removal of remaining OCT from slides. Slides were washed by placing sections in distilled water for 2 mins and shaking slide rack gently. Slides were fixed in 4% buffered formalin (4% Paraformaldehyde, Cambridge Bioscience, UK) for 30 minutes. Slides were again washed by placing sections in distilled water for 2 mins and shaking slide rack gently. Samples were placed into PSR dye (Picrosirius Red Solution, Abcam, UK) for 15 minutes in the dark based on optimisation outlined above. Samples were washed using 0.05% acetic acid solution (glacial acetic acid, Scientific Laboratory Supplies, UK) for 10 seconds whilst shaking slide rack gently to remove excess dye, twice. Slides were dehydrated using two washes in 100% EtOH for 2 minutes. Slides were transferred to xylene for three changes, slides were mounted using coverslips (Menzel-Gläser cover slips: 22x60x1.5mm, Epredia, UK) using Pertex mounting medium (Histolab Products AB, Sweden) and left to dry overnight in a fume hood. Once dry, slides were imaged using a brightfield profile on a Axio Scan Z1 slide scanner (Zeiss, Germany).

Table 4. 1 Atrial Sample numbers for histological analysis

Sex	Sample Numbers				
	1 Month	3 Month	6 Month	12 Month	18 Month
Male	5	6	6	6	5
Female	6	6	5	4	5

Histological analysis was performed using QuPath version 5.0.1 (Queen's University Belfast, UK) for quantification of positive (red) PSR staining (PSR+ %) (224). Tissue images were imported into QuPath and then tissue detection thresholder was created through the creation of atrial classifications. A threshold-based approach was utilised to detect tissue at a high resolution, thresholds were set as above threshold to ignore values and below threshold to mark as tissue, a Gaussian prefilter was selected and a threshold value of 200 was selected based on values observed on tissue – this classifier was named WT_1. This classifier was tested on several separate sections to ensure adequate tissue detection was occurring. Another pixel classifier was carried out by drawing regions of interest (ROIs) highlighting PSR positive stains, PSR negative areas on a section and regions to ignore such as artefacts/blood cells. For this classifier a random trees classification at a high resolution was utilised and Gaussian and Laplacian features were selected. The classifier was then trained and its accuracy to detect positive PSR stain was assessed across several sections. Batch analysis was carried out by manually defining atria (see figure 3.5) to ensure that non-cardiac areas were not included and then applying both the tissue detection classifier and PSR stain trained classifier to these regions. This provided average intensity values for PSR positive areas and PSR negative areas across samples. Note that atria regions were not separated into left and right due to challenges orientating the different regions.

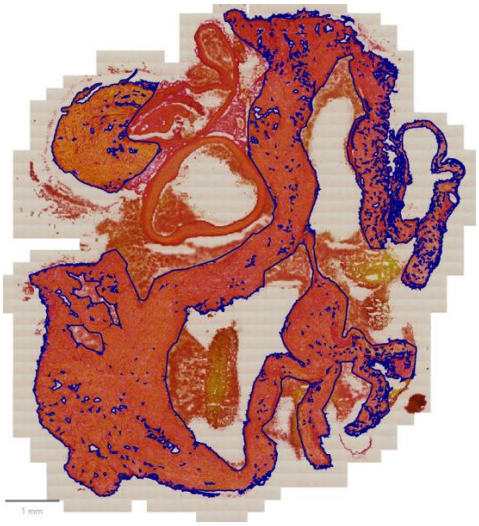

Figure 4. 1 Representative image showing the regions of interest in the atria excluding vessels and artefacts for subsequent analysis

4.2.2 Hydroxyproline colorimetric assay

Tissue homogenisation was carried out to prepare samples for hydroxyproline assay, samples are shown in Table 4.2. Samples were defrosted on ice and then weighed and diluted in deionised (DI) water at 1:10 or 100 µl/10mg. For the atria removal of all major blood vessels was carried to ensure that only atrial cardiac tissue was homogenised. Samples cut into smaller sections using scissors and then tissue was mechanically homogenised using an Ultra-Turrax ® homogeniser (T 10 basic Disperser, IKA, UK) on ice in 10sec bursts to prevent overheating of samples. Tissue homogenisation continued till a uniform suspension observed. Samples were aliquoted into 110µl to prevent repeated freeze-thaw cycles and placed in - 80◦C for storage till analysis.

Table 4. 2 Atrial sample numbers for hydroxyproline colorimetric assay

Sex	Sample Numbers				
	1 Month	3 Month	6 Month	12 Month	18 Month
Male	6	6	6	4	6
Female	5	5	4	4	6

A colorimetric assay kit (Abcam; Cambridge,UK) was used to measure the total hydroxyproline content in the atria. Samples were defrosted on ice and then 100µl of sample homogenate was transferred into a screw-capped polypropylene tube and then equal volumes (100µl) of 10N concentrated NaOH was added and then sample was heated at 120◦C on a heat block for 1 hour. Following incubation, samples were cooled on ice and then samples were neutralised using 100µl of 10N of concentrated from HCl (diluted from VMR concentrated chemical). Samples were vortexed and then samples were centrifuged for 5 mins at 10,000g at 4◦C. The supernatant was collected and kept on ice, ready for the assay to begin.

Hydroxyproline standards were prepared according the kit protocol and then 10µl of each standard was placed in duplicate into the 96-well plate. Then 10µl of each sample was placed in duplicate into the 96-well plate. The plate was placed on heating block at 65◦C to allow for samples to evaporate for a minimum of 45mins. Oxidation mix (94 µl of oxidation buffer and 6 µl chloramine T concentrate per sample) provided in the kit were added to each well and then the plate was incubated at room temperature (RT) for 20mins in the dark. Following Incubation, then 50 µl of developer was added to

the reaction and incubated at 37◦C for 5 mins. Next, 50µl DMAB concentrated was added to plate a and plate was gently mixed and sealed using plate seal supplied by the kit and then the plate was incubated at 65◦C for 45mins. The plate was read using a microplate reader within 10 mins of the incubation completion, an absorbance at OD 560nm was used.

Total hydroxyproline content was calculated on Microsoft excel and was based on the standard curve generated by plotting the average of each duplicated standard minus the background (calculated from the blank). The background was subtracted from the samples and then valued were averaged A best-fit linear trend line was calculated and the equation was used to calculate the total amount of hydrolysed hydroxyproline in each sample. To calculate the concentration of hydroxyproline in each well (µg/µl) the identified value was divided by the sample volume (10µl) and then multiplied by a factor of 3 to account for dilution occurring during preparation.

4.2.3 Soluble/Insoluble colorimetric assay

Tissue homogenisation was carried out to prepare samples for Sircol soluble/insoluble collagen assay (Biocolor, UK) samples numbers are shown in Table 4.3. Samples were defrosted on ice and then weighed and diluted in Acetic (0.5M) Pepsin (sigma-aldrich, USA) 0.1mg/ml at 1:10 or 100 µl/10mg and left overnight (18 hours) at 4◦C as detailed in figure 4.3. Samples were then spun at 3000g for 10mins at 4◦C and then the supernatant containing the soluble collagen was collected and frozen at -20◦C. The pellet containing insoluble collagen was collected and frozen at -20◦C.

Table 4. 3 Atrial sample numbers for insoluble/soluble colorimetric assay

Sex	Sample Numbers				
	1 Month	3 Month	6 Month	12 Month	18 Month
Male	5	6	6	4	6
Female	6	6	5	4	6

Soluble and insoluble were assayed in separate runs due to differences in assay protocol. Soluble samples were defrosted on ice. Whilst samples were defrosting, soluble collagen standards (provided in the assay kit) were made up ranging from 0µg - 50µg in 100µl volumes. Once samples were defrosted, 10µl of each sample was transferred and made up to 100µl using DI water. Following sample preparation, 1ml of Sircol Dye (provided in the assay kit) was added to each standard and

sample tube to fully saturate the collagen molecules in the volume, tubes were then inverted. Samples were incubated at RT for 30mins on a mechanical shaker at a gentle speed. Tubes were then centrifuged at 13000g for 10 minutes at 4◦C and supernatant was discarded. Samples were then washes with 750µl of acid-salt wash reagent to remove unbound dye from the pellet and tube. Samples were then centrifuged at 13000g for 10 minutes at 4◦C and supernatant was discarded. Finally, 1ml of alkali reagent was added to all standards and samples, which were vortexed and incubated for 5 mins to allow for bound dye to dissolve. In duplicate, standards and samples were placed into a 96 well plate. The plate was read using a microplate reader within 2 hours of assay completion with an absorbance at OD 556nm.

Insoluble samples were defrosted on ice. Fragmentation reagent was added to each sample (50µl/mg of tissue) and the sample was placed onto a heatblock at 65◦C for 2 hours in screw capped round bottom 2 ml digestion tubes. Samples were then centrifuged at 13000g for 10mins at 4◦C. The remainder of the assay was run as described in the previous paragraph.

Total soluble and insoluble content was calculated on Microsoft excel Version 16.0 and was based on the standard curve generated by plotting the average of each duplicated standard minus the background (calculated from the blank). The background was subtracted from the samples and then valued were averaged A best-fit linear trend line was calculated and the equation was used to calculate the total amount of hydrolysed hydroxyproline in each sample. To calculate the concentration of soluble and insoluble content in each well (µg/µl) the identified value was then multiplied by a factor of 10 or 2 for soluble and insoluble respectively, to account for dilution occurring during preparation.

4.3 Results

This study looked to assess the effect of aging and sex on cardiac collagen synthesis in the atria in Sprague Dawley rats up to 18 months of age. Furthermore, we wished to characterise in this model the effect of sex and age on atrial collagen deposition *ex vivo*. Finally, we wish to compare the two different processes to assess whether changes in synthesis can be correlated with collagen deposited in the tissue. These findings will provide a comprehensive understanding of changes in collagen synthesis and deposition *in vivo* and *ex vivo.*

4.3.1 LA *cis*-4-[^{18}F]fluoro-*L*-proline uptake peaks at 3 months and is not affected by advanced aging

The synthesis of unhydroxylated collagen in the LA was quantified using *cis*-4-[^{18}F]fluoro-*L*-proline PET imaging. To evaluate sex differences, measurements were taken over an 18-month period – the template was manually applied to each scan to ensure accurate matching of the atria . No significant differences between males and females were observed at any of the time points (Figure 4.2). Both sexes exhibited similar uptake values at 1 month (males: 0.90 ± 0.05 SUVr; females: 0.90 ± 0.08 SUVr) and at 18 months (males: 0.95 ± 0.05 SUVr; females: 0.95 ± 0.07 SUVr).

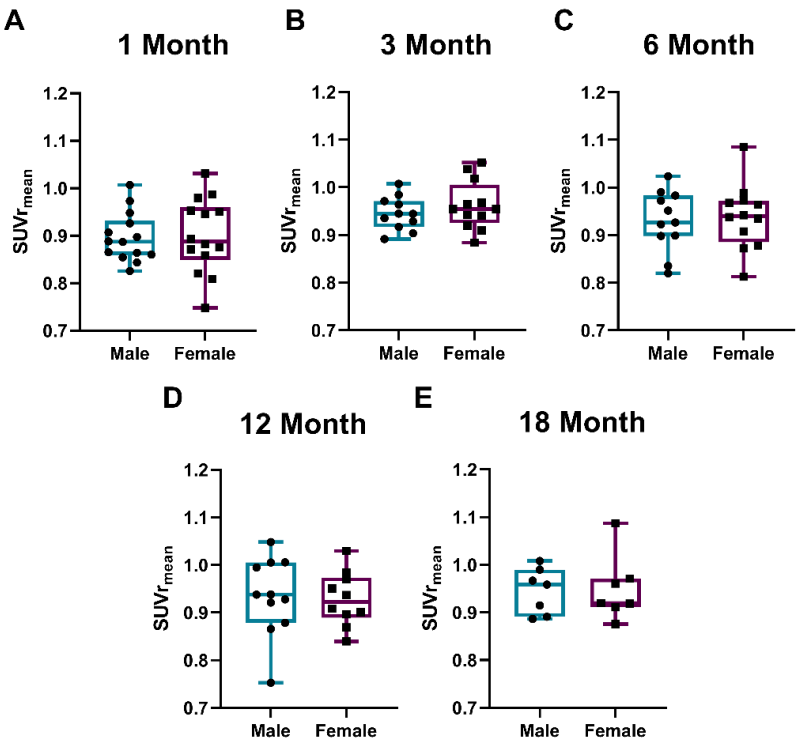

Figure 4. 2 Evaluating the impact of sex on LA *cis*-4-[^{18}F]fluoro-*L*-proline uptake Across timepoints. *cis*-4-[^{18}F]fluoro-*L*-proline uptake was measured in the LA at each imaging time point: 1 month (A), 3 month (B), 6 month (C), 12 month (D) and 18 month (E). Results reported as min to max range, n=7-14 males and n=7-14 females; Changes were assessed using a Student's t-test; results were not statistically significant.

The impact of age on unhydroxylated collagen synthesis in the LA was evaluated in both sexes. No significant age-related differences were observed in unhydroxylated collagen synthesis in males with some early change's females but not in advanced aging (Figure 4.3). Males exhibited a non-significant trend towards increased uptake (p=0.06) between 1 and 3 months, approximately 5.4%. In contrast, females showed a significant increase (p=0.04) in tracer uptake between 1 and 3 months by 6.9%, indicating higher rates of unhydroxylated collagen synthesis in the LA during early adult life. Given the lack of significant sex differences, data from both sexes were combined to assess the effect of age on the LA. This combined analysis revealed a significant increase (p=0.001) in uptake from 1 month (0.90 ± 0.07 SUVr) to 3 months (0.95 ± 0.04 SUVr), representing a 6.21% increase (Figure 4.4). This elevated level was maintained from 6 months (p=0.05) to 18 months (p=0.14), although the changes were not statistically significant.

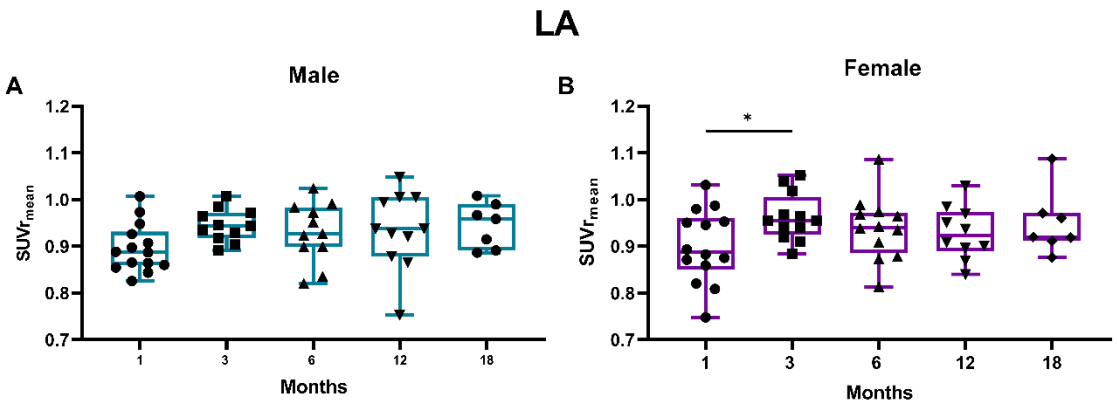

Figure 4. 3 Evaluating the impact of age on LA *cis*-4-[^{18}F]fluoro-*L*-proline in both sexes. Longitudinal changes in males (A) and females (B) *cis*-4-[^{18}F]fluoro-*L*-proline uptake in the LA over 18 months. Results reported as min to max range, n=7-14 males and n=7-14 females; p values were obtained a Mixed-effects Analysis and Dunnett's Post hoc test when comparing longitudinal data to the first timepoint. *p<0.05

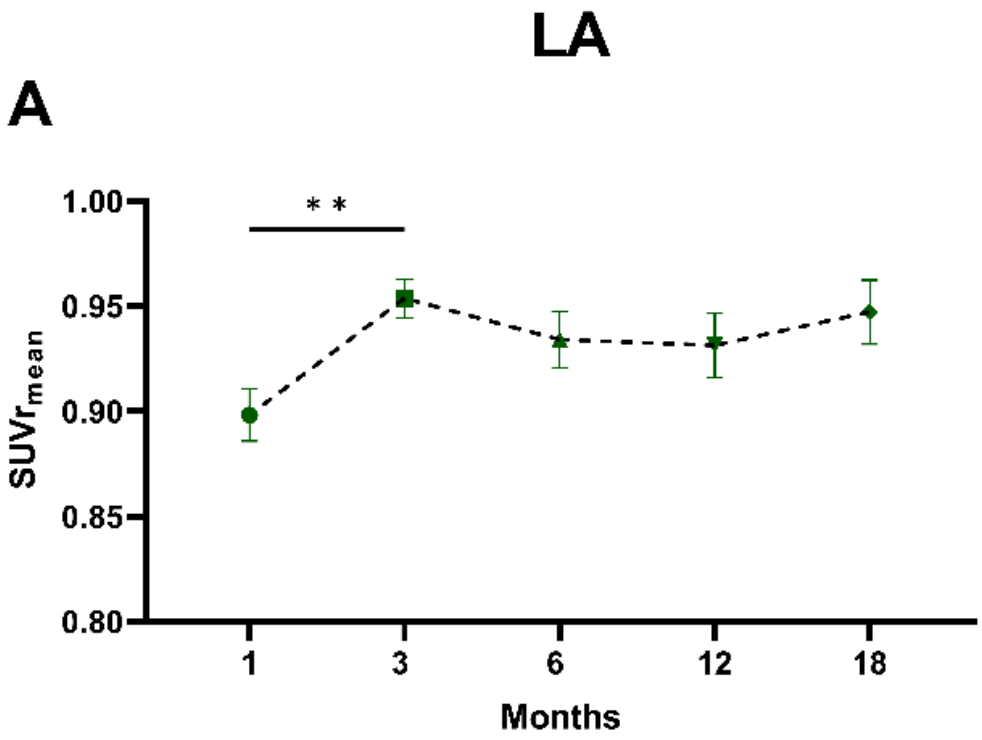

Figure 4. 4 Assessing the longitudinal effect of age in on LA *cis*-4-[^{18}F]fluoro-*L*-proline uptake. Longitudinal changes in *cis*-4-[^{18}F]fluoro-*L*-proline uptake in the LA over 18 months. Results reported as min to max range, n=7-14 males and n=7-14 females; p values were obtained a Mixed-effects Analysis and Dunnett's Post hoc test when comparing longitudinal data to the first timepoint. **p<0.01

4.3.2 LA *trans*-4-[^{18}F]fluoro-*L*-proline uptake increases at 18 months but is unaffected by sex

Hydroxylated collagen synthesis in the LA was measured using *trans*-4-[^{18}F]fluoro-*L*-proline PET imaging. No significant sex differences were observed in *trans*-4-[^{18}F]fluoro-*L*-proline uptake between males and females (Figure 4.5). Both sexes exhibited similar uptake values at 1 month (males: 0.92 ± 0.02 SUVr; females: 0.92 ± 0.04 SUVr) and at 18 months (males: 0.99 ± 0.02 SUVr; females: 0.97 ± 0.07 SUVr).

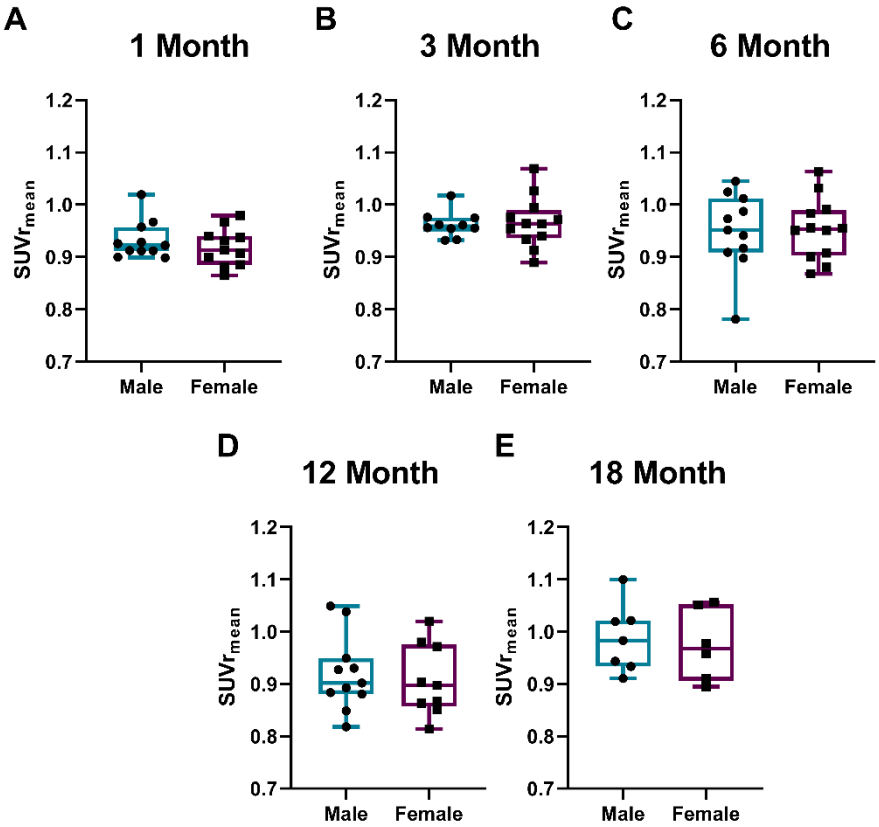

Figure 4. 5 Evaluating the impact of sex on LA *trans*-4-[^{18}F]fluoro-*L*-proline uptake across timepoints. *trans*-4-[^{18}F]fluoro-*L*-proline uptake was measured in the LA at each imaging time point: 1 month (A), 3 month (B), 6 month (C), 12 month (D) and 18 month (E). Results reported as min to max range, n=7-14 males and n=7-14 females; Changes were assessed using a Student's t-test; results were not statistically significant.

The effect of age on hydroxylated collagen synthesis in the LA was assessed in both sexes over an 18-month period. In males, age was found to significantly affect hydroxylated collagen synthesis, with a 4.2% increase at 3 months (0.96±0.02 SUVr; p=0.0051) and a 6.9% increase at 18 months (0.99±0.07 SUVr; p=0.027) compared to baseline at 1 month (0.92±0.02 SUVr) (Figure 4.6 A). No notable trends were observed at 6 and 12 months. In females, no significant effects of aging on LA hydroxylated collagen synthesis were detected; however, similar increasing trends were observed at 3 months (0.97±0.05 SUVr; p=0.12) with a 5.2% increase and at 18 months (0.97±0.07 SUVr; p=0.28) with a 6.1% increase compared to baseline measurements at 1 month (0.92±0.04 SUVr).

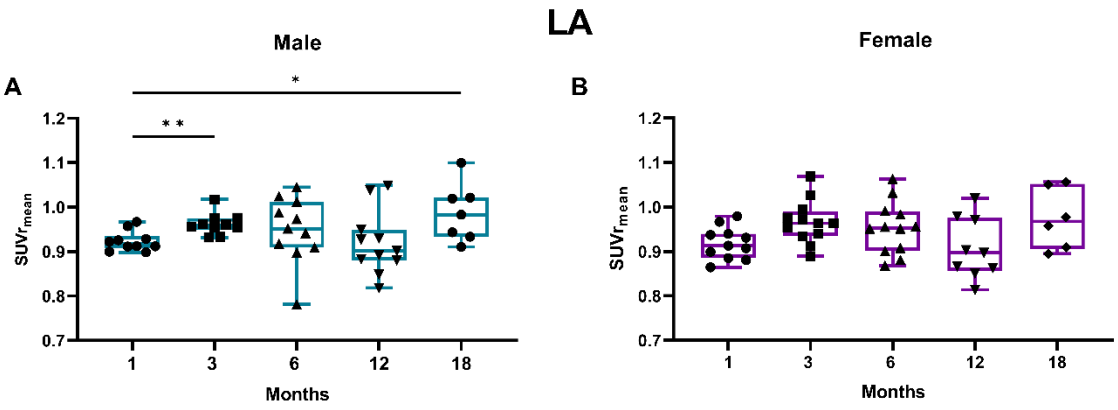

Figure 4. 6 Evaluating the impact of age on LA *trans*-4-[^{18}F]fluoro-*L*-proline in both sexes. Longitudinal changes in males (A) and females (B) *trans*-4-[^{18}F]fluoro-*L*-proline uptake in the LA over 18 months. Results reported as min to max range, n=7-14 males and n=7-14 females; p values were obtained a Mixed-effects Analysis and Dunnett's Post hoc test when comparing longitudinal data to the first timepoint. *p<0.05; **p<0.01

Given the absence of significant sex differences, the effect of age was assessed across the entire cohort. Consistent with previous findings, two main peaks in *trans*-4-[^{18}F]fluoro-*L*-proline uptake in the LA were observed: a 4.2% increase at 3 months (0.96 ± 0.04 SUVr; p=0.02) and a 6.1% increase at 18 months (0.98 ± 0.06 SUVr; p=0.01) (Figure 4.7). This suggests that hydroxylated collagen synthesis in the LA increases with aging.

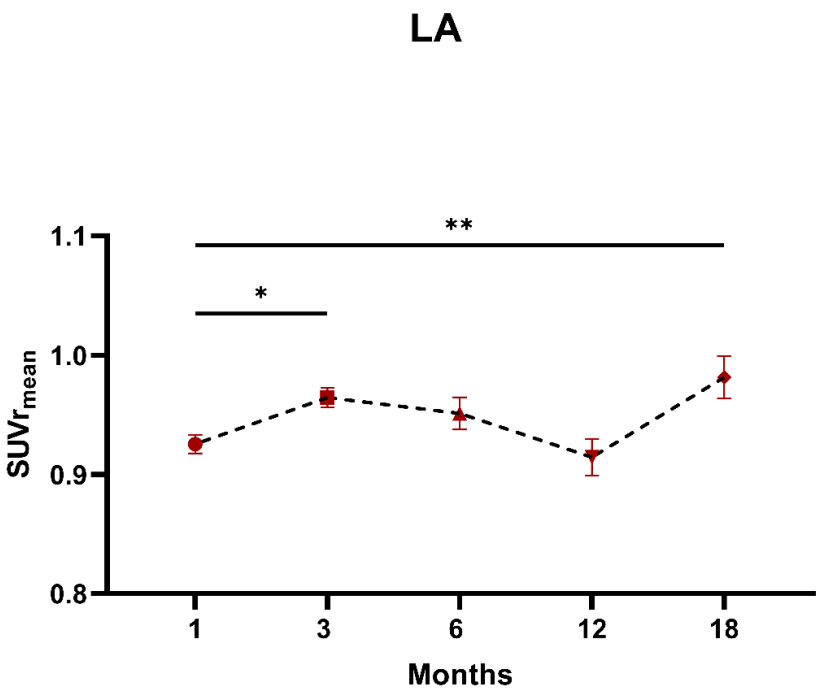

Figure 4. 7 Assessing the longitudinal effect of age in on LA *trans*-4-[^{18}F]fluoro-*L*-proline uptake. Longitudinal changes in *trans*-4-[^{18}F]fluoro-*L*-proline uptake in the LA over 18 months. Results reported as min to max range, n=7-14 males and n=7-14 females; p values were obtained a Mixed-effects Analysis and Dunnett's Post hoc test when comparing longitudinal data to the first timepoint. *p<0.05; **p<0.01

4.3.3 RA *cis*-4-[^{18}F]fluoro-*L*-proline uptake peaks at 6 months and is not affected by advanced aging

Unhydroxylated collagen synthesis in the RA was measured using *cis*-4-[^{18}F]fluoro-*L*-proline PET imaging. No significant sex differences were observed in *cis*-4-[^{18}F]fluoro-*L*-proline uptake within the RA over the 18-month period (Figure 4.8). Both males and females exhibited comparable uptake levels at 1 month (0.91 ± 0.06 SUVr) and at 18 months (0.98 ± 0.05 SUVr).

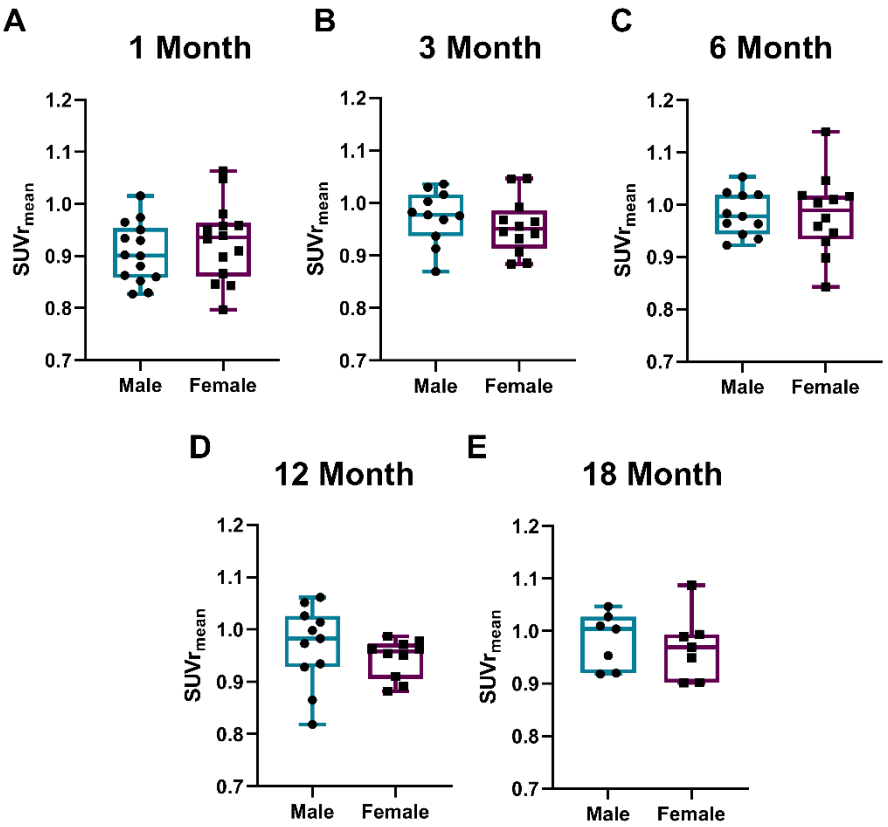

Figure 4. 8 Evaluating the impact of age on RA *cis*-4-[^{18}F]fluoro-*L*-proline in both sexes. Longitudinal changes in males (A) and females (B) *cis*-4-[^{18}F]fluoro-*L*-proline uptake in the RA over 18 months. Results reported as min to max range, n=7-14 males and n=7-14 females; p values were obtained using unpaired parametric students t-test when comparing two groups

The effect of age on unhydroxylated collagen synthesis in the RA was assessed in both sexes over 18 months. Males showed significant age-related increases in *cis*-4-[^{18}F]fluoro-*L*-proline uptake at 6 months (0.98 ±0.04 SUVr; p=0.01), representing an 8.4% increase compared to baseline measurements at 1 month (0.91±0.06 SUVr) (Figure 4.9 A). Similar increases were observed at other time points: 7.5% at 3 months (0.97±0.05 SUVr; p=0.05), 6.9% at 12 months (p=0.10), and 8.4% at 18 months (p=0.11), though these increases were not statistically significant. The 3-month time point approached significance (p=0.0539), and the lack of significance at later time points was likely due to the reduction in sample size over the course of the study. In females, no significant changes were observed over the 18-month period. However, there was a trend towards increased uptake: 3% at 3 months (0.96±0.05 SUVr), 5.8% at 6 months (0.98±0.08 SUVr), and 4.6% at 18 months (0.97±0.06 SUVr) compared to baseline at 1 month (0.93±0.08 SUVr) (Figure 4. 9 B).

Given the lack of significant sex differences, data from both sexes were combined to assess the effect of age on the RA. This combined analysis identified a significant increase in uptake at 6 months (7.1%, Figure 4.10). Additionally, there were trends towards significance at 3 months (5.2%, p=0.052) and at 18 months (6.5%, p=0.096). These findings suggest that unhydroxylated collagen synthesis in the RA increases with age, particularly at 6 months.

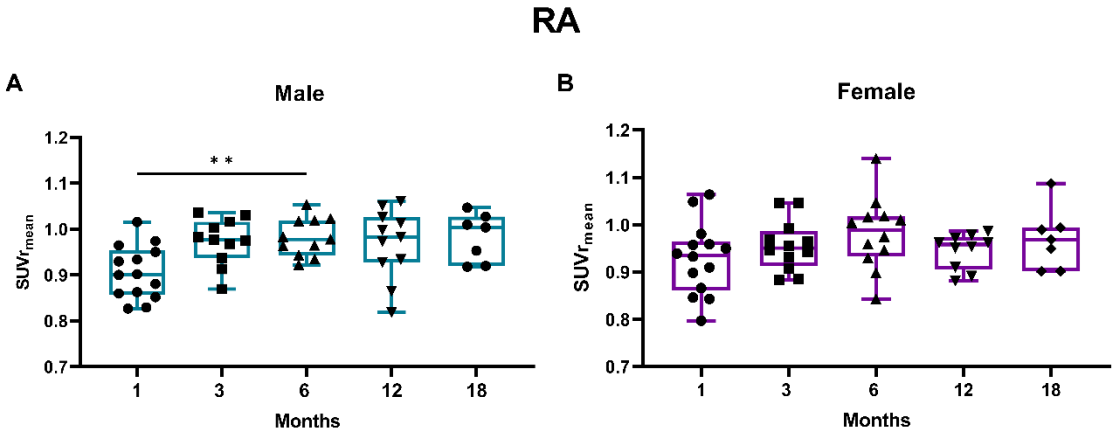

Figure 4. 9 Evaluating the Impact of Age on RA *cis*-4-[^{18}F]fluoro-*L*-proline in both sexes. Longitudinal changes in males (A) and females (B) *cis*-4-[^{18}F]fluoro-*L*-proline uptake in the RA over 18 months. Results reported as min to max range, n=7-14 males and n=7-14 females; p values were obtained a when comparing longitudinal data to the first timepoint. **p<0.01

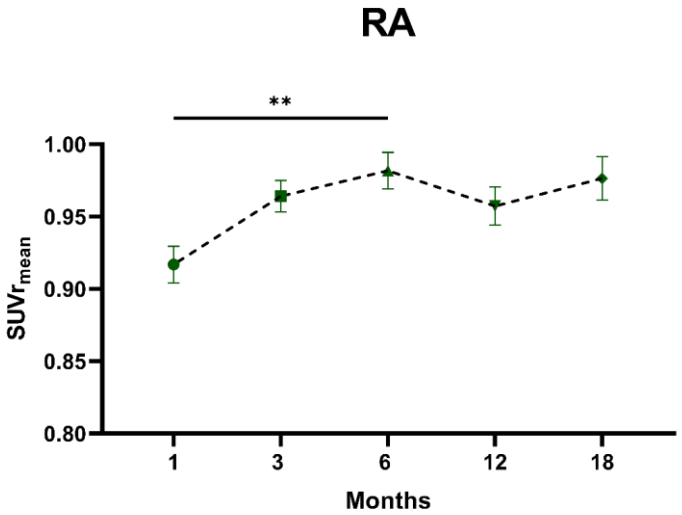

Figure 4. 10 Assessing the longitudinal effect of age in on RA *cis*-4-[^{18}F]fluoro-*L*-proline uptake. Longitudinal changes in *cis*-4-[^{18}F]fluoro-*L*-proline uptake in the RA over 18 months. Results reported as min to max range, n=7-14 males and n=7-14 females; p values were obtained a Mixed-effects Analysis and Dunnett's Post hoc test when comparing longitudinal data to the first timepoint. **p<0.01;

4.3.4 RA *trans*-4-[^{18}F]fluoro-*L*-proline uptake increases in aging but is unaffected by sex

Hydroxylated collagen synthesis in the RA was assessed over an 18-month period. No significant sex differences were identified at any time point (Figure 4.11). Both males and females exhibited comparable levels of uptake from 1 month (males: 0.94 ± 0.04 SUVr; females: 0.92 ± 0.05 SUVr) to 18 months (males: 1.1 ± 0.09 SUVr; females: 0.99 ± 0.07 SUVr). These findings indicate that hydroxylated collagen synthesis in the RA is consistent between sexes throughout the aging process.

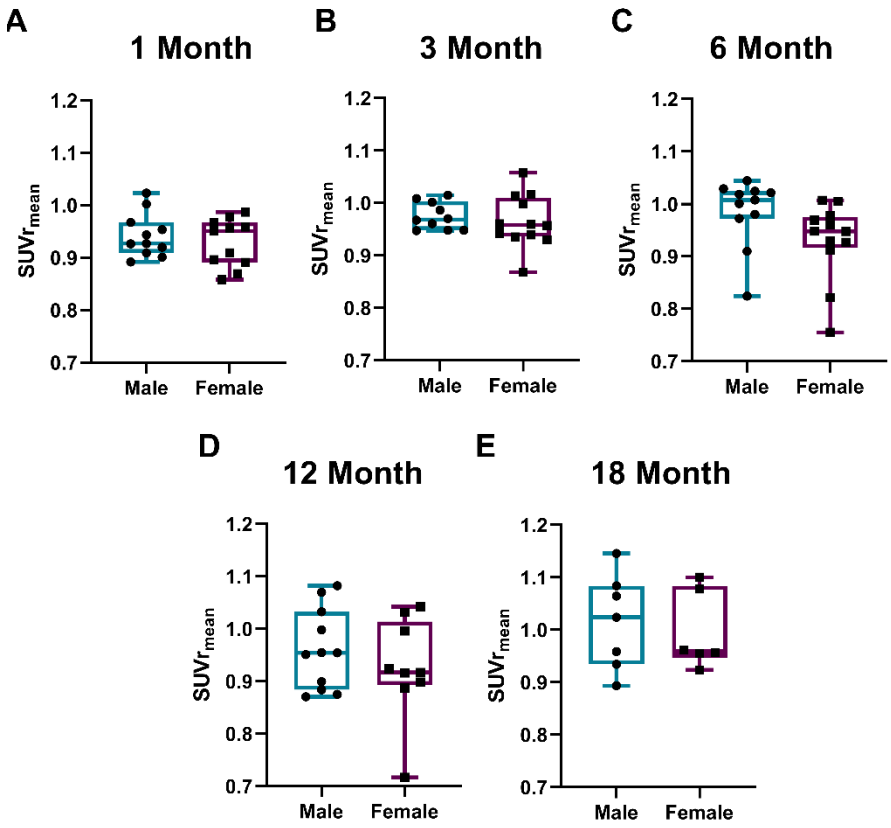

Figure 4. 11 Evaluating the impact of sex on RA *trans*-4-[^{18}F]fluoro-*L*-proline uptake across timepoints. *trans*-4-[^{18}F]fluoro-*L*-proline uptake was measured in the RA at each imaging time point: 1 month (A), 3 month (B), 6 month (C), 12 month (D) and 18 month (E). Results reported as min to max range, n=7-14 males and n=7-14 females; p values were obtained using unpaired parametric students t-test when comparing two groups

The effect of age on RA hydroxylated collagen synthesis was assessed in both sexes over 18 months. No significant sex differences were observed (Figure 4.12). However, there was a trend towards increased uptake with age in both sexes. Males showed a 7.7% increase at 18 months (1.01 ± 0.09 SUVr; p=0.15) compared to the 1-month time point (0.94 ± 0.04 SUVr). Similarly, females exhibited a 7.2% increase at 18 months (0.99 ± 0.07 SUVr; p=0.23) compared to the 1-month time point (0.93 ± 0.05 SUVr). Given the absence of sex differences, data from both sexes were combined to assess the overall effect of age. This combined analysis revealed that aging significantly increased hydroxylated collagen synthesis in the RA (Figure 4.13). Significant changes were observed at 3 months (0.97 ± 0.04 SUVr; p= 0.04), representing a 3.6% increase, at 6 months (0.98 ± 0.04 SUVr; p=0.01), with a 4.7% increase, and at 18 months (1.0±0.08 SUVr; p=0.018), showing a 7.5% increase. These findings indicate that hydroxylated collagen synthesis in the RA increases with age.

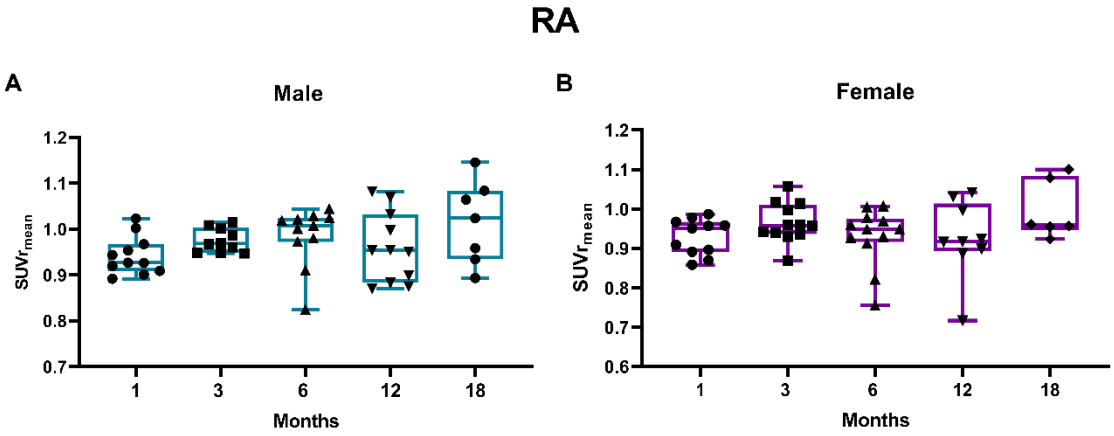

Figure 4. 12 Evaluating the impact of age on RA *trans*-4-[^{18}F]fluoro-*L*-proline in both sexes. Longitudinal changes in males (A) and females (B) *trans*-4-[^{18}F]fluoro-*L*-proline uptake in the RA over 18 months. Results reported as min to max range, n=7-14 males and n=7-14 females; p values were obtained a Mixed-effects Analysis and Dunnett's Post hoc test when comparing longitudinal data to the first timepoint.

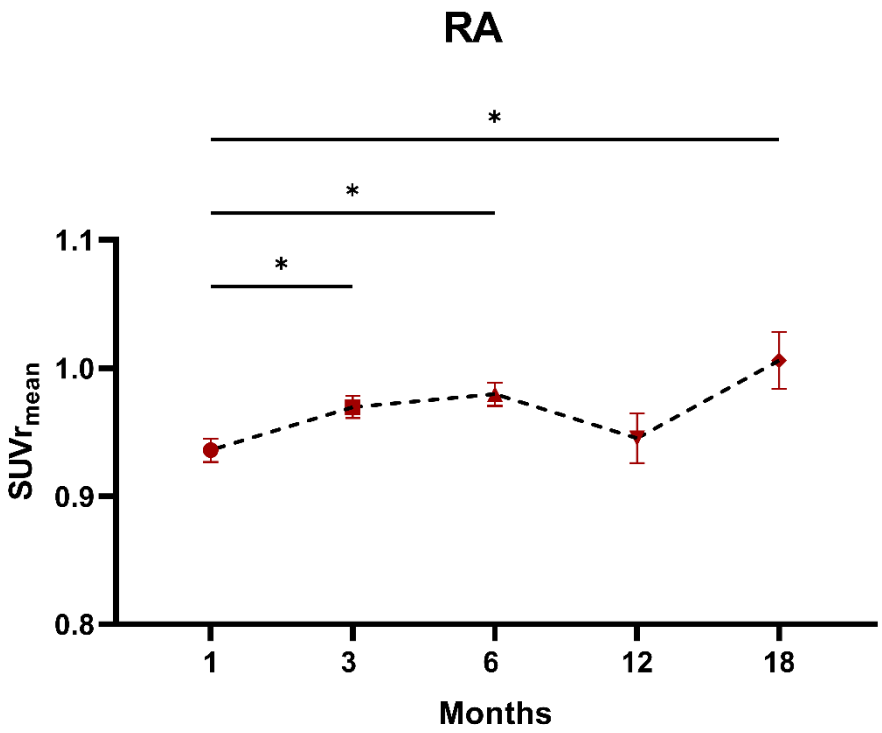

Figure 4. 13 Assessing the longitudinal effect of age in on RA *trans*-4-[^{18}F]fluoro-*L*-proline uptake. Longitudinal changes in *trans*-4-[^{18}F]fluoro-*L*-proline uptake in the RA over 18 months. Results reported as min to max range, n=7-14 males and n=7-14 females; p values were obtained a Mixed-effects Analysis and Dunnett's Post hoc test when comparing longitudinal data to the first timepoint. *p<0.05

4.3.5 Whole atrial *cis*-4-[^{18}F]fluoro-*L*-proline uptake increases with aging

Due to the limited availability of tissue, most of our *ex vivo* analyses did not differentiate between the left and right atria. Therefore, we assessed the overall uptake of atrial unhydroxylated collagen synthesis. This analysis revealed that the atria as a whole exhibited increased uptake of *cis*-4-[^{18}F]fluoro-*L*-proline, indicating elevated unhydroxylated collagen synthesis with age (Figure 4.14). A significant increase in uptake was observed at 3 months, with a 6.5% rise (p=0.0005). This increase was maintained over time, with further increases noted at 6 months (6.5%) (p=0.01), 12 months (4.9%), and 18 months (6.7%). These findings suggest a progressive increase in unhydroxylated collagen synthesis in the atria as a function of aging.

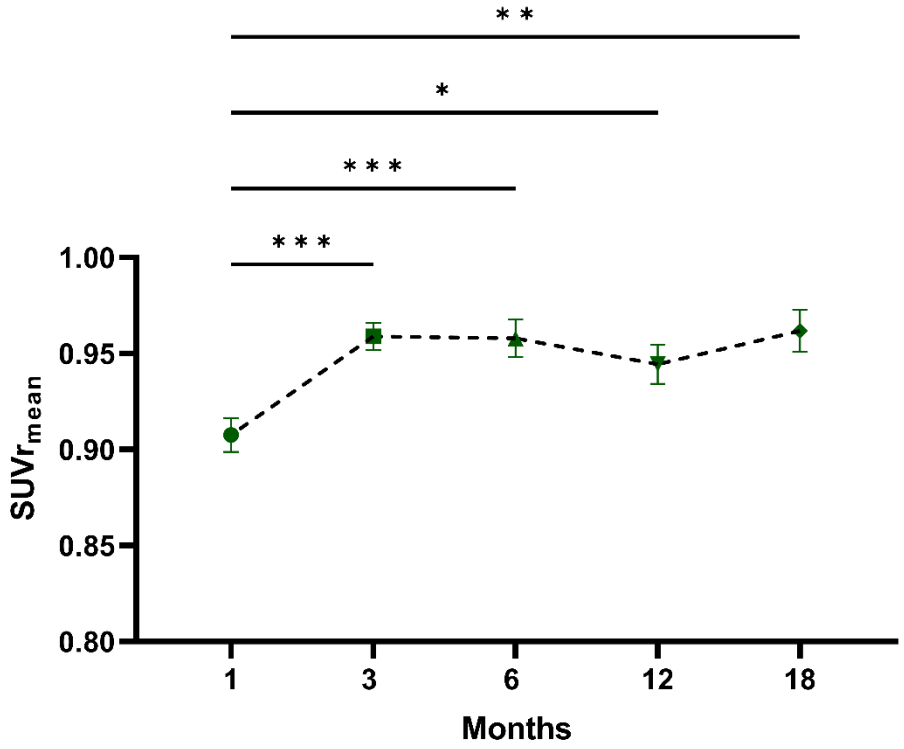

Figure 4. 14 Assessing the longitudinal effect of age in on whole atrial *cis*-4-[^{18}F]fluoro-*L*-proline uptake. Longitudinal changes in *cis*-4-[^{18}F]fluoro-*L*-proline uptake in the Whole Atrial over 18 months. Results reported as min to max range, n=7-14 males and n=7-14 females; p values were obtained a *Mixed-effects Analysis and Dunnett's Post hoc test* when comparing longitudinal data to the first timepoint. *p<0.05; **p<0.01 and ***p<0.001

4.3.6 Whole atrial *trans*-4-[^{18}F]fluoro-*L*-proline uptake increases with aging

Whole atrial uptake of *trans*-4-[^{18}F]fluoro-*L*-proline was measured to assess hydroxylated collagen synthesis. The analysis indicated that hydroxylated collagen synthesis in the atria increases with age. The most significant increase was observed at 18 months, with a 6.8% rise (p=0.001) (Figure 4.15). Additional increases were noted at 3 months (3.9%; p=0.0005) and 6 months (3.6%; p=0.01), followed by a notable return to baseline levels at 12 months of age. These findings suggest a trend of increasing hydroxylated collagen synthesis in the atria up to 18 months, with a temporary stabilization at 12 months.

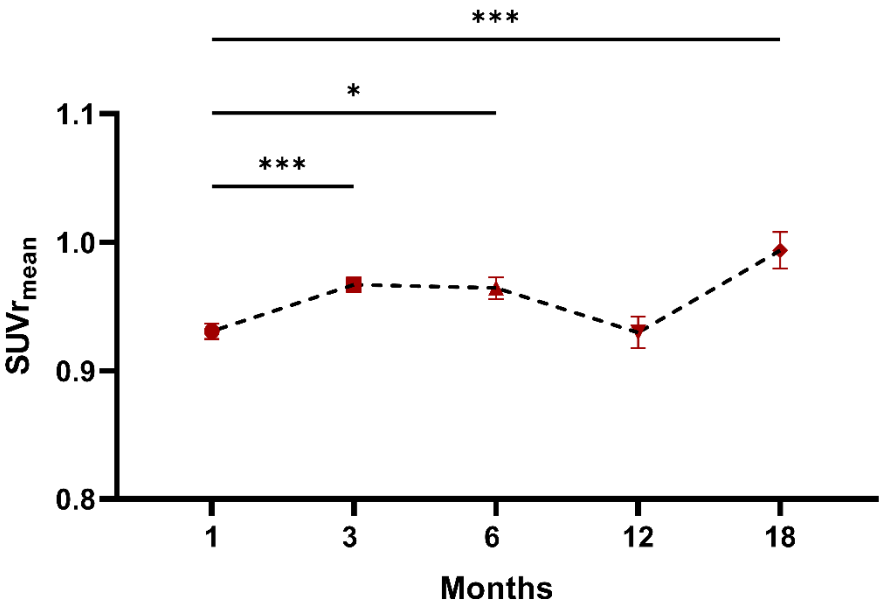

Figure 4. 15 **Assessing the longitudinal effect of age in on whole atrial *trans*-4-[^{18}F]fluoro-*L*-proline uptake.** Longitudinal changes in *trans*-4-[^{18}F]fluoro-*L*-proline uptake in the Whole Atrial over 18 months. Results reported as min to max range, n=7-14 males and n=7-14 females; p values were obtained a Mixed effects Analysis and Dunnett's Post hoc test when comparing longitudinal data to the first timepoint. *p<0.05; ***p<0.001

4.3.7 Atrial total deposited collagen does not alter with age but shows some sex differences

Histological analysis of total deposited collagen was completed within the atria, assessing sex differences over an 18-month period. No sex differences in early adult life were observed at 1 month (males: 64.8%±5.5%; females: 65.0%±3.2%) and 6 months of age (males: 58.9%±4.2%; females: 62.9%±5.8%), with both sexes showing relatively comparable total deposited collagen (Figure 4.16 A-C). However, as aging advanced, significant differences emerged between the sexes. At 12 months, females (69.7%±9.1%; p=0.026) had significantly higher atrial collagen deposition compared to males (57.6%±5.1%), with an 11.1% difference (Figure 4.16 D). This trend reversed at 18 months, with males (66.0%±5.1%; p=0.0073) showing significantly higher deposited collagen than females (56.2%±3.6%) (Figure 4.16 E). These findings highlight dynamic sex-specific differences in atrial collagen deposition over time.

The effect of aging on total deposited atrial collagen was assessed over 18 months in both sexes. No significant effects of age were observed on atrial deposited collagen (Figure 4.17 A). However, a trend was noted where total collagen decreased below baseline expression over the first 12 months and increased again at 18 months. Due to high variability, a greater number of samples would be needed to accurately assess these changes. In females, a significant decrease (p=0.045) in total atrial collagen deposition of 13.7% was observed at 18 months compared to baseline, suggesting that collagen deposition is maintained over 12 months and then declines in females at 18 months (Figure 4.17 B).

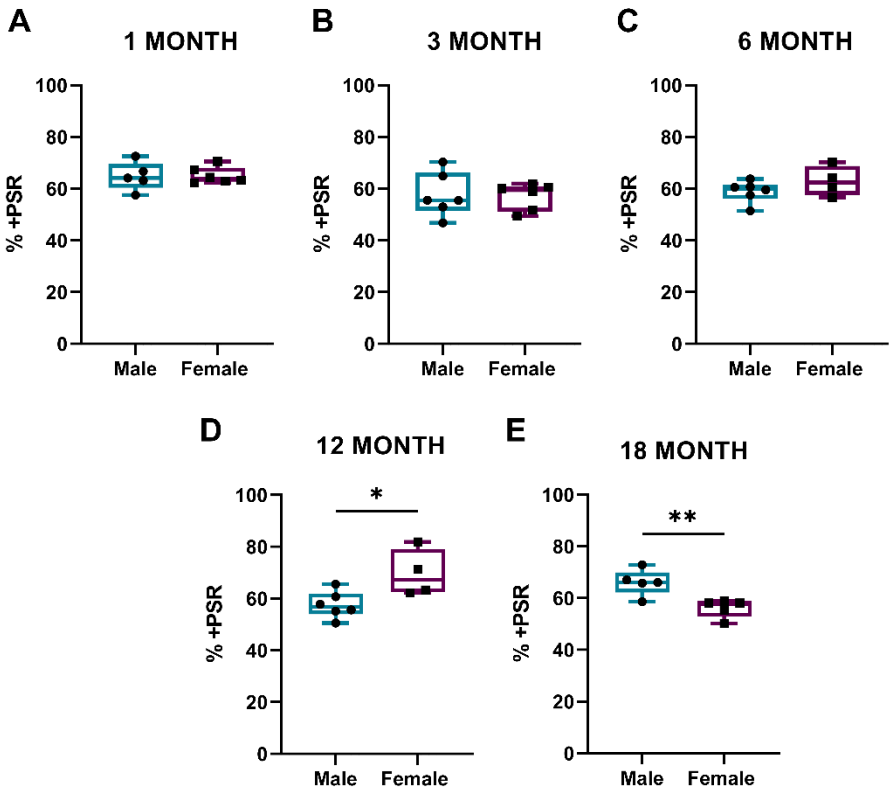

Figure 4. 16 Evaluating the impact of sex on total whole atria collagen deposition across timepoints. *%* positive PSR stain (%+PSR) was measured in the whole atria at each imaging time point: 1 month (A), 3 month (B), 6 month (C), 12 month (D) and 18 month (E). Results reported as min to max range, n=5-6 males and n=5-6 females; p values were obtained using unpaired parametric students t-test when comparing two groups *p<0.05; **p<0.01

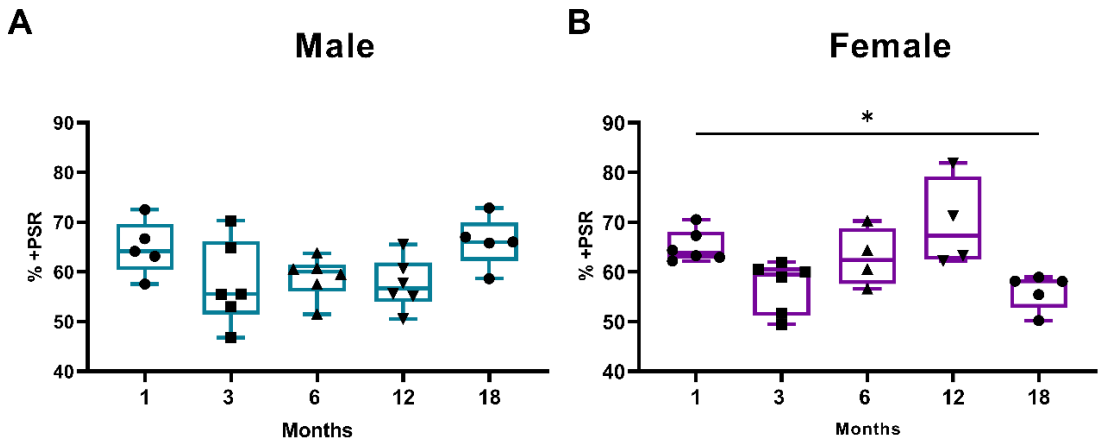

Figure 4. 17 Evaluating the impact of age on total whole atria in both sexes. Longitudinal changes in males (A) and females (B) % positive PSR stain (%+PSR) in the Whole Atria over 18 months. Results reported as min to max range, n=7-14 males and n=7-14 females; p values were obtained a one-way ANOVA and Dunnett's Post hoc test when comparing longitudinal data to the first timepoint. *p<0.05

4.3.8 Atrial hydroxyproline analysis peaks in adult life, but falls by 18 months

Total hydroxyproline content, a marker exclusively found in collagen and indicative of collagen abundance, was measured to assess sex differences over 18 months. Significant sex differences in hydroxyproline content were only identified in early adult life at 1 month and 3 months of age (Figure 4.18). At 1 month, females had significantly lower hydroxyproline levels (males: 0.26±0.10 µg/mg; females: 0.11 ± 0.01 µg/mg; p=0.02) compared to males. This trend reversed at 3 months, with females showing significantly higher hydroxyproline content (males: 0.26 ± 0.10µg/mg; females: 0.40 ±0 .19 µg/mg; p=0.03) compared to males.

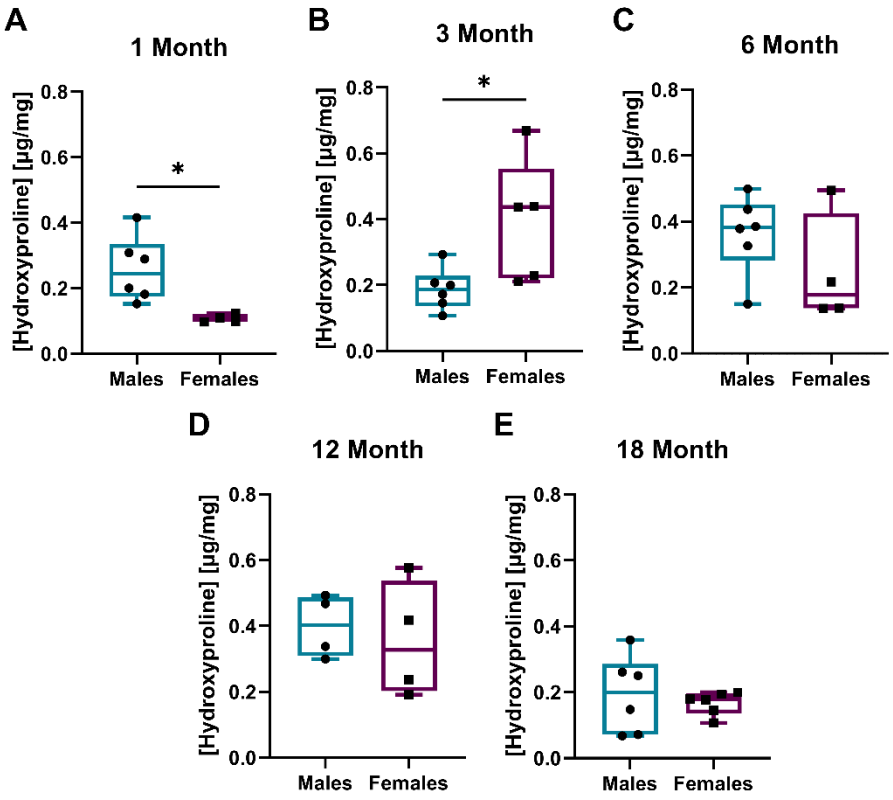

Figure 4. 18 Evaluating the Impact of Sex on total Whole Atrial hydroxyproline content Across Timepoints. Hydroxyproline content (µg/mg) was measured in the whole atrial at each imaging time point: 1 month (A), 3 month (B), 6 month (C), 12 month (D) and 18 months (E). Results reported as min to max range, n=5-6 males and n=5-6 females; p values were obtained using unpaired parametric students t-test when comparing two groups' *p<0.05

The effect of age on atrial hydroxyproline content was assessed over 18 months in both sexes. Males showed a significant increase in hydroxyproline content at 6 months (0.41 ± 0.07 µg/mg; p=0.04), representing a 57.1% increase, followed by a significant decline at 18 months (0.19 ± 0.12 µg/mg), comparable to baseline levels at 1 month (0.26 ± 0.10 µg/mg) (Figure 4.19 A). In females, peak hydroxyproline content was observed at 3 months (0.40 ± 0.19 µg/mg; p=0.04), with an average increase of 270.9% compared to baseline (0.11 ± 0.01 µg/mg), followed by a significant decrease at 18 months (0.17 ± 0.04 µg/mg) (Figure 4.19 B). These findings suggest that hydroxyproline content, and consequently collagen abundance, exhibits distinct age-related patterns in males and females.

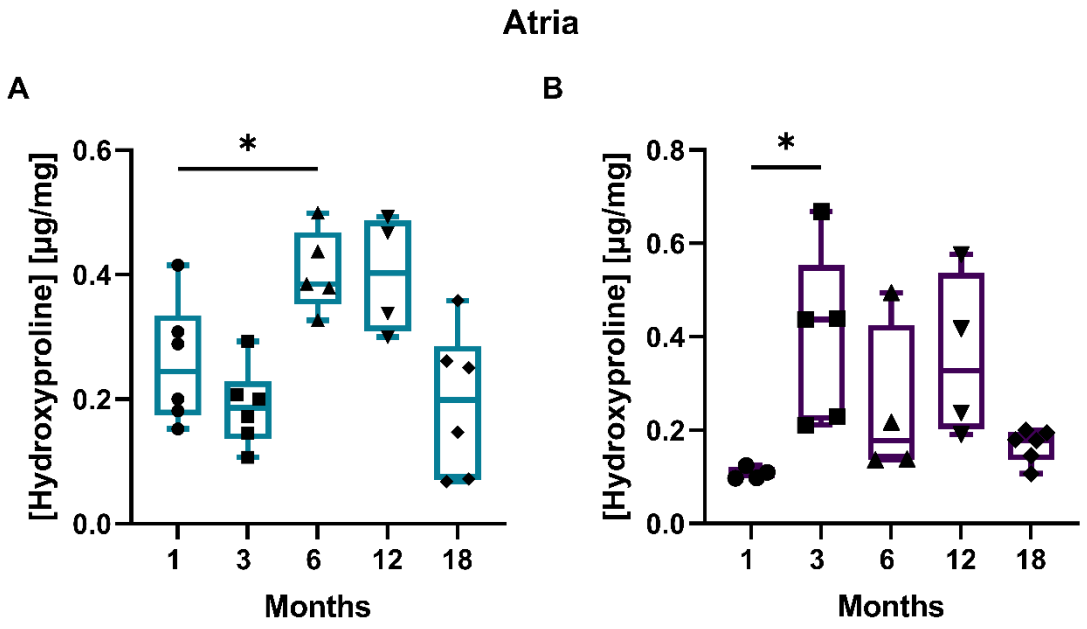

Figure 4. 19 Evaluating the impact of age on total whole atrial hydroxyproline content in both sexes. Longitudinal changes in males (A) and females (B) Hydroxyproline content (µg/mg) uptake in the whole atria over 18 months. Results reported as min to max range, n=5-6 males and n=5-6 females; p values were obtained a one-way ANOVA and Dunnett's Post hoc test when comparing longitudinal data to the first timepoint *p<0.05

4.3.9 Atrial soluble collagen analysis increases in males with aging but not females

Soluble collagen was measured to assess the abundance of newly synthesized collagen that has yet to mature and be crosslinked. Over 12 months, no significant sex differences were observed, with males and females showing comparable levels of soluble collagen at 1 month (males: 7650 ±3 691 µg/µl; females: 8081 ± 719 µg/µl) and 12 months of age (males: 13027 ± 2883 µg/µl; females: 11499 ± 3280 µg/µl) (Figure 4.20 A-D). Interestingly, a striking sex difference was found at 18 months, with males having significantly higher soluble collagen compared to females, showing a 92% difference (males:

44234 ± 8208 µg/µl; females: 3504 ± 3280 µg/µl) (Figure 4.20 E). These results indicate a pronounced divergence in soluble collagen levels between males and females as they age.

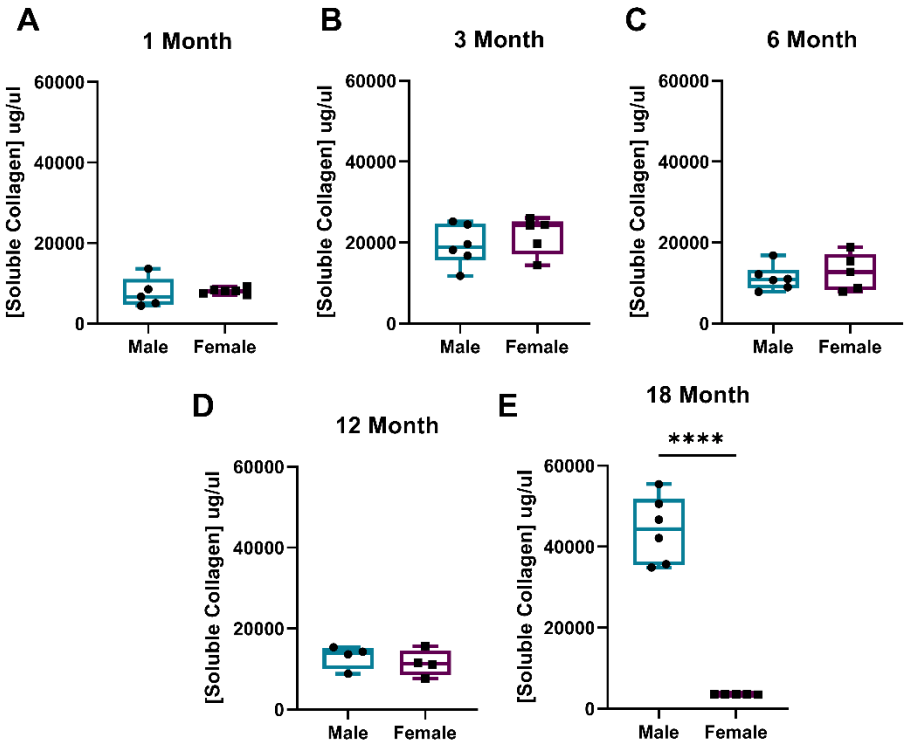

Figure 4. 20 Evaluating the impact of sex on total whole atria soluble collagen content across timepoints. Soluble collagen (µg/µl) was measured in the Whole Atria at each imaging time point: 1 month (A), 3 month (B), 6 month (C), 12 month (D) and 18 months (E). Results reported as min to max range, n=3-6 males and n=3-6 females; p values were obtained using unpaired parametric students t-test when comparing two groups' ****p<0.0001

The effect of age on soluble collagen was assessed in the atria of both sexes over 18 months. In males, aging caused a significant increase in soluble collagen, predominantly at 18 months (Figure 4.21 A). Males exhibited two significant peaks in soluble collagen: one at 3 months with a 152.9% increase (p=0.01), and a much larger increase at 18 months with a 478.2% rise (p<0.0001), suggesting that these are key time points for increased soluble collagen prevalence. In females, there was a significant increase at 3 months of 91.1%, followed by a gradual return to baseline values (Figure 4.21 B). These findings highlight distinct age-related patterns in soluble collagen levels between males and females.

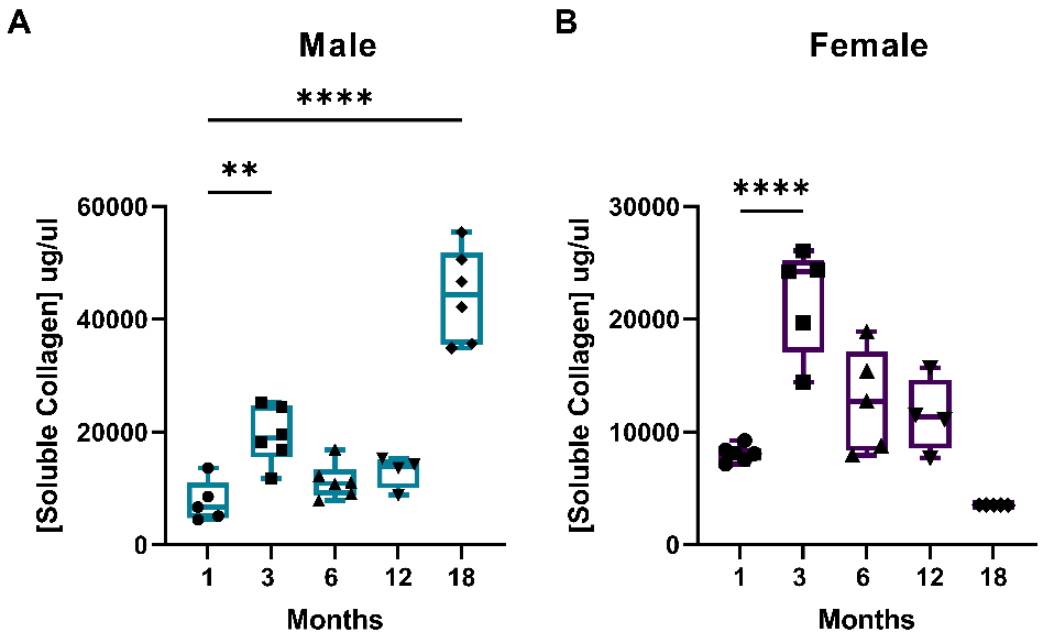

Figure 4. 21 Evaluating the impact of age on total whole atrial soluble collagen content in both sexes. Longitudinal changes in males (A) and females (B) Soluble collagen (µg/µl) uptake in the whole atria over 18 months. Results reported as min to max range, n=5-6 males and n=5-6 females; p values were obtained a one-way ANOVA and Dunnett's Post hoc test when comparing longitudinal data to the first timepoint. **p<0.01; ****p<0.0001

4.3.10 Atrial insoluble collagen is not affected by age or sex

Insoluble collagen content, a metric of mature collagen abundance, was assessed and compared in the atria of males and females over 18 months. No sex differences were identified in insoluble collagen content over this period (Figure 4.22). Males and females showed comparable levels of insoluble collagen from 1 month (males: 1158 ± 658 µg/µl; females: 1187 ± 179 µg/µl) to 18 months (males: 478 ± 220 µg/µl; females: 637 ± 457 µg/µl), suggesting that sex does not influence insoluble collagen content in the atria.

The effect of age on insoluble collagen synthesis was also assessed over 18 months in the atria. Aging was found to have no significant effect on atrial insoluble collagen content (Figure 4.23). Males showed sustained levels of insoluble collagen from 1 month to 18 months of age, and similarly, females showed no significant changes in insoluble collagen with aging in the atria. These results indicate that both sex and aging have no substantial impact on insoluble collagen levels in the atria.

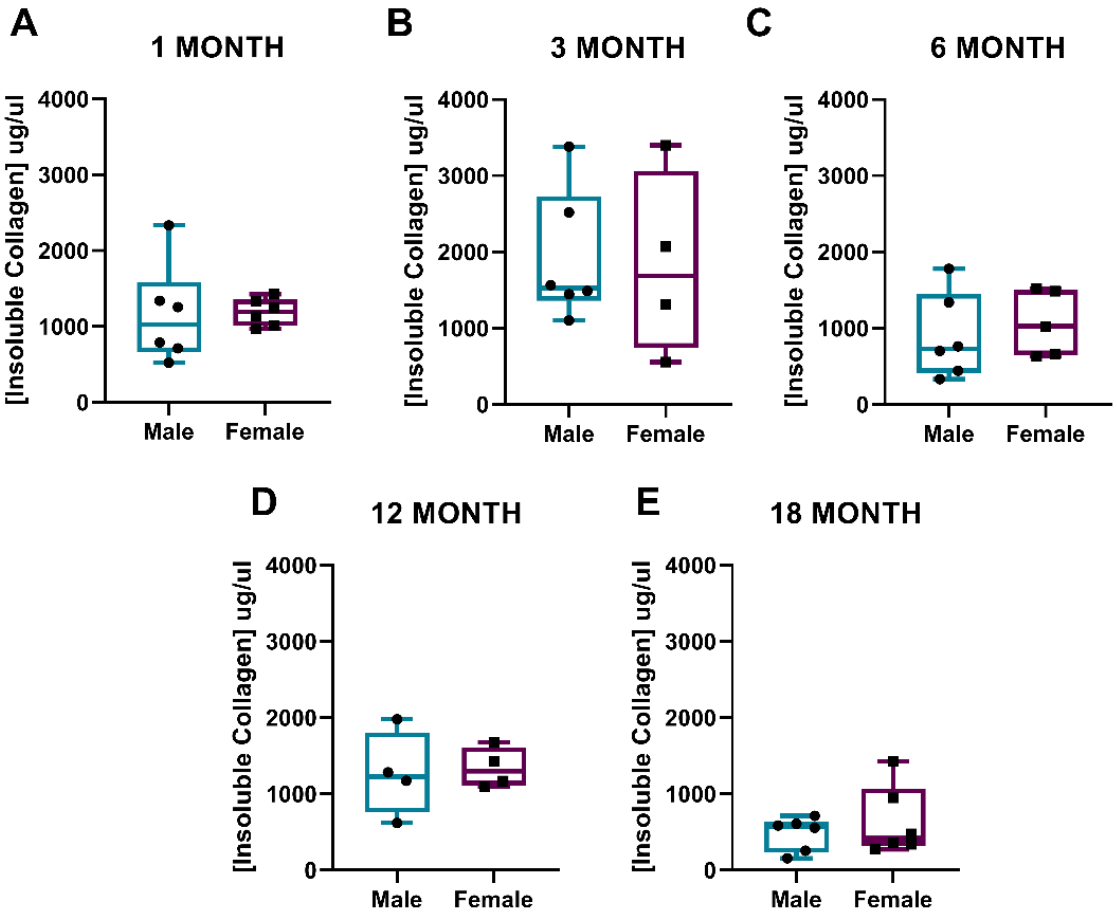

Figure 4. 22 Evaluating the impact of sex on total whole atria insoluble collagen content across timepoints. Insoluble collagen (µg/µl) was measured in the whole atria at each imaging time point: 1 month (A), 3 month (B), 6 month (C), 12 month (D) and 18 months (E). Results reported as min to max range, n=5-6 males and n=5-6 females; Changes were assessed using a Student's t-test; results were not statistically significant.

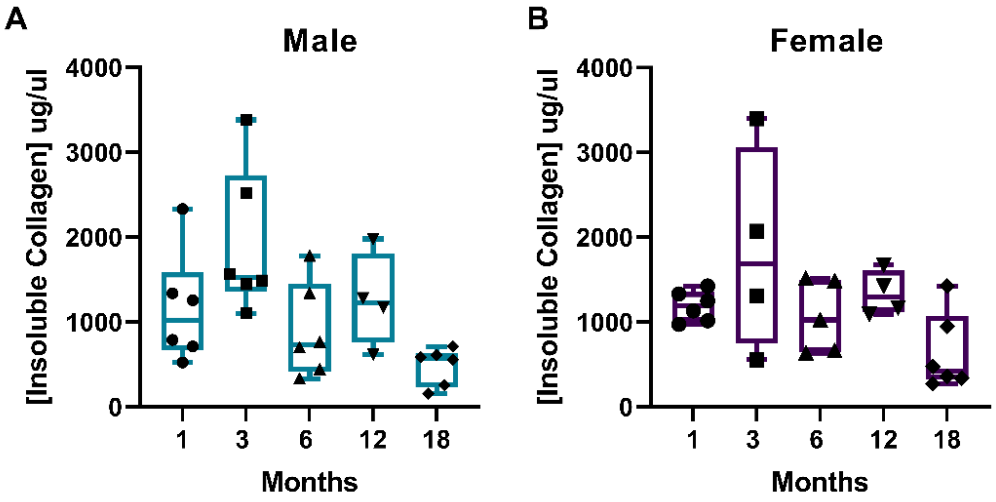

Figure 4. 23 Evaluating the impact of age on total whole atria insoluble collagen content in both sexes. Longitudinal changes in males (A) and females (B) insoluble collagen (µg/µl) uptake in the whole atria over 18 months. Results reported as min to max range, n=5-6 males and n=5-6 females; Changes were assessed using a one-way ANOVA and Dunnett's Post-hoc test; results were not statistically significant.

4.3.11 Atrial soluble: insoluble collagen ratio shows a male specific reduction at 18 months

The insoluble:Soluble collagen ratio was calculated in the atria as an indicator of tissue integrity. No sex differences were observed in this ratio up to 12 months of age (Figure 4.24 A-D). However, at 18 months, males exhibited a significantly lower insoluble: Soluble collagen ratio compared to females. This difference is likely due to a substantial decrease in soluble collagen observed in males at 18 months of age (Figure 4.24 E).

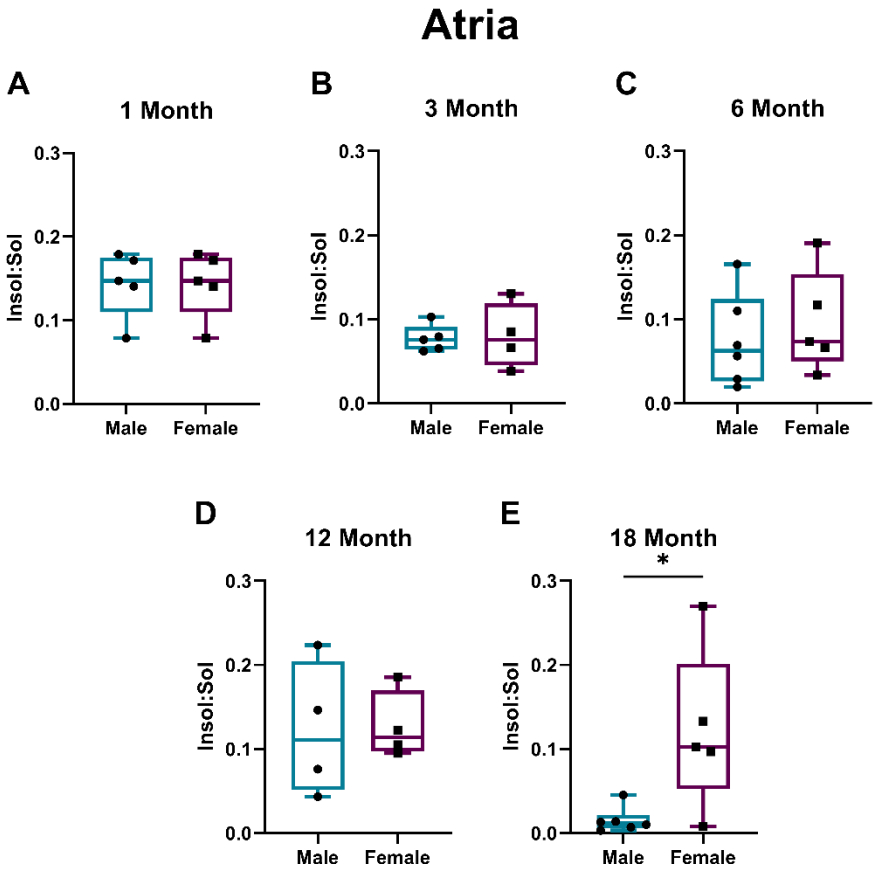

Figure 4. 24 Evaluating the impact of sex on total whole atria insoluble: soluble collagen content ratio across timepoints. Insoluble: soluble collagen ratio was calculated for the whole atria at each imaging time point: 1 month (A), 3 month (B), 6 month (C), 12 month (D) and 18 months (E). Results reported as min to max range, n=4-6 males and n=4-6 females; p values were obtained using unpaired parametric students t-test when comparing two groups'

The effect of age on the insoluble:soluble collagen ratio in the atria was assessed. In males, the insoluble:soluble collagen ratio remained stable over 12 months; however, a significant decline of 89.2% was observed at 18 months. This suggests an increase in soluble collagen relative to insoluble collagen, leading to changes in tissue integrity (Figure 4.25 A). In contrast, females showed no significant age-related changes in the insolublecollagen ratio, indicating that atrial tissue structure is maintained with age.

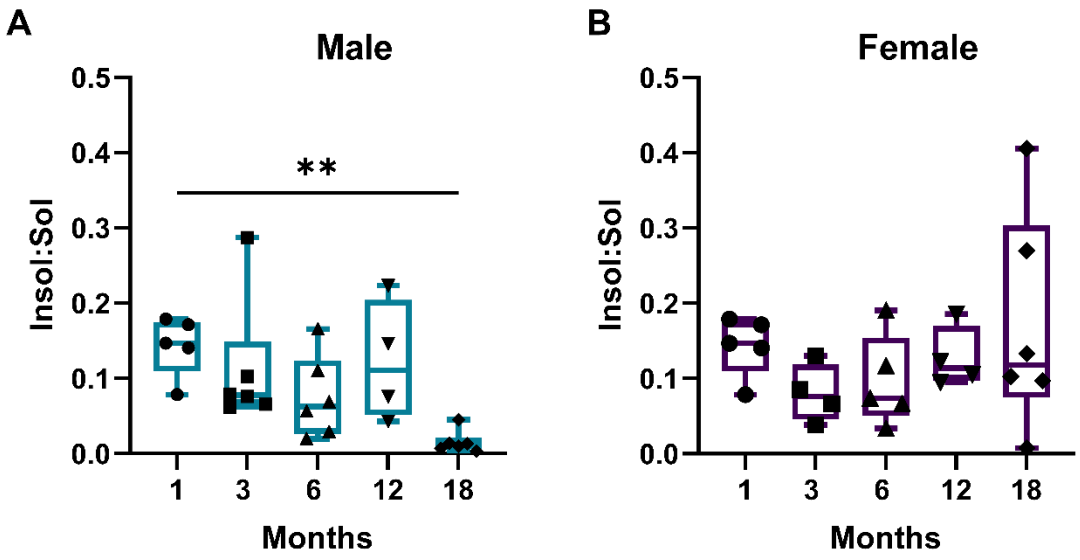

Figure 4. 25 Evaluating the impact of age on total whole atrial insoluble: soluble collagen ratio in both sexes. Longitudinal changes in males (A) and females (B) insoluble: soluble collagen content ratio was calculated for the whole atrial over 18 months. Results reported as min to max range, n=4-6 males and n=4-6 females; p values were obtained a one-way ANOVA when comparing longitudinal data to the first timepoint. **p<0.01

4.3.12 Atrial collagen synthesis outcomes do not predict functional outcomes

Linear regression analysis was carried out to assess whether RA or LA hydroxylated or unhydroxylated collagen synthesis over 18 months was associated with aged EF outcomes. In the LA, no significant associations were found between *cis*-4-[^{18}F]fluoro-*L*-proline uptake from 1 to 18 months and EF at 18 months (Figure 4.26 A). Similarly, *trans*-4-[^{18}F]fluoro-*L*-proline uptake from 1 to 18 months showed no significant associations with aged EF outcomes (Table 4.4). When analysing the RA, no significant associations were observed between *cis*-4-[^{18}F]fluoro-*L*-proline and *trans*-4-[^{18}F]fluoro-*L*-proline uptake from 1 to 18 months and EF in aged animals (Table 4.5). These findings suggest that collagen synthesis, whether hydroxylated or unhydroxylated, does not significantly impact ejection fraction outcomes with aging in either atrial region.

Table 4. 4 Longitudinal correlation analysis of collagen synthesis and cardiac functional outcomes in the LA. *cis*-4-[^{18}F]fluoro-*L*-proline and *trans*-4-[^{18}F]fluoro-*L*-proline uptake was compared with EF measures over 18 months in the RA

Radiotracer	Outcome Measure	Months				
		1	3	6	12	18
***cis*-[^{18}F]-Pro**	**R Squared**	0.02225	0.001741	0.002700	0.01999	0.2396
	P Value	0.6267	0.8923	0.8661	0.6450	0.0896
***trans*-[^{18}F]-Pro**	**R Squared**	0.007096	0.08544	0.09083	0.07389	0.09295
	P Value	0.7946	0.3566	0.3170	0.3690	0.3111

Table 4. 5 Longitudinal correlation analysis of collagen synthesis and cardiac functional outcomes in the RA. *cis*-4-[^{18}F]fluoro-*L*-proline and *trans*-4-[^{18}F]fluoro-*L*-proline uptake was compared with ejection fraction measures over 18 months in the RA.

Radiotracer	Outcome Measure	Months				
		1	3	6	12	18
***cis*-[^{18}F]-Pro**	**R Squared**	0.0003668	0.01475	0.001460	0.02299	0.05241
	P Value	0.9505	0.6927	0.9014	0.6210	0.4518
***trans*-[^{18}F]-Pro**	**R Squared**	0.05100	0.09111	0.2718	0.09627	0.09767
	P Value	0.4803	0.3403	0.0677	0.3022	0.2985

Atrial collagen synthesis outcomes were evaluated for correlations with collagen deposition and cardiac function over an 18-month period. In males, a significant negative correlation was observed between *trans*-4-[^{18}F]fluoro-*L*-proline uptake and PSR histological analysis of collagen deposition (Figure 4.26 A). This suggests an inverse relationship between *trans*-4-[^{18}F]fluoro-*L*-proline uptake and collagen deposition. No other significant correlations were identified between collagen synthesis and deposition, indicating that these processes operate independently of each other. In females, no significant correlations were found among collagen synthesis and degradation parameters (Figure 4.26 B). Upon examining the relationship between atrial collagen synthesis outcomes and cardiac functions, several significant correlations were noted. Both males and females showed a significant negative correlation between *trans*-4-[^{18}F]fluoro-*L*-proline uptake over 18 months and frailty measurements, indicating that higher uptake is associated with lower frailty. This suggests that PET imaging of *trans*-4-[^{18}F]fluoro-*L*-proline uptake may not reliably reflect frailty levels (Figure 4.27). Additionally, in females, a significant positive correlation was identified between atrial *cis*-4-[^{18}F]fluoro-*L*-proline uptake and diastolic blood pressure, highlighting a potential link between collagen synthesis and blood pressure regulation in this sex.

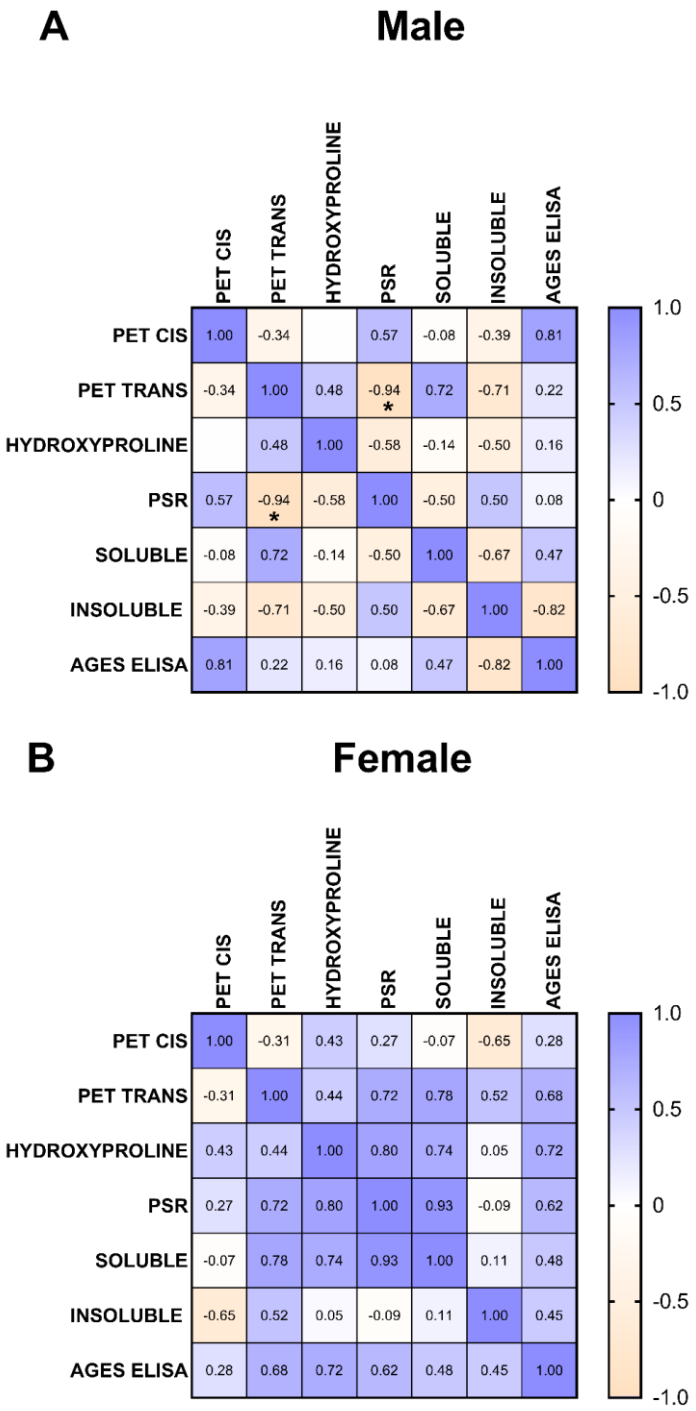

Figure 4. 26 Correlation analysis of atrial collagen synthesis and deposition outcomes. Correlation analysis was carried out comparing longitudinal collagen synthesis outcomes and longitudinal collagen deposition outcomes in males (A) and females (B) Correlation matrix analysis was performed using Pearson correlation to assess the relationships between various parameters. Statistical significance was determined Pearson rank correlation analysis. Significance levels are indicated as follows: *p<0.05;

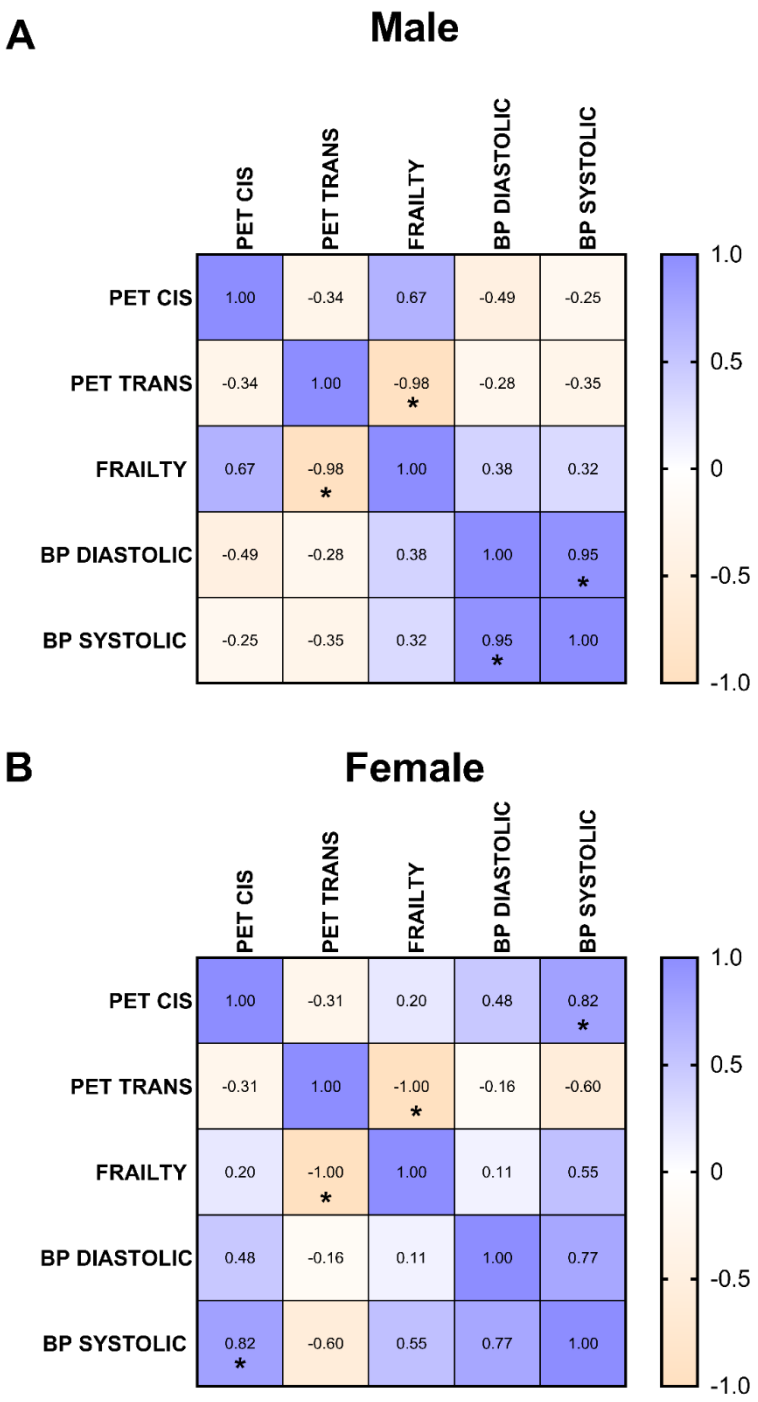

Figure 4. 27 Correlation analysis of atrial collagen synthesis and functional outcomes. Correlation analysis was carried out comparing longitudinal collagen synthesis outcomes and longitudinal cardiac functional outcomes in males (A) and females (B) Correlation matrix analysis was performed using Pearson correlation to assess the relationships between various parameters. Statistical significance was determined Pearson rank correlation analysis. Significance levels are indicated as follows *p<0.05;

4.3.13 No meaningful atrial clustering between PET outcomes and collagen deposition

Hierarchical clustering was conducted to determine whether distinct clusters based on age, sex, or collagen metabolism outcomes were identifiable in the atria. Within the atria, when comparing collagen synthesis and deposition metrics, no visible clustering by sex was observed, indicating that sex is not a significant determinant of collagen metabolism in this study (Figure 4.28). Interestingly, two main clusters emerged, with 18-month-old males forming a distinct, isolated cluster from the other groups. In contrast to the ventricles, the clustering of the tracers in the atria was distinct. Atrial cis-4-[18F]fluoro-L-proline uptake was closely associated with AGEs ELISA outcomes, whereas trans-4-[18F]fluoro-L-proline uptake was closely associated with insoluble collagen outcomes. This suggests that the atria exhibit a less clear association between collagen synthesis and deposition outcomes compared to the ventricles. These findings highlight age-related differences in collagen metabolism within the atria, particularly in older males, and suggest that the relationship between collagen synthesis and deposition in the atria is complex and distinct from that in the ventricles. Further research is needed to elucidate the mechanisms underlying these associations and their implications for atrial tissue integrity and function.

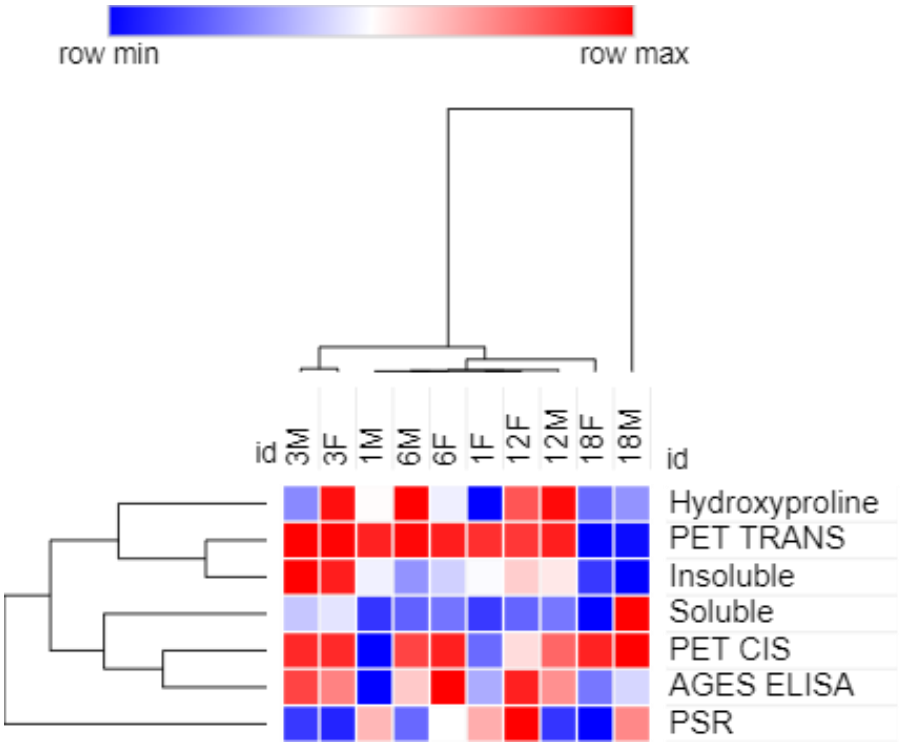

Figure 4. 28 Hierarchical clustering analysis of collagen synthesis and deposition in the atria. Hierarchical clustering using Morpheus was performed to compare collagen synthesis and deposition across different time points and sexes. The heatmap shows clustering patterns in male and female subjects at 1 month (1M, 1F), 3 months (3M, 3F), 6 months (6M, 6F), 12 months (12M, 12F), and 18 months (18M, 18F). The dendrogram indicates the relationships among groups, highlighting similarities and differences in collagen metabolism over time.

Similarly, hierarchical clustering comparing PET outcomes with functional measures was conducted. Distinct clustering by age was observed, with 18-month-old males and females, as well as 12-month-old males and females, forming separate clusters (Figure 4.29). Similar to the findings in the ventricles, collagen synthesis outcomes and cardiac function outcomes clustered independently, suggesting no significant association between these two processes.

These results reinforce the observation that age is a significant determinant in clustering patterns related to collagen metabolism and cardiac function. Additionally, the independent clustering of collagen synthesis and cardiac function outcomes suggests that these processes operate separately in both the atria and the ventricles. This indicates a complex and multifaceted relationship between collagen metabolism and cardiac function that warrants further investigation to fully understand their interactions and implications for cardiac health.

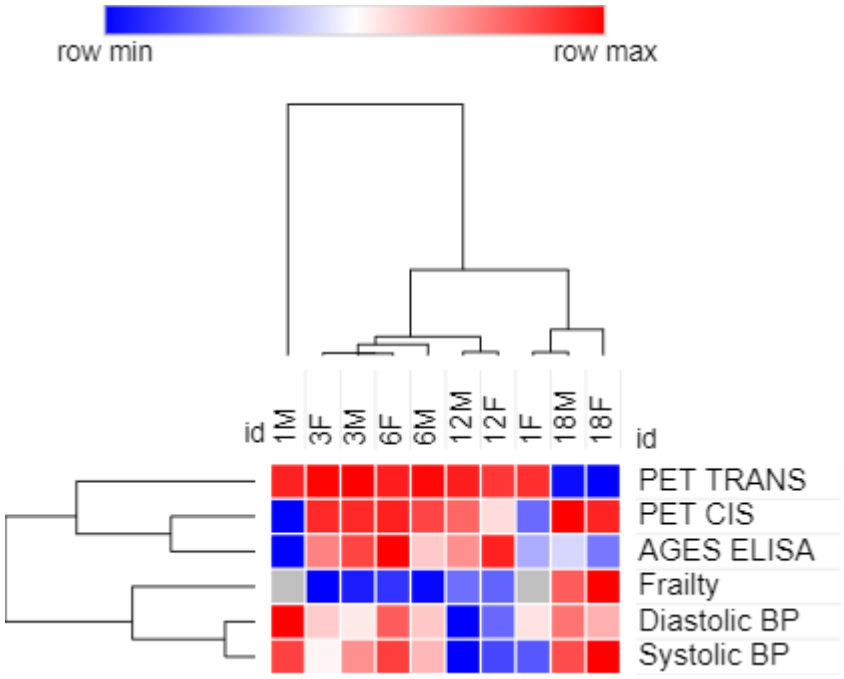

Figure 4. 29 Hierarchical clustering analysis of collagen synthesis and cardiac function in the atria. Hierarchical clustering using Morpheus was performed to compare collagen synthesis and cardiac function across different time points and sexes. The heatmap shows clustering patterns in male and female subjects at 1 month (1M, 1F), 3 months (3M, 3F), 6 months (6M, 6F), 12 months (12M, 12F), and 18 months (18M, 18F). The dendrogram indicates the relationships among groups, highlighting similarities and differences in collagen metabolism over time.

4.4 Discussion

This chapter explored the impact of aging and sex on atrial collagen metabolism, with a focus on collagen synthesis and deposition in the LA and RA over 18 months. Building on the previous chapter's work on ventricular collagen, this study applied similar methodologies to the atria, using both *cis*-4-[^{18}F]fluoro-*L*-proline and *trans*-4-[^{18}F]fluoro-*L*-proline radiotracers to quantify *in vivo* collagen synthesis, allowing differentiation between unhydroxylated (*cis*-) and hydroxylated (*trans*-) collagen forms. Notably, both *cis* and *trans* tracers revealed consistent patterns across age and sex, suggesting that the primary drivers of collagen turnover may be similar regardless of hydroxylation status, an insight which could simplify future tracer selection.

The findings addressed three main hypotheses. First, it was hypothesized that atrial collagen synthesis would decline with age. Consistent with this hypothesis, both *cis* and *trans* tracers indicated an age-related decrease in synthesis. Second, it was hypothesized that male rats would exhibit a higher rate of atrial collagen synthesis than female rats examining the idea that sex-based differences influence collagen metabolism. Third, an increase in atrial collagen accumulation with age, especially in male rats, was hypothesized.

In addition to confirming these hypotheses, this study provided a comparative view of *cis- and trans*-4-[^{18}F]fluoro-*L*-proline tracer behaviours, which may offer insights into the specific contributions of unhydroxylated and hydroxylated collagen forms in the aging atria. Overall, these findings further support a model where age- and sex-driven changes in collagen metabolism contribute to atrial fibrosis distinct from ventricular fibrosis, with potential implications for understanding sex differences in age-related cardiac function and fibrotic remodelling (see Figure 4.4.1 for a summary of key findings).

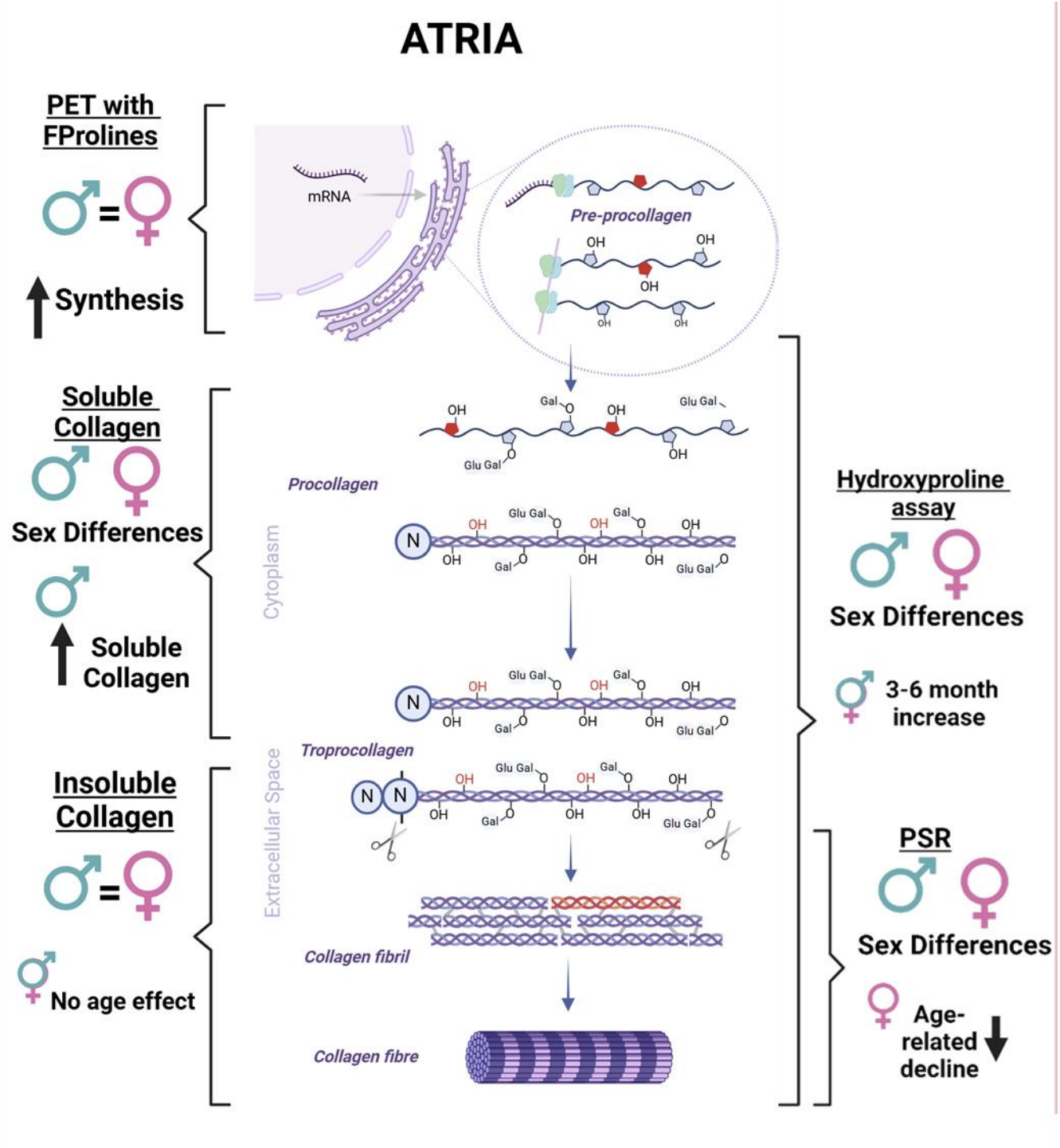

Figure 4.4.1. Summary of findings regarding atrial collagen metabolism in this study. Key changes in the Atria collagen metabolism comprising od collagen synthesis and collagen accumulation outcomes. Abbreviations: PSR – Picrosirius Red staining; AGES- Advanced Glycation End Products Crosslinking. Figure created using Biorender.

4.4.1 No sex differences in atrial collagen synthesis

This study evaluated the effect of sex on collagen synthesis and deposition over 18 months in Sprague Dawley rats. Consistent with the findings reported in Chapter 3, no significant differences were observed in the synthesis of hydroxylated and unhydroxylated collagen in both the LA and RA, with males and females remaining comparable throughout the study period. The scarcity of studies examining collagen synthesis in the atria during healthy aging makes it challenging to contextualize these findings. To our knowledge, no studies have specifically addressed the effect of sex on atrial collagen synthesis during healthy aging.

Most existing research on sex differences in the atria has primarily focused on remodelling in the context of dysfunction, particularly AFib. Studies investigating the impact of sex on AFib development have noted increased atrial remodelling in females (279). One study identified sex-specific differences in gene expression in patients with AFib, revealing an upregulation of eight genes in females, including TGF-β2, SMAD3, COL1A2, COL1A3, and PARP1, suggesting that collagen synthesis in atrial dysfunction is influenced by sex, similar to what is observed in the ventricles (279). However, there is a significant gap in research directly exploring these effects in humans, leaving this area largely unexplored. Given the strong association between aging in females, AFib, and atrial fibrosis, further research in this domain is clearly needed (280).

Future studies should prioritize longitudinal analyses of collagen synthesis in the atria across a broader age range, particularly in humans, to better understand the interplay between sex and aging in the development of atrial fibrosis. Unlike the ventricles, where the effect of sex on specific collagen subtypes is better understood, knowledge regarding these differences in the atria is limited. This gap may contribute to differences in age-related atrial dysfunction. Additionally, research exploring the molecular pathways regulating collagen synthesis in both males and females could provide valuable insights into sex-specific therapeutic targets for the prevention of AFib.

4.4.2 Atrial collagen synthesis increases with age

This study identified a significant increase in collagen synthesis in the atria over 18 months in Sprague Dawley rats. This observation contrasts with previous reports in the literature, which have generally

described a decline in atrial collagen synthesis with age. For instance, in Wistar rats, Northern blot analysis revealed a fivefold decline in atrial collagen type III mRNA between 10 and 40 weeks of age(281). Conversely, another study found a threefold increase in atrial collagen III mRNA in SHR over 40 weeks, suggesting a distinct pattern from injury-related fibrosis. This finding aligns with the differences between age-related fibrosis and injury-induced fibrosis discussed in the previous chapter. However, other studies suggest that collagen I and III mRNA expression remain unchanged in the LA and RA of aged (101 weeks old) C57BL/6 mice compared to younger counterparts. Similarly, no effect of age or frailty was observed on the expression of TGFβ, a profibrotic gene (17).

Based on the limited available murine studies, our findings challenge the current understanding of the effect of age on atrial collagen synthesis, as we observed a significant increase in collagen synthesis in both atria. Several potential factors may explain this discrepancy, including strain and species differences, which were discussed in the previous chapter. Additionally, the increase may be influenced by the analysis methodology. Despite applying stringent criteria, there remains a possibility of contamination from blood pools or non-atrial tissue. This issue is partly due to the lack of cardiac gating during imaging, which was necessitated by low tracer uptake but led to increased cardiac motion. The decision to use an *ex vivo* cardiac template for analysis was driven by the low resolution of our CT images, as contrast agents were not utilized due to their renal toxicity and the risks associated with repeated exposure in a longitudinal study (282). Consequently, contamination from non-atrial tissues may have influenced our outcomes. However, stringent criteria were consistently applied during image analysis, with the same individual performing template placements, reducing the margin of error. The low variability observed in our data suggests that the results are robust, but these limitations should be considered when interpreting the findings.

Interestingly, within the ECM, collagen synthesis is not the only atria-specific ECM protein increase observed. Fibronectin synthesis also increased in the atria compared to the ventricles, indicating a potential broader pattern of age-related changes in ECM protein synthesis (283). However, this study also identified a decline in fibronectin mRNA with aging between 10 and 40 weeks in Wistar rats (281). These findings suggest that while certain ECM components may increase with age, the overall regulation of ECM protein synthesis is complex and may involve compensatory mechanisms or differential regulation at the mRNA level. This complexity underscores the need for further investigation into the interplay between various ECM proteins in the aging atria.

This PhD project found no significant correlations between RA and LA collagen synthesis outcome measures and either age-related EF or frailty. Previous studies have reported similar findings, with no

significant correlation between atrial collagen synthesis and frailty index outcomes (17). These results further suggest that collagen synthesis alone may not be sufficient to predict aging-related changes in cardiac function.

4.4.3 Atrial collagen deposition does not show clear age-associated accumulation

This study assessed collagen deposition and accumulation in the atria over 18 months in male and female Sprague Dawley rats. The findings revealed that, unlike in the ventricles, total collagen deposition in the atria did not show the same pattern of accumulation. Males exhibited stable levels of total deposited collagen, while females showed a decline at 18 months compared to baseline measurements. Notably, some sex differences in atrial hydroxyproline content were identified, with females displaying higher hydroxyproline levels in early adulthood compared to males; however, this difference was lost in later adulthood. Age-related changes in hydroxyproline content were also observed, with a peak at 6 months followed by a return to baseline at 18 months in males, and a similar pattern in females, though their peak occurred at 3 months.

Interestingly, previous studies have reported a consistent increase in atrial collagen content and fibrils with advanced aging (75, 174, 284). For example, in aged canines (9 years old), a significant increase in collagen fibre ratio (%) was observed in the LA compared to adult canines (4 years old). This increase was further exacerbated by atrial pacing-induced AFib in aged canines, highlighting an increased vulnerability to AFib development due to the observed remodelling (75). It is important to note that this study did not assess the effect of aging on RA collagen content, likely due to the predominant impact of AFib on the LA, and no change in LA or RA diameter was observed (75). Similarly, increased collagen volume fraction with age has been documented in male Kumming mice in both the LA and RA, with a greater level of fibrosis observed in the RA of 24-month-old mice compared to 2-month-old counterparts (284). This has also been illustrated in C57BL/6 male mice, where an increase in hydroxyproline content was identified in aged mice in both the RA and LA (17).

Our study did not observe this unidirectional accumulation of collagen in the atria, which could be partly due to the methodology employed, where the LA and RA were combined for analysis. This approach may have reduced the ability to detect region-specific differences in collagen deposition, as averaging values from both atria could obscure localized fibrosis. In cases where fibrosis is more pronounced in one atrial chamber than the other, combining the data can result in average values that fail to accurately reflect the extent or pattern of collagen accumulation in each region. This suggests the need for more granular, chamber-specific analyses in future studies. It is also unclear

whether the LA and RA accumulation observed in mice and canines is species-specific (75, 284). This discrepancy may stem from the fact that, as the atria age, they contribute more to ventricular filling compared to younger hearts, a change linked to age-related remodelling of cardiac tissue composition (53). However, it remains challenging to fully understand the potential causes of these reported changes due to the scarcity of research on atrial collagen metabolism in healthy aging.

A study examining the relationship between aging and hypertension found that Wistar-Kyoto (WKY) rats did not exhibit age-related collagen accumulation, with a non-significant decline observed instead (285). This suggests that rats may experience different effects of aging on atrial collagen metabolism, as discussed in the previous chapter. However, the extracellular matrix (ECM) is highly conserved across species, implying that similar patterns of collagen deposition in the atria may occur in Sprague Dawley rats, though with low sample numbers, these patterns might not be clearly discernible in this analysis (286).

In humans, atrial tissue collected during open-heart surgery revealed a 5.5% increase in collagen deposition from patients younger than 50 years to those older than 70, suggesting that the aged human atria may follow a similar fibrosis mechanism to those observed in murine and canine models (271). However, this study likely reflects injury-related remodelling, despite strict inclusion criteria (e.g., lack of atrial fibrillation, malignancies, chronic inflammatory diseases, or acute infections). Given that patients were undergoing open-heart surgery, some degree of cardiac dysfunction was likely present (271). Collectively, these findings suggest that while we have some understanding of atrial aging, however, our study identified no clear increase in atrial collagen deposition.

Our study did not identify pronounced sex differences in atrial collagen in Sprague Dawley rats. Preclinical research on atrial collagen deposition in both sexes is limited, as is the case in humans, where understanding of healthy atrial aging is constrained by the low availability of control tissue. A study investigating atrial remodelling and hypertrophic obstructive cardiomyopathy found no significant differences in collagen volume fraction in the LA between control males and females. However, this control tissue was only middle-aged (45 years), and therefore may not provide insights into sex differences in advanced age-related atrial remodelling (287). Interestingly, females with hypertrophic obstructive cardiomyopathy were found to have worse LA function due to increased susceptibility to atrial fibrosis (287). This increased atrial stiffness in females has also been observed in heart failure (287). These findings suggest that sex differences in aging may contribute to the disparities seen in atrial dysfunction, particularly as they become more pronounced with age. However, the study would have benefited from a larger sample size, as detecting these differences can be

challenging, and the limited availability of truly representative control tissue hinders our understanding of how these processes evolve, especially in advanced atrial aging.

4.4.4 Collagen turnover appears increased in atrial aging

In contrast to the ventricles, this study did not identify a clear dysregulation between collagen synthesis and deposition in the atria. Analysis of soluble and insoluble collagen fractions revealed no significant effect of age on insoluble collagen levels; however, an age-related increase in soluble collagen content was observed in aged males. Since soluble collagen reflects both newly synthesized and newly degraded collagen, and given that PET outcomes identified increased collagen synthesis, this finding suggests a potential rise in collagen turnover in the aging atria, particularly in males (288). Increased collagen turnover is considered a secondary fibrotic mechanism, associated with the dynamic turnover of deposited collagen (289). This phenomenon has been documented in conditions such as ventricular volume overload, indicating ongoing cardiac remodelling and early signs of potential atrial injury (290). Similar findings have been observed in canine studies subjected to RV pacing-induced heart failure, where increased collagen synthesis (measured using ^{14}C-proline) and increased collagen degradation (assessed through zymography) were noted in both atrial chambers (289). These observations suggest that aging in the atria leads to increased collagen turnover, which may reflect heightened structural remodelling and potential early signs of atrial dysfunction.

However, this finding contrasts with the prevailing understanding of aging's impact on collagen metabolism in the atria, where most studies report an increase in atrial collagen accumulation accompanied by a decline in collagen synthesis (174). For instance, a dissociation between collagen synthesis (observed through mRNA analysis) and collagen protein expression was identified in the atria of 40-week-old Wistar rats (281). Further studies have explored collagen degradation despite unchanged collagen synthesis and increased collagen deposition in the atria (17). One study, for example, found that MMP-2 expression remained unchanged in the RA but was reduced in the LA, while MMP-9 expression increased in the RA but was unchanged in the LA. Additionally, specific changes in TIMP expression were identified in both the LA and RA, linking excessive collagen deposition to these alterations (17). Similar findings have been observed in the sinoatrial node during aging, suggesting that these processes are conserved across different regions of the atria (291). These results highlight the complexity of collagen turnover in the atria and suggest that age-related remodelling may vary depending on specific atrial regions and underlying mechanisms.

While our study suggests one potential mechanism of aging-related changes in atrial collagen, canine and murine studies indicate another, leaving it unclear which model would be most applicable to humans. Therefore, further research is needed in both humans and preclinical models, with higher-powered analyses, to clarify these mechanisms given the often-subtle nature of age-related changes. Additionally, our study would have greatly benefited from assessing collagen degradation markers such as MMP and TIMP expression in the atria to fully understand whether atrial collagen degradation is altered during aging in Sprague Dawley rats.

4.4.5 Atrial laterality impact collagen metabolism in aging

This study is the first to assess collagen synthesis within each atrial chamber individually. However, a similar pattern of both hydroxylated and unhydroxylated collagen synthesis during aging was observed in both the LA and RA. Due to limited tissue availability, given the small proportion of the heart that comprises the atria, we were unable to assess the effects of aging on the LA and RA individually *ex vivo*. This limitation poses challenges in directly comparing PET imaging outcomes, which allowed for region-specific analysis. To address the absence of LA/RA separation, we averaged the data from both sides to assess overall atrial collagen synthesis. However, the study would have greatly benefited from conducting *ex vivo* analysis on each chamber individually.

Nevertheless, it is crucial to conduct research on atrial laterality, particularly in the context of aging and dysfunction. Limited studies on aging-related atrial dysfunction have indicated that atrial laterality plays a significant role in disease progression or functional decline. For instance, echocardiographic analysis of the atria in aged humans identified LA-specific dilation, specifically citing the deterioration of the left atrium's ability to passively conduct blood from the pulmonary veins into the left ventricle during diastole (292). Interestingly, this dilation was observed in both sexes, suggesting that left atrial function declines in both males and females with aging (292). The same study noted that altered LA performance can contribute to atrial fibrosis and subsequent heart failure due to increased LA pressure. This implies that collagen metabolism could be altered under these conditions and should be further investigated to understand its role in age-related atrial changes. In conclusion, the potential impact of atrial laterality on collagen metabolism and overall atrial function underscores the need for more detailed, region-specific studies to better understand the differential aging processes in the LA and RA.

4.4.6 Conclusion

This thesis chapter examined the effects of age and sex on atrial collagen metabolism by employing both *in vivo* PET imaging and *ex vivo* analysis of collagen deposition in Sprague Dawley rats. For the first time, our study identified an increase in collagen synthesis in both atria over 18 months, with no significant impact of sex on this phenomenon. These findings contradict our initial hypothesis that the rate of atrial collagen synthesis would decline with age in rats, instead revealing the opposite trend. Furthermore, our second hypothesis, which proposed the presence of sex differences in atrial collagen synthesis, was also disproved.

Interestingly, while our study did not demonstrate a clear age-related accumulation of collagen deposition in the atria over 18 months, we observed peak collagen deposition at 6 months in males and 3 months in females. Notably, we detected an age-related increase in soluble collagen specifically in males, which, combined with the findings on collagen synthesis, suggests enhanced collagen turnover in the aging atria. This indicates a remodelling process distinct from simple collagen accumulation. Consequently, our final hypothesis, which posited an increase in atrial collagen accumulation with age, particularly in males, was also refuted. Although some outcomes hinted at male-specific increases in collagen deposition, the evidence for sex differences remains inconclusive.

Our findings suggest an alternative mechanism of age-related atrial remodelling, indicated by stable collagen synthesis rates without evidence of accumulation, which may point to increased collagen turnover, although we have not directly assessed collagen degradation. However, due to the limited availability of comparative data, particularly concerning sex differences, it is challenging to contextualize these results fully. Species differences, as discussed in the previous chapter, may also play a role, with less adverse remodelling observed in this model compared to current understanding in murine and canine studies. Nonetheless, this study provides valuable insights into non-invasive assessment of collagen synthesis in humans, offering a potential avenue for exploring age- and sex-related effects *in vivo*, which circumvents the difficulties associated with obtaining 'control' human tissue.

There are limitations to our study, particularly related to the image analysis methodology, which may have impacted the *in vivo* findings. Despite the challenges posed by the lack of cardiac gating and contrast agents, we believe we employed the most conservative and appropriate analytical methods. Additionally, the study would have benefited from larger sample sizes for *ex vivo* analysis, given the

observed variations and the subtle differences that may occur in aging and sex in the absence of overt dysfunction.

Chapter 5 – *The Impact of Age and Sex on Cardiac fibroblast Collagen Metabolism*

5.1 Introduction

cFbs are the primary cell type responsible for collagen metabolism and have been implicated in adverse remodelling in aging and cardiac dysfunction (18). This has been described in detail in the introduction - Chapter 1.3.2. cFbs have two main phenotypes: resident/inactivated and myofibroblasts/activated fibroblast, each have vital roles in tissue integrity maintenance and injury response respectively (27, 28). Therefore, cFbs are one of the main targets for understanding age-related fibrosis. Sex has been shown to influence cardiac fibroblast mediated remodelling in injury, with female cFbs found to have oestrogen mediated dampening of remodelling (40). Therefore, we aimed to explore the effect of sex and age on cFbs collagen synthesis and deposition.

This fifth chapter will examine how cellular sex and age at explantation affect cFbs, with a specific focus on collagen synthesis and deposition. We will investigate how age and sex influence these processes at a cellular level, including the effects of inhibiting collagen crosslinking. Given the critical role of cFbs in collagen homeostasis, understanding these influences will shed light on potential sex- and age-related variations in collagen metabolism. *In vitro* studies have previously highlighted the impact of cFbs aging in the form of cellular senescence, with strong links identified between senescence in cFbs and fibrosis, primarily through elevated TGF-β expression—a factor associated with inducing cFb senescence (293). This relationship has been further examined by assessing senescence-associated secretory phenotype (SASP) expression, which is known to promote tissue remodelling and fibrosis (294). Despite the critical role of cFbs in collagen metabolism, research on aged cFbs and their physiological changes, particularly in collagen synthesis, remains limited.

Our study seeks to explore aging *in vitro*, not by relying on multiple-passage-induced senescence—a commonly used but limited model—but by culturing cFbs derived from naturally aged rats. Unlike stress-induced senescence models, which may not accurately replicate the gradual cellular and metabolic changes of natural aging, culturing chronologically aged cFbs may better capture the authentic aging phenotype (295). Addressing this gap is essential, as a more accurate model of fibroblast aging can provide critical insights into collagen homeostasis and fibrosis mechanisms, leading to more effective age-specific therapeutic targets for cardiac health.

Additionally, little has been established on whether aging promotes reactive or replacement fibrosis, a question that will be addressed in this chapter using both *cis*- and *trans*-4-[^{18}F]fluoro-*L*-proline PET radiotracers. By exploring these aspects, we aim to gain insight into age- and sex-specific shifts in collagen metabolism at the cellular level, advancing the understanding of fibrosis and collagen homeostasis in aging.

In chapter 3, it was observed that aging caused a significant increase in ECM crosslinking in the LV of males, specifically in AGEs. Therefore, this chapter not only set out to assess the impact of cellular sex and age on collagen crosslinking but also explore the impact of inhibiting the formation of AGEs on collagen synthesis and collagen deposition. Previously studies have identified, that in the LV reducing collagen crosslinking can lead to decreased collagen synthesis with a reduction in collagen type I and III mRNA observed (63). However, other papers have suggested the inverse that inhibition of collagen crosslinking causes an increase in collagen synthesis to compensate for the reduction crosslinking (296). Therefore, this chapter aimed to understand whether inhibition of AGEs formation would alter collagen synthesis using both *cis*-4-[^{18}F]fluoro-*L*-proline and *trans*-4-[^{18}F]fluoro-*L*-proline *in vitro*.

Hypotheses:

- Age-related dysregulation of collagen metabolism will be observed in cardiac fibroblasts *in vitro*, with older cells displaying a disconnect between collagen synthesis and deposition.
- Age-related changes in collagen metabolism will be more pronounced in male versus female cardiac fibroblasts, revealing sex-specific differences.
- ALT711 will reduce collagen synthesis and deposition *in vitro*

The objectives of this study are to: 1) investigate how collagen synthesis by cardiac fibroblasts is influenced by age and sex at explanation *in vitro*; 2) evaluate the impact of age and sex at explanation on collagen accumulation in cardiac fibroblasts cultures *in vitro* and 3) assess the effects of the AGEs inhibitor ALT711 on collagen synthesis and deposition *in vitro*, with a focus on age- and sex-specific differences.

5.2 Materials & methods

5.2.1 Animal care and experimental handling

All *in vivo* experiments were carried out in accordance with the Home Office Animals (Scientific Procedures) Act 1986 and experimental plans were approved by the University of Edinburgh animal welfare and ethical review committee. All *in vivo* data is reporter according to the ARRIVE recommended criteria (182). Animals used for study were 3 weeks old Sprague-Dawley rats (Charles River, Tranent) and were given 1 week to acclimatise. 18-month animals were aged in house and monitored bi-weekly till ready for cell extraction. Animals were housed under standard conditions with a 12 h light: 12h dark cycle (7am – 7pm lights) at 22±2◦C and 55% humidity. Rats were fed a standard chow diet and water available ad libitum. It should be noted due to the increased prevalence of foot pressure sores as a result of sedentary behaviour from 12 months animals were exercised for 15 mins, twice a week for the remainder of the study.

5.2.2 Rat cardiac fibroblast isolation and maintenance

Primary rat cardiac fibroblast cell culture methodology was developed and optimised based on previously established methods (297-299). Animals were culled using an overdose of anaesthetic and following shaving of fur and sterilising with ethanol, hearts were dissected and placed in warmed DMEM/F-12 (Thermo Fisher, US). Following dissection, pericardium and atria are removed using sterile tool and ventricles were weighed. Cardiac tissue was manually dissociated into 1-2 mm^2 placed in the Miltenyi C tube (Miltenyi Biotec, Germany). Tissue was then digested using the enzyme mix from Multi Tissue Dissociation Kit 2 (Miltenyi Biotec, Germany). Tissue was incubated for 15 minutes at 37◦C and the further dissociated using the gentleMACS Dissociator (Miltenyi Biotec, Germany), these steps were repeated twice further. Sample was then resuspended in DMEM/F-12 with 20% FBS (Thermo Fisher, US) and filtered using a 70 µm strainer (Miltenyi Biotec, Germany). Cell suspension was then centrifuged at 600×g for 5 minutes and supernatant was discarded and pellet was resuspended in DMEM/10% FBS/ 1% Penstrep (Thermo Fisher, US). The single cell suspension was then placed onto a poly-L-lysine (Sigma-Aldrich, US) coated T25 flask and incubated for 2 hours. Following incubation, single-cell suspension is removed and fibroblasts are adhered to the coated flask. Note that aged female cells were cultured but experiments were not completed due to widespread contamination in the cell culture facility leading to loss of cells.

5.2.3 Immunocytochemistry

Cells were seeded onto poly-L-lysine coated glass coverslips in a 24 well plate. Once cells reached 70-80% confluence they were fixed using 4% PFA (Sigma-Aldrich, US) for 5 mins and then stored at 4◦C in PBS (Thermo Fisher, US)– to ensure cells did not dry out. At time of staining cells were washed twice in PBS for 5 minutes on a shaker and then permeabilised for 15 minutes using 0.1% TritonX 100 (Scientific Lab Supplies, UK). Following permeabilization, cells were washed twice in PBS for 5 minutes on a shaker and placed in the relevant blocking agent (see Table 5.1 for specific conditions used). Coverslips were placed on a droplet of primary antibody overnight at 4◦C, with no primary applied to the negative control. The following day, coverslips were washed and then secondary antibody (1:500) was applied for 1hr at RT in the dark. DAPI was used to stain for nuclei in the cells (1:1000 in PBS; 5 minutes; RT) (Thermo Fisher, US). Coverslips were washed and then mounted onto slides using permaflour mounting liquid (Fisher Scientific, UK) and left to dry. Coverslips were imaged using the slide scanner, acquired images were resized to 20% of original size and converted to a TIFF filed. Following stain intensity was analysed for each marker using ImageJ (Fiji version, ImageJ, US). Regions of interest (ROIs) were drawn around coverslips, disregarding any artefacts. Intensity was then measured and analysed for each stain.

Table 5. 1 Antibodies for specific cardiac cell types.

Marker	Antibody tested	Blocking	Primary Dilutions
Vimentin	Anti-vimentin (Ab8979;Abcam)	10% Donkey Serum (1 hour)	1:100
CD45	Anti-CD45 (Ab33923;Abcam)	10% Donkey Serum (1 hour)	1:250
αSMA	Anti-Actin (C6198.2ML; Scientific laboratory supplies)	10% Goat Serum (1 hour)	1:1000
PDGFRα	Anti-PDGFRα (PA5-16571; Invitrogen)	10% Donkey Serum (1 hour)	2µg/ml

RECA-1	Anti-RECA1 (MA140240; ThermoFisher)	1% Hydrogen peroxide (15 mins) & 10% Donkey Serum (1 hour)	1:50

5.2.4 Radiosynthesis of *cis*- and *trans*-4-[^{18}F]fluoro-*L*-proline

Radiosynthesis methodology are as describe Chapter 3 Section 2.2.

5.2.5 *cis*-4-[^{18}F]fluoro-*L*-proline and *trans*-4-[^{18}F]fluoro-*L*-proline cell incubation assay

cFbs were seeded at 250,000 cells and maintained using in DMEM/10% FBS/1% Penstrep/100µm Ascorbic Acid (Sigma-Aldrich, Spain). Optimisation was run by incubating cells for 0, 15, 30, 60, 90 or 120 min with *cis*-4-[^{18}F]fluoro-*L*-proline and *trans*-4-[^{18}F]fluoro-*L*-proline and uptake was measured. After the radiotracer incubation, the supernatant was collected and cells were washed using PBS, twice – each wash was collected. Following washes, cells were lysed using RIPA Lysis Buffer System with protease inhibitor (Santa Cruz Biotechnology, USA) for 1 min and manually dislodged using a cell scraper. Following aliquoting of supernatant, washes and cell suspension were placed in the gamma counter (Wizzard2, PerkinElmer, USA) and the activity of each sample was measured and optimal incubation time was determined to be 90 mins. Following optimisation, cells were cultured in 12.5 mM glucose medium and treatment occurred when cells reached 80-90% confluence at which time cells were supplemented with either a vehicle (PBS) or 100 mM of ALT711 (Cambridge Bioscience, UK) in DMEM-F-12/10%FBS/1%Penstrep. Cells were incubated with drug or control medium for 7 days. Following treatment, cells were washed and 1 ml of *cis*-4-[^{18}F]fluoro-*L*-proline and *trans*-4-[^{18}F]fluoro-*L*-proline (5 MBq/ml) in PBS was administered and left to incubate for 90 min (at 37°C, 5% CO_2, 100% humidity). The data was analyzed by converting the F-18 disintegrations per minutes into kilo Becquerel (kBq) per ml. Then the percentage of activity present in each sample was calculated from total activity in the supernatant, wash 1, wash 2 and cells. Lysed cells were spun at 13,000g for 20 min at 4°C and supernatant was collected and kept on ice. Protein analysis was carried out using 4 µl of lysed cells placed into 800 µl of tris buffer (Sigma-Aldrich, Germany) pH 7.4 with 200 µl of optical density of 595nm was then measured with a microplate reader (Optimax, UK). Percentage of cell radiotracer uptake was normalized by total protein.

5.2.6 Protein assay

Following incubation assays protein from cells was frozen at -80◦C until commencement of assay. On the day of assay samples were defrosted on ice, once defrosted samples were spun at 13,200g at 4◦C for 10 min. The supernatant was collected and kept on ice till the beginning of the assay. Standards were set up by adding 21.5µl of BSA standard (Bio-Rad Laboratories, USA) in 1600µl of 50mM Tris Buffer, pH 7.4 (Sigma-Aldrich, USA) and then serial diluted 4 times and blank with Tris Buffer only. Optimisation of sample volume was carried and an optimal sample volume of 4 µl was identified. Therefore, 4 µl of samples was added to 800 µl of tris buffer and vortexed. Once all samples and standards are prepped, 200 µl of protein assay dye (Bio-Rad Laboratories, USA) was added to each sample and standard, each tube was vortexed and incubated at RT in the dark for 10 min. Following the incubation, 200 µl off each sample and standard were aliquoted in triplicate into a 96 well plate which was then read using a microplate reader using the 595nm filter. Total protein assay was calculated on Microsoft Excel and was based on the standard curve generated by plotting the average of each duplicated standard minus the background (calculated from the blank). The background was subtracted from the samples and then valued were averaged a best-fit linear trend line was calculated and the equation was used to calculate the total protein concentration in each sample. To calculate the concentration of protein per well (µg/µl) the identified value was then multiplied 200, to account for dilution occurring during preparation.

5.2.7 Soluble and insoluble colorimetric assay for *in vitro* samples

Total soluble and insoluble collagen was measured using a colorimetric assay from Sircol™ Soluble plus Sircol™ Insoluble Collagen assay kit. Young (4 weeks) and aged (18 months) cells were used, approximately 250,000 cells were seeded per well in a 6 well plate. Cells were treated with either DMEM containing 10% FBS, 100 µM L-ascorbic acid or DMEM containing 10% FBS, 100 µM L-ascorbic acid with 100mM of ALT711/Alagebrium Chloride (Cambridge Bioscience, UK). The following day, DMEM containing 10% FBS, 100 µM L-ascorbic acid was added to each well. On day 12, the spent medium is removed and volumes were recorded. Following removal of medium, cell monolayer was rinsed using PBS to remove any remaining traces of serum. Cells were digested using 0.5 M acetic acid and 0.1 mg/ml pepsin (2.0ml per well) and incubated overnight at 4°C with mechanical shaking. Then the wells were further manually detached using a cell-scrapper and then the cell mixture was centrifuged at 3000 x g for 10 minutes. The supernatant was collected for the soluble collagen assay

and stored at -20°C, until ready for processing. The pellet was collected for the insoluble assay for processing.

Soluble and insoluble were assayed in separate runs due to differences in assay protocol. Soluble samples were defrosted on ice. For the soluble collagen assay, 1.0 ml of the supernatant from each sample was added to a 1.5 ml low protein binding conical microcentrifuge tubes. To each sample 200µl of Isolation and concentration reagent was added and vortex for 5 seconds in thrice. Samples were incubated at 4◦C for 15 minutes and then centrifuged at 13,000g for 10 minutes. Supernatant was discarded and inverted to remove residual fluid and made up to 100µl using DI water. Following sample preparation, 1ml of Sircol Dye (provided in the assay kit) was added to each standard and sample tube to fully saturate the collagen molecules in the volume, tubes were then inverted. Samples were incubated at RT for 30mins on a mechanical shaker at a gentle speed. Tubes were then centrifuged at 13000g for 10 minutes at 4◦C and supernatant was discarded. Samples were then washes with 750µl of acid-salt wash reagent to remove unbound dye from the pellet and tube. Samples were then centrifuged at 13000g for 10 minutes at 4◦C and supernatant was discarded. Finally, 1ml of alkali reagent was added to all standards and samples, which were vortexed and incubated for 5 mins to allow for bound dye to dissolve. In duplicate, standards and samples were placed into a 96 well plate. The plate was read using a microplate reader within 2 hours of assay completion with an absorbance at OD 556nm.

For the insoluble collagen assay, the pellet is taken and placed into a screw capped round bottom 2 ml digestion tube (Supplied in S2000 Assay kit). Then per 1 µl of sample 50 µl of fragmentation reagent was added and the sample was placed onto a heatblock at 65◦C for 2 hours in screw capped round bottom 2 ml digestion tubes. Samples were then centrifuged at 13000g for 10mins at 4◦C. The remainder of the assay was run as described in the previous paragraph.

Total soluble and insoluble content was calculated on Microsoft excel and was based on the standard curve generated by plotting the average of each duplicated standard minus the background (calculated from the blank). The background was subtracted from the samples and then valued were averaged A best-fit linear trend line was calculated and the equation was used to calculate the total amount of hydrolysed hydroxyproline in each sample. To calculate the concentration of soluble and insoluble content in each well (µg/µl) the identified value was then multiplied by a factor of 10 or 2 for soluble and insoluble respectively, to account for dilution occurring during preparation.

5.2.8 Data analysis

Data fitting, statistical analysis and production of graphs were completed using GraphPad Prism version 9 (GraphPad Software Inc., USA). Normality of the data was assessed for each group and paired or unpaired student T tests were used to statistically compare two groups. Values are expressed as min to max range and the threshold for statistical significance is $p<0.05$.

5.3 Results

5.3.1 Cardiac fibroblast culture is Vimentin + PDGFRα+ and heterogeneously αSMA+

cFbs were isolated following established protocols to ensure the purity and viability of the cell population. After isolation, cells from both male and female hearts were imaged at each passage to evaluate their morphological characteristics and verify their identity as cFbs or myofibroblasts. Visual inspection confirmed that the isolated cells exhibited a largely homogeneous population with classical fibroblast morphology. These cells appeared large, flat, and spindle-shaped, with processes extending from the cell body—features consistent with commercially available rat cFbs, as shown in Figure 5.1.

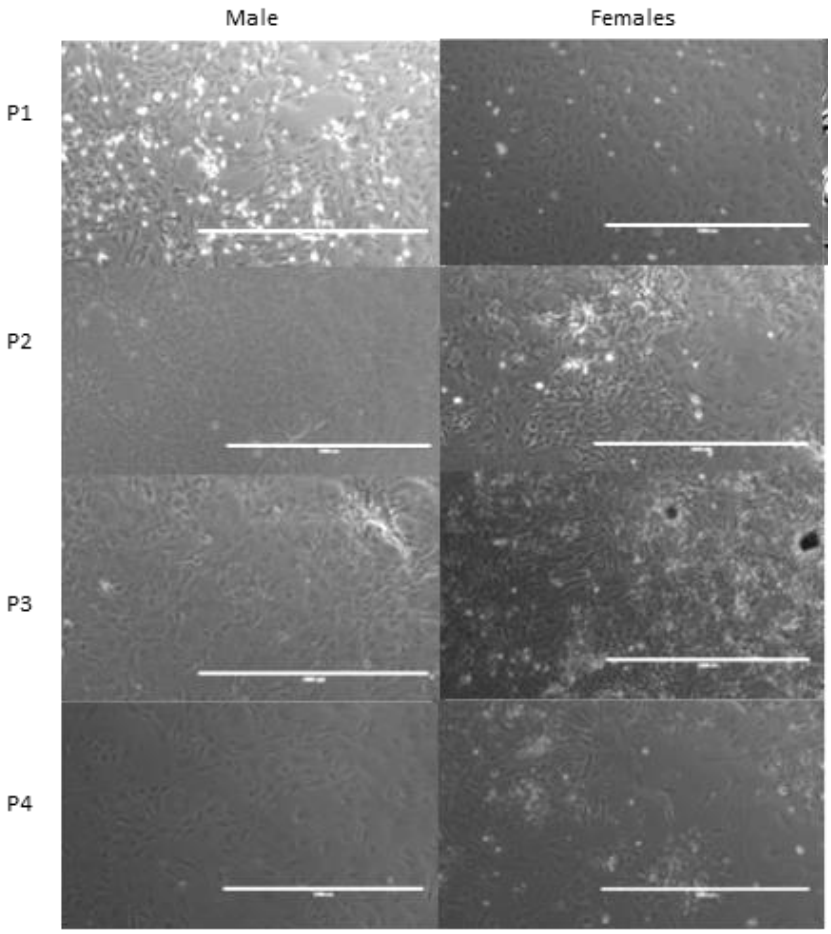

Figure 5. 1 – Rat derived primary cardiac fibroblasts progression through passages 1-4

Morphological evaluation was conducted at each passage to track potential phenotypic changes over time. Between passages 1 and 4, the cells consistently retained their fibroblast-like morphology. However, after passage 4, the fibroblasts began to exhibit changes, including increased adherence, reduced proliferation rates, and alterations in cell morphology with male cells showing greater projections in the cells (data not shown). No morphological differences were observed between male and female cFbs up to passage 4. However, female fibroblasts appeared to proliferate at a slower rate compared to their male counterparts, which could be partially attributed to the smaller heart size, and therefore lower initial seeding density, at the time of isolation. However, these findings are purely observational and further analysis would need to be carried out to confirm this. Post-passage 4, female fibroblasts displayed a more heterogeneous morphology, which suggests a shift in cell phenotype with extended passaging. This is likely due to extended cell culture and cellular senescence.

To confirm the identity of isolated cFbs, we characterized cells using immunostaining techniques with specific markers: vimentin (fibroblasts), PDGFRα (fibroblasts), αSMA (myofibroblasts/smooth muscle cells), CD45 (leukocytes), and RECA-1 (endothelial cells). Antibody optimization followed protocols detailed in Table 5.1. The results revealed a heterogeneous population of vimentin+ and PDGFRα+ cells, with some cells also expressing αSMA (Figure 5.1). Minor contamination with CD45+ cells was observed, comprising approximately 3-5% of the population based on visual inspection. No RECA-1+ endothelial cells were detected in the population, consistent with our rat cardiac tissue positive control (Figure 5.2).

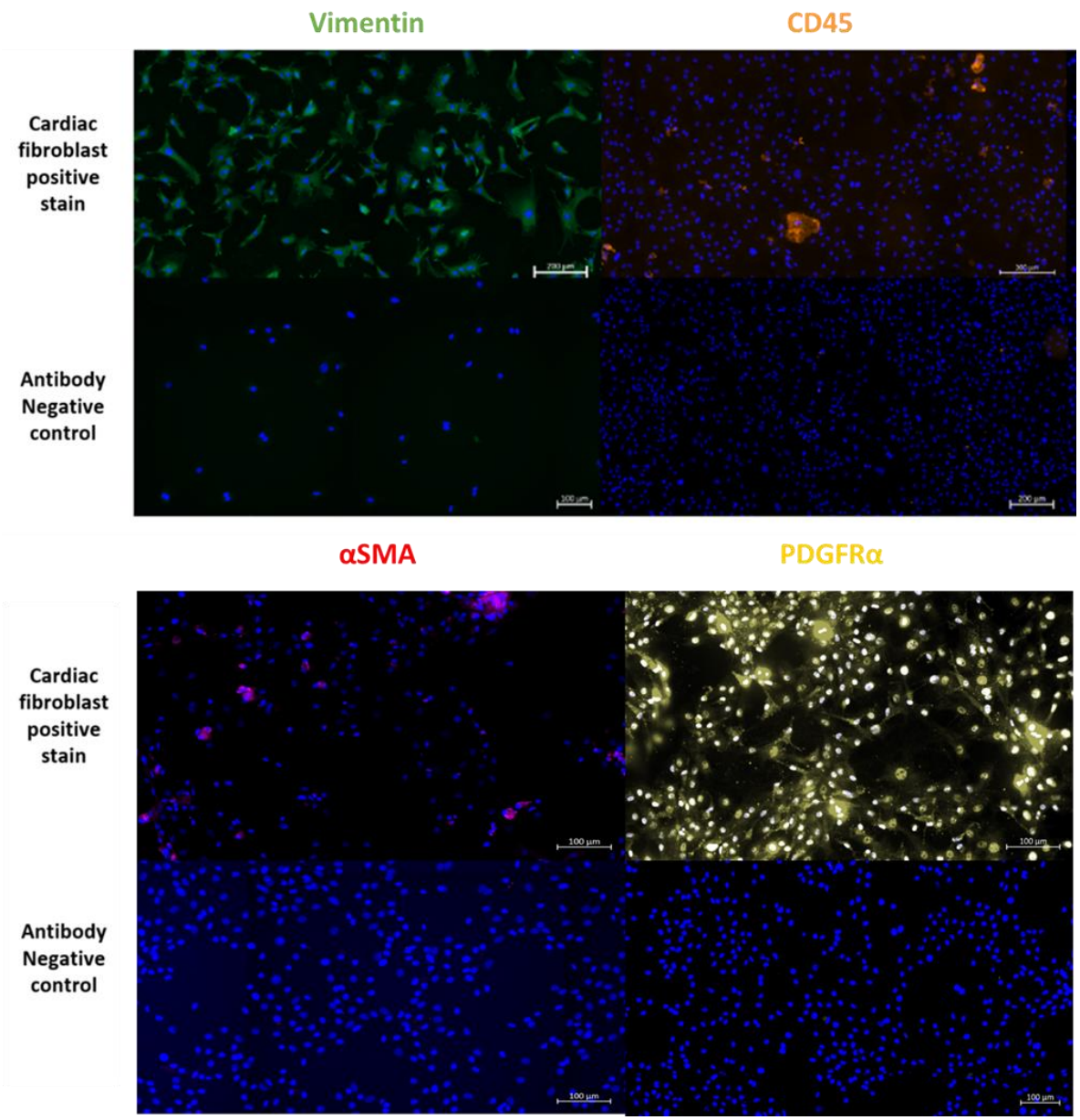

Figure 5. 2 Immunocytochemistry characterisation of cells present in primary cell culture. Images of single-stains for DAPI (blue), Vimentin (green), CD45 (orange), PDGFRα (yellow) and αSMA (red).

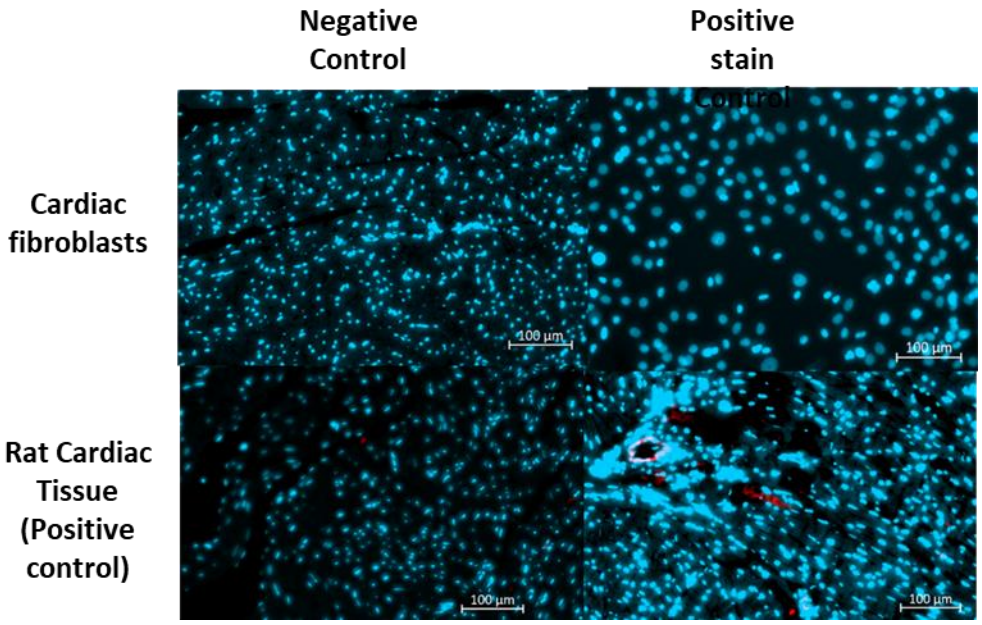

Figure 5. 3. Assessment of present of rat endothelial cells in *in vitro* cardiac fibroblasts culture. Cells and rat cardiac tissue (positive control) were stained with RECA-1 (red) and DAPI (light blue) to assess whether culture included endothelial cells.

5.3.2 Faster equilibration of *trans*-4-[^{18}F]fluoro-*L*-proline compared to *cis*-4-[^{18}F]fluoro-*L*-proline in optimized uptake conditions

The optimization of tracer uptake for *cis*-4-[^{18}F]fluoro-*L*-proline and *trans*-4-[^{18}F]fluoro-*L*-proline was assessed by measuring tracer accumulation in biological triplicates over time intervals ranging from 0 to 120 minutes. The uptake of *cis*-4-[^{18}F]fluoro-*L*-proline achieved approximately 90% uptake at 90 minutes, with a calculated doubling time (Td) of 52 minutes (Figure 5.4 A). In contrast, *trans*-4-[^{18}F]fluoro-*L*-proline reached 90% occupancy at approximately 35 minutes, with a Td of 30 minutes (Figure 5.4 B). These findings demonstrate that *trans*-4-[^{18}F]fluoro-*L*-proline equilibrated faster than *cis*-4-[^{18}F]fluoro-*L*-proline. Consequently, an incubation period of 90 minutes was established for both tracers to ensure consistent experimental conditions and the attainment of equilibrium.

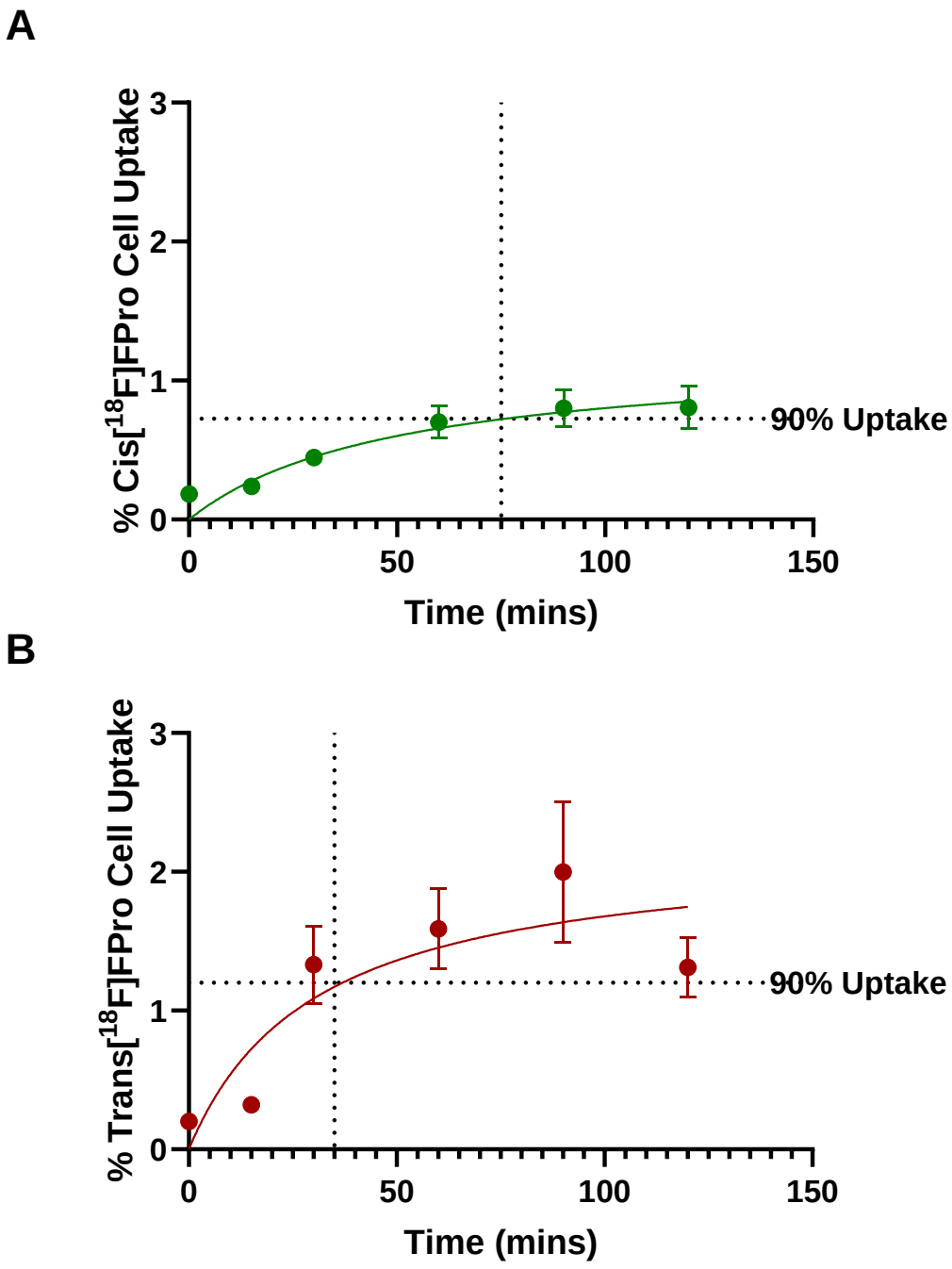

Figure 5. *4* Kinetics of *cis*-4-[^{18}F]fluoro-*L*-proline and *trans*-4-[^{18}F]fluoro-*L*-proline uptake in male cardiac fibroblasts over 120 Minutes. Uptake was analysed using non-linear regression to model equillibrium. (A) *cis*-4-[^{18}F]fluoro-*L*-proline uptake over time, (B) *trans*-4-[^{18}F]fluoro-*L*-proline uptake over time per well. Results are reported as min to max range, with n = 3 biological replicates per group.

5.3.3 Cardiac fibroblast *cis*-4-[^{18}F]fluoro-*L*-proline uptake is affected by both sex and age

The impact of sex and age on unhydroxylated collagen synthesis in cFbs was evaluated *in vitro* using *cis*-4-[^{18}F]fluoro-*L*-proline. Young male cFbs (4 weeks) exhibited significantly higher *cis*-4-[^{18}F]fluoro-*L*-proline uptake compared to their female counterparts (males: 0.1767 ± 0.05 %/ng; females: 0.05 ± 0.03 %/ng; p = 0.026), indicating elevated rates of unhydroxylated collagen synthesis in young male fibroblasts versus young female fibroblasts (Figure 5.5 A). When comparing young male (4 weeks) to aged male (18 months) cFbs, aged fibroblasts demonstrated significantly higher *cis*-4-[^{18}F]fluoro-*L*-proline uptake (young: 0.18 ± 0.05 %/ng; aged: 0.33 ± 0.05 %/ng; p = 0.012), suggesting that aging increases unhydroxylated collagen synthesis *in vitro* (Figure 5.5 B). These results indicate that both sex and age significantly influence unhydroxylated collagen synthesis in cFbs *in vitro.* However, it is important to acknowledge that effect of sex in aging was not explored due to the lack of aged female cells available and therefore conclusions cannot be made on the effect of sex in aged cells.

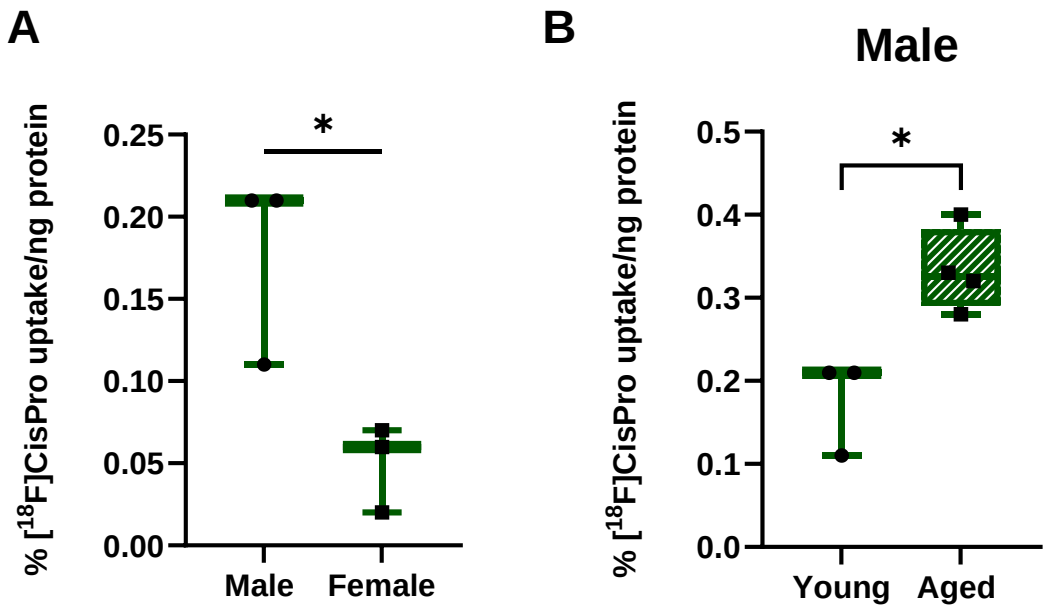

Figure 5. 5 Assessing the effect of sex and age on cardiac fibroblast *cis*-4-[^{18}F]fluoro-L-proline uptake. % *cis*-4-[^{18}F]fluoro-*L*-proline uptake normalised to protein content was measured to assess the effect of sex in young (4 week) males and females (A) and the effect of age (18 months) in males (B). Results reported as min to max range, n= 3/group (biological replicates) except for aged males where n=4; young male data is the same for both panels in the figure. p values were obtained using a student's t-test; *p<0.05

5.3.4 Cardiac fibroblast *trans*-4-[^{18}F]fluoro-*L*-proline uptake is affected by age but not sex

Hydroxylated collagen synthesis was assessed using *trans*-4-[^{18}F]fluoro-*L*-proline in cFbs from both male and female 4-week-old rats, as well as aged male 18-month-old rats, to evaluate the effects of sex and age on collagen synthesis *in vitro*. No significant sex differences were observed in *trans*-4-[^{18}F]fluoro-*L*-proline uptake, with males showing a slightly higher but not significantly different average uptake compared to females (males: 0.13 ± 0.1; females: 0.05 ± 0.01; p = 0.25) (Figure 5.6 A). However, in aged male cFbs, a significant increase in *trans*-4-[^{18}F]fluoro-*L*-proline uptake was observed (young: 0.09 ± 0.05; aged: 0.3 ± 0.09; p = 0.022) (Figure 5.6 B). These findings suggest that hydroxylated collagen synthesis is primarily influenced by age in male cFbs.

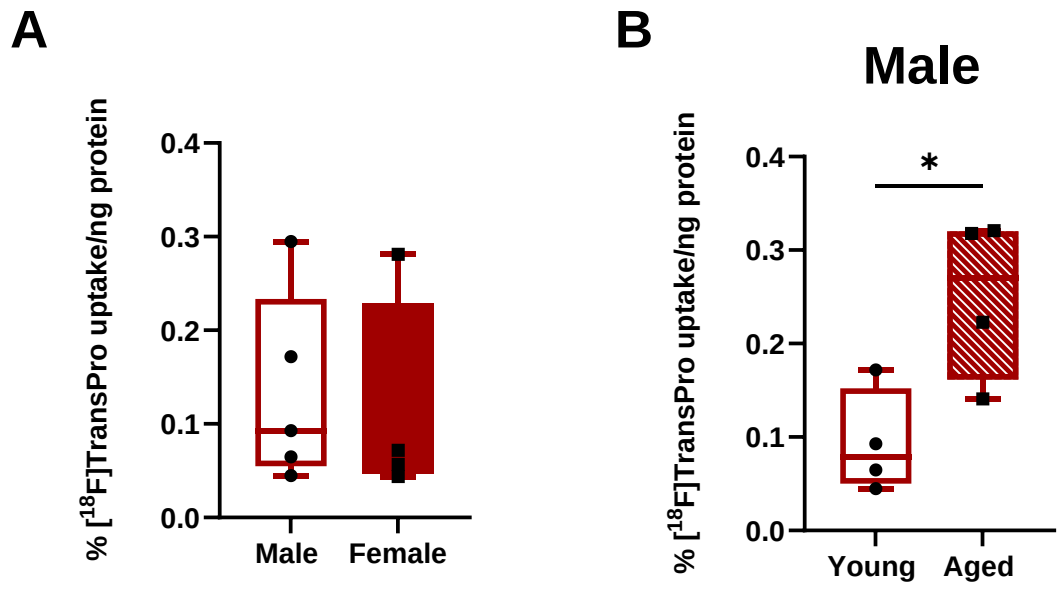

Figure 5. 6 Assessing the effect of sex and age on cardiac fibroblast *trans*-4-[^{18}F]fluoro-*L*-proline uptake. % *trans*-4-[^{18}F]fluoro-*L*-proline uptake normalised to protein content was measured to assess the effect of sex in young (4 week) males and females (A) and the effect of age (18 months) in males (B). Results reported as min to max range, n= 3/group except for aged males where n=4; young male data is the same for both panels in the figure; p values were obtained using a student's t-test; *p<0.05

5.3.5 Cardiac fibroblast insoluble collagen content is affected by sex and age, but soluble collagen remains unaffected

The impact of age and sex on collagen deposition in cFbs was evaluated by measuring soluble and insoluble collagen *in vitro*. Soluble collagen, which reflects newly synthesized and degraded collagen, did not exhibit significant differences related to sex or age, with all groups showing comparable values and no discernible trends (Figure 5.7). This indicates that collagen turnover is stable *in vitro* and is not significantly influenced by aging or sex in young cFbs. In contrast, insoluble collagen, indicative of crosslinked collagen, demonstrated significant effects due to both age and sex (Figure 5.8). Young male cFbs deposited markedly more insoluble collagen compared to their female counterparts (males: 953 ± 540 ng/µl; females: 300 ± 231 ng/µl; p = 0.04) (Figure 5.8 A). Additionally, in male cFbs, aging led to a substantial reduction in insoluble collagen deposition compared to younger counterparts (young: 928 ± 581.5 ng/µl; aged: 90 ± 77 ng/µl; p = 0.02) (Figure 5.8 B). These findings suggest that while soluble collagen production remains unaffected by age and sex, insoluble collagen deposition is significantly influenced by both factors.

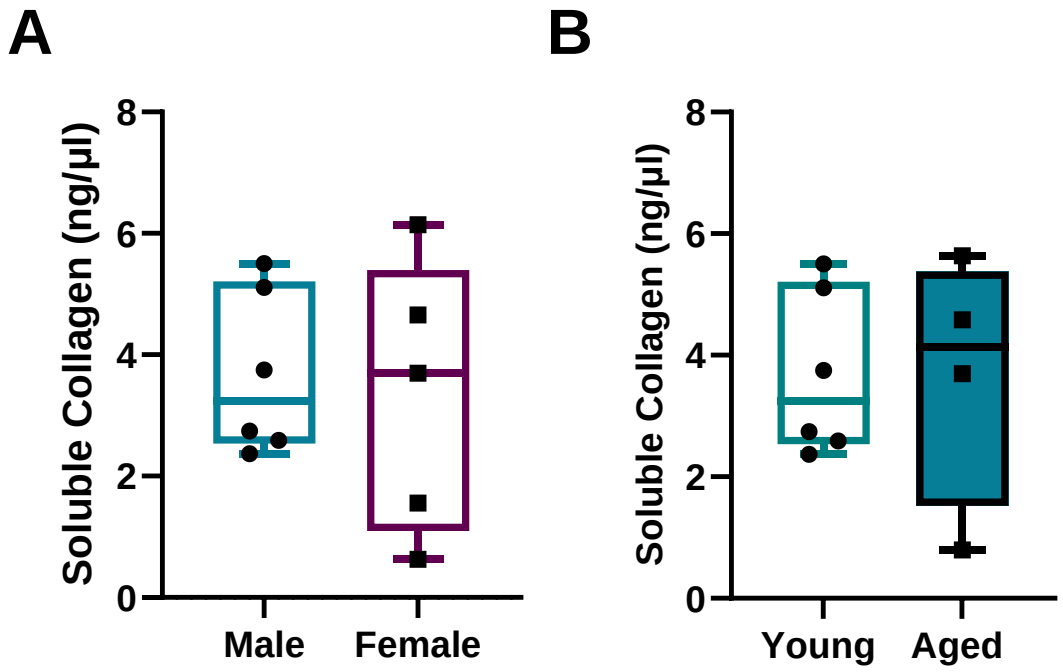

Figure 5. 7 Effect of sex and age on soluble collagen content in cardiac fibroblasts. Soluble collagen content (ng/µl) was measured to assess the effect of sex in young (4 week) males and females (A) and the effect of age (18 months) in males (B). Results reported as min to max range, n= 6/group except for aged males where n=4; young male data is the same for both panels in the figure; p values were obtained using a student's t-test

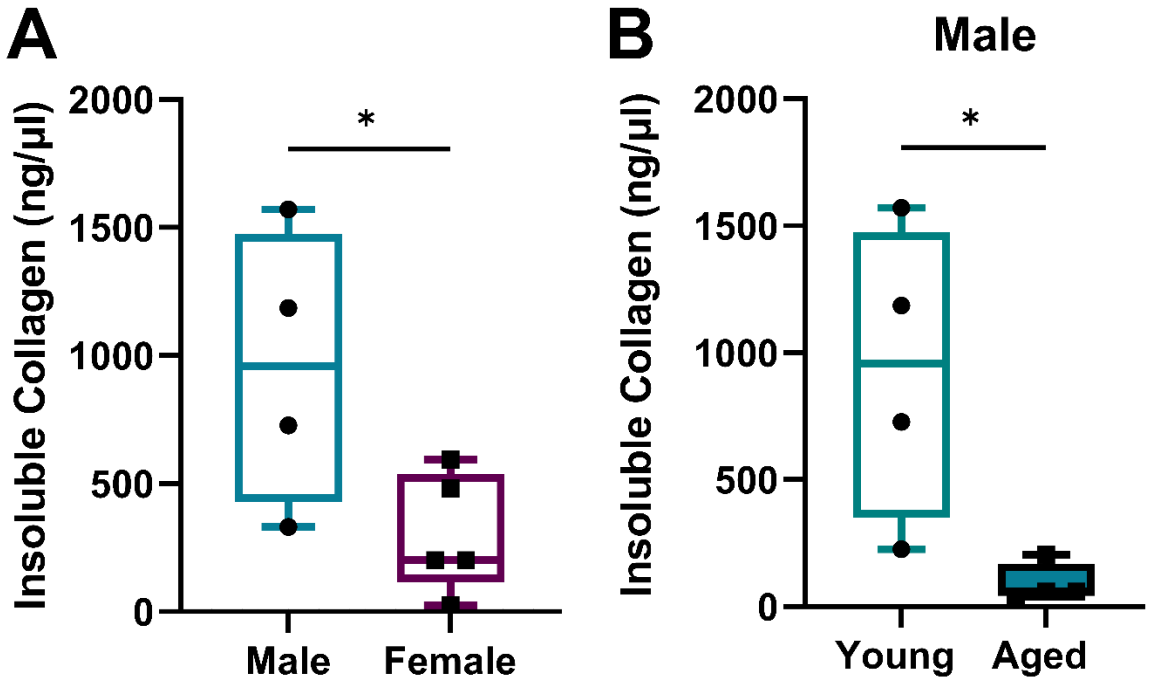

Figure 5. 8 Effect of sex and age on insoluble collagen content in cardiac fibroblasts. Insoluble collagen content (ng/µl) was measured to assess the effect of sex in young (4 week) males and females (A) and the effect of age (18 months) in males (B). Results reported as min to max range, n= 6/group except for aged males where n=4; young male data is the same for both panels in the figure; p values were obtained using a student's t-test; *p<0.05

5.3.6 ALT711 does not alter unhydroxylated collagen synthesis across groups

In Chapter 3, we found increased accumulation of AGEs in the left ventricle of male rats over time. To explore this further, we investigated the effects of AGEs inhibition on collagen synthesis and deposition *in vitro*, accounting for age and sex differences. We assessed unhydroxylated collagen synthesis using *cis*-4-[^{18}F]fluoro-*L*-proline in both young male and female cFbs, comparing those treated with either a vehicle or ALT711, an AGEs inhibitor. Our results showed that inhibition of AGEs formation did not significantly alter unhydroxylated collagen synthesis in either sex (Figure 5.9 A & B). Similarly, no significant effect of AGEs inhibition was observed in aged cFbs with respect to unhydroxylated collagen synthesis *in vitro* (Figure 5.9 C). However, there was a trend indicating a reduction in collagen synthesis in the aged, treated group, with an average decrease of 30.8% (p=0.06). This trend suggests a potential effect of AGEs inhibition on unhydroxylated collagen synthesis.

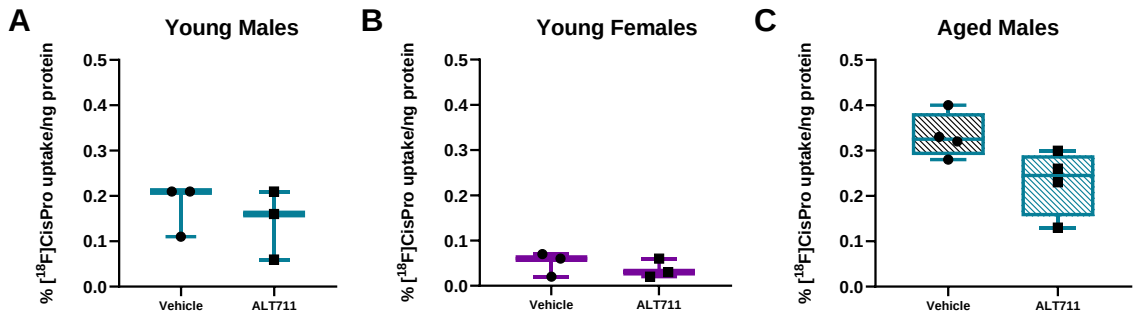

Figure 5. 9 Effect of AGEs inhibition on unhydroxylated collagen synthesis in young and aged cardiac fibroblasts. % *cis*-4-[^{18}F]fluoro-*L*-proline uptake normalised to protein content was measured to assess the effect of drug treatment with ALT711 in young (4 week) males (A) and females (B) and the effect of age (18 months) in males (C). Results reported as min to max range, n= 6/group except for aged males where n=4; young male data is the same for both panels in the figure; p values were obtained using a student's t-test;

5.3.7 ALT711 does not alter hydroxylated collagen synthesis across groups

We evaluated the effect of ALT711 treatment on hydroxylated collagen synthesis using *trans*-4-[^{18}F]fluoro-*L*-proline across different groups. The treatment did not result in statistically significant changes in hydroxylated collagen synthesis in young cFbs of either sex (Figure 5.10 A & B). Nonetheless, a trend towards a decline was observed, with young males exhibiting a 48.3% decrease (p = 0.15) and young females a 46.2% decrease (p = 0.12) following ALT711 treatment. These results suggest that ALT711 treatment did not significantly affect hydroxylated collagen synthesis.

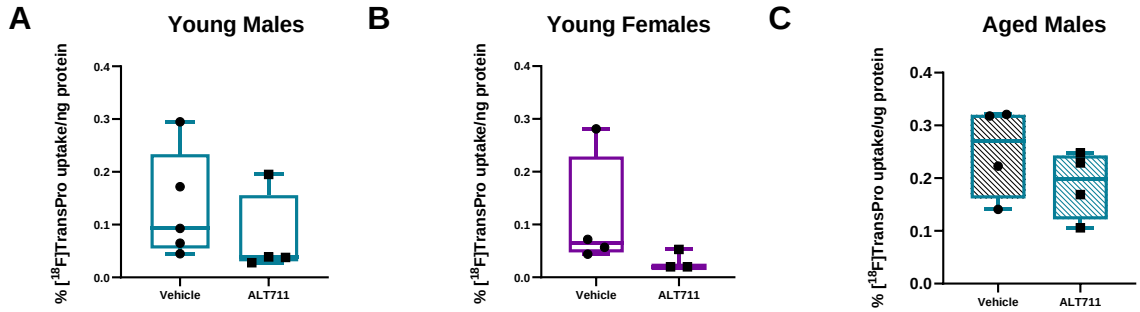

Figure 5. 10 Effect of AGEs inhibition on hydroxylated collagen synthesis in young and aged cardiac fibroblasts. % *trans*-4-[^{18}F]fluoro-*L*-proline uptake normalised to protein content was measured to assess the effect of drug treatment with ALT711 in young (4 week) males (A) and females (B) and the effect of age (18 months) in males (C). Results reported as min to max range, n= 6/group except for aged males where n=4; young male data is the same for both panels in the figure; p values were obtained using a student's t-test

5.3.8 Cardiac fibroblasts soluble and insoluble collagen content are unaffected by ALT711 treatment Groups

Soluble and insoluble collagen content was assessed following treatment with ALT711 in cFbs across various groups. No significant effect of the drug treatment was observed on either soluble or insoluble collagen content (Figures 5.11 & 5.12). In male (young and aged) and female cFbs, both soluble and insoluble collagen content were similar between vehicle- and drug-treated cells, regardless of age.

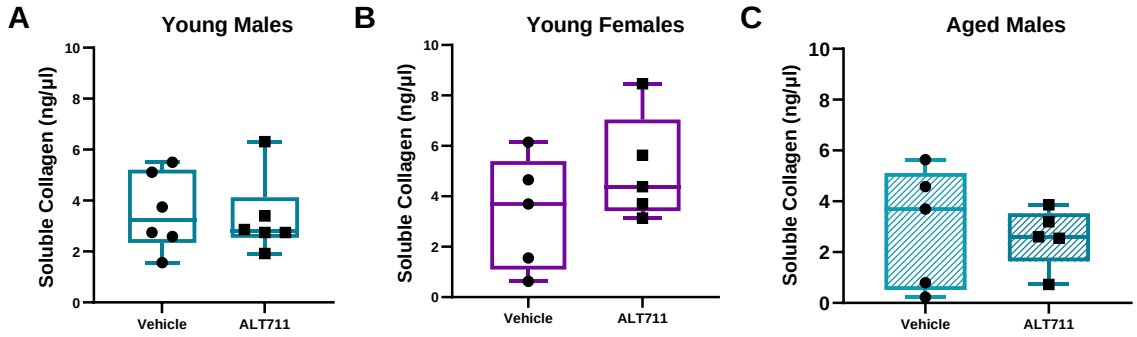

Figure 5. 11 Effect of AGEs inhibition on soluble collagen content in young and aged cardiac fibroblasts. Soluble collagen content (ng/µl) was measured to assess the effect of drug treatment with ALT711 in young (4 week) males (A) and females (B) and the effect of age (18 months) in males (C). Results reported as min to max range, n= 4-6/group; p values were obtained using a student's t-test

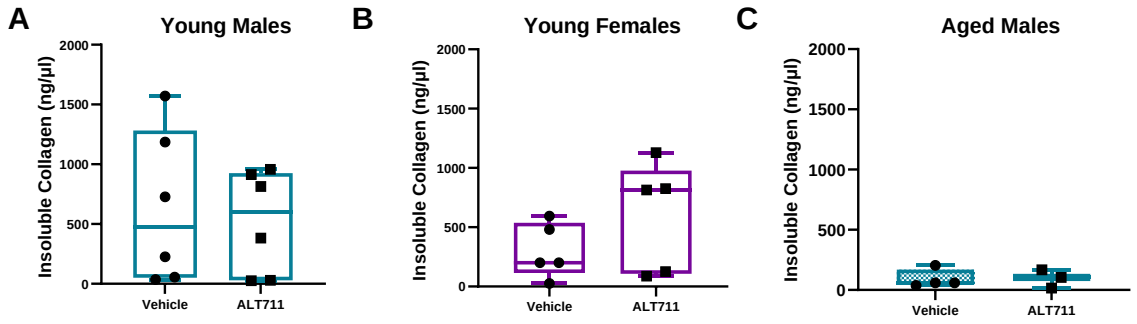

Figure 5. 12 Effect of AGEs inhibition on insoluble collagen content in young and aged cardiac fibroblasts. Insoluble collagen content (ng/µl) was measured to assess the effect of drug treatment with ALT711 in young (4 week) males (A) and females (B) and the effect of age (18 months) in males (C). Results reported as min to max range, n= 6/group except for aged males where n=3-4; p values were obtained using a student's t-test

5.4 Discussion

This chapter investigated the effects of sex and age on collagen metabolism in cFbs *in vitro*, focusing on collagen synthesis and deposition. Collagen synthesis was quantified using PET radiotracer incubation experiments, while collagen deposition was evaluated through soluble and insoluble collagen biochemical assays. This chapter examined the influence of age and sex on collagen metabolism in cFbs *in vitro*, with a specific focus on collagen synthesis and deposition, addressing the study's primary objectives. Based on our hypotheses, we anticipated that aging would disrupt collagen homeostasis in cFbs, resulting in a decoupling of collagen synthesis and deposition, particularly in aged cells. We also hypothesized that age-related alterations would be more pronounced in male fibroblasts than in female fibroblasts, revealing sex-specific differences, and that treatment with the AGE crosslink breaker ALT-711 would reduce collagen synthesis and deposition in an age- and sex-dependent manner.

Our findings largely aligned with these hypotheses. Collagen synthesis was quantified using PET radiotracer assays, while collagen deposition was assessed through soluble and insoluble colorimetric assays. Both sex and age significantly affected unhydroxylated collagen synthesis, while hydroxylated collagen synthesis appeared predominantly influenced by age, suggesting divergent regulatory pathways in collagen synthesis within cFbs. Furthermore, insoluble collagen deposition was modulated by both sex and age, supporting our premise of differential collagen accumulation patterns based on these factors.

The study also explored the impact of ALT-711 on collagen metabolism in both young and aged fibroblasts. Although significant changes were not observed, trends suggested potential age- and sex-specific effects, indicating that further studies with larger sample sizes may be required to substantiate these findings. Collectively, our results suggest that aging disrupts the balance between collagen synthesis and deposition in cFbs, with sex-specific variations that may have implications for age-related cardiac fibrosis. A detailed summary of the key findings is provided in Figure 5.4.1. c. The study demonstrates that both sex and age significantly influence unhydroxylated collagen synthesis. In contrast, hydroxylated collagen synthesis is primarily affected by age, indicating distinct regulatory roles for these factors in collagen synthesis pathways within cFbs. Additionally, the findings show that insoluble collagen deposition is regulated by both sex and age in a heterogeneous population of activated cFbs. The study also investigates the effects of the AGEs breaker ALT-711 on collagen metabolism in young and aged cFbs. Although no significant effects were observed, trends indicative

of potential impacts were noted, underscoring the need for larger sample sizes to draw more definitive conclusions. A comprehensive summary of the key findings is illustrated in Figure 5.4.1.

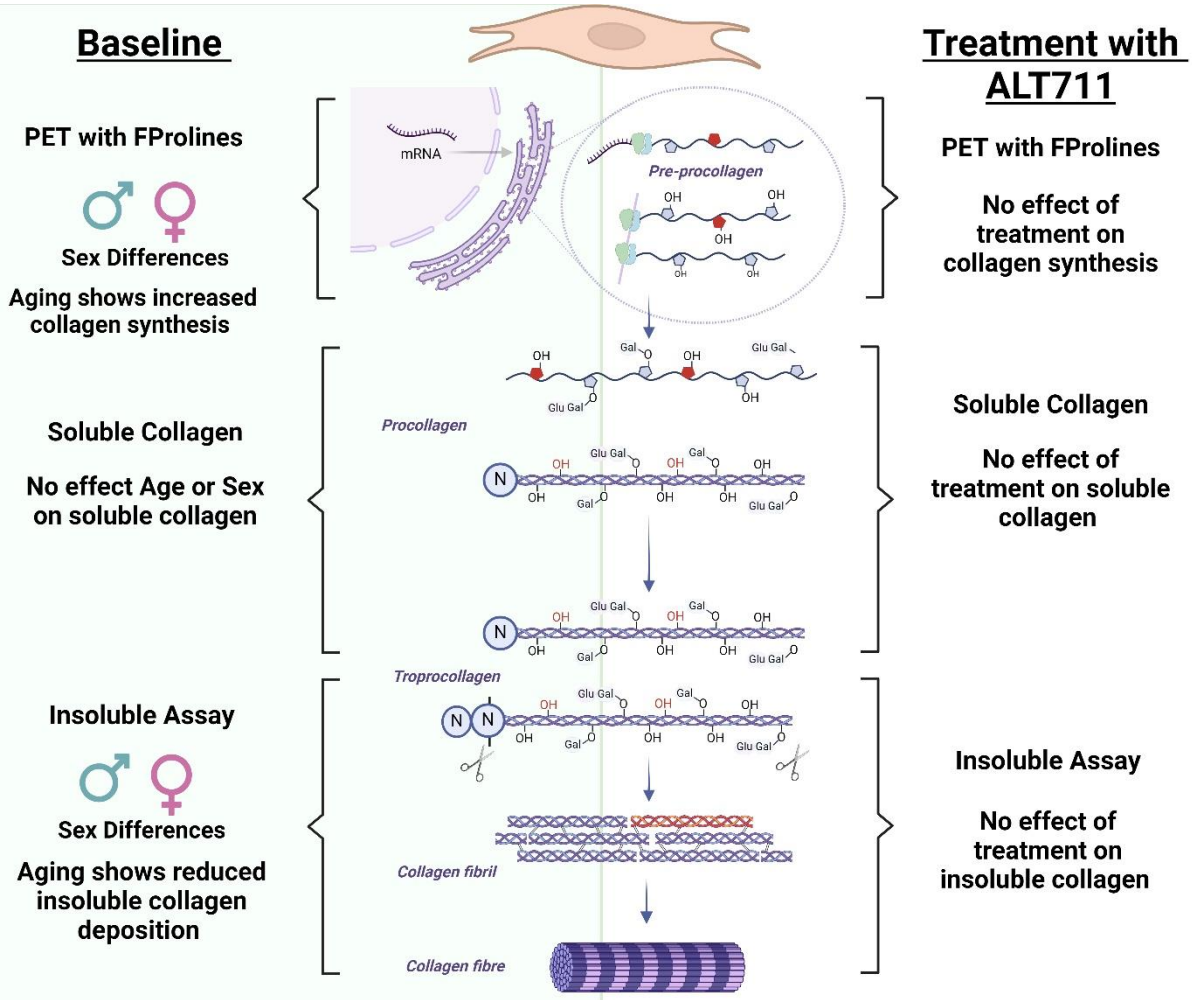

Figure 5. 13 Summary of key findings from chapter 5. Note that aging was only explored in male cells Figure created using Biorender.

5.4.1 Cardiac fibroblasts are heterogeneously activated *in vitro*

The study identified a heterogeneous population of cFbs, characterized by uniform expression of vimentin and PDGFRα across the culture, but with variable αSMA expression. This suggests that the primary cell culture predominantly contained cFbs, as indicated by morphology and antibody staining, with some cells transitioning into activated myofibroblasts while others remained inactivated. Such heterogeneity among fibroblasts is consistent with previous reports. For instance, single-cell analyses of primary murine cFbs 15 days post-isolation revealed four main groups: contractile fibroblasts, matrix-producing fibroblasts, fibroblast-marker-expressing macrophages, and endothelial cells (300).

In contrast, previous studies have typically described a homogeneous activation of cFbs *in vitro*, with consistent αSMA expression observed in both human and rat cultures (301, 302).

Fibroblast activation is generally associated with tissue remodelling following injury, but this activation might not fully capture the cellular changes occurring during aging. Fibroblast activation in injury models is driven by acute stress and inflammation, which differs from the chronic, progressive processes linked to aging (303). Although activation of cFbs with aging has been documented, the mechanisms involved may differ significantly, potentially affecting the relevance of our findings (304). Future studies should explore fibroblast dynamics in both injury and aging contexts to gain a more comprehensive understanding of their behaviour.

Our cultured cells exhibited minor contamination by CD45+ hematopoietic cells. Given the low proportion of CD45+ cells, this contamination is unlikely to significantly influence our results. Previous studies have identified subpopulations of macrophages expressing fibroblast markers—such as Acta2, vimentin, Col1a1, and Lox—alongside weaker macrophage markers (Lyz2 and CD68) in primary murine cardiac fibroblast cultures (300). This may explain our observation of homogeneous PDGFRα and vimentin expression, suggesting that the CD45+ population in our study might include CD45+ fibroblasts, a cell type described in the context of cardiac injury (305). The role of CD45+ hematopoietic-derived fibroblasts has been extensively studied in injury models. For example, MCP-1 deletion in mice results in reduced interstitial fibrosis following angiotensin II infusion, likely due to the absence of fibrocyte-derived CD45+ fibroblasts suggesting that in remodelling (306). Additionally, CD45+ fibroblasts have been found to play a role in non-adaptive fibrosis in ischemia/reperfusion cardiomyopathy (306). The presence of CD45+ fibroblasts in our culture might have been induced by the stress of cell isolation, reflecting immune-to-fibroblast transitions observed in injury models(307). To confirm the identity and proportions of these cells, co-staining or flow cytometry would be necessary for a more accurate assessment of subpopulations. These analyses would provide a clearer understanding of the cellular composition within our cultures and elucidate the role of CD45+ cells in our findings.

It is also crucial to consider the limitations of *in vitro* cFbs culture in accurately modelling 'healthy' fibroblast dynamics. Characterizing cFbs is challenging due to their morphological similarities to mesenchymal stem cells, and they have been described as "phenotypically indistinguishable" (308). Attempts to differentiate these populations have shown that all mesenchymal cells begin expressing myofibroblast markers when cultured (300). Furthermore, no single marker specifically identifies fibroblasts, complicating their precise characterization. Fibroblasts exhibit high phenotypic plasticity,

allowing them to rapidly alter their phenotype in response to environmental cues (309). This phenotypic flexibility adds another layer of complexity to their identification and study.

Several limitations of this study should be acknowledged. Due to time constraints and the preliminary nature of this study and low cFbs cell yield from aged hearts, we were unable to thoroughly characterize the cells across experimental groups. Such characterization would have provided greater insight into the impact of aging on fibroblast morphology, as increased fibroblast activation in adult cFbs compared to foetal counterparts is associated with higher periostin and αSMA gene expression therefore there are likely significant changes in activation with advanced aging (310). Specifically, we did not perform co-staining analyses, which would have enabled more precise identification of specific cell populations, including CD45+ fibroblasts. Detailed characterization is crucial for validating the phenotypes observed in our cultures and for understanding the cellular heterogeneity present. Prior studies have identified approximately six fibroblast subpopulations in culture (300). Incorporating this level of detail would have enhanced our understanding of how distinct fibroblast subtypes contribute to the cellular responses observed, potentially highlighting unique pathways or responses within specific fibroblast lineages (300). Furthermore, characterisation of senescence in culture was not carried out, this was due to the reasons previously stated above, however, would have provided key insights into this essential component of aging research with markers such as Senescence-associated β-galactosidase (SA-β-gal), SASP, DNA damage response (DDR).

5.4.2 Collagen synthesis in cardiac fibroblasts is affected by both age and sex

Our study identified that age and sex directly impact cFbs collagen synthesis, however due to loss of aged females cells sex was only assessed in the younger group. cFbs cells from young males exhibited significantly higher *cis*-4-[^{18}F]fluoro-*L*-proline uptake compared to their female counterparts, and aging in males had a further increase unhydroxylated (interstitial) collagen synthesis. Interestingly, hydroxylated (structural) collagen synthesis was affected by age but not by sex, with aged males showing significantly higher uptake compared to their younger counterparts.

This observation is consistent with previous findings that chronological age impacts cFbs function *in vitro*. For example, a comparison of fetal (2-day) and adult (3-5 month) Sprague Dawley rat ventricular cFbs in 3D co-culture with cardiomyocytes demonstrated that aging disrupted cFbs collagen deposition and function, and also led to deterioration in cardiomyocyte mechanical and electrical function (310). Similarly, aged cFbs have been reported to show increased collagen synthesis (mRNA

expression of collagen I and III) compared to fetal counterparts, with notable upregulation of collagen I and III expression (310). Although our study does not investigate advanced aging (e.g. > 2 years), it clearly illustrates that aging increases collagen synthesis.. With some studies identifying that adult rat cFbs found to exhibit pro-fibrotic actions in 3D cultures, leading to increased stiffness and diminished electrophysiological function compared to young counterparts (310). Conversely, other studies comparing neonatal (4-day-old) and adult (2-3 month-old) Sprague Dawley cFbs have suggested reduced collagen mRNA expression in aging (22). This lack of consensus on the effect of aging on collagen synthesis in cFbs *in vitro* highlights the variability in research findings, with most studies focusing on young-adult and neonatal cells. To our knowledge, this is the first study to clearly explore the effect of aging on cardiac fibroblast collagen synthesis.

Our study also identified significant sex differences in cFbs collagen synthesis. Males showed higher uptake of *cis*-4-[^{18}F]fluoro-*L*-proline, indicating that sex influences unhydroxylated (interstitial) collagen synthesis *in vitro*. Previous *in vitro* studies have demonstrated sex differences in collagen synthesis in rat and human cFbs through mRNA analysis, with E2 administration affecting collagen synthesis (92). Female rat cFbs exhibited decreased collagen synthesis (collagen I and III mRNA expression) and MMP expression when treated with E2, compared to males, who showed increased collagen synthesis following E2 treatment (92). Interestingly, this study did not find differences in collagen synthesis without E2 treatment, with both males and females showing similar expression profiles (92). This discrepancy may reflect the use of mRNA measurements in previous studies, whereas our study employed sensitive radiotracers to assess synthesis. Another study found that E2 inhibited collagen degradation in both male and female cFbs but only reduced collagen mRNA expression in females (99). Our study is the first to demonstrate the effect of sex on collagen synthesis in the absence of hormonal supplementation, suggesting that intrinsic cellular sex-specific factors lead to differential collagen synthesis profiles. This is particularly relevant as clinical trials using hormonal replacement therapies have not consistently shown a clear benefit of E2 treatment on cardiac fibrosis in females (311, 312). Our findings suggest that the reduced collagen synthesis pathways observed in females may involve non-hormonal components. Although our study could have benefited from comparing collagen synthesis rates following E2 administration to assess hormonal intervention effects, this was beyond the scope of the project.

Our study did not include a detailed analysis of fibroblast subtypes from various cardiac regions, such as atrial tissues, which could have enriched our exploration of collagen synthesis changes observed *in vivo* (chapters 3 & 4). Previous research using [^{3}H]proline to compare fibroblast populations from the

atria and ventricles in WKY and SHR rats showed no differences in uptake, suggesting that collagen synthesis in fibroblasts from different cardiac regions does not differ *in vitro* (313). However, given the advancements in understanding cFbs heterogeneity, further research using newer techniques to assess different fibroblast populations would provide valuable insights into their specific roles under stress or aging conditions (314).

5.4.3 *In vitro* cardiac fibroblasts culture as a model of cardiac injury

In this study, we assessed the effects of aging and sex on collagen metabolism and identified the heterogeneous activation of cFbs. We propose that our findings offer insights into age- and sex-specific responses in the context of cardiac injury rather than natural aging. This is primarily due to the increased collagen synthesis and deposition of insoluble collagen, reminiscent of thick collagen fibres deposited during replacement fibrosis following injury to prevent rupture. These findings directly contrast with our *in vivo* results illustrating that both models show divergent responses. Our study found that insoluble collagen deposition varied with both sex and age, with young male cFbs depositing greater levels of insoluble collagen compared to females. In aging, insoluble collagen content was notably lower compared to younger counterparts, suggesting potential dysregulation of collagen metabolism in aged fibroblasts, characterized by decreased deposition and increased synthesis mechanisms.

cFb culture as a model of injury associated remodelling have previously been proposed in studies comparing single-cell gene expression of primary murine cFbs from control and HF samples, which found that *in vitro* murine cFbs had a gene expression profile more similar to diseased samples than controls, suggesting that primary cFbs cultures can be used to assess injury-related cardiac remodelling (300). Cartledge *et al.* identified that *in vitro* cFbs represent an injury phenotype, comparing 'healthy' rat cFbs with myofibroblasts from pressure-overload hypertrophic rat hearts, showing similarities in gene expression and collagen deposition (315). CF is associated with increased ECM content, particularly collagen deposition. Several studies have demonstrated that TGF-β1 promotes collagen synthesis and/or deposition in cultured cFbs, reflecting mechanisms found following cardiac injury and dysfunction (24).

Interestingly, despite increased collagen synthesis in our aged male group, insoluble collagen deposition was lower compared to younger counterparts. This suggests dysregulation in collagen metabolism in aging, similar to our *in vivo* findings where despite collagen synthesis declining collagen

accumulation continues, and may indicate less efficient reparative collagen deposition and scar formation following injury. Research has shown that aging impairs the reparative response following cardiac injury, largely due to dysfunctional cFbs (29). Aging patients have been observed to form weaker scars due to reduced fibroblast response and dampened fibrotic cues (52). This weakness in scar formation has been attributed to reduced collagen production and unstable matrix due to loose connective tissues (316). Our findings may model the remodelling process in the senescent heart and could serve as an alternative to animal MI models, which are challenging to perform in aged animals.

Sex differences in cardiac injury, such as MI, show that females have a dampened remodelling process (92). This was observed in our study, with female cFbs exhibiting reduced unhydroxylated/interstitial collagen synthesis. These findings are consistent with current understanding of remodelling processes in cardiac dysfunction or post-injury, where human females have been shown to have reduced collagen I and III expression compared to males (92). Preclinical studies have also extensively reported that ovariectomized (OVX) mice, when supplemented with E2, exhibit reduced fibrosis following TAC and MI (317-319). The similarities between our *in vitro* findings and existing preclinical and clinical understanding of sex differences post injury further supports the case for classical 2D culture of primary cFbs as a model of injury related remodelling.

Interestingly, efforts have been made to produce a cFbs culture environment that recapitulated the *in vivo* environment more closely (310). Basic 2D cell culture methodologies using rigid glass or plastic materials can lead to spontaneous activation due to fibroblasts' responsiveness to substrate stiffness (320). Studies have attempted to produce unstimulated/inactivated cultures through alterations in culturing protocols, such as using different serum types and flexible substrates like polydimethylsiloxane (321, 322). These modifications have promoted a quiescent phenotype and reduced fibroblast activation (323). Future *in vitro* studies exploring age-related cardiac fibroblast remodelling would benefit from these advancements to better model physiological age-related changes rather than injury-related changes.

5.4.4 AGEs inhibition does not alter collagen synthesis or deposition *in vitro*

In the LV, we observed increased AGEs crosslinking in males (chapter 3) a factor which has been shown to increase cardiac stiffness in aging directly contributing to CF development (48). To understand the effect of AGEs inhibition on collagen metabolism, we evaluated the impact of the AGEs inhibitor ALT711 on collagen synthesis and deposition. Our study did not identify significant effects of ALT711 on collagen metabolism across young and aged groups *in vitro*. However, we observed trends suggesting that the treatment may reduce collagen synthesis, with lower uptake of *cis*-4-[^{18}F]fluoro-*L*-proline and *trans*-4-[^{18}F]fluoro-*L*-proline compared to vehicle controls. This trend is consistent with one study in rodents, which observed reduced cardiac collagen synthesis following inhibition of collagen crosslinking (63). However, research in this area is limited, and the effects of AGEs inhibition on collagen synthesis and cFbs remain poorly understood both *in vivo* and *in vitro*. Studies in aged canines have shown that ALT711 reduces LV stiffness, suggesting potential effects on collagen metabolism in aging (259). Further research is needed to determine if AGEs inhibition has any true therapeutic effects on collagen synthesis and metabolism.

To gain a clearer understanding of whether the trends observed in this study reflect genuine biological effects, it would be necessary to increase the study's statistical power. The challenges associated with culturing aging cells (i.e. 2 hearts needed per batch of cells) and the associated costs limited our ability to include large sample sizes, which in turn reduced the likelihood of detecting significant changes. Additionally, the lack of observed direct effects on collagen deposition are likely attributable to the fact that AGEs were not directly measured in this study and potential incorrect drug dosage – however, this was selected based on previous studies utilising the drug *in vitro*. The low cell numbers obtained from aging samples complicated the execution of multiple assays. Future studies should include direct measurements of AGEs to better understand their impact on collagen crosslinking and metabolism.

5.4.5 Conclusion

In this chapter, we investigated the effects of aging and sex on collagen metabolism in cFbs *in vitro*, focusing on both collagen synthesis and deposition. Our findings revealed that age significantly impacts hydroxylated collagen synthesis, while sex predominantly modulates unhydroxylated collagen synthesis. Specifically, young male fibroblasts exhibited higher unhydroxylated collagen synthesis than females, with aging amplifying this trend in males. Additionally, both age and sex influenced insoluble collagen deposition, highlighting a complex interplay between these factors in collagen regulation.

These results align with our first hypothesis, which predicted age-related dysregulation of collagen metabolism in cFbs. Older fibroblasts showed dyssynchronisation between collagen synthesis and deposition, supporting the notion of age-driven changes in fibroblast function. Moreover, our findings supported the second hypothesis, suggesting more pronounced fluoroproline uptake in young male fibroblasts compared to young females cells, highlighting potential sex-specific differences in collagen metabolism, though this requires further validation in aged female cells to understand the effect in aged cells.

However, our examination of ALT-711, an AGEs breaker, did not produce significant effects on collagen synthesis or deposition. While there were trends suggesting reduced collagen synthesis, the results were not statistically significant, thus failing to fully support our third hypothesis. This suggests that while ALT-711 may influence collagen metabolism, its effects may be more subtle than anticipated, requiring larger sample sizes to detect or exclude potential changes.

Overall, this study supports our hypotheses regarding age-related dysregulation and sex-specific differences in collagen metabolism, but it does not provide definitive evidence for ALT-711's impact on collagen synthesis. Future work with larger sample sizes and more targeted analyses will be necessary to clarify these findings and further explore therapeutic strategies targeting collagen metabolism in aging cFbs.

Chapter 6 - Discussion and concluding remarks

6.1 The challenges in cardiac aging research

Aging studies have consistently presented significant challenges in both clinical and preclinical research for several reasons: 1) aging can be measured by various parameters such as chronological age, biological aging, and frailty, which leads to variability in findings across different models; 2) research tends to focus on pathophysiology, often providing limited robust data on "healthy" aging; 3) aging studies frequently detect only subtle changes, necessitating sensitive methods and large sample sizes to identify meaningful trends; 4) there is a scarcity of "healthy" aging tissue, particularly from human subjects, making it difficult to assess natural age-related changes; and 5) aging studies are expensive, leading to research gaps due to limited funding, high animal maintenance costs, and the extended time required to generate meaningful outcomes. As a result, few comprehensive studies have adequately assessed baseline physiological changes associated with aging.

Moreover, there has been little focus on understanding sex differences in natural cardiac aging in both clinical and preclinical research. Most studies are still conducted predominantly in male subjects or combine sexes into a single group, which limits the ability to explore sex-specific differences. This limitation is partly due to the inherent difficulties in assessing sex differences, compounded by the aforementioned challenges, as well as the added complexity of physiological variations caused by hormonal fluctuations. Consequently, there remains a lack of understanding regarding the nuances of aging and the role sex plays in these physiological processes. In the case of cardiac remodelling, this knowledge gap restricts exploration into why females seem to be better protected against adverse remodelling, a factor that could unlock critical insights into protective mechanisms and potential therapeutic targets.

6.2 The importance of cardiac aging research

Given the critical role of cardiac aging as a major risk factor for the development of cardiac dysfunction, poor clinical outcomes following cardiac events, and the progression to heart failure, it is essential to characterize this process in detail. While chronological aging has been clearly associated with a deterioration in cardiac function, these age-related modifications are not uniform across individuals. The rate of deterioration is influenced by both genetic and environmental factors, making it challenging to isolate intrinsic aging-related mechanisms in humans (324, 325). Preclinical assessments of cardiac aging are thus crucial, as they allow for the investigation of these intrinsic

mechanisms within a controlled environment, minimizing genetic variability (324). In-depth rodent studies, although limited by cost and time constraints, help mitigate some of these challenges and provide valuable insights into natural cardiac aging (325).

Additionally, given the high degree of conservation in the ECM, particularly collagen, across species, aging research in rodents offers a significant opportunity to study cardiac aging with potential direct relevance to human aging (326). Furthermore, advancements in techniques for measuring ECM dynamics, such as the utilization of PET imaging, now enable longitudinal assessment of aging cohorts in a non-invasive manner. These techniques allow for the sensitive measurement of ECM processes through specific targets, and this project leveraged these tools to assess collagen metabolism *in vivo*.

6.3 Hypotheses and Key Findings

This PhD thesis set out to explore the hypothesis that aging disrupts cardiac collagen metabolism, leading to a decrease in collagen synthesis despite significant collagen accumulation. Furthermore, it hypothesized that both collagen synthesis and accumulation would be higher in males compared to females. These hypotheses were tested through both *in vivo* and *in vitro* models of cardiac aging. Specifically, this thesis characterized the *in vivo* effects of aging in both male and female Sprague Dawley rats, providing comprehensive measurements of cardiovascular health. Collagen synthesis was assessed both *in vitro* and *in vivo* using PET radiotracers, *cis*-4-^{18}F-fluoro-*L*-proline and *trans*-4-^{18}F-fluoro-*L*-proline. A summary of the key findings from this PhD project is shown in Figure 6.1.

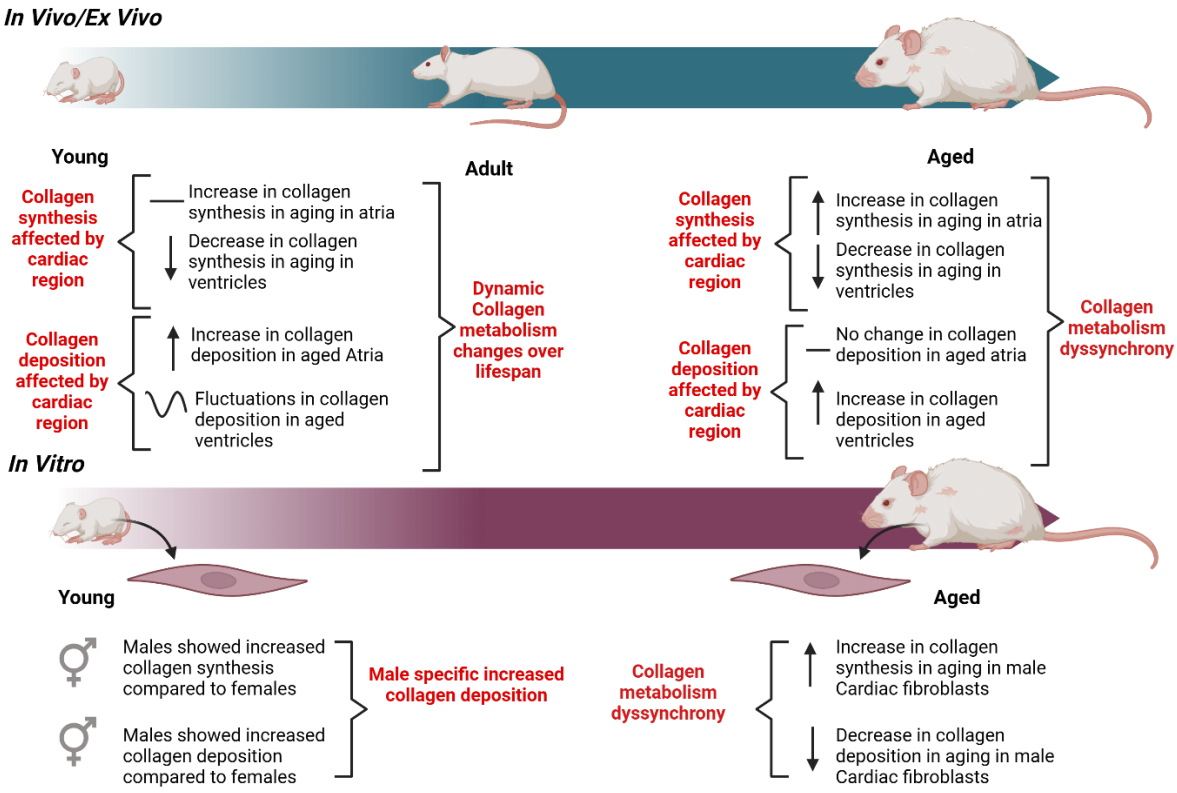

Figure 6. 1 Summary of key findings across this PhD project. Figure created using Biorender.

The selection of these radiotracers was informed by previous work by Balogh *et al*. and Reid et al., who had employed [^{18}F]fluoroproline radiotracers to measure collagen synthesis (135, 142, 162, 165). However, the uptake mechanisms are not yet fully characterised. Nevertheless, strong evidence from previous *in vivo* preclinical and clinical studies—primarily involving *cis*-[^{18}F]-fluoro-*L*-proline in the liver and heart—supports their relevance(136, 235, 327). These studies identified that fluoroproline PET tracers did not correlate directly with deposited collagen and attributed to this to the tracers measuring active collagen *in vivo*(235). Additionally, emerging data suggest the potential utility of *trans*-[^{18}F]-fluoro-*L*-proline in cardiac fibrosis in models of pressure overload (162).This approach addresses a significant challenge in collagen research, as measuring collagen synthesis has traditionally relied on mRNA in the tissue *(ex vivo)* or proxy measures like PIP in the blood. While useful, these proxies provide a limited view, as they focus on specific collagen types rather than capturing the overall rate of collagen synthesis (247). Although fluoroproline radiotracers were originally developed in the 1960s, their utility had been limited due to synthesis impurities and lack of targeted applications

(153). However, advancements in radiosynthesis methodology and recent applications in fibrosis models, such as myocardial infarction and angiotensin II-mediated pressure overload have revitalized their potential for assessing collagen metabolism (142, 161, 162). In addition to the use of PET radiotracers, collagen accumulation was measured using classical biochemical assays and histological analysis to evaluate the effect of aging on collagen deposition and explore whether these changes were sex-dependent. This multi-faceted approach aimed to provide a more complete understanding of the interplay between aging, collagen metabolism, and sex differences.

At 18 months, both male and female Sprague Dawley rats exhibited increased frailty, indicative of advanced biological aging, a finding that contrasts with the prevailing literature suggesting advanced aging typically occurs between 2 and 3 years of age (187, 188). Cardiovascular parameters such as blood pressure and cardiac volume remained within the 'healthy' range, yet males displayed a notable reduction in EF, likely driven by increased cardiac stiffening, a phenomenon consistently observed in aging male rats (190). Although Chapter 2 did not directly investigate collagen metabolism, it addressed a significant gap by providing a comprehensive longitudinal assessment of natural aging up to 18 months in both sexes, a timeframe for which well-reported data remains limited. These findings establish essential physiological context for interpreting later observations on collagen metabolism. Additionally, the study supports the suitability of Sprague Dawley rats for modelling cardiac aging, as they exhibited fewer signs of dysfunction compared to other rodent strains (213).

The third chapter demonstrated that aging was associated with a decline in *cis*-4-^{18}F-fluoro-*L*-proline and *trans*-4-^{18}F-fluoro-*L*-proline uptake by 12 months, indicating a downregulation of both hydroxylated and unhydroxylated collagen synthesis. This aligns with previous studies utilizing mRNA or [^{14}C]Proline (61, 244). But the longitudinal design of this study uniquely captured dynamic changes in early collagen synthesis, a process not previously well-characterized. The high sensitivity of the PET tracers enabled the detection of subtle yet significant alterations in collagen metabolism, addressing a critical limitation of aging research, which often requires large sample sizes and sensitive methodologies to detect meaningful physiological changes. Importantly, while much of the existing research focuses on pathophysiological aging, this study contributes valuable data on 'healthy' aging mechanisms. Contrary to earlier mRNA studies, no significant sex-specific differences in collagen synthesis were observed (234). Collagen accumulation increased with age in both sexes, with males exhibiting significantly greater deposition by 12 months. Unexpectedly, a decline in collagen accumulation was observed at 18 months, challenging the conventional view of a linear increase with age. This may reflect intrinsic, 'healthy' aging processes, as no overt signs of cardiac dysfunction were

observed in this cohort. Although the study was constrained by termination at 18 months due to welfare considerations and time constraints, it provides critical insights into early aging processes, often overlooked in favour of pathophysiological models.

A key finding of this study is that ventricular fibrotic mechanisms in aging differ from those observed in injury models. While injury models typically show an upregulation of collagen synthesis, our results indicated a reduction in collagen synthesis with aging, corroborated by previous unpublished data from our group and other studies (246). Furthermore, we observed a dyssynchrony between collagen synthesis and deposition, suggesting that collagen degradation processes may be disrupted, contributing to increased collagen accumulation. Notably, collagen crosslinking was found to be elevated. These results largely support the hypothesis that aging disrupts cardiac collagen metabolism, evidenced by decreased uptake of cis- and trans-4-18F-fluoro-L-proline. While we expected males to exhibit higher collagen synthesis than females, this hypothesis was not supported, as no significant sex-specific differences were detected. However, males did demonstrate greater collagen accumulation than females, partially aligning with the hypothesis regarding sex-specific variations in collagen metabolism.

The fourth chapter examined collagen metabolism within the atria, revealing a significant increase in both *cis*-4-^{18}F-fluoro-*L*-proline and *trans*-4-^{18}F-fluoro-*L*-proline uptake with aging. To our knowledge, this is the first study to identify divergent effects of aging on atrial versus ventricular collagen synthesis, underscoring the importance of considering both cardiac chambers in aging research. Interestingly, despite the increased collagen synthesis, no corresponding accumulation was observed, leading to the hypothesis that the atria may exhibit enhanced collagen turnover with aging. This hypothesis is supported by the detection of increased soluble collagen in aged male samples, which aligns with the proposed mechanism of fibrosis leading to tissue expansion (289).

Finally, we investigated the effects of aging on cFbs, the primary cells responsible for collagen metabolism in the heart (Chapter 5). Our *in vitro* experiments revealed that unhydroxylated collagen synthesis was influenced by both age and sex, whereas hydroxylated collagen synthesis was predominantly age-dependent. In young female cFbs, we observed a significantly lower level of collagen synthesis and deposition, consistent with established collagen dynamics in females. Notably, aged cells demonstrated reduced collagen deposition despite elevated synthesis rates, indicating a dysregulation in collagen metabolism in male cells. These finding parallels previous research highlighting inefficient scar formation in aged patients' post-cardiac injury (328).

While we aimed to characterize the effects of inhibiting AGEs formation using ALT-711, we found no significant impact on collagen synthesis or deposition. Challenges in culturing aging cells resulted in low cell numbers, limiting the assessment of AGEs and restricting exploration of the effects of aging on female cells due to contamination in the culture of the aged female animals. Overall, the results support the hypothesis that aging disrupts cardiac collagen metabolism, as evidenced by reduced collagen deposition in aged male fibroblasts. However, while the expected reduction in collagen synthesis and deposition was confirmed in young female cells, the predominant effect of aging on hydroxylated collagen synthesis was observed across both sexes. These findings suggest that aging fibroblasts exhibit characteristics resembling those seen in cardiac remodelling following injury, highlighting the need for further investigation into the underlying mechanisms of collagen dysregulation.

6.4 Limitations of the study

This thesis acknowledges several limitations in assessing age- and sex-related changes in collagen metabolism, which should be considered when interpreting the findings. First, the study's design lacked longitudinal cardiac function data beyond terminal time points. Measurement intervals were chosen to capture critical developmental and reproductive phases in rodents—early development, adolescence, adulthood, and post-reproductive stages—that coincide with shifts in cardiac ECM remodelling. However, gaps between these intervals may have missed significant time points, potentially obscuring dynamic age-related changes. Jackson *et al.* underscore this issue in aging research, as increased variability and compromised findings often result from insufficient attention to system-specific development and cellular aging (329).

Further, stress-induced variability in BP data due to tail-cuff plethysmography highlights the limitations in tracking physiological changes *in vivo*. Hormonal confirmation of reproductive phases was also absent, relying instead on reproductive life stage estimation. Ongoing mass spectrometry analyses of sex organs and blood samples may provide additional information on reproductive status, which could add critical context to understanding sex differences in collagen turnover and the aging process.

Another technical limitation exists in the use of CT measurements for heart size, which provided a composite view without distinguishing diastolic and systolic phases. While these measures were normalized to body weight—a standard in clinical and preclinical settings (183)—this approach

assumes isometric growth and may not be accurate for metabolic variations, as observed in cases of obesity. For the Sprague Dawley cohort, given its potential metabolic variability, an allometric scaling approach might have improved the accuracy of these measurements.

The PET aspect of the imaging study faced certain limitations. Notably, there was limited indication of specific uptake of PET tracers, no definitive proof of incorporation into collagen, and no observed competition uptake *in vitro*. Furthermore, the use of a static method for analysing PET images—relying on a template derived from an *ex vivo* heart—had inherent constraints, particularly the potential to overlook smaller chambers such as the atria and right ventricle. However, given the experimental conditions, this approach remained the most rigorous method available for analysing the dataset. Finally, the inability to control for reproductive cycle stages in females may have introduced variability in collagen production, though observed data variability was generally low, suggesting minimal impact from this factor. We also could not confirm reproductive senescence in female subjects, leading to uncertainty in attributing observed effects to post-menopausal changes. Additionally, loss of animals at the final time point may have underpowered the study, limiting the ability to detect sex differences reliably—a challenge noted in studies where high variability and low dysfunction necessitate greater statistical power (240).

The study also faced limitations in cellular characterization, particularly in aged cFbs. Due to time and preliminary data constraints, as well as low cell yields from aged hearts, comprehensive phenotyping and quantification was not achieved, which would have clarified the impact of aging on fibroblast activation and morphological changes. Literature indicates that fibroblast activation increases with age and is associated with periostin and αSMA upregulation, suggesting a shift toward heightened fibrotic activity in aging (310). Previous studies have identified up to six fibroblast subpopulations ; thus, co-staining analysis for cell-specific markers, such as CD45+ cells, would have better captured these distinct cell lineages and their unique roles in collagen homeostasis (300). Furthermore, assessment of cellular senescence was not conducted and would provide key information regarding the functional capacity would be essential for future studies.

Despite these limitations, careful assessment of intragroup variability against expected collagen turnover within the imaging timeframe, alongside the high sensitivity of PET imaging and radiotracers' capability to capture both hydroxylated and unhydroxylated collagen synthesis, supports the robustness of our observations. Addressing these limitations in future studies—particularly through enhanced cellular profiling, hormonal status verification, and refined functional cardiac measures—will be vital to deepen the insights presented in this work. However, the absence of longitudinal

cardiac function data beyond the terminal time points and the high variability in blood pressure measurements, influenced by stress-induced artifacts from tail cuff plethysmography, were limitations to consider.

6.5 Future work and clinical implications

This study addressed several unknowns regarding collagen metabolism in aging, yet critical aspects remain unexplored. Notably, we did not investigate collagen degradation—a vital process in collagen homeostasis that likely influences collagen accumulation with age (262, 263). A longitudinal *in vivo* study focusing on overall MMP activity, rather than isolated MMPs as in previous studies, could reveal broader degradation dynamics in aging. Utilizing tracers like ^{64}Cu-RYM2, which enables imaging of MMP activity across the cardiac ECM, would provide valuable insights into age-related degradation shifts (173). Complementary classical assays, such as gelatine zymography, could offer detailed quantitative data, creating a more comprehensive understanding of collagen degradation processes in aged Sprague Dawley rats. This would pave the way for establishing a reference framework for cardiac collagen metabolism in aging, which is currently lacking.

Furthermore, assessment of skeletal muscle collagen synthesis and its age-related changes would provide valuable insights into the broader physiological implications of collagen turnover across different tissues. Investigating skeletal muscle collagen metabolism alongside other tissues could develop our understanding of age-associated connective tissue remodelling, revealing tissue-specific differences in collagen synthesis rates, regulatory mechanisms, and responses to therapeutic interventions. Future studies employing [^{18}F]Fluoroprolines could extend these findings by assessing skeletal muscle collagen dynamics, contributing to a more comprehensive view of age-related extracellular matrix changes.

Additionally, combining collagen metabolism tracers, such as ^{68}Ga-FAPI, in tandem with [^{18}F]fluoroproline radiotracers would allow for detailed analysis of cardiac fibroblast activation and its impact on collagen turnover. This approach could illuminate the role of fibroblast activation in aging—an area currently underexplored but increasingly recognized for its significance in MI and HF patients and animals' models (143). Characterizing these mechanisms in aging models could provide foundational insights for potential anti-fibrotic therapies and deepen our understanding of ECM remodelling's role in age-related cardiac dysfunction, ultimately expanding therapeutic options in aging populations.

This project, alongside prior work in preclinical models of cardiac injury, has underscored the translational promise of [^{18}F]fluoroproline radiotracers (162). Both tracers exhibited consistent patterns of uptake in aging models, and in models of pressure overload, they showed differential uptake, highlighting their ability to sensitively distinguish various types of collagen synthesis (162, 235). However, it is important to note that once again a clear mechanism of uptake has yet to be published. This distinction suggests potential diagnostic and prognostic applications for collagen fibrosis in clinical settings, particularly for patients with CF.

While the diagnostic application of these tracers for aging clinically may be challenging—since aging itself is not classified as a disease—they nonetheless offer a valuable opportunity to investigate changes in cardiac collagen synthesis *in vivo*. This area has yet to be systematically explored in humans but could yield clinically relevant insights. The recent advent of Total Body PET (TB-PET) scanners enhances this potential, as they enable high-resolution, whole-body imaging that captures age-related physiological changes in real time. By facilitating a comprehensive analysis of fibrotic processes across multiple organ systems under natural physiological conditions, TB-PET provides an in-depth view into the systemic effects of aging on collagen metabolism. This capability holds significant implications for studying age-related fibrosis, particularly in understanding how collagen synthesis and degradation are coordinated—or uniquely varied—among organs such as the heart, lungs, kidneys, and liver. Through TB-PET imaging, it may be possible to discern distinct patterns of collagen turnover and fibrosis progression specific to aging, potentially linked to systemic factors like inflammation, hormonal changes, and metabolic alterations. Importantly, these insights could refine our understanding of cardiac fibrosis within the broader aging context, suggesting new, multi-organ therapeutic targets that account for the complex interplay between aging, collagen metabolism, and fibrotic disease development.

In future studies, applying TB-PET in longitudinal analyses of aging populations could reveal biomarkers predictive of fibrotic progression, contributing not only to fibrosis research but also to geriatric medicine and healthy aging strategies. Detecting significant changes in collagen synthesis even in the absence of overt dysfunction highlights the critical synthetic shifts occurring with age. This capability to detect subclinical alterations emphasizes the diagnostic potential of these tracers for early intervention. Our findings suggest that collagen synthesis and accumulation become dysregulated with age, aligning with existing literature and underscoring the need for further patient-based studies to deepen our understanding of these age-related changes. Expanding this research to

include diverse age groups could help identify early metabolic shifts that may serve as therapeutic targets, potentially delaying or preventing the progression of age-related cardiac fibrosis.

Understanding healthy aging in humans is essential in tackling age-related diseases, particularly CF, as it allows us to identify precise targets for therapeutic intervention and to determine optimal intervention points. Characterizing age-dependent shifts in collagen metabolism across the lifespan would enable us to pinpoint when in the aging process treatments could effectively mitigate dysregulated collagen deposition and, ultimately, fibrosis. Such insights could guide the development of therapies that aim not only to address established cardiac fibrosis but also to intervene pre-emptively, maintaining ECM balance and healthy cardiac function over time.

6.6 Conclusion

This thesis provides conclusive evidence that cardiac collagen metabolism undergoes significant dysregulation with aging, emphasizing the importance of using age-relevant models to study cardiac diseases. Through the application of advanced imaging techniques, such as PET imaging, this work demonstrates novel insights into collagen protein synthesis across the heart's chambers. The findings reveal dynamic, chamber-specific changes in collagen metabolism with aging, including increased collagen synthesis in the atria without net accumulation, suggesting enhanced collagen turnover, in contrast to the ventricles.

These results underscore the complexity of age-related remodeling processes and highlight the challenges in translating findings from young animal models to aged populations. Notably, the lack of distinct sex-specific differences in collagen synthesis observed here underscores the need for further investigation into hormonal and physiological influences on aging processes. Moreover, the challenges encountered with in vitro aging models, including sex-based differences and cell culturing variability, reflect the inherent intricacies of studying fibroblast behavior and extracellular matrix (ECM) dynamics in aging.

This research contributes to the understanding of cardiac aging and lays a foundation for future studies to explore baseline physiological changes across sexes and optimize cardiac injury models in aged animals. Investigating mechanisms of collagen degradation and refining experimental models to account for hormonal influences will be critical for unraveling the complexities of aging in cardiac

pathology. Ultimately, these efforts could lead to more effective therapeutic strategies for addressing age-related cardiac dysfunction, improving outcomes for aging populations.

References

1. (BHF) BHF. Global Heart & Circulatory Diseases Factsheet United Kingdom 2024 [Available from: https://www.bhf.org.uk/-/media/files/for-professionals/research/heart-statistics/bhf-cvd-statistics-global-factsheet.pdf?rev=ee25ba7e8aea4c1cb057af4cfd66d4b3&hash=9EF0A4CF1541E28747390514C7100F38.
2. Groenewegen A, Rutten FH, Mosterd A, Hoes AW. Epidemiology of heart failure. European Journal of Heart Failure. 2020;22(8):1342-56.
3. James SL, Abate D, Abate KH, Abay SM, Abbafati C, Abbasi N, et al. Global, regional, and national incidence, prevalence, and years lived with disability for 354 diseases and injuries for 195 countries and territories, 1990–2017: a systematic analysis for the Global Burden of Disease Study 2017. The Lancet. 2018;392(10159):1789-858.
4. Yazdanyar A, Newman AB. The burden of cardiovascular disease in the elderly: morbidity, mortality, and costs. Clin Geriatr Med. 2009;25(4):563-77, vii.
5. Humeres C, Frangogiannis NG. Fibroblasts in the infarcted, remodeling, and failing heart. JACC: Basic to Translational Science. 2019;4(3):449-67.
6. Aoki T, Fukumoto Y, Sugimura K, Oikawa M, Satoh K, Nakano M, et al. Prognostic Impact of Myocardial Interstitial Fibrosis in Non-Ischemic Heart Failure–Comparison Between Preserved and Reduced Ejection Fraction Heart Failure–. Circulation journal. 2011:1108041373-.
7. Kannel WB. Risk stratification in hypertension: new insights from the Framingham Study. Am J Hypertens. 2000;13(1 Pt 2):3s-10s.
8. Christiansen MN, Køber L, Weeke P, Vasan RS, Jeppesen JL, Smith JG, et al. Age-specific trends in incidence, mortality, and comorbidities of heart failure in Denmark, 1995 to 2012. Circulation. 2017;135(13):1214-23.
9. Dworatzek E, Baczko I, Kararigas G. Effects of aging on cardiac extracellular matrix in men and women. PROTEOMICS–Clinical Applications. 2016;10(1):84-91.
10. Lawson CA, Zaccardi F, Squire I, Ling S, Davies MJ, Lam CS, et al. 20-year trends in cause-specific heart failure outcomes by sex, socioeconomic status, and place of diagnosis: a population-based study. The Lancet Public Health. 2019;4(8):e406-e20.
11. Rajendran A, Minhas AS, Kazzi B, Varma B, Choi E, Thakkar A, Michos ED. Sex-specific differences in cardiovascular risk factors and implications for cardiovascular disease prevention in women. Atherosclerosis. 2023;384:117269.
12. Cleutjens JP. The role of matrix metalloproteinases in heart disease. Cardiovascular research. 1996;32(5):816-21.
13. Lindsey ML, Goshorn DK, Squires CE, Escobar GP, Hendrick JW, Mingoia JT, et al. Age-dependent changes in myocardial matrix metalloproteinase/tissue inhibitor of metalloproteinase profiles and fibroblast function. Cardiovascular research. 2005;66(2):410-9.
14. Meschiari CA, Ero OK, Pan H, Finkel T, Lindsey ML. The impact of aging on cardiac extracellular matrix. Geroscience. 2017;39:7-18.
15. Kennedy BK, Berger SL, Brunet A, Campisi J, Cuervo AM, Epel ES, et al. Aging: a common driver of chronic diseases and a target for novel interventions. Cell. 2014;159(4):709.
16. Wynn TA, Ramalingam TR. Mechanisms of fibrosis: therapeutic translation for fibrotic disease. Nature medicine. 2012;18(7):1028-40.
17. Jansen HJ, Moghtadaei M, Mackasey M, Rafferty SA, Bogachev O, Sapp JL, et al. Atrial structure, function and arrhythmogenesis in aged and frail mice. Scientific Reports. 2017;7(1):44336.
18. Jugdutt BI. Ventricular remodeling after infarction and the extracellular collagen matrix: when is enough enough? Circulation. 2003;108(11):1395-403.

19. Litviňuková M, Talavera-López C, Maatz H, Reichart D, Worth CL, Lindberg EL, et al. Cells of the adult human heart. Nature. 2020;588(7838):466-72.
20. Frangogiannis NG. The extracellular matrix in myocardial injury, repair, and remodeling. The Journal of clinical investigation. 2017;127(5):1600-12.
21. Talman V, Ruskoaho H. Cardiac fibrosis in myocardial infarction—from repair and remodeling to regeneration. Cell and tissue research. 2016;365(3):563-81.
22. Wilson CG, Stone JW, Fowlkes V, Morales MO, Murphy CJ, Baxter SC, Goldsmith EC. Age-dependent expression of collagen receptors and deformation of type I collagen substrates by rat cardiac fibroblasts. Microscopy and Microanalysis. 2011;17(4):555-62.
23. Stephens EH, Grande-Allen KJ. Age-related changes in collagen synthesis and turnover in porcine heart valves. The Journal of heart valve disease. 2007;16(6):672-82.
24. Horn MA, Graham HK, Richards MA, Clarke JD, Greensmith DJ, Briston SJ, et al. Age-related divergent remodeling of the cardiac extracellular matrix in heart failure: collagen accumulation in the young and loss in the aged. Journal of molecular and cellular cardiology. 2012;53(1):82-90.
25. Dworatzek E, Mahmoodzadeh S, Schriever C, Kusumoto K, Kramer L, Santos G, et al. Sex-specific regulation of collagen I and III expression by 17β-Estradiol in cardiac fibroblasts: role of estrogen receptors. Cardiovasc Res. 2019;115(2):315-27.
26. EGHBALI M, EGHBALI M, ROBINSON TF, SEIFTER S, BLUMENFELD OO. Collagen accumulation in heart ventricles as a function of growth and aging. Cardiovascular research. 1989;23(8):723-9.
27. Bujak M, Kweon HJ, Chatila K, Li N, Taffet G, Frangogiannis NG. Aging-related defects are associated with adverse cardiac remodeling in a mouse model of reperfused myocardial infarction. Journal of the American College of Cardiology. 2008;51(14):1384-92.
28. Cieslik KA, Trial J, Entman ML. Defective myofibroblast formation from mesenchymal stem cells in the aging murine heart rescue by activation of the AMPK pathway. Am J Pathol. 2011;179(4):1792-806.
29. Biernacka A, Frangogiannis NG. Aging and cardiac fibrosis. Aging and disease. 2011;2(2):158.
30. New SEP, Aikawa E. Cardiovascular calcification-an inflammatory disease. Circulation Journal. 2011;75(6):1305-13.
31. Kajstura J, Cheng W, Sarangarajan R, Li P, Li B, Nitahara JA, et al. Necrotic and apoptotic myocyte cell death in the aging heart of Fischer 344 rats. American Journal of Physiology-Heart and Circulatory Physiology. 1996;271(3):H1215-H28.
32. Kung G, Konstantinidis K, Kitsis RN. Programmed necrosis, not apoptosis, in the heart. Circulation research. 2011;108(8):1017-36.
33. Mirza M, Strunets A, Shen W-K, Jahangir A. Mechanisms of arrhythmias and conduction disorders in older adults. Clinics in geriatric medicine. 2012;28(4):555-73.
34. Dzeshka MS, Lip GY, Snezhitskiy V, Shantsila E. Cardiac fibrosis in patients with atrial fibrillation: mechanisms and clinical implications. Journal of the American College of Cardiology. 2015;66(8):943-59.
35. Strait JB, Lakatta EG. Aging-associated cardiovascular changes and their relationship to heart failure. Heart failure clinics. 2012;8(1):143-64.
36. Debessa CRG, Maifrino LBM, de Souza RR. Age related changes of the collagen network of the human heart. Mechanisms of ageing and development. 2001;122(10):1049-58.
37. Sun B. The mechanics of fibrillar collagen extracellular matrix. Cell Reports Physical Science. 2021;2(8).
38. Karamanos NK, Theocharis AD, Piperigkou Z, Manou D, Passi A, Skandalis SS, et al. A guide to the composition and functions of the extracellular matrix. The FEBS journal. 2021;288(24):6850-912.
39. Stamov DR, Pompe T. Structure and function of ECM-inspired composite collagen type I scaffolds. Soft Matter. 2012;8(40):10200-12.

40. Hortells L, Johansen AKZ, Yutzey KE. Cardiac fibroblasts and the extracellular matrix in regenerative and nonregenerative hearts. Journal of cardiovascular development and disease. 2019;6(3):29.
41. Achkar A, Saliba Y, Fares N. Differential gender-dependent patterns of cardiac fibrosis and fibroblast phenotypes in aging mice. Oxidative medicine and cellular longevity. 2020;2020(1):8282157.
42. Aisagbonhi O, Rai M, Ryzhov S, Atria N, Feoktistov I, Hatzopoulos AK. Experimental myocardial infarction triggers canonical Wnt signaling and endothelial-to-mesenchymal transition. Disease models & mechanisms. 2011;4(4):469-83.
43. Möllmann H, Nef HM, Kostin S, von Kalle C, Pilz I, Weber M, et al. Bone marrow-derived cells contribute to infarct remodelling. Cardiovascular research. 2006;71(4):661-71.
44. Watanabe T, Akishita M, He H, Miyahara Y, Nagano K, Nakaoka T, et al. 17β-Estradiol inhibits cardiac fibroblast growth through both subtypes of estrogen receptor. Biochemical and biophysical research communications. 2003;311(2):454-9.
45. Horn MA, Trafford AW. Aging and the cardiac collagen matrix: Novel mediators of fibrotic remodelling. Journal of molecular and cellular cardiology. 2016;93:175-85.
46. Eyre DR, Paz MA, Gallop PM. Cross-linking in collagen and elastin. Annual review of biochemistry. 1984;53(1):717-48.
47. López Ba, González A, Díez J. Circulating biomarkers of collagen metabolism in cardiac diseases. Circulation. 2010;121(14):1645-54.
48. Hartog JW, Voors AA, Bakker SJ, Smit AJ, van Veldhuisen DJ. Advanced glycation end-products (AGEs) and heart failure: pathophysiology and clinical implications. European journal of heart failure. 2007;9(12):1146-55.
49. López B, Querejeta R, González A, Beaumont J, Larman M, Díez J. Impact of treatment on myocardial lysyl oxidase expression and collagen Cross-linking in patients with heart failure. Hypertension. 2009;53(2):236-42.
50. Horn MA. Cardiac physiology of aging: extracellular considerations. Comprehensive Physiology. 2011;5(3):1069-121.
51. LeBar K, Wang Z. Extracellular Matrix in Cardiac Tissue Mechanics and Physiology: Role of Collagen Accumulation. Extracellular Matrix-Developments and Therapeutics. 2021.
52. Tracy E, Rowe G, LeBlanc AJ. Cardiac tissue remodeling in healthy aging: the road to pathology. American Journal of Physiology-Cell Physiology. 2020;319(1):C166-C82.
53. Ribeiro ASF, Zerolo BE, López-Espuela F, Sánchez R, Fernandes VS. Cardiac system during the aging process. Aging and disease. 2023;14(4):1105.
54. Sasaki T, Göhring W, Mann K, Maurer P, Hohenester E, Knäuper V, et al. Limited cleavage of extracellular matrix protein BM-40 by matrix metalloproteinases increases its affinity for collagens. Journal of Biological Chemistry. 1997;272(14):9237-43.
55. Zile MR, Baicu CF, Stroud RE, Van Laer AO, Jones JA, Patel R, et al. Mechanistic relationship between membrane type-1 matrix metalloproteinase and the myocardial response to pressure overload. Circulation: Heart Failure. 2014;7(2):340-50.
56. Brew K, Dinakarpandian D, Nagase H. Tissue inhibitors of metalloproteinases: evolution, structure and function. Biochimica et Biophysica Acta (BBA)-Protein Structure and Molecular Enzymology. 2000;1477(1-2):267-83.
57. Grilo GA, Shaver PR, Stoffel HJ, Morrow CA, Johnson OT, Iyer RP, de Castro Brás LE. Age-and sex-dependent differences in extracellular matrix metabolism associate with cardiac functional and structural changes. Journal of molecular and cellular cardiology. 2020;139:62-74.
58. Cappelli V, Forni R, Poggesi C, Reggiani C, Ricciardi L. Age-dependent variations of diastolic stiffness and collagen content in rat ventricular myocardium. Archives internationales de physiologie et de biochimie. 1984;92(2):93-106.

59. Jugdutt BI, Jelani A, Palaniyappan A, Idikio H, Uweira RE, Menon V, Jugdutt CE. Aging-related early changes in markers of ventricular and matrix remodeling after reperfused ST-segment elevation myocardial infarction in the canine model: effect of early therapy with an angiotensin II type 1 receptor blocker. Circulation. 2010;122(4):341-51.
60. Raya TE, Gaballa M, Anderson P, Goldman S. Left ventricular function and remodeling after myocardial infarction in aging rats. American Journal of Physiology-Heart and Circulatory Physiology. 1997;273(6):H2652-H8.
61. Mays P, McANULTY RJ, Campa JS, Laurent GJ. Age-related changes in collagen synthesis and degradation in rat tissues. Importance of degradation of newly synthesized collagen in regulating collagen production. Biochemical Journal. 1991;276(2):307-13.
62. Annoni G, Luvarà G, Arosio B, Gagliano N, Fiordaliso F, Santambrogio D, et al. Age-dependent expression of fibrosis-related genes and collagen deposition in the rat myocardium. Mechanisms of ageing and development. 1998;101(1-2):57-72.
63. Thomas DP, Zimmerman SD, Hansen TR, Martin DT, McCormick RJ. Collagen gene expression in rat left ventricle: interactive effect of age and exercise training. Journal of Applied Physiology. 2000;89(4):1462-8.
64. Chiao YA, Ramirez TA, Zamilpa R, Okoronkwo SM, Dai Q, Zhang J, et al. Matrix metalloproteinase-9 deletion attenuates myocardial fibrosis and diastolic dysfunction in ageing mice. Cardiovascular research. 2012;96(3):444-55.
65. Mays PK, Bishop JE, Laurent GJ. Age-related changes in the proportion of types I and III collagen. Mechanisms of ageing and development. 1988;45(3):203-12.
66. Besse S, Robert V, Assayag Pa, Delcayre C, Swynghedauw B. Nonsynchronous changes in myocardial collagen mRNA and protein during aging: effect of DOCA-salt hypertension. American Journal of Physiology-Heart and Circulatory Physiology. 1994;267(6):H2237-H44.
67. Bradshaw AD, Baicu CF, Rentz TJ, Van Laer AO, Bonnema DD, Zile MR. Age-dependent alterations in fibrillar collagen content and myocardial diastolic function: role of SPARC in post-synthetic procollagen processing. American Journal of Physiology-Heart and Circulatory Physiology. 2010;298(2):H614-H22.
68. Cieslik KA, Taffet GE, Carlson S, Hermosillo J, Trial J, Entman ML. Immune-inflammatory dysregulation modulates the incidence of progressive fibrosis and diastolic stiffness in the aging heart. Journal of molecular and cellular cardiology. 2011;50(1):248-56.
69. Rahkonen O, Su M, Hakovirta H, Koskivirta I, Hormuzdi SG, Vuorio E, et al. Mice with a deletion in the first intron of the Col1a1 gene develop age-dependent aortic dissection and rupture. Circulation research. 2004;94(1):83-90.
70. Du X-J, Samuel CS, Gao X-M, Zhao L, Parry LJ, Tregear GW. Increased myocardial collagen and ventricular diastolic dysfunction in relaxin deficient mice: a gender-specific phenotype. Cardiovascular research. 2003;57(2):395-404.
71. Masutomo K, Makino N, Sugano M, Miyamoto S, Hata T, Yanaga T. Extracellular matrix regulation in the development of Syrian cardiomyopathic Bio 14.6 and Bio 53.58 hamsters. Journal of molecular and cellular cardiology. 1999;31(9):1607-15.
72. Burgess ML, McCrea JC, Hedrick HL. Age-associated changes in cardiac matrix and integrins. Mechanisms of ageing and development. 2001;122(15):1739-56.
73. Wagner JU, Chavakis E, Rogg E-M, Muhly-Reinholz M, Glaser SF, Günther S, et al. Switch in laminin β2 to laminin β1 isoforms during aging controls endothelial cell functions—brief report. Arteriosclerosis, thrombosis, and vascular biology. 2018;38(5):1170-7.
74. Deckx S, Heggermont W, Carai P, Rienks M, Dresselaers T, Himmelreich U, et al. Osteoglycin prevents the development of age-related diastolic dysfunction during pressure overload by reducing cardiac fibrosis and inflammation. Matrix Biology. 2018;66:110-24.

75. Wang FF, Han YF, Liang XY, Zhang GG, Lu YM, Li YD, Tang BP. Aging-induced atrial fibrosis in If current change and its effect on atrial fibrillation in dogs. Annals of Noninvasive Electrocardiology. 2022;27(4):e12951.
76. de Castro Brás LE, Toba H, Baicu CF, Zile MR, Weintraub ST, Lindsey ML, Bradshaw AD. Age and SPARC change the extracellular matrix composition of the left ventricle. BioMed research international. 2014;2014(1):810562.
77. Mendes A, Ferro M, Rodrigues B, Souza Md, Araujo RC, Souza Rd. Quantification of left ventricular myocardial collagen system in children, young adults, and the elderly. Medicina (B Aires). 2012;72(3):216-20.
78. Chiao YA, Dai Q, Zhang J, Lin J, Lopez EF, Ahuja SS, et al. Multi-analyte profiling reveals matrix metalloproteinase-9 and monocyte chemotactic protein-1 as plasma biomarkers of cardiac aging. Circulation: Cardiovascular Genetics. 2011;4(4):455-62.
79. Nguyen NT, Yabluchanskiy A, de Castro Brás LE, Jin Y-F, Lindsey ML. Aging-related changes in extracellular matrix: implications for ventricular remodeling following myocardial infarction. Aging and Heart Failure: Mechanisms and Management. 2014:377-89.
80. Thomas DP, McCormick RJ, Zimmerman SD, Vadlamudi RK, Gosselin LE. Aging-and training-induced alterations in collagen characteristics of rat left ventricle and papillary muscle. American Journal of Physiology-Heart and Circulatory Physiology. 1992;263(3):H778-H83.
81. Oneglia A, Nelson MD, Merz CNB. Sex differences in cardiovascular aging and heart failure. Current heart failure reports. 2020;17:409-23.
82. Gazoti Debessa CR, Mesiano Maifrino LB, Rodrigues de Souza R. Age related changes of the collagen network of the human heart. Mechanisms of Ageing and Development. 2001;122(10):1049-58.
83. Angello JC, Pendergrass WR, Norwood TH, Prothero J. Proliferative potential of human fibroblasts: an inverse dependence on cell size. Journal of cellular physiology. 1987;132(1):125-30.
84. Chen W, Frangogiannis NG. The role of inflammatory and fibrogenic pathways in heart failure associated with aging. Heart failure reviews. 2010;15(5):415-22.
85. Miyata T, Sugiyama S, Saito A, Kurokawa K. Reactive carbonyl compounds related uremic toxicity ("carbonyl stress"). Kidney International. 2001;59:S25-S31.
86. Smit AJ, Lutgers H. The clinical relevance of advanced glycation endproducts (AGE) and recent developments in pharmaceutics to reduce AGE accumulation. Current medicinal chemistry. 2004;11(20):2767-84.
87. Dyer DG, Dunn JA, Thorpe SR, Bailie KE, Lyons TJ, McCance DR, Baynes JW. Accumulation of Maillard reaction products in skin collagen in diabetes and aging. The Journal of clinical investigation. 1993;91(6):2463-9.
88. Grilo GA, Shaver PR, Stoffel HJ, Morrow CA, Johnson OT, Iyer RP, de Castro Brás LE. Age- and sex-dependent differences in extracellular matrix metabolism associate with cardiac functional and structural changes. J Mol Cell Cardiol. 2020;139:62-74.
89. Ivey MJ, Tallquist MD. Defining the cardiac fibroblast. Circulation Journal. 2016:CJ-16-1003.
90. Bonnema DD, Webb CS, Pennington WR, Stroud RE, Leonardi AE, Clark LL, et al. Effects of age on plasma matrix metalloproteinases (MMPs) and tissue inhibitor of metalloproteinases (TIMPs). Journal of cardiac failure. 2007;13(7):530-40.
91. Achkar A, Saliba Y, Fares N. Differential Gender-Dependent Patterns of Cardiac Fibrosis and Fibroblast Phenotypes in Aging Mice. Oxidative medicine and cellular longevity. 2020;2020.
92. Dworatzek E, Mahmoodzadeh S, Schriever C, Kusumoto K, Kramer L, Santos G, et al. Sex-specific regulation of collagen I and III expression by 17β-Estradiol in cardiac fibroblasts: role of estrogen receptors. Cardiovascular research. 2019;115(2):315-27.

93. Queirós AM, Eschen C, Fliegner D, Kararigas G, Dworatzek E, Westphal C, et al. Sex-and estrogen-dependent regulation of a miRNA network in the healthy and hypertrophied heart. International journal of cardiology. 2013;169(5):331-8.
94. Angelini A, Ortiz-Urbina J, Trial J, Reddy AK, Malovannaya A, Jain A, et al. Sex-specific Phenotypes in the Aging Mouse Heart and Consequences for Chronic Fibrosis. American Journal of Physiology-Heart and Circulatory Physiology.0(0):null.
95. Xu Y, Arenas IA, Armstrong SJ, Davidge ST. Estrogen modulation of left ventricular remodeling in the aged heart. Cardiovasc Res. 2003;57(2):388-94.
96. Barasch E, Gottdiener JS, Aurigemma G, Kitzman DW, Han J, Kop WJ, Tracy RP. Association between elevated fibrosis markers and heart failure in the elderly: the cardiovascular health study. Circ Heart Fail. 2009;2(4):303-10.
97. Fliegner D, Schubert C, Penkalla A, Witt H, Kararigas G, Dworatzek E, et al. Female sex and estrogen receptor-beta attenuate cardiac remodeling and apoptosis in pressure overload. Am J Physiol Regul Integr Comp Physiol. 2010;298(6):R1597-606.
98. Bustamante M, Garate-Carrillo A, B RI, Garcia R, Carson N, Ceballos G, et al. Unmasking of oestrogen-dependent changes in left ventricular structure and function in aged female rats: a potential model for pre-heart failure with preserved ejection fraction. J Physiol. 2019;597(7):1805-17.
99. Mahmoodzadeh S, Dworatzek E, Fritschka S, Pham TH, Regitz-Zagrosek V. 17beta-Estradiol inhibits matrix metalloproteinase-2 transcription via MAP kinase in fibroblasts. Cardiovasc Res. 2010;85(4):719-28.
100. Zhou L, Shao Y, Huang Y, Yao T, Lu LM. 17beta-estradiol inhibits angiotensin II-induced collagen synthesis of cultured rat cardiac fibroblasts via modulating angiotensin II receptors. Eur J Pharmacol. 2007;567(3):186-92.
101. Pedram A, Razandi M, O'Mahony F, Lubahn D, Levin ER. Estrogen receptor-beta prevents cardiac fibrosis. Mol Endocrinol. 2010;24(11):2152-65.
102. Voloshenyuk TG, Gardner JD. Estrogen improves TIMP-MMP balance and collagen distribution in volume-overloaded hearts of ovariectomized females. Am J Physiol Regul Integr Comp Physiol. 2010;299(2):R683-93.
103. Yatsushiro S, Akamine R, Yamamura S, Hino M, Kajimoto K, Abe K, et al. Quantitative analysis of serum procollagen type I C-terminal propeptide by immunoassay on microchip. PLoS One. 2011;6(4):e18807.
104. Arnold AP, Cassis LA, Eghbali M, Reue K, Sandberg K. Sex hormones and sex chromosomes cause sex differences in the development of cardiovascular diseases. Arteriosclerosis, thrombosis, and vascular biology. 2017;37(5):746-56.
105. Grilo GA, Shaver PR, Stoffel HJ, Morrow CA, Johnson OT, Iyer RP, de Castro Brás LE. Age- and sex-dependent differences in extracellular matrix metabolism associate with cardiac functional and structural changes. Journal of Molecular and Cellular Cardiology. 2020;139:62-74.
106. Kehlet SN, Willumsen N, Armbrecht G, Dietzel R, Brix S, Henriksen K, Karsdal MA. Age-related collagen turnover of the interstitial matrix and basement membrane: Implications of age-and sex-dependent remodeling of the extracellular matrix. PloS one. 2018;13(3):e0194458.
107. Florea VG, Anand IS. Troponin T and plasma collagen peptides in heart failure. Am Heart Assoc; 2012. p. 394-7.
108. Chen W-C, Tran KD, Maisel AS. Biomarkers in heart failure. Heart. 2010;96(4):314-20.
109. Suthahar N, Meijers WC, Silljé HH, de Boer RA. From inflammation to fibrosis—molecular and cellular mechanisms of myocardial tissue remodelling and perspectives on differential treatment opportunities. Current heart failure reports. 2017;14(4):235-50.

110. Anand A, Lee KK, Chapman AR, Ferry AV, Adamson PD, Strachan FE, et al. High-sensitivity cardiac troponin on presentation to rule out myocardial infarction: a stepped-wedge cluster randomized controlled trial. Circulation. 2021;143(23):2214-24.
111. Asher A. A review of endomyocardial biopsy and current practice in England: out of date or underutilised. Br J Cardiol. 2017;24:108-12.
112. King M, Kingery JE, Casey B. Diagnosis and evaluation of heart failure. American family physician. 2012;85(12):1161-8.
113. Marwick TH. Methods used for the assessment of LV systolic function: common currency or tower of Babel? Heart. 2013;99(15):1078-86.
114. Members ATF, Dickstein K, Cohen-Solal A, Filippatos G, McMurray JJ, Ponikowski P, et al. ESC Guidelines for the diagnosis and treatment of acute and chronic heart failure 2008: the Task Force for the Diagnosis and Treatment of Acute and Chronic Heart Failure 2008 of the European Society of Cardiology. Developed in collaboration with the Heart Failure Association of the ESC (HFA) and endorsed by the European Society of Intensive Care Medicine (ESICM). European heart journal. 2008;29(19):2388-442.
115. Edelmann F, Bobenko A, Gelbrich G, Hasenfuss G, Herrmann‐Lingen C, Duvinage A, et al. Exercise training in Diastolic Heart Failure (Ex‐DHF): rationale and design of a multicentre, prospective, randomized, controlled, parallel group trial. European journal of heart failure. 2017;19(8):1067-74.
116. Holland DJ, Prasad SB, Marwick TH. Prognostic implications of left ventricular filling pressure with exercise. Circulation: Cardiovascular Imaging. 2010;3(2):149-56.
117. Habib G, Bucciarelli-Ducci C, Caforio AL, Cardim N, Charron P, Cosyns B, et al. Multimodality Imaging in Restrictive Cardiomyopathies: An EACVI expert consensus document In collaboration with the "Working Group on myocardial and pericardial diseases" of the European Society of Cardiology Endorsed by The Indian Academy of Echocardiography. European Heart Journal-Cardiovascular Imaging. 2017;18(10):1090-121.
118. Adigopula S, Grapsa J. Advances in Imaging and Heart Failure: Where are we Heading? Cardiac failure review. 2018;4(2):73.
119. Angelidis G, Giamouzis G, Karagiannis G, Butler J, Tsougos I, Valotassiou V, et al. SPECT and PET in ischemic heart failure. Heart failure reviews. 2017;22(2):243-61.
120. Aziz W, Claridge S, Ntalas I, Gould J, de Vecchi A, Razeghi O, et al. Emerging role of cardiac computed tomography in heart failure. ESC heart failure. 2019;6(5):909-20.
121. Webb J, Fovargue L, Tøndel K, Porter B, Sieniewicz B, Gould J, et al. The Emerging Role of Cardiac Magnetic Resonance Imaging in the Evaluation of Patients with HFpEF. Curr Heart Fail Rep. 2018;15(1):1-9.
122. Su M-YM, Lin L-Y, Tseng Y-HE, Chang C-C, Wu C-K, Lin J-L, Tseng W-YI. CMR-Verified Diffuse Myocardial Fibrosis Is Associated With Diastolic Dysfunction in HFpEF. JACC: Cardiovascular Imaging. 2014;7(10):991-7.
123. Melero-Ferrer JL, López-Vilella R, Morillas-Climent H, Sanz-Sánchez J, Sánchez-Lázaro IJ, Almenar-Bonet L, Martínez-Dolz L. Novel imaging techniques for heart failure. Cardiac Failure Review. 2016;2(1):27.
124. Walsh TF, Hundley WG. Assessment of ventricular function with cardiovascular magnetic resonance. Magnetic resonance imaging clinics of North America. 2007;15(4):487-504.
125. Azarisman SM, Carbone A, Shirazi M, Bradley J, Teo KS, Worthley MI, Worthley SG. Characterisation of Myocardial Injury via T1 Mapping in Early Reperfused Myocardial Infarction and its Relationship with Global and Regional Diastolic Dysfunction. Heart Lung Circ. 2016;25(11):1094-106.

126. Ugander M, Oki AJ, Hsu L-Y, Kellman P, Greiser A, Aletras AH, et al. Extracellular volume imaging by magnetic resonance imaging provides insights into overt and sub-clinical myocardial pathology. European heart journal. 2012;33(10):1268-78.
127. Giubbini R, Milan E, Bertagna F, Mut F, Metra M, Rodella C, Dondi M. Nuclear cardiology and heart failure. European journal of nuclear medicine and molecular imaging. 2009;36(12):2068-80.
128. Mc Ardle B, Ziadi MC, Ruddy TD, Beanlands RS. Nuclear perfusion imaging for functional evaluation of patients with known or suspected coronary artery disease: the future is now. Future cardiology. 2012;8(4):603-22.
129. Verberne HJ, Acampa W, Anagnostopoulos C, Ballinger J, Bengel F, De Bondt P, et al. EANM procedural guidelines for radionuclide myocardial perfusion imaging with SPECT and SPECT/CT: 2015 revision. European journal of nuclear medicine and molecular imaging. 2015;42(12):1929-40.
130. Georgoulias P, Tsougos I, Tzavara C, Valotassiou V, Demakopoulos N. Incremental prognostic value of 99mTc-tetrofosmin early poststress pulmonary uptake. Determination of the optimal cut-off value. Nuclear medicine communications. 2012;33(5):470-5.
131. Hesse B, Tägil K, Cuocolo A, Anagnostopoulos C, Bardiès M, Bax J, et al. EANM/ESC procedural guidelines for myocardial perfusion imaging in nuclear cardiology. European journal of nuclear medicine and molecular imaging. 2005;32(7):855-97.
132. Anagnostopoulos C, Georgakopoulos A, Pianou N, Nekolla SG. Assessment of myocardial perfusion and viability by positron emission tomography. International journal of cardiology. 2013;167(5):1737-49.
133. Albaugh VL, Mukherjee K, Barbul A. Proline precursors and collagen synthesis: biochemical challenges of nutrient supplementation and wound healing. The Journal of nutrition. 2017;147(11):2011-7.
134. Barbul A. Proline precursors to sustain mammalian collagen synthesis. The Journal of nutrition. 2008;138(10):2021S-4S.
135. Balogh V, Spath N, Alcaide-Corral C, Walton T, Lennen R, Jansen M, et al. P16 Assessment of myocardial fibrosis activity using 18f-fluoroproline positron emission tomography (pet) in rat models of cardiovascular disease. BMJ Publishing Group Ltd and British Cardiovascular Society; 2020.
136. Geisler S, Ermert J, Stoffels G, Willuweit A, Galldiks N, P Filss C, et al. Isomers of 4-[18F] fluoro-proline: radiosynthesis, biological evaluation and results in humans using PET. Current radiopharmaceuticals. 2014;7(2):123-32.
137. Zhong Y, Jin C, Zhang X, Zhou R, Dou X, Wang J, et al. Aging imaging: the future demand of health management. European Journal of Nuclear Medicine and Molecular Imaging. 2023;50(13):3820-3.
138. Tian M, He X, Jin C, He X, Wu S, Zhou R, et al. Transpathology: molecular imaging-based pathology. European journal of nuclear medicine and molecular imaging. 2021;48:2338-50.
139. Yang F, Wang J, Li W, Xu Y, Wan K, Zeng R, Chen Y. The prognostic value of late gadolinium enhancement in myocarditis and clinically suspected myocarditis: systematic review and meta-analysis. Eur Radiol. 2020;30(5):2616-26.
140. van den Borne SW, Isobe S, Verjans JW, Petrov A, Lovhaug D, Li P, et al. Molecular imaging of interstitial alterations in remodeling myocardium after myocardial infarction. J Am Coll Cardiol. 2008;52(24):2017-28.
141. Ylä-Herttuala E, Saraste A, Knuuti J, Liimatainen T, Ylä-Herttuala S. Molecular imaging to monitor left ventricular remodeling in heart failure. Current cardiovascular imaging reports. 2019;12:1-13.
142. Balogh V, MacAskill MG, Hadoke PW, Gray GA, Tavares AA. Positron Emission Tomography Techniques to Measure Active Inflammation, Fibrosis and Angiogenesis: Potential for Non-invasive Imaging of Hypertensive Heart Failure. Frontiers in Cardiovascular Medicine. 2021;8.

143. Varasteh Z, Mohanta S, Robu S, Braeuer M, Li Y, Omidvari N, et al. Molecular Imaging of Fibroblast Activity After Myocardial Infarction Using a (68)Ga-Labeled Fibroblast Activation Protein Inhibitor, FAPI-04. J Nucl Med. 2019;60(12):1743-9.
144. Balogh V, Spath N, Alcaide-Corral C, Walton T, Lennen R, Jansen M, et al. P16 Assessment of myocardial fibrosis activity using ¹⁸f-fluoroproline positron emission tomography (pet) in rat models of cardiovascular disease. Heart. 2020;106(Suppl 1):A11-A.
145. Garin-Chesa P, Old LJ, Rettig WJ. Cell surface glycoprotein of reactive stromal fibroblasts as a potential antibody target in human epithelial cancers. Proc Natl Acad Sci U S A. 1990;87(18):7235-9.
146. Tillmanns J, Hoffmann D, Habbaba Y, Schmitto JD, Sedding D, Fraccarollo D, et al. Fibroblast activation protein alpha expression identifies activated fibroblasts after myocardial infarction. J Mol Cell Cardiol. 2015;87:194-203.
147. Siebermair J, Köhler M, Kupusovic J, Nekolla S, Kessler L, Ferdinandus J, et al. Cardiac fibroblast activation detected by Ga-68 FAPI PET imaging as a potential novel biomarker of cardiac injury/remodeling. Journal of Nuclear Cardiology. 2021;28(3):812-21.
148. Zhang M, Quan W, Zhu T, Feng S, Huang X, Meng H, et al. [68Ga] Ga-DOTA-FAPI-04 PET/MR in patients with acute myocardial infarction: potential role of predicting left ventricular remodeling. European journal of nuclear medicine and molecular imaging. 2023;50(3):839-48.
149. Neuman RE, Logan MA. The determination of collagen and elastin in tissues. Journal of Biological Chemistry. 1950;186(2):549-56.
150. Bach TMH, Takagi H. Properties, metabolisms, and applications of L-proline analogues. Applied microbiology and biotechnology. 2013;97:6623-34.
151. Dai D-F, Chen T, Johnson SC, Szeto H, Rabinovitch PS. Cardiac aging: from molecular mechanisms to significance in human health and disease. Antioxidants & redox signaling. 2012;16(12):1492-526.
152. Barnes M, Constable B, Morton L, Kodicek E. Studies in vivo on the biosynthesis of collagen and elastin in ascorbic acid-deficient guinea pigs. Evidence for the formation and degradation of a partially hydroxylated collagen. Biochemical Journal. 1970;119(3):575-85.
153. Gottlieb AA, Fujita Y, Udenfriend S, Witkop B. Incorporation of cis-and trans-4-Fluoro-L-prolines into Proteins and Hydroxylation of the trans Isomer During Collagen Biosynthesis. Biochemistry. 1965;4(11):2507-13.
154. Uitto J, Tan EM, Ryhänen L. Inhibition of collagen accumulation in fibrotic processes: review of pharmacologic agents and new approaches with amino acids and their analogues. Journal of Investigative Dermatology. 1982;79(1):113-20.
155. Skovgaard D, Kjaer A, Heinemeier KM, Brandt-Larsen M, Madsen J, Kjaer M. Use of cis-[18F] fluoro-proline for assessment of exercise-related collagen synthesis in musculoskeletal connective tissue. PLoS One. 2011;6(2):e16678.
156. Vitagliano L, Berisio R, Mastrangelo A, Mazzarella L, Zagari A. Preferred proline puckerings in cis and trans peptide groups: implications for collagen stability. Protein Science. 2001;10(12):2627-32.
157. Qiu R, Li X, Huang K, Bai W, Zhou D, Li G, et al. Cis-trans isomerization of peptoid residues in the collagen triple-helix. Nature Communications. 2023;14(1):7571.
158. Sarkar SK, Young PE, Sullivan CE, Torchia DA. Detection of cis and trans X-Pro peptide bonds in proteins by 13C NMR: application to collagen. Proc Natl Acad Sci U S A. 1984;81(15):4800-3.
159. Sun Z. Aging, arterial stiffness, and hypertension. Hypertension. 2015;65(2):252-6.
160. Wallace WE, Gupta NC, Hubbs AF, Mazza SM, Bishop HA, Keane MJ, et al. Cis-4-[18F] fluoro-L-proline PET imaging of pulmonary fibrosis in a rabbit model. Journal of Nuclear Medicine. 2002;43(3):413-20.

161. Morgan TE, Riley LM, Tavares AA, Sutherland A. Automated radiosynthesis of cis-and trans-4-[18F] Fluoro-l-proline using [18F] Fluoride. The Journal of Organic Chemistry. 2021;86(20):14054-60.
162. Balogh V. Non-invasive imaging of fibrosis with positron emission tomography in a rat model with systemic hypertension and myocardial fibrosis. 2023.
163. Brüel A, Oxlund H. Biosynthetic growth hormone increases the collagen deposition rate in rat aorta and heart. European journal of endocrinology. 1995;132(2):195-9.
164. Jacobs A, Reid VJ, Macaskill MG, Pandya K, Alcaide-Coral C, Morgan TE, et al. Quantification of extra-cardiac damage following acute myocardial infarction using cis-and trans-4-[18F] fluoro-L-proline PET imaging. The PET is Wonderful Journal. 2024;1(1).
165. EANM'23 Abstract Book Congress Sep 9-13, 2023. European Journal of Nuclear Medicine and Molecular Imaging. 2023;50(1):1-898.
166. Takeuchi T, Rosenbloom J, Prockop DJ. Biosynthesis of abnormal collagens with amino acid analogues: II. Inability of cartilage cells to extrude collagen polypeptides containing L-azetidine-2-carboxylic acid or cis-4-fluoro-L-proline. Biochimica et Biophysica Acta (BBA)-Protein Structure. 1969;175(1):156-64.
167. Takeuchi T, Prockop DJ. Biosynthesis of abnormal collagens with amino acid analogues: I. Incorporation of l-azetidine-2-carboxylic acid and cis-4-fluoro-l-proline into protocollagen and collagen. Biochimica et Biophysica Acta (BBA)-Protein Structure. 1969;175(1):142-55.
168. Chemaly ER, Kang S, Zhang S, McCollum L, Chen J, Bénard L, et al. Differential patterns of replacement and reactive fibrosis in pressure and volume overload are related to the propensity for ischaemia and involve resistin. The Journal of physiology. 2013;591(21):5337-55.
169. Désogère P, Tapias LF, Rietz TA, Rotile N, Blasi F, Day H, et al. Optimization of a collagen-targeted PET probe for molecular imaging of pulmonary fibrosis. Journal of Nuclear Medicine. 2017;58(12):1991-6.
170. Désogère P, Tapias LF, Hariri LP, Rotile NJ, Rietz TA, Probst CK, et al. Type I collagen–targeted PET probe for pulmonary fibrosis detection and staging in preclinical models. Science translational medicine. 2017;9(384):eaaf4696.
171. Izquierdo-Garcia D, Désogère P, Fur ML, Shuvaev S, Zhou IY, Ramsay I, et al. Biodistribution, Dosimetry, and Pharmacokinetics of ⁶⁸Ga-CBP8: A Type I Collagen–Targeted PET Probe. Journal of Nuclear Medicine. 2023;64(5):775-81.
172. Moon BF, Zhou IY, Ning Y, Chen Y-CI, Fur ML, Shuvaev S, et al. Simultaneous PET and molecular MR imaging of cardiopulmonary fibrosis in a mouse model of left ventricular dysfunction. bioRxiv. 2023:2023.12.15.571959.
173. Toczek J, Gona K, Liu Y, Ahmad A, Ghim M, Ojha D, et al. Positron emission tomography imaging of vessel wall matrix metalloproteinase activity in abdominal aortic aneurysm. Circulation: Cardiovascular Imaging. 2023;16(1):e014615.
174. Ringström N, Edling C, Nalesso G, Jeevaratnam K. Framing heartaches: The cardiac ECM and the effects of age. International journal of molecular sciences. 2023;24(5):4713.
175. Sengupta P. The laboratory rat: relating its age with human's. International journal of preventive medicine. 2013;4(6):624.
176. Howlett SE, Rockwood K. New horizons in frailty: ageing and the deficit-scaling problem. Age and ageing. 2013;42(4):416-23.
177. Phillips PM, Jarema KA, Kurtz DM, MacPhail RC. An observational assessment method for aging laboratory rats. Journal of the American Association for Laboratory Animal Science. 2010;49(6):792-9.
178. Yorke A, Kane AE, Hancock Friesen CL, Howlett SE, O'Blenes S. Development of a rat clinical frailty index. Journals of Gerontology Series A: Biomedical Sciences and Medical Sciences. 2017;72(7):897-903.

179. Whitehead JC, Hildebrand BA, Sun M, Rockwood MR, Rose RA, Rockwood K, Howlett SE. A clinical frailty index in aging mice: comparisons with frailty index data in humans. J Gerontol A Biol Sci Med Sci. 2014;69(6):621-32.
180. Xu B, Daimon M. Cardiac aging phenomenon and its clinical features by echocardiography. Journal of Echocardiography. 2016;14(4):139-45.
181. Masugata H, Senda S, Goda F, Hirao T, Yoshihara Y, Yoshikawa K, et al. A New Index of "Cardiac Age" Derived from Echocardiography: Influence of Hypertension and Comparison with Pulse Wave Velocity. Hypertension Research. 2008;31(8):1573-81.
182. Percie du Sert N, Hurst V, Ahluwalia A, Alam S, Avey MT, Baker M, et al. The ARRIVE guidelines 2.0: Updated guidelines for reporting animal research. Journal of Cerebral Blood Flow & Metabolism. 2020;40(9):1769-77.
183. Kim SH. Normalization of cardiac measurements: isometric vs. Allometric Method. Journal of Cardiovascular Imaging. 2020;28(1):18-20.
184. Nohynek G, Longeart L, Geffray B, Provost J, Lodola A. Fat, frail and dying young: survival, body weight and pathology of the Charles River Sprague-Dawley-derived rat prior to and since the introduction of the VAFR variant in 1988. Sage Publications Sage CA: Thousand Oaks, CA; 1993. p. 87-98.
185. Davis R, Stevenson G, Busch K. Tumor incidence in normal Sprague-Dawley female rats. Cancer Research. 1956;16(3):194-7.
186. Altun M, Bergman E, Edström E, Johnson H, Ulfhake B. Behavioral impairments of the aging rat. Physiology & behavior. 2007;92(5):911-23.
187. Chawla S, Jena S. The Anatomy and Physiology of Laboratory Rat. Essentials of Laboratory Animal Science: Principles and Practices. 2021:187-209.
188. Ghasemi A, Jeddi S, Kashfi K. The laboratory rat: Age and body weight matter. EXCLI journal. 2021;20:1431.
189. Yamashita Y, Kawai N, Ueno O, Matsumoto Y, Oohashi T, Honda M. Induction of prolonged natural lifespans in mice exposed to acoustic environmental enrichment. Scientific Reports. 2018;8(1):7909.
190. McAdams RM, McPherson RJ, Dabestani NM, Gleason CA, Juul SE. Left ventricular hypertrophy is prevalent in Sprague–Dawley rats. Comparative medicine. 2010;60(5):357-63.
191. Ho KM, Morgan DJ, Johnstone M, Edibam C. Biological age is superior to chronological age in predicting hospital mortality of the critically ill. Internal and emergency medicine. 2023;18(7):2019-28.
192. Brower M, Grace M, Kotz C, Koya V. Comparative analysis of growth characteristics of Sprague Dawley rats obtained from different sources. Laboratory Animal Research. 2015;31:166.
193. Soto JE, Burnett CM, Ten Eyck P, Abel ED, Grobe JL. Comparison of the effects of high‐fat diet on energy flux in mice using two multiplexed metabolic phenotyping systems. Obesity. 2019;27(5):793-802.
194. Keenan KP, Smith PF, Hertzog P, Soper K, Ballam GC, Clark RL. The effects of overfeeding and dietary restriction on Sprague-Dawley rat survival and early pathology biomarkers of aging. Toxicologic pathology. 1994;22(3):300-15.
195. Welsh A, Hammad M, Piña IL, Kulinski J. Obesity and cardiovascular health. European Journal of Preventive Cardiology. 2024;31(8):1026-35.
196. Nixon JP, Zhang M, Wang C, Kuskowski MA, Novak CM, Levine JA, et al. Evaluation of a quantitative magnetic resonance imaging system for whole body composition analysis in rodents. Obesity. 2010;18(8):1652-9.
197. Cressey D. Fat rats skew research results. Nature. 2010;464(19):10.1038.

198. Collard RM, Boter H, Schoevers RA, Oude Voshaar RC. Prevalence of frailty in community-dwelling older persons: a systematic review. Journal of the american geriatrics society. 2012;60(8):1487-92.
199. Bisset ES, Howlett SE. The biology of frailty in humans and animals: understanding frailty and promoting translation. Aging Medicine. 2019;2(1):27-34.
200. Howlett SE, Rockwood K. Ageing: Develop models of frailty. Nature. 2014;512(7514).
201. Miller MG, Thangthaeng N, Shukitt-Hale B. A clinically relevant frailty index for aging rats. Journals of Gerontology Series A: Biomedical Sciences and Medical Sciences. 2017;72(7):892-6.
202. Kane AE, Bisset ES, Keller KM, Ghimire A, Pyle WG, Howlett SE. Age, sex and overall health, measured as frailty, modify myofilament proteins in hearts from naturally aging mice. Scientific Reports. 2020;10(1):10052.
203. Bisset ES, Howlett SE. Sex-specific effects of frailty on cardiac structure and function: Insights from preclinical models. Canadian Journal of Physiology and Pharmacology. 2024.
204. Soltis EE. Effect of age on blood pressure and membrane-dependent vascular responses in the rat. Circulation Research. 1987;61(6):889-97.
205. Randall DC, Speakman RO, Silcox DL, Brown LV, Brown DR, Gong MC, et al. Longitudinal analysis of arterial blood pressure and heart rate response to acute behavioral stress in rats with type 1 diabetes mellitus and in age-matched controls. Frontiers in Physiology. 2011;2:53.
206. Tuma RF, Irion GL, Vasthare US, Heinel LA. Age-related changes in regional blood flow in the rat. American Journal of Physiology-Heart and Circulatory Physiology. 1985;249(3):H485-H91.
207. Barsha G, Denton KM, Mirabito Colafella KM. Sex-and age-related differences in arterial pressure and albuminuria in mice. Biology of sex differences. 2016;7:1-15.
208. Fentie IH, Greenwood MM, Wyss JM, Clark JT. Age-related decreases in gonadal hormones in Long-Evans rats: relationship to rise in arterial pressure. Endocrine. 2004;25(1):15-22.
209. Pinto E. Blood pressure and ageing. Postgraduate medical journal. 2007;83(976):109-14.
210. Lin J, Lopez EF, Jin Y, Van Remmen H, Bauch T, Han H-C, Lindsey ML. Age-related cardiac muscle sarcopenia: Combining experimental and mathematical modeling to identify mechanisms. Experimental gerontology. 2008;43(4):296-306.
211. Kitpipatkun P, Sukwan C. Echocardiographic parameters in different age and sex of Sprague-Dawley rats under isoflurane anesthesia. 2021.
212. Routledge FS, McFetridge-Durdle JA, Dean C. Stress, menopausal status and nocturnal blood pressure dipping patterns among hypertensive women. Canadian Journal of Cardiology. 2009;25(6):e157-e63.
213. Deschepper CF, Olson JL, Otis M, Gallo-Payet N. Characterization of blood pressure and morphological traits in cardiovascular-related organs in 13 different inbred mouse strains. J Appl Physiol (1985). 2004;97(1):369-76.
214. Joyner MJ, Barnes JN, Hart EC, Wallin BG, Charkoudian N. Neural control of the circulation: how sex and age differences interact in humans. Comprehensive Physiology. 2015;5(1):193.
215. Maas A, Franke H. Women's health in menopause with a focus on hypertension. Netherlands Heart Journal. 2009;17:68-72.
216. Harrison D, Bader M, Lerman L, Fink G, Karumanchi S, Reckelhoff J, et al. Tail-cuff versus radiotelemetry to measure blood pressure in mice and rats. Hypertension. 2024;81(1):3-5.
217. Feng M, Whitesall S, Zhang Y, Beibel M, Alecy LD, DiPetrillo K. Validation of volume–pressure recording tail-cuff blood pressure measurements. American journal of hypertension. 2008;21(12):1288-91.
218. Martin TG, Leinwand LA. Hearts apart: sex differences in cardiac remodeling in health and disease. The Journal of Clinical Investigation. 2024;134(13).
219. Watson LE, Sheth M, Denyer RF, Dostal DE. Baseline echocardiographic values for adult male rats. Journal of the American Society of Echocardiography. 2004;17(2):161-7.

220. Murakami M, Niwa H, Kushikata T, Watanabe H, Hirota K, Ono K, Ohba T. Inhalation anesthesia is preferable for recording rat cardiac function using an electrocardiogram. Biological and Pharmaceutical Bulletin. 2014;37(5):834-9.
221. Stupfel M, Costagliola D. Lifelong variations in heart rates in SPF Sprague Dawley rats of both sexes: Statistical correlations with body weights. Pflügers Archiv. 1979;380:189-95.
222. Zhang TY, Zhao BJ, Wang T, Wang J. Effect of aging and sex on cardiovascular structure and function in wildtype mice assessed with echocardiography. Scientific Reports. 2021;11(1):22800.
223. Arias T, Chen J, Fayad ZA, Fuster V, Hajjar RJ, Chemaly ER. Comparison of echocardiographic measurements of left ventricular volumes to full volume magnetic resonance imaging in normal and diseased rats. J Am Soc Echocardiogr. 2013;26(8):910-8.
224. Redfield MM, Jacobsen SJ, Burnett JC, Mahoney DW, Bailey KR, Rodeheffer RJ. Burden of systolic and diastolic ventricular dysfunction in the community: appreciating the scope of the heart failure epidemic. Jama. 2003;289(2):194-202.
225. Chung AK, Das SR, Leonard D, Peshock RM, Kazi F, Abdullah SM, et al. Women have higher left ventricular ejection fractions than men independent of differences in left ventricular volume: the Dallas Heart Study. Circulation. 2006;113(12):1597-604.
226. Wei JY. Age and the cardiovascular system. New England Journal of Medicine. 1992;327(24):1735-9.
227. Qin F, Siwik DA, Lancel S, Zhang J, Kuster GM, Luptak I, et al. Hydrogen peroxide–mediated SERCA cysteine 674 oxidation contributes to impaired cardiac myocyte relaxation in senescent mouse heart. Journal of the American Heart Association. 2013;2(4):e000184.
228. Flecknell P. Laboratory animal anaesthesia: Academic press; 2015.
229. Liu Y, Beyer A, Aebersold R. On the Dependency of Cellular Protein Levels on mRNA Abundance. Cell. 2016;165(3):535-50.
230. Segmentation AHAWGoM, Imaging: RfC, Cerqueira MD, Weissman NJ, Dilsizian V, Jacobs AK, et al. Standardized myocardial segmentation and nomenclature for tomographic imaging of the heart: a statement for healthcare professionals from the Cardiac Imaging Committee of the Council on Clinical Cardiology of the American Heart Association. Circulation. 2002;105(4):539-42.
231. Bankhead P, Loughrey MB, Fernández JA, Dombrowski Y, McArt DG, Dunne PD, et al. QuPath: Open source software for digital pathology image analysis. Scientific reports. 2017;7(1):1-7.
232. Gould J. Morpheus 2017 [cited 2024 28th July]. Available from: https://software.broadinstitute.org/morpheus.
233. Pappritz K, Puhl S-L, Matz I, Brauer E, Shia YX, El-Shafeey M, et al. Sex-and age-related differences in the inflammatory properties of cardiac fibroblasts: impact on the cardiosplenic axis and cardiac fibrosis. Frontiers in Cardiovascular Medicine. 2023;10:1117419.
234. Yusifov A, Chhatre VE, Koplin EK, Wilson CE, Schmitt EE, Woulfe KC, Bruns DR. Transcriptomic analysis of cardiac gene expression across the life course in male and female mice. Physiological Reports. 2021;9(13):e14940.
235. Duan N, Chen H, Pi L, Ali Y, Cao Q. Cis-4-[18F] fluoro-L-proline PET/CT molecular imaging quantifying liver collagenogenesis: No existing fibrotic deposition in experimental advanced-stage alcoholic liver fibrosis. Frontiers in Nuclear Medicine. 2022;2:952943.
236. Yusifov A, Woulfe KC, Bruns DR. Mechanisms and implications of sex differences in cardiac aging. J Cardiovasc Aging. 2022;2.
237. Petrov G, Regitz-Zagrosek V, Lehmkuhl E, Krabatsch T, Dunkel A, Dandel M, et al. Regression of myocardial hypertrophy after aortic valve replacement: faster in women? Circulation. 2010;122(11_suppl_1):S23-S8.
238. Fliegner D, Schubert C, Penkalla A, Witt H, Kararigas G, Dworatzek E, et al. Female sex and estrogen receptor-β attenuate cardiac remodeling and apoptosis in pressure overload. American Journal of Physiology-Regulatory, Integrative and Comparative Physiology. 2010;298(6):R1597-R606.

239. Iwańska D, Kęska A, Dadura E, Wójcik A, Mastalerz A, Urbanik C. The effect of the menstrual cycle on collagen metabolism, growth hormones and strength in young physically active women. Biology of Sport. 2021;38(4):721-8.
240. Rich-Edwards JW, Kaiser UB, Chen GL, Manson JE, Goldstein JM. Sex and gender differences research design for basic, clinical, and population studies: essentials for investigators. Endocrine reviews. 2018;39(4):424-39.
241. Shaw RC, Tamagnan GD, Tavares AAS. Rapidly (and successfully) translating novel brain radiotracers from animal research into clinical use. Frontiers in Neuroscience. 2020;14:871.
242. Salvador RA, Tsai I, Marcel RJ, Felix AM, Kerwar S. The in vivo inhibition of collagen synthesis and the reduction of prolyl hydroxylase activity by 3, 4-dehydroproline. Archives of Biochemistry and Biophysics. 1976;174(2):381-92.
243. Muratsubaki H, Yamaki A. Profile of plasma amino acid levels in rats exposed to acute hypoxic hypoxia. Indian Journal of Clinical Biochemistry. 2011;26:416-9.
244. Annoni G, Luvarà G, Arosio B, Gagliano N, Fiordaliso F, Santambrogio D, et al. Age-dependent expression of fibrosis-related genes and collagen deposition in the rat myocardium1This study was presented in part at the 49th Annual Meeting of the `Gerontological Society of America', Washington, November 17–21, 1996.1. Mechanisms of Ageing and Development. 1998;101(1):57-72.
245. Boluyt MO, O'Neill L, Meredith AL, Bing O, Brooks WW, Conrad CH, et al. Alterations in cardiac gene expression during the transition from stable hypertrophy to heart failure. Marked upregulation of genes encoding extracellular matrix components. Circulation research. 1994;75(1):23-32.
246. Varo N, Etayo JC, Zalba G, Beaumont J, Iraburu MJ, Montiel C, et al. Losartan inhibits the post-transcriptional synthesis of collagen type I and reverses left ventricular fibrosis in spontaneously hypertensive rats. J Hypertens. 1999;17(1):107-14.
247. Querejeta R, López B, González A, Sánchez E, Larman M, Martínez Ubago JL, Díez J. Increased collagen type I synthesis in patients with heart failure of hypertensive origin: relation to myocardial fibrosis. Circulation. 2004;110(10):1263-8.
248. Schalla S, Bekkers SC, Dennert R, van Suylen RJ, Waltenberger J, Leiner T, et al. Replacement and reactive myocardial fibrosis in idiopathic dilated cardiomyopathy: comparison of magnetic resonance imaging with right ventricular biopsy. European journal of heart failure. 2010;12(3):227-31.
249. Liu C-Y, Liu Y-C, Wu C, Armstrong A, Volpe GJ, Van der Geest RJ, et al. Evaluation of age-related interstitial myocardial fibrosis with cardiac magnetic resonance contrast-enhanced T1 mapping: MESA (Multi-Ethnic Study of Atherosclerosis). Journal of the American College of Cardiology. 2013;62(14):1280-7.
250. Fannin J, Rice KM, Thulluri S, Dornon L, Arvapalli RK, Wehner P, Blough ER. Age-associated alterations of cardiac structure and function in the female F344xBN rat heart. Age. 2014;36:1-12.
251. Capitanio D, Leone R, Fania C, Torretta E, Gelfi C. Sprague Dawley rats: A model of successful heart aging. EuPA Open Proteomics. 2016;12:22-30.
252. Coleman GL, Barthold SW, Osbaldiston GW, Foster SJ, Jonas AM. Pathological Changes During Aging in, Barrier-Reared Fischer 344 Male Rats. Journal of Gerontology. 1977;32(3):258-78.
253. Andersen S, Nielsen-Kudsk JE, Vonk Noordegraaf A, de Man FS. Right ventricular fibrosis: a pathophysiological factor in pulmonary hypertension? Circulation. 2019;139(2):269-85.
254. Qiu B, Wei F, Sun X, Wang X, Duan B, Shi C, et al. Measurement of hydroxyproline in collagen with three different methods. Molecular medicine reports. 2014;10(2):1157-63.
255. Forman DE, Cittadini A, Azhar G, Douglas PS, Wei JY. Cardiac morphology and function in senescent rats: gender-related differences. Journal of the American College of Cardiology. 1997;30(7):1872-7.

256. Hung C-L, Gonçalves A, Shah AM, Cheng S, Kitzman D, Solomon SD. Age-and sex-related influences on left ventricular mechanics in elderly individuals free of prevalent heart failure: the ARIC Study (Atherosclerosis Risk in Communities). Circulation: Cardiovascular Imaging. 2017;10(1):e004510.
257. Bi X, Song Y, Song Y, Yuan J, Cui J, Zhao S, Qiao S. Collagen Cross-Linking Is Associated With Cardiac Remodeling in Hypertrophic Obstructive Cardiomyopathy. Journal of the American Heart Association. 2021;10(1):e017752.
258. Campbell DJ, Somaratne JB, Jenkins AJ, Prior DL, Yii M, Kenny JF, et al. Diastolic dysfunction of aging is independent of myocardial structure but associated with plasma advanced glycation end-product levels. PLoS One. 2012;7(11):e49813.
259. Asif M, Egan J, Vasan S, Jyothirmayi GN, Masurekar MR, Lopez S, et al. An advanced glycation endproduct cross-link breaker can reverse age-related increases in myocardial stiffness. Proceedings of the National Academy of Sciences. 2000;97(6):2809-13.
260. Sharma A, Weber D, Raupbach J, Dakal TC, Fließbach K, Ramirez A, et al. Advanced glycation end products and protein carbonyl levels in plasma reveal sex-specific differences in Parkinson's and Alzheimer's disease. Redox biology. 2020;34:101546.
261. Thomas PD, Cotter TA, Li X, McCormick RJ, Gosselin LE. Exercise training attenuates aging-associated increases in collagen and collagen crosslinking of the left but not the right ventricle in the rat. European journal of applied physiology. 2001;85:164-9.
262. Vigetti D, Moretto P, Viola M, Genasetti A, Rizzi M, Karousou E, et al. Matrix metalloproteinase 2 and tissue inhibitors of metalloproteinases regulate human aortic smooth muscle cell migration during in vitro aging. The FASEB Journal. 2006;20(8):1118-30.
263. Wang M, Kim SH, Monticone RE, Lakatta EG. Matrix metalloproteinases promote arterial remodeling in aging, hypertension, and atherosclerosis. Hypertension. 2015;65(4):698-703.
264. Varani J, Spearman D, Perone P, Fligiel SE, Datta SC, Wang ZQ, et al. Inhibition of type I procollagen synthesis by damaged collagen in photoaged skin and by collagenase-degraded collagen in vitro. The American journal of pathology. 2001;158(3):931-42.
265. Fisher GJ, Quan T, Purohit T, Shao Y, Cho MK, He T, et al. Collagen fragmentation promotes oxidative stress and elevates matrix metalloproteinase-1 in fibroblasts in aged human skin. The American journal of pathology. 2009;174(1):101-14.
266. McNair BD, Shorthill SK, Bruns DR. More than just a small left ventricle: the right ventricular fibroblast and ECM in health and disease. American Journal of Physiology-Heart and Circulatory Physiology. 2023;325(2):H385-H97.
267. Moore-Morris T, Guimarães-Camboa N, Banerjee I, Zambon AC, Kisseleva T, Velayoudon A, et al. Resident fibroblast lineages mediate pressure overload–induced cardiac fibrosis. The Journal of clinical investigation. 2014;124(7):2921-34.
268. Tucker NR, Chaffin M, Fleming SJ, Hall AW, Parsons VA, Bedi Jr KC, et al. Transcriptional and cellular diversity of the human heart. Circulation. 2020;142(5):466-82.
269. He T, Melgarejo JD, Clark AL, Yu YL, Thijs L, Díez J, et al. Serum and urinary biomarkers of collagen type-I turnover predict prognosis in patients with heart failure. Clinical and translational medicine. 2021;11(1).
270. Raafs AG, Adriaans BP, Henkens MT, Verdonschot JA, Abdul Hamid MA, Díez J, et al. Biomarkers of collagen metabolism are associated with left ventricular function and prognosis in dilated cardiomyopathy: a multi-modal study. Journal of Clinical Medicine. 2023;12(17):5695.
271. Gramley F, Lorenzen J, Knackstedt C, Rana OR, Saygili E, Frechen D, et al. Age-related atrial fibrosis. Age. 2009;31:27-38.
272. Lin K-b, Chen K-k, Li S, Cai M-q, Yuan M-j, Wang Y-p, et al. Impaired left atrial performance resulting from age-related arial fibrillation is associated with increased fibrosis burden: insights from

a clinical study combining with an in vivo experiment. Frontiers in Cardiovascular Medicine. 2021;7:615065.
273. Nakajima H, Nakajima HO, Salcher O, Dittiè AS, Dembowsky K, Jing S, Field LJ. Atrial but not ventricular fibrosis in mice expressing a mutant transforming growth factor-β1 transgene in the heart. Circulation research. 2000;86(5):571-9.
274. Burstein B, Libby E, Calderone A, Nattel S. Differential behaviors of atrial versus ventricular fibroblasts: a potential role for platelet-derived growth factor in atrial-ventricular remodeling differences. Circulation. 2008;117(13):1630-41.
275. O'Brien D, Fu Y, Parker H, Chan S, Idikio H, Scott P, Jugdutt B. Differential morphometric and ultrastructural remodelling in the left atrium and left ventricle in rapid ventricular pacing-induced heart failure. The Canadian Journal of Cardiology. 2000;16(11):1411-9.
276. Booz GW, Baker KM. Molecular signalling mechanisms controlling growth and function of cardiac fibroblasts. Cardiovascular research. 1995;30(4):537-43.
277. Swynghedauw B. Molecular mechanisms of myocardial remodeling. Physiological reviews. 1999;79(1):215-62.
278. Siddiqi HK, Vinayagamoorthy M, Gencer B, Ng C, Pester J, Cook NR, et al. Sex differences in atrial fibrillation risk: the VITAL rhythm study. JAMA cardiology. 2022;7(10):1027-35.
279. Li Z, Wang Z, Yin Z, Zhang Y, Xue X, Han J, et al. Gender differences in fibrosis remodeling in patients with long-standing persistent atrial fibrillation. Oncotarget. 2017;8(32):53714.
280. Nattel S. Molecular and cellular mechanisms of atrial fibrosis in atrial fibrillation. JACC: Clinical Electrophysiology. 2017;3(5):425-35.
281. Mamuya W, Chobanian A, Brecher P. Age-related changes in fibronectin expression in spontaneously hypertensive, Wistar-Kyoto, and Wistar rat hearts. Circulation research. 1992;71(6):1341-50.
282. Vandenberghe W, Hoste E. Contrast-associated acute kidney injury: does it really exist, and if so, what to do about it? F1000Research. 2019;8.
283. Mamuya WS, Brecher P. Fibronectin expression in the normal and hypertrophic rat heart. The Journal of clinical investigation. 1992;89(2):392-401.
284. Luo T, Chang CX, Zhou X, Gu SK, Jiang TM, Li YM. Characterization of atrial histopathological and electrophysiological changes in a mouse model of aging. Int J Mol Med. 2013;31(1):138-46.
285. Lau DH, Shipp NJ, Kelly DJ, Thanigaimani S, Neo M, Kuklik P, et al. Atrial arrhythmia in ageing spontaneously hypertensive rats: unraveling the substrate in hypertension and ageing. PloS one. 2013;8(8):e72416.
286. Statzer C, Ewald CY. The extracellular matrix phenome across species. Matrix biology plus. 2020;8:100039.
287. Bi X, Song Y, Yang C, Song Y, Zhao S, Qiao S, Zhang J. Sex differences in atrial remodeling and its relationship with myocardial fibrosis in hypertrophic obstructive cardiomyopathy. Frontiers in Cardiovascular Medicine. 2022;9:947975.
288. Kronenberg D, Michel PA, Hochstrat E, Wei M, Brinckmann J, Müller M, et al. Increased Collagen Turnover Impairs Tendon Microstructure and Stability in Integrin α2β1-Deficient Mice. International Journal of Molecular Sciences. 2020;21(8):2835.
289. Khan A, Moe GW, Nili N, Rezaei E, Eskandarian M, Butany J, Strauss BH. The cardiac atria are chambers of active remodeling and dynamic collagen turnover during evolving heart failure. Journal of the American College of Cardiology. 2004;43(1):68-76.
290. Dolgilevich S, Siri F, Atlas S, Eng C. Changes in collagenase and collagen gene expression after induction of aortocaval fistula in rats. American Journal of Physiology-Heart and Circulatory Physiology. 2001;281(1):H207-H14.

291. Moghtadaei M, Jansen HJ, Mackasey M, Rafferty SA, Bogachev O, Sapp JL, et al. The impacts of age and frailty on heart rate and sinoatrial node function. The Journal of physiology. 2016;594(23):7105-26.
292. Nikitin N, Witte K, Thackray S, Goodge L, Clark A, Cleland J. Effect of age and sex on left atrial morphology and function. European Journal of Echocardiography. 2003;4(1):36-42.
293. Lyu G, Guan Y, Zhang C, Zong L, Sun L, Huang X, et al. TGF-β signaling alters H4K20me3 status via miR-29 and contributes to cellular senescence and cardiac aging. Nature communications. 2018;9(1):2560.
294. Osorio JM, Espinoza-Pérez C, Rimassa-Taré C, Machuca V, Bustos JO, Vallejos M, et al. Senescent cardiac fibroblasts: a key role in cardiac fibrosis. Biochimica et Biophysica Acta (BBA)-Molecular Basis of Disease. 2023;1869(4):166642.
295. González-Gualda E, Baker AG, Fruk L, Muñoz-Espín D. A guide to assessing cellular senescence in vitro and in vivo. The FEBS journal. 2021;288(1):56-80.
296. Wells RG. Tissue mechanics and fibrosis. Biochimica et Biophysica Acta (BBA)-Molecular Basis of Disease. 2013;1832(7):884-90.
297. Brilla CG, Zhou G, Matsubara L, Weber KT. Collagen metabolism in cultured adult rat cardiac fibroblasts: response to angiotensin II and aldosterone. Journal of molecular and cellular cardiology. 1994;26(7):809-20.
298. Gündüz D, Hamm CW, Aslam M. Simultaneous Isolation of High Quality Cardiomyocytes, Endothelial Cells, and Fibroblasts from an Adult Rat Heart. J Vis Exp. 2017(123).
299. Melzer M, Beier D, Young PP, Saraswati S. Isolation and Characterization of Adult Cardiac Fibroblasts and Myofibroblasts. J Vis Exp. 2020(157).
300. Herum KM, Weng G, Kahnert K, Waikel R, Milburn G, Conger A, et al. Cardiac fibroblast sub-types in vitro reflect pathological cardiac remodeling in vivo. Matrix Biology Plus. 2022;15:100113.
301. Hall C, Law JP, Reyat JS, Cumberland MJ, Hang S, Vo NT, et al. Chronic activation of human cardiac fibroblasts in vitro attenuates the reversibility of the myofibroblast phenotype. Scientific Reports. 2023;13(1):12137.
302. Goldsmith RS, Tsan YC, Scissors RE, Helms AS, Brody MJ. In Vitro Assessment of Cardiac Fibroblast Activation at Physiologic Stiffness. Current Protocols. 2024;4(4):e1025.
303. Salminen A. The role of immunosuppressive myofibroblasts in the aging process and age-related diseases. Journal of Molecular Medicine. 2023;101(10):1169-89.
304. Lu L, Guo J, Hua Y, Huang K, Magaye R, Cornell J, et al. Cardiac fibrosis in the ageing heart: contributors and mechanisms. Clinical and Experimental Pharmacology and Physiology. 2017;44:55-63.
305. Turner NA, Porter KE. Function and fate of myofibroblasts after myocardial infarction. Fibrogenesis & tissue repair. 2013;6:1-10.
306. Haudek SB, Gupta D, Dewald O, Schwartz RJ, Wei L, Trial J, Entman ML. Rho kinase-1 mediates cardiac fibrosis by regulating fibroblast precursor cell differentiation. Cardiovascular research. 2009;83(3):511-8.
307. Mescher AL. Macrophages and fibroblasts during inflammation and tissue repair in models of organ regeneration. Regeneration. 2017;4(2):39-53.
308. Denu RA, Nemcek S, Bloom DD, Goodrich A, Kim J, Mosher DF, Hematti P. Fibroblasts and mesenchymal stromal/stem cells are phenotypically indistinguishable. Acta haematologica. 2016;136(2):85-97.
309. Santiago JJ, Dangerfield AL, Rattan SG, Bathe KL, Cunnington RH, Raizman JE, et al. Cardiac fibroblast to myofibroblast differentiation in vivo and in vitro: expression of focal adhesion components in neonatal and adult rat ventricular myofibroblasts. Developmental dynamics. 2010;239(6):1573-84.

310. Li Y, Asfour H, Bursac N. Age-dependent functional crosstalk between cardiac fibroblasts and cardiomyocytes in a 3D engineered cardiac tissue. Acta Biomaterialia. 2017;55:120-30.
311. Grodstein F, Stampfer MJ, Colditz GA, Willett WC, Manson JE, Joffe M, et al. Postmenopausal hormone therapy and mortality. New England Journal of Medicine. 1997;336(25):1769-76.
312. Rossouw JE, Anderson GL, Prentice RL, LaCroix AZ, Kooperberg C, Stefanick ML, et al. Risks and benefits of estrogen plus progestin in healthy postmenopausal women: principal results From the Women's Health Initiative randomized controlled trial. Jama. 2002;288(3):321-33.
313. Fullerton MJ, Funder JW. Aldosterone and cardiac fibrosis: in vitro studies. Cardiovascular research. 1994;28(12):1863-7.
314. Zhang H, Tian L, Shen M, Tu C, Wu H, Gu M, et al. Generation of quiescent cardiac fibroblasts from human induced pluripotent stem cells for in vitro modeling of cardiac fibrosis. Circulation research. 2019;125(5):552-66.
315. Cartledge JE, Kane C, Dias P, Tesfom M, Clarke L, Mckee B, et al. Functional crosstalk between cardiac fibroblasts and adult cardiomyocytes by soluble mediators. Cardiovascular research. 2015;105(3):260-70.
316. Chen W, Frangogiannis NG. The role of inflammatory and fibrogenic pathways in heart failure associated with aging. Heart Fail Rev. 2010;15(5):415-22.
317. Westphal C, Schubert C, Prelle K, Penkalla A, Fliegner D, Petrov G, Regitz-Zagrosek V. Effects of estrogen, an ERα agonist and raloxifene on pressure overload induced cardiac hypertrophy. PloS one. 2012;7(12):e50802.
318. Lee T-M, Lin S-Z, Chang N-C. Membrane ERα attenuates myocardial fibrosis via RhoA/ROCK-mediated actin remodeling in ovariectomized female infarcted rats. Journal of Molecular Medicine. 2014;92:43-51.
319. Zhan E, Keimig T, Xu J, Peterson E, Ding J, Wang F, Yang XP. Dose‐dependent cardiac effect of oestrogen replacement in mice post‐myocardial infarction. Experimental Physiology. 2008;93(8):982-93.
320. Childers RC, Lucchesi PA, Gooch KJ. Decreased substrate stiffness promotes a hypofibrotic phenotype in cardiac fibroblasts. International journal of molecular sciences. 2021;22(12):6231.
321. Yeh Y-C, Corbin EA, Caliari SR, Ouyang L, Vega SL, Truitt R, et al. Mechanically dynamic PDMS substrates to investigate changing cell environments. Biomaterials. 2017;145:23-32.
322. Palchesko RN, Zhang L, Sun Y, Feinberg AW. Development of polydimethylsiloxane substrates with tunable elastic modulus to study cell mechanobiology in muscle and nerve. PloS one. 2012;7(12):e51499.
323. Landry NM, Rattan SG, Dixon IM. An improved method of maintaining primary murine cardiac fibroblasts in two-dimensional cell culture. Scientific reports. 2019;9(1):12889.
324. Hastings MH, Zhou Q, Wu C, Shabani P, Huang S, Yu X, et al. Cardiac aging: from hallmarks to therapeutic opportunities. Cardiovascular Research. 2024:cvae124.
325. Palliyaguru DL, Vieira Ligo Teixeira C, Duregon E, di Germanio C, Alfaras I, Mitchell SJ, et al. Study of longitudinal aging in mice: presentation of experimental techniques. The Journals of Gerontology: Series A. 2021;76(4):552-60.
326. Özbek S, Balasubramanian PG, Chiquet-Ehrismann R, Tucker RP, Adams JC. The evolution of extracellular matrix. Molecular biology of the cell. 2010;21(24):4300-5.
327. Cao Q, Lu X, Azad BB, Pomper M, Smith M, He J, et al. cis-4-[18F] fluoro-L-proline molecular imaging experimental liver fibrosis. Frontiers in Molecular Biosciences. 2020;7:90.
328. Bujak M, Kweon HJ, Chatila K, Li N, Taffet G, Frangogiannis NG. Aging-related defects are associated with adverse cardiac remodeling in a mouse model of reperfused myocardial infarction. J Am Coll Cardiol. 2008;51(14):1384-92.
329. Jackson SJ, Andrews N, Ball D, Bellantuono I, Gray J, Hachoumi L, et al. Does age matter? The impact of rodent age on study outcomes. Laboratory animals. 2017;51(2):160-9.

330. Shin HS, Shin HH, Shudo Y. Current status and limitations of myocardial infarction large animal models in cardiovascular translational research. Frontiers in bioengineering and biotechnology. 2021;9:673683.
331. Van der Worp HB, Howells DW, Sena ES, Porritt MJ, Rewell S, O'Collins V, Macleod MR. Can animal models of disease reliably inform human studies? PLoS medicine. 2010;7(3):e1000245.

Chapter 7 – Appendix

The appendix contains supplementary tables and graphs that further support the findings presented in the main thesis.

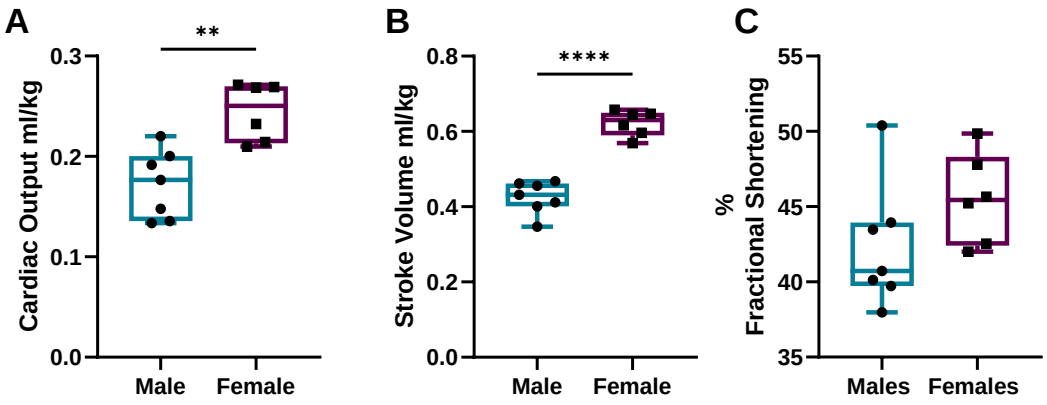

Figure 7. 1 Echocardiography derived functional parameters. Echocardiography measurements were taken at the terminal timepoints (18 months). Cardiac Output (A), Stroke Volume (B), % Fractional Shortening (C) was assessed in both aged males and females. Results reported as min to max range, axis range was decided based on the physiologically 'healthy' ranges, n=7 males and n=7 females; p values were obtained using unpaired Students t-test when comparing two groups; *p<0.05; **p<0.01

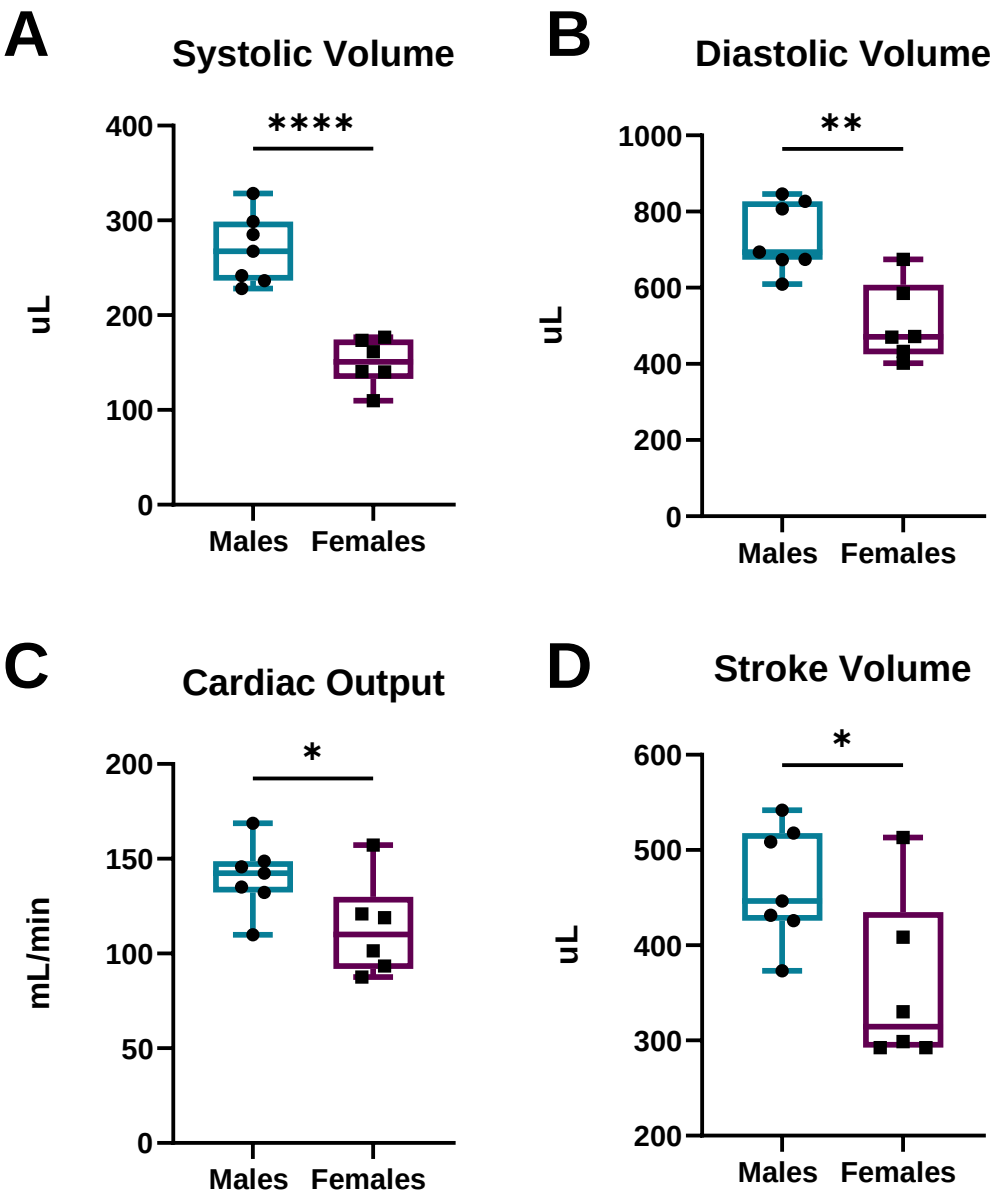

Figure 7. 2 Raw echocardiography measurements. Raw echocardiography measurements were taken at the terminal timepoints (18 months). Systolic volume (A), Diastolic Volume (B), Cardiac Output (C), Stroke Volume (D) was assessed in both aged males and females. Results reported as min to max range, axis range was decided based on the physiologically 'healthy' ranges, n=7 males and n=7 females; p values were obtained using unpaired Students t-test when comparing two groups; *p<0.05; **p<0.01

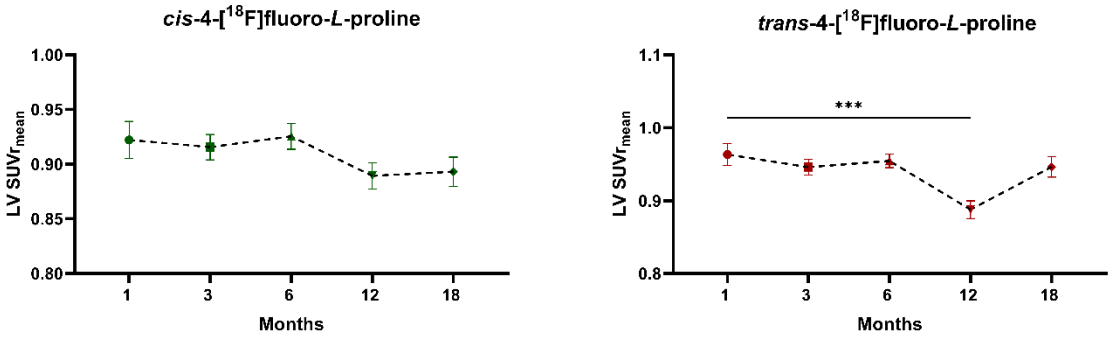

Figure 7. 3 LV *cis*-4-[^{18}F]fluoro-L-proline and *trans*-4-[18F]fluoro-L-proline analysis assessing whether survival bias altered the trends. Longitudinal changes in *cis*-4-[^{18}F]fluoro-*L*-proline and *trans*-4-[^{18}F]fluoro-*L*-proline uptake in the LV over 18 months of animals that survived all timepoints. Results reported as min to max range, n=7 males and n=7 females; p values were obtained a Mixed-effects Analysis and Dunnett's Post hoc test when comparing longitudinal data to the first timepoint. *p<0.05

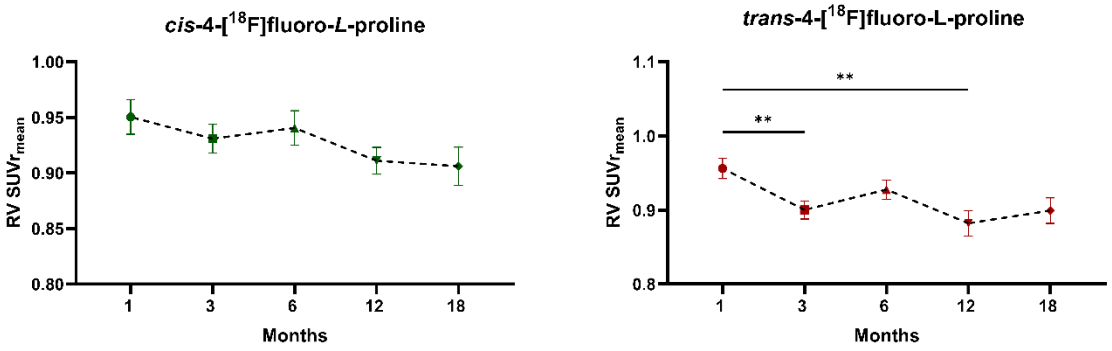

Figure 7. 4 RV cis-4-[^{18}F]fluoro-L-proline and trans-4-[^{18}F]fluoro-L-proline analysis assessing whether survival. Longitudinal changes in *cis*-4-[^{18}F]fluoro-*L*-proline and *trans*-4-[^{18}F]fluoro-*L*-proline uptake in the RV over 18 months of animals that survived all timepoints. Results reported as min to max range, n=7 males and n=7 females; p values were obtained a Mixed-effects Analysis and Dunnett's Post hoc test when comparing longitudinal data to the first timepoint. *p<0.05

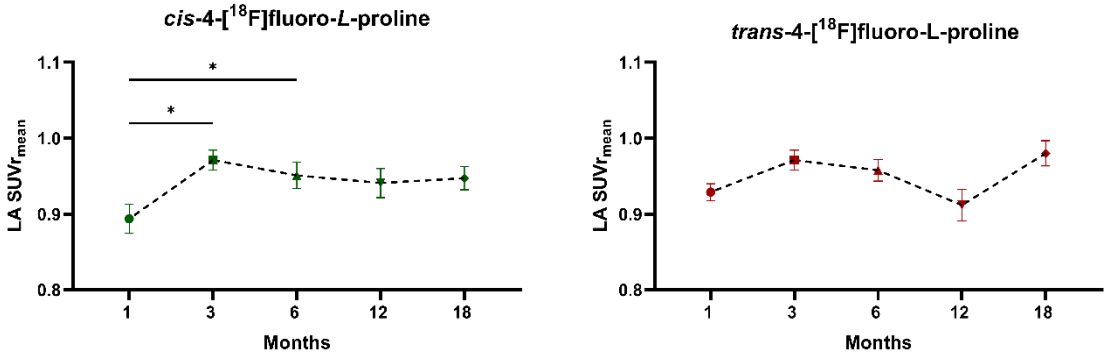

Figure 7. 5 LA cis-4-[^{18}F]fluoro-L-proline and trans-4-[^{18}F]fluoro-L-proline analysis assessing whether survival bias altered trends. Longitudinal changes in *cis*-4-[^{18}F]fluoro-*L*-proline and *trans*-4-[^{18}F]fluoro-*L*-proline uptake in the LA over 18 months of animals that survived all timepoints. Results reported as min to max range, n=7 males and n=7 females; p values were obtained a Mixed-effects Analysis and Dunnett's Post hoc test when comparing longitudinal data to the first timepoint. *p<0.05

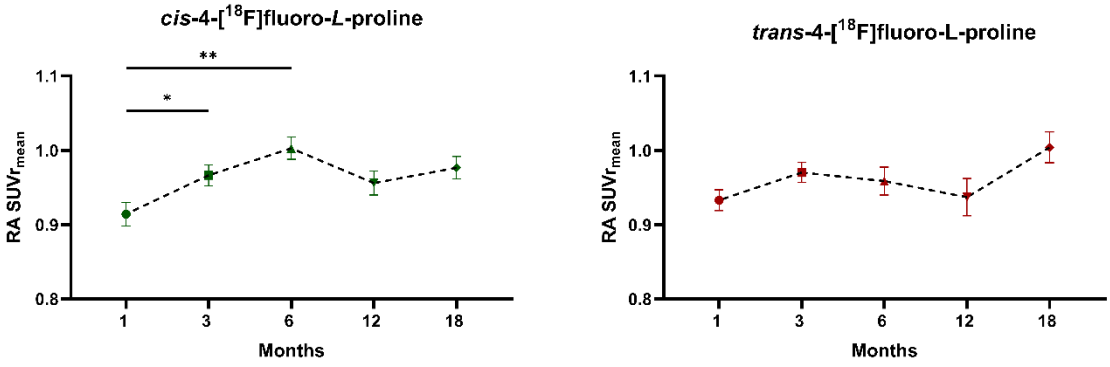

Figure 7.6 RA cis and trans analysis assessing whether survival bias altered trends. Longitudinal changes in *cis*-4-[^{18}F]fluoro-*L*-proline and *trans*-4-[^{18}F]fluoro-*L*-proline uptake in the RA over 18 months of animals that survived all timepoints. Results reported as min to max range, n=7 males and n=7 females; p values were obtained a Mixed-effects Analysis and Dunnett's Post hoc test when comparing longitudinal data to the first timepoint. *p<0.05